Geochemical and petrological evolution of La Palma (Canary Islands) and its rift zone during the last 1.0 Ma

Dissertation for the doctorate degree
of the Department of Geoscience
at the University of Bremen

submitted by
Karsten Galipp
Bremen 2005

“Ach was alles Unsinn:
Lava und Magma und Fumarolen und Eruptionen -
im Berg sitzt ein scheußlich schwarzer Teufelskerl,
der mit glühenden Steinen schmeißt.”

Urmel aus dem Eis, Max Kruse

Tag des Kolloquiums:

23.06.05

Gutachter:

Prof. Dr. M. Olesch

Dr. habil. T. H. Hansteen

Prüfer:

Prof. Dr. O. Brockamp

Dr. A. Klügel

Table of contents

Abstract _____ **1**

Zusammenfassung _____ **3**

1. Introduction _____ **6**

2. Magma storage and underplating beneath Cumbre Vieja volcano, La Palma (Canary Islands) _____ **21**

Andreas Klügel, Thor H. Hansteen, Karsten Galipp
Submitted to Earth and Planetary Science Letters: Received revised manuscript, 18 February 2005

3. Thermobarometry _____ **46**

Changing depths of magma fractionation and stagnation during the evolution of an oceanic island volcano: La Palma (Canary Islands)
Karsten Galipp, Andreas Klügel, Thor H. Hansteen
Submitted to Journal of Volcanology and Geothermal Research: Received 03.11.04

4. Geochemistry _____ **78**

Petrogenesis and geochemical evolution of lavas from La Palma (Canary Islands): implications for plume-lithosphere interaction
Karsten Galipp, Andreas Klügel, Tor S. Johansen, Folkmar Hauff, Kaj Hoernle
To be submitted to Chemical Geology

5. Geochronology _____ **124**

6. Conclusions _____ **140**

Appendix _____ **143**

Erklärung _____ **198**

Danksagung _____ **199**

Lebenslauf _____ **200**

Abstract

Rift zones on ocean island volcanoes have a strong control over magmatic processes such as differentiation, crustal assimilation and magma transport mechanisms. Our knowledge of the magmatic evolution beneath rift zones at ocean islands is still limited. The aim of this thesis is to better understand the geochemical and petrological evolution of a rift zone in space and time focusing on La Palma (Canary Islands) as a case study. In order to model the magmatic evolution of the rift zone major, trace elements and radiogenic isotope compositions of representative rocks from the last 1.0 Ma were determined. This timespann encompasses the volcanic activity of the Taburiente shield volcano (1.2 - 0.4 Ma) and the Cumbe Nueva ridge (830 – 560 ka) as well as the short Bejenado volcanic phase (560 – 490 ka) which followed the Cumbre Nueva collapse (~560 ka), and the presently active Cumbre Vieja rift phase (125 ka to present).

Clinopyroxene-melt thermobarometry and microthermometry of fluid inclusions were applied to constrain magma pathways and main levels of magma stagnation. CO_2-rich fluid inclusions in Taburiente dunite xenoliths correspond to equilibrium pressures of 0.4 to 0.6 GPa (10 – 17 km). Inclusion data of Cumbre Nueva ankaramites and Bejenado cumulate xenoliths yield pressure estimates of 0.25 to 0.45 GPa (8 – 14 km). In comparison, fluid inclusions in Recent Cumbre Vieja rocks yield a pronounced pressure range of 0.20 to 0.40 GPa (5 – 14 km), which partly overlaps with the Cumbre Nueva data but is shallower than that for Taburiente. Clinopyroxene-melt barometry of phenocrysts and glassy groundmass yield equilibrium pressures between 0.60 and 1.05 GPa (19 – 34 km, Taburiente) and 0.50 to 0.85 GPa (16 – 28 km; Cumbre Nueva and Bejenado). This pressure range partly overlaps with that for Cumbre Vieja which is characterized by values of 0.45 to 0.64 GPa (14 – 25 km) but has a tendency to higher pressures. The combined data indicate that two separate magma stagnation levels existed for each rift phase: (1) a main fractionation level within the upper mantle, and (2) intermittent stagnation close to the Moho for the Taburiente volcano and above the Moho for Bejenado, Cumbre Nueva and Cumbre Vieja. A possible relationship of the magma plumbing systems of the extinct Taburiente shield volcano and the active Cumbre Vieja rift can be excluded due to the thermobarometric data obtained.

Trace element and isotope ratios reveal distinct geochemical signatures for the active Cumbre Vieja and the extinct volcanoes. Sr, Nd and Pb isotopic ratios for the older Taburiente and Bejenado volcanoes show considerable variability ($^{87}Sr/^{86}Sr$ = 0.703001 - 0.703110, $^{143}Nd/^{144}Nd$ = 0.512880 - 0.512971, $^{206}Pb/^{204}Pb$ = 19.142 - 19.947, $^{207}Pb/^{204}Pb$ = 15.544 - 15.639; $^{208}Pb/^{204}Pb$ = 38.829 - 39.758), whereas the range for Cumbre Vieja is rather limited ($^{87}Sr/^{86}Sr$ = 0.703087 - 0.703169, $^{143}Nd/^{144}Nd$ = 0.512888 - 0.512901, $^{206}Pb/^{204}Pb$ = 19.497 - 19.715, $^{207}Pb/^{204}Pb$ = 15.609 - 15.888; $^{208}Pb/^{204}Pb$ = 39.159 - 39.488) and has a tendency to more depleted compositions than Taburiente. Much of the isotope

variations can be explained by binary mixing between an enriched HIMU-type plume component and a more depleted lithospheric component. Cumbre Vieja rocks are systematically more enriched in incompatible trace elements (Ba, Rb, P, Th, U, Nb, Sr, LREE) and show larger La/Yb (27.1 - 49.1) and Sm/Yb (4.6 – 7.3) ratios than the older Taburiente, Cumbre Nueva and Bejenado rocks (La/Yb = 19.1 – 37.2; Sm/Yb = 3.7 – 6.3). Remarkably, La/Yb and Sm/Yb ratios of Cumbre Vieja lavas are also higher than those of most ocean island basalts (OIB) wordwide. Slight concave-upward chondrite-normalized rare earth element (REE) patterns, negative K anomalies as well as relative depletion in Rb and Ba on mantle-normalized diagrams of fractionation-corrected La Palma basalts require the presence of residual amphibole in their melting region. It is suggested that this amphibole is of metasomatic origin as a consequence of infiltrating melts, which were derived from rising plume material penetrating the lithosphere at its base during the early submarine stage of La Palma volcanism. Model calculations for the variation of trace element ratios as a function of source composition and degree of melting illustrate that the observed rare earth element ratios and the high contents of P, Sr, Th, U and LREE of Cumbre Vieja lavas cannot be derived by a single-stage melting process from amphibole-bearing garnet lherzolite, garnet pyroxenite, or a combination of both. The compositions rather require assimilation of ~1% apatite by Cumbre Vieja melts during their ascent through the lithosphere. The geochemical data indicate that there is no progressive geochemical evolution of La Palma magmas but a compositional break between Taburiente volcanism in the north and Cumbre Vieja volcanism in the south. This conclusion is also supported by significant differences of Nb/U ratios between Cumbre Vieja lavas (33.8 – 52.3) and those of Taburiente and Bejenado (49.7 – 87.6), the latter being clearly above the global OIB range (47 ± 10) probably due to amphibole assimilation. The combined data suggest that the active Cumbre Vieja rift and the extinct volcanoes represent distinct volcanic systems, rather than a progressively evolving volcano.

Incremental $^{39}Ar/^{40}Ar$ laserdating was carried out in order to extend the existing age data set of La Palma and to adress the question whether the apparent gap in volcanic activity between 410 and 125 ka could be related to sampling bias or a volcanic hiatus. However, $^{39}Ar/^{40}Ar$ age determination and step heating experiments of basaltic groundmass and glass separates yielded geologicallly unreasonable results due to strong contamination of the samples by atmospheric argon. Therefore, only one Bejenado (550 ± 20 ka) and one Cumbre Nueva (730 ± 70 ka) sample revealed reliable crystallization ages.

Zusammenfassung

Riftzonen von Ozeaninsel-Vulkanen haben einen starken Einfluß auf magmatische Prozesse wie Differentiation, Mischung und Assimilation. Jedoch sind die Prozesse der Magmenentwicklung von Riftzonen nur wenig erforscht. Ziel dieser Arbeit ist es deshalb, ein besseres Verständnis über die zeitlich-räumliche geochemische und petrologische Entwicklung einer Riftzone zu erhalten. Als exemplarisches Fallbeispiel wurde La Palma gewählt. Um die zeitliche magmatische Entwicklung zu rekonstruieren, wurden die Zusammensetzungen der Haupt- und Spurenelemente sowie die Sr-Nd-Pb Isotopen-Verhältnisse repräsentativer Gesteine der letzten 1.0 Ma ermittelt. Diese Zeitspanne umfasst sowohl das Aktivitätsstadium des Taburiente Vulkans (1.2 – 0.4 Ma) und des Cumbre Nueva Rückens (830 – 560 ka), als auch die kurze Phase des Bejenado Vulkans (560 – 490 ka) nach dem Cumbre Nueva Kollaps (~ 560 ka), sowie das aktive Cumbre Vieja Riftstadium (von 125 ka bis rezent).

Tiefen von Magmenreservoirs und temporäre Stagnationsniveaus wurden anhand eines Klinopyroxen-Schmelz-Barometers und mikrothermometrischen Untersuchungen von Fluideinschlüssen bestimmt. CO_2-reiche Fluideinschlüsse in Taburiente Xenolithen weisen auf Gleichgewichtsdrücke von 0.40 bis 0.60 GPa hin, entsprechend Stagnationstiefen von 10 bis 17 km. Fluideinschlußdaten von Cumbre Nueva Ankaramiten und Bejenado Kumulaten ergaben Drücke von 0.25 bis 0.45 GPa (8 bis 14 km). Im Vergleich dazu wurden in rezenten Cumbre Vieja-Proben geringere Drücke von 0.25 bis 0.40 GPa (5 bis 14 km) ermittelt, die aber z.T. mit den Cumbre Nueva Daten überlappen, jedoch niedriger als die des Taburiente Vulkans sind.

Das Klinopyroxen-Schmelz-Barometer ergab Fraktionierung von Klinopyroxen bei Drücken zwischen 0.60 und 1.05 GPa (19 bis 34 km, Taburiente) und 0.50 bis 0.85 GPa (16 bis 28 km, Cumbre Nueva und Bejenado). Dieser Druckbereich überschneidet sich z.T. mit dem Bereich für die Cumbre Vieja, der jedoch bei etwas geringeren Drücken zwischen 0.45 und 0.64 GPa (14 bis 25 km) liegt. Die kombinierten barometrischen und mikrothermometrischen Daten weisen auf zwei separate Stagnationsniveaus für jede vulkanische Phase hin: (1) Ein Hauptfraktionierungsniveau innerhalb des oberen Mantels und (2) ein temporäres Stagnationsniveau im Bereich der Moho für den Taburiente Vulkan und oberhalb der Moho für die Cumbre Nueva, den Bejenado Vulkan und die Cumbre Vieja. Eine mögliche Verbindung der Magmenaufstiegswege des erloschenen Taburiente Schildvulkans und dem aktiven Cumbre Vieja Rift kann aufgrund der ermittelten thermobarometrischen Daten ausgeschlossen werden.

Die Spurenelementanalysen und die Isotopendaten offenbaren deutliche geochemische Unterschiede zwischen dem Cumbre Vieja Rift und den erloschenen Vulkanen.

Die Sr-Nd-Pb-Isotopen Daten ergaben große Variationen für den Taburiente und Bejenado Vulkan ($^{87}Sr/^{86}Sr$ = 0.703001 - 0.703110, $^{143}Nd/^{144}Nd$ = 0.512880 - 0.512971, $^{206}Pb/^{204}Pb$ = 19.142 - 19.947, $^{207}Pb/^{204}Pb$ = 15.544 - 15.639; $^{208}Pb/^{204}Pb$ = 38.829 - 39.758). Im Vergleich dazu weisen die Isotopenverhältnisse des aktiven Rifts (Cumbre Vieja) eine geringere Spannbreite auf und neigen tendenziell zu verarmteren Verhältnissen ($^{87}Sr/^{86}Sr$ = 0.703087 - 0.703169, $^{143}Nd/^{144}Nd$ = 0.512888 - 0.512901, $^{206}Pb/^{204}Pb$ = 19.497 - 19.715, $^{207}Pb/^{204}Pb$ = 15.609 - 15.888; $^{208}Pb/^{204}Pb$ = 39.159 - 39.488). Die Isotopenzusammensetzung der La Palma Magmen kann mit einem Model erklärt werden, bei dem sich eine isotopisch angereicherte asthenospherische Komponente mit einer isotopisch verarmten lithospherischen Komponente mischt.

Die Gesteine der Cumbre Vieja sind am stärksten angereichert an inkompatiblen Spurenelementen (Ba, Rb, P, Th, U, Nb, Sr, LREE) und weisen höhere La/Yb- (27.1 bis 49.1) und Sm/Yb-Verhältnisse (4.6 – 7.3) auf als die älteren Taburiente-, Cumbre Nueva- und Bejenado-Gesteine. Auch im Vergleich zu anderen Ozean Insel Basalten sind die La/Yb- und Sm/Yb-Verhältnisse der Cumbre Vieja Laven außergewöhnlich hoch. Die Mantelquelle und deren mögliche zeitliche Änderung wurde mit Hilfe von korrigierten Spurenelementdaten für die Olivin- und Klinopyroxen-Fraktionierung modelliert. Die konkav-aufwärts verlaufenden chondrit-normierten Seltenen Erden Muster (SEE), sowie die negative K-Anomalie und die relative Verarmung an Rb und Ba in mantel-normierten Diagrammen sprechen für eine amphibolhaltige Mantelquelle. Die Entstehung des Amphibols wird erklärt durch eine metasomatische Überprägung, hervorgerufen durch infiltrierende Schmelzen des aufsteigenden Plumes, welche die tiefere Lithosphere durchdrungen haben. Jedoch ergaben Modellierungen, daß ein amphibolführender Granat Lherzolith bzw. Granat Pyroxenit als mögliche Quellen nicht die extreme Anreicherung von P, Sr, Th, U und den leichten SEE in den Cumbre Vieja Proben erklären können. Die hohen Gehalte an inkompatiblen Spurenelementen der Cumbre Vieja Magmen erfordert die Assimilation von ~1% Apatit innerhalb der Lithosphere während des Magmenaufstiegs. Die geochemischen Daten schließen eine progressive geochemische Entwicklung zwischem den Magmen des Taburiente Vulkanismus im Norden und dem Cumbre Vieja Vulkanismus im Süden aus. Diese Schlußfolgerung wird u.a. durch unterschiedliche Nb/U-Verhältnisse zwischen den Cumbre Vieja Basalten (33.8 – 52.3) und den Basalten der alten Vulkane gestützt (49.7 – 87.6), wobei die Verhältnisse der Letzteren deutlich höher sind, als für andere Ozean Insel Basalte (47 ± 10). Insgesamt sprechen die zusammengefassten Daten dafür, daß das aktive Cumbre Vieja Rift und die erloschenen Vulkane keinen sich progressiv entwickelnden Vulkan darstellen, sondern zwei unabhängige vulkanische Systeme.

$^{40}Ar/^{39}Ar$-Laserdatierungen wurden durchgeführt, um kritische Lücken im Altersdatensatz zu schließen und die Frage zu klären, ob der Hiatus zwischen 410 und 125 ka eine Pause in der

vulkanischen Aktivität wiederspiegelt oder auf die Beprobungstrategie zurückzuführen ist. Altersbestimmungen und Stufenheizexperimente an basaltischer und glasiger Grundmasse führten auf Grund von starker Kontamination der Proben durch atmosphärisches Argon zu geologisch unschlüssigen Resultaten. Für eine Bejenado- und Cumbre Nueva**-**Probe wurden sinnvolle Kristallisationsalter von 550 ± 20 ka bzw. 730 ± 70 ka ermittelt

1. Introduction

Many oceanic intraplate volcanoes are surface manifestations of deep-seated mantle plumes. The global occurrence of such volcanoes thus reflects recurrent magma generation processes, which are of central importance to our understanding of regional and global mantle dynamics. Due to the dense and thin oceanic crust underlying ocean islands, ascending magmas are less prone to crustal contamination than their continental counterparts. The compositions of oceanic islands basalts (OIB) are thus commonly interpreted to reflect deep-seated magma generation and evolution processes (e.g. Class et al., 1998; Simonsen et al., 2000). A number of studies have shown, however, that the evolution of oceanic intraplate magmas may be directly linked to intermittent stagnation, fractionation and wall-rock assimilation in the crust (e.g. Hansteen et al., 1998; Caroff et al., 1999; Harris et al., 2000; Klügel et al., 2000; Schwarz et al., 2004). Evidence for crustal influence on mantle magmas is particularly pronounced for volcanoes consisting of rift zones, such as the Hawaiian volcanoes (e.g. Kilauea: Garcia et al., 1989; Yang et al., 1999).

Rift zones are fundamental components in many ocean islands volcanoes and influence spatial evolution and constitution of volcanoes (e.g. Garcia et al., 1989; Yang et al., 1999). They define narrow zones along which the islands preferably grow by intrusions and extrusion (Carracedo, 1994; Carracedo, 1999; Walker, 1999) resulting in elongated volcano piles. Characteristic features are (i) parallel, subvertical dyke swarms, (ii) alignment of scoria and cinder cones stacked one on another, (iii) lava flows extending from the rift zone and (iv) parallel graben structures (Fig. 1).

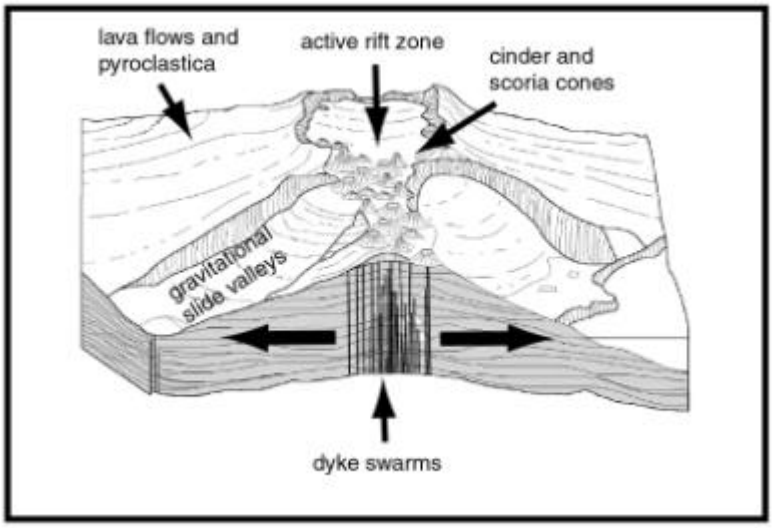

Fig. 1. Profile through a rift zone (modified after Carracedo, 1994). At the surface the sublinear, elongated rift zone is characterized by eruptive fissures, cinder and spatter cones and lava flows extending from the rift. Subparallel, steeply dipping dikes are concentrated at the center (axis) of the rift zone.

Rift zones also have a strong influence on destructive processes. For example, subaerial and submarine landslides together with flank collapses and associated tsunamis are linked to rift zones (Moore et al., 1994; Day et al., 1999). The relationship between rift zones and flank

stability is given by the occurrence of normal faults parallel to the rift axes and shallowly-dipping detachments faults subparallel to the surface. Alternatively they may buttress and effectively strengthen volcanic cones (Walker, 1999; Walter and Troll, 2003) if overlapping volcanic edifices are connected by a rift zone

Studies of Hawaiian volcanoes have shown that rift zones have a strong control on magmatic processes such as differentiation and crustal assimilation and on magma transport mechanisms (e.g. Garcia et al., 1989; Delaney et al., 1990; Yang et al., 1999). Despite their importance only few studies have dealt with the geochemical and petrological evolution of the magmatic system of ocean island rift zones. Our knowledge is mainly based on the eruptive sequence of a single eruption or a short period of activity (< 1000 a) (e.g. Hofmann et al., 1984; Wolfe et al., 1987; Garcia et al., 1996; Klügel et al., 2000;) or on Iceland (e.g. (Gudmundsson, 1995; Hardarson et al., 1997; Gudmundsson, 2000;) and on the Hawaiian islands (e.g. Walker, 1987; Feigenson et al., 1983; Dieterich, 1988; Frey et al., 1991;).

However, Iceland and the Hawaiian islands are not representative for rift zones worldwide: Iceland is located directly above the Atlantic mid-ocean ridge and therefore represents a special tectonic and geochemical location and the Hawaiian islands are regarded as the most intense hotspot system on Earth in terms of the buoyancy flux of the Hawaiian plume (Table 1). Interdisciplinary studies at Hawaiian volcanoes have revealed deeper insights into the stucture and dynamics of rift zones (e.g. Tilling and Dvorak, 1993) and references therein). These volcanoes are characterized by a central volcano underlain by a shallow magma chamber at 2 to 6 km depths from where two or three rift arms emanate. The general importance of case studies of volcanic islands other than Hawaii is underlined by previous studies of magmatic systems and submarine deposits at the Canary Islands (Schmincke and Sumita, 1998; Klügel et al., 2000) and Madeira (Schwarz et al., 2004), which have shown that results from Hawaii are not necessarily transferable to other ocean islands.

Table 1: Overview of main geodynamical and volcanological parameters of Hawaiian (Kilauea) and Canary Islands (La Palma)

	Canary Islands	Hawaii
buoyancy flux	1.0×10^3 kg/s[1]	8.7×10^3 kg/S[1]
magma supply rate	0.15 – 0.37 km^2/ka^3 (La Palma)	10.0 – 18.0 km^3/ka^3 (Kilauea)
plate velocity	19 cm/a[4]	10 cm/a[5]

1 Sleep (1990), 2 Ancochea et al. (1994), 3 Dzurisin et al. (1984), 4 Carracedo (1999) 5 Clague (1987)

Scope of the thesis

The main purpose of this thesis is to improve our understanding of magma evolution processes and transport mechanisms in rift zones in general, using La Palma as a case study.

Petrographical and whole rock analyses, including major, trace element, isotopic and geochronological investigations were undertaken to understand magma genesis during the last 1.0 Ma years at La Palma. A combination of major and trace element chemistry is used to interpret the origin and the evolution of the basaltic rocks. Isotopic composition of the rocks studied allow constraints on magma sources and/or contamination processes, while age dating of basalts and glass by $^{40}Ar/^{39}Ar$ analyses give better temporal constraints on the geological evolution. Thermobarometric and fluid inclusion data is also used to gain insights into the magma plumbing system during the evolution of the rift system. The objectives in detail are to determine:

- Information about temporal variations of the source composition and mineralogy and the role of possible crustal contamination on ascending magmas
- Temporal and spatial geochemical variations of the magmas
- Depths of major fractionation levels and temporary stagnation levels
- Whether the currently active Cumbre Vieja rift is zone genetically related to the extinct Taburiente stratovolcano, or whether they represent two distinct volcanoes with their own magma plumbing systems
- Whether the petrologic model for 1949 eruption (Klügel et al., 2000) is transferable to pre-historic eruptions
- The role of a major flank collapse on magma pathways within the crust
- Principal differences between the model for Hawaiian rift zones and rift zones on North Atlantic ocean islands
- Whether the apparent gap in activity between 410 and 125 ka is related to sampling bias or a volcanic hiatus

Why La Palma

Most of our knowledge about rift zones is based on Hawaiian rift zones (e.g. Tilling and Dvorak, 1993; Garcia et al., 1996; Garcia et al., 1998) which are characterized by shallow magma chambers from which two or three rift arms emanate. However, other ocean islands volcanoes can differ substantially from such a rift zone configuration. For example, studies of rift zones at the Madeira Archipelago (North Atlantic; Schwarz et al., 2004) show differences to Hawaiian rift systems and resembles those of the Cumbre Vieja lacking a shallow magma chamber and a summit caldera (Klügel et al., 2000). However, the Desertas rift arm at the Madeira achipelago represents a deeply eroded fossile rift arm (3 – 4 Ma) which was active for a relatively short period, whereas on La Palma eruptions occurred since 0.8 Ma until present along a well-developed rift zone. In summary, the reasons why La Palma is suitable for the study of the evolution of a rift zone are as follows*:*

1. The buoyancy flux of the Canary plume is lower than that of Hawaii (Table 1), but can be regarded as representative for plumes worldwide (0.3 – 3.3 Mg/s; Sleep, 1990).
2. La Palma with low magma supply rates (Table 1) can be viewed as a typical example of intraplate volcanism on the slowly moving North Atlantic plate. In contrast, Hawaii (Kilauea) has higher magma supply rates and is located on a fast moving plate which probably has influence on the formation of rift zones.
3. La Palma offers a great opportunity to analyse the development of a juvenile shield volcano from the seamount stage, as well as the structural changes giving place to development of rifts.
4. The geochronological evolution of La Palma has been thoroughly been reconstructed by K/Ar and Ar/Ar dating methods (Guillou et al., 1998; Carracedo et al., 1999; Guillou et al., 2001). Therefore, La Palma is an ideal place to study the temporal evolution of a rift zone.
5. Previous petrological-geochemical studies of the 1971 and 1949 eruptions (Praegel, 1986; Klügel, 1997; Klügel et al., 2000) have revealed important constraints on magmatic processes (differentiation, assimilation, stagnation and fractionation depths, transport mechanisms). These results provide an important basis for this work.
6. La Palma together with El Hierro and Tenerife are the only Canary Islands which are still in a shield-stage (Carracedo et al., 2001). Furthermore, La Palma has the most active volcano at the Canary Islands, the Cumbre Vieja.
7. Another important advantage of La Palma over other ocean island is the easy access.

Geological setting

Geology of the Canary Islands. The Canary Archipelago represents a 600 km long chain of seven volcanic islands off the coast of Africa (Fig. 2). Subaerial volcanic activity started more than 20 million years ago with the formation of the eastern islands and shows a westward decrease in age from Lanzarote and Fuerteventura to El Hierro (1.3 Ma) (Schmincke and Sumita, 1998). La Palma is the westernmost and volcanically most active of the Canary Islands. All islands rest on oceanic Jurassic crust indicated by magnetic and seismic data (e.g. Hayes and Rabinowitz, 1975; Roeser, 1982; Verhoef et al., 1991) and by tholeiitic mid-ocean ridge basalt (MORB) gabbro xenoliths (Hoernle, 1998; Schmincke et al., 1998). The age of the crust is bracketed by magnetic anomalies S1 (175 Ma) between the easternmost Islands and the African coast, and M25 (155 Ma) between La Palma and El Hierro. Thickness estimates of the lithosphere range from 10 km to 36 km (Watts, 1994; Arana, 1995; Canales and Danobeitia, 1998). Previous studies of mantle xenoliths suggest that oceanic lithosphere extends underneath all Canary Islands (Neumann, 1991; Neumann et al., 1995; Klügel, 1998).

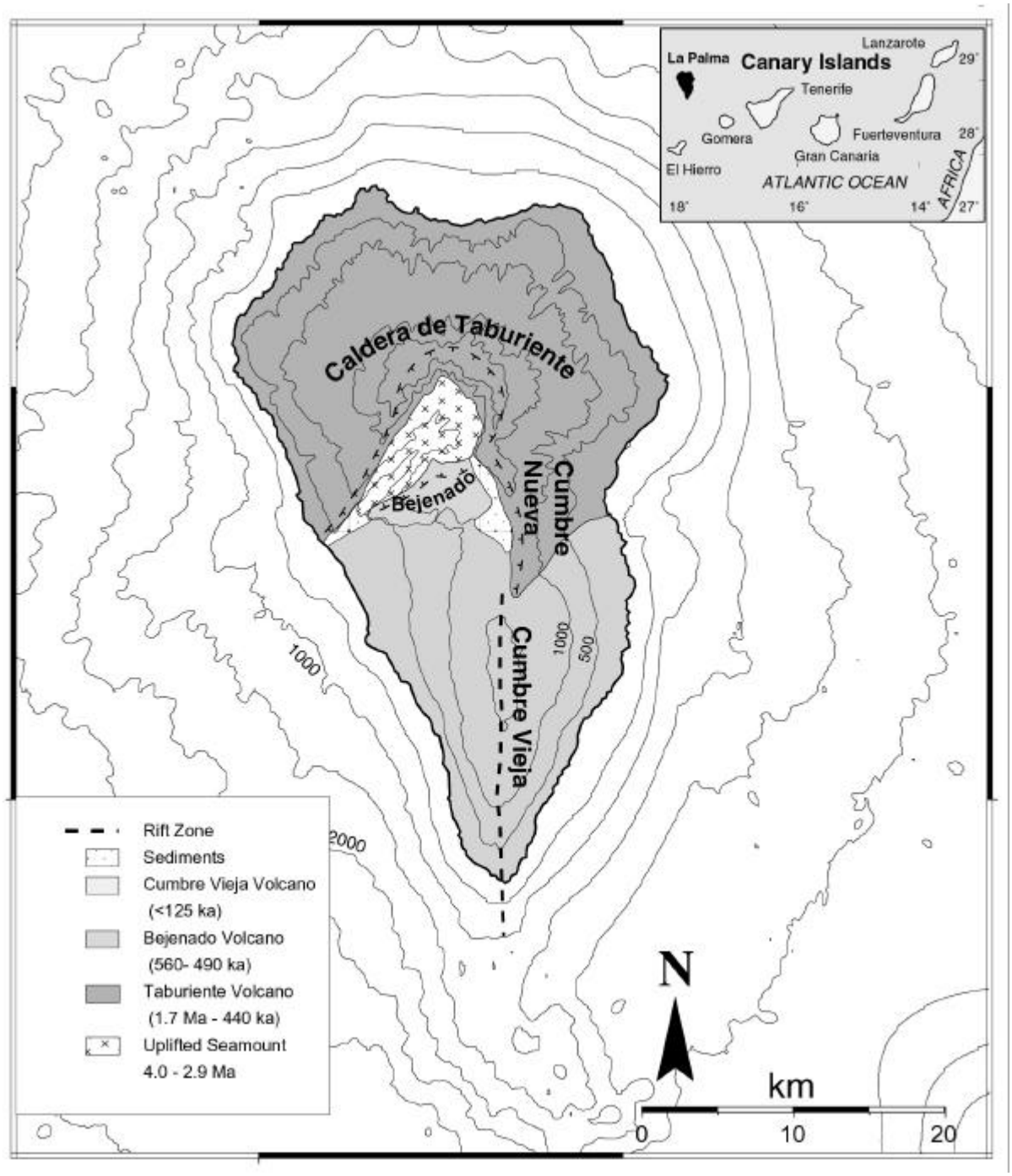

Fig. 2 Simplified geological map of La Palma (modified after Ancochea et al., 1994 and Carracedo et al., 1999). Age range of volcanic units are from Staudigel et al. (1986) and Guillou et al. (1998, 2001). Bathymetric data are partly based on D. G. Masson et al. (2002), compiled by S. Krastel, Universität Bremen.

At present Tenerife, La Palma and El Hierro are the Canary Islands in the shield-stage of growth. Lanzarote, Fuerteventura, Gran Canaria and La Gomera are already in the post-erosional stage of their development. (Carracedo, 1999). The Canary Islands are believed to result from volcanism above a hotspot that impinges beneath the oceanic lithosphere (Morgan et al., 1983; Holik and Rabinowitz, 1991; Hoernle at al., 1993). Differences to the classic hotspot model for Hawaii and alternative hypotheses are discussed in detail by

Schmincke (1976, 1982), Carracedo (1999) and (Mitchell et al., 2002). The different hypotheses for the source of magmatism for the Canary Island is summarized in (Anguita and Hernán, 2000). These authors suggest that the thermal anomaly beneath the eastern Atlantic and western and central Europe (Hoernle et al., 1995) is part of a plume which was instrumental in the opening of the central Atlantic. This model is supported by the overall islands alignment in the central Atlantic (Fig. 3), where islands to the west and east of the Mid-Atlantic ridge appear to trace the motion of the underlying Atlantic plate. This suggest the Canary Islands and New England seamount are derived from a similar magma source, a hypothesis which is supported by isotope ratio diagrams where both island groups overlap (Arana, 1995).

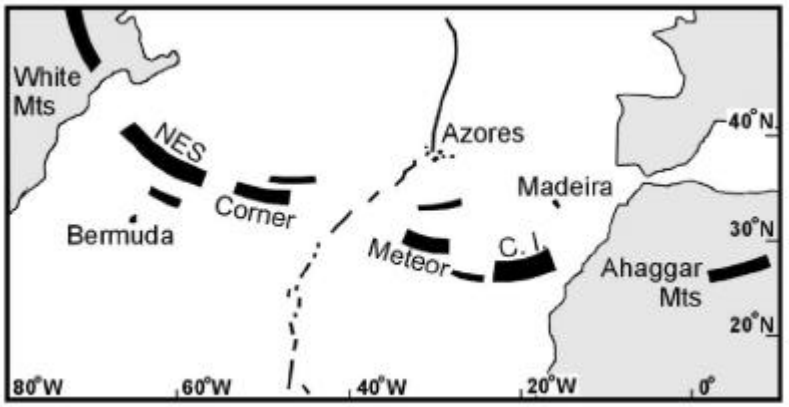

Fig. 3 Simplified map of the central Atlantic; NES = New England Seamounts, C.I. = Canary Islands, redrawn from Arana (1995), taken from Triepold (2004). The Canary Islands and the New England Seamounts are ascribed to the same magma source**.**

Geology of La Palma. The island of La Palma rises to 2426 m above sea level and can be divided into three major units (Fig. 2) (Hausen, 1969; Abdel-Monem et al., 1972; Middlemost, 1972; Schmincke, 1976): (i) the older basal complex (ca. 4.0 to 3.0 Ma) comprised of a Pliocene seamount complex exposed in the Caldera de Taburiente, and a plutonic complex, uplifted and tiled by intrusions coeval with the later subaerial activity (Staudigel and Schmincke, 1984), (ii) the older volcanic series (1.7 to 0.4 Ma) which include the Garafia volcano, the Taburiente shield volcano, the Bejenado edifice, and the Cumbre Nueva series, and (iii) the recent Cumbre Vieja series (125 ka to present) which is confined to the southern half of the island. The first subaerial volcanism formed the Garafia volcano (1.7 – 1.2 Ma) which overlies and mantles the uplifted seamount. Outcrops of the Garafia volcano are limited to erosive windows on the north and southwest flanks of the northern shield. The Taburiente shield-volcano (1.2 to 0.4 Ma) forms the northern part of La Palma (Fig. 1) (Ancochea et al., 1994; Guillou et al., 1998; Guillou et al., 2001). From about 830 ka, the Taburiente volcano began to extend to the south forming the morphologically prominent Cumbre Nueva ridge which is interpreted as a volcanic rift zone. This rift was partially destroyed by a giant lateral collapse at 560 ka (Fig. 4). New chronological and structural data revealed that the Cumbre Nueva series is a younger part of Taburiente, whose >400 m thick

lava sequences formed in <200 ka (Carracedo et al., 1999). Immediately after the collapse, a new episode of volcanic activity occurred within the collapsed embayment and produced the Bejenado volcano. The growth of this stratovolcano occurred rapidly from about 560 to 490 ka (Guillou et al., 1998; Guillou et al., 2001) with little concomitant activity from Taburiente. Carracedo et al (2001) have subdivided the Taburiente shield volcano in a lower sequence (~1.2 to 0.8 Ma) characterized by the predominance of pyroclastic deposits, and in an upper sequence (~0.8 to 0.4 Ma) where eruptions changed to more effusive style with emission of large volumes of alkaline lavas.

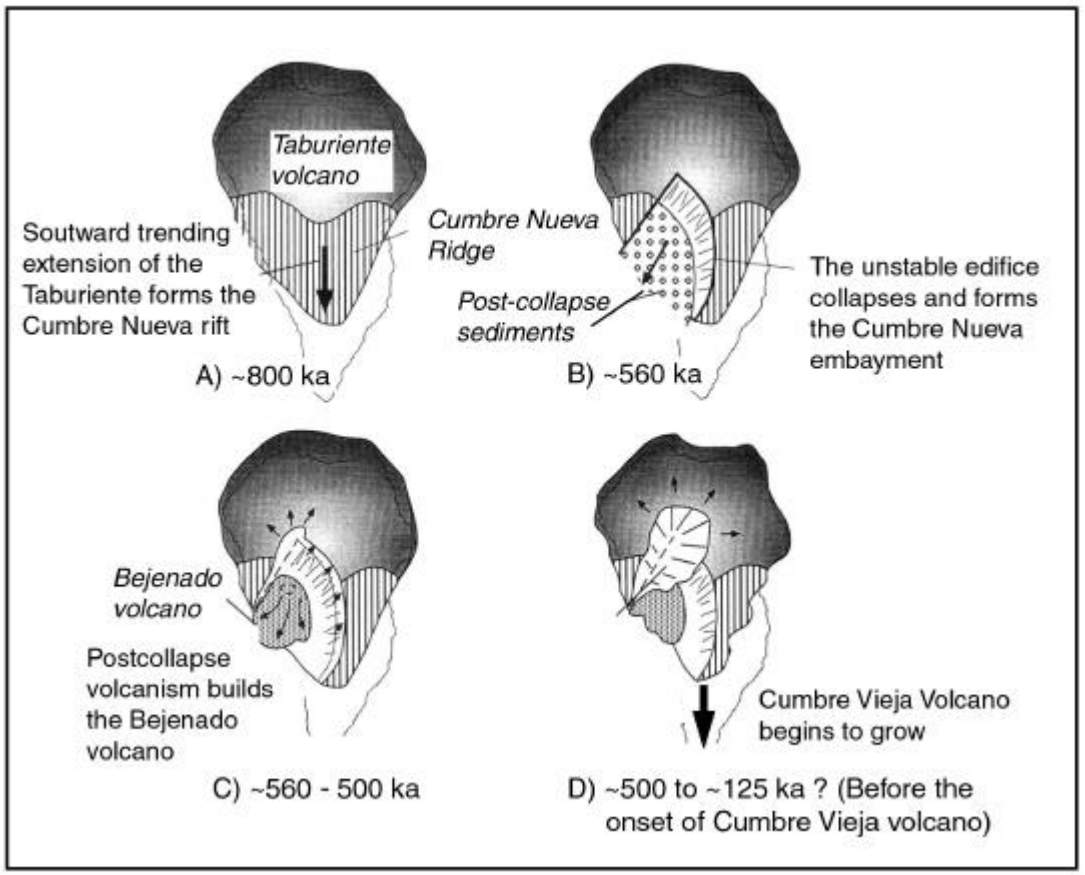

Fig. 4 Evolution of (A) the Cumbre Nueva rift, (B) the Cumbre Nueva collapse, (C) Bejenado volcano and of (C) the N-S trending presently active rift zone at La Palma (modified after Carracedo et al., 1999).

After cessation of volcanism at Bejenado, the activity shifted to the south forming the Cumbre Vieja volcano (Fig. 4). This volcano is still active to the present. The apparent gap from 400 to 125 ka, separating the volcanism at Taburiente and Cumbre Vieja, may correspond to a period of volcanic quiescence. However, a more likely explanation is that volcanism continued but older rocks at the Cumbre Vieja are completely covered by younger lavas.

Recent eruptive activity on La Palma is largely confined to the N-S trending Cumbre Vieja ridge. This is a pronounced rift zone as indicated by the prominent north-south alignment of vents, fissures and faults (Middlemost, 1972; Carracedo, 1994). Morphologically, the Cumbre Vieja rests on the southern flank of the older Cumbre Nueva ridge and represents a separate

volcanic edifice. Historic eruptions at the Cumbre Vieja were recorded in 1430/1440, 1585, 1646, 1677, 1712, 1949 and 1971. A detailed geological map of La Palma and new age determinations of La Palma rocks are given in Carracedo et al. (2001, 2001b) and references therein.

La Palma vs. Hawaii

One purpose of this thesis is to compare the La Palma rift system with those of Hawaiian Islands in order to elucidate principal differences between both rift configurations and to verify if the model for the 1949 eruption on La Palma (Klügel et al. 2000) is transferable to pre-historic eruptions. Therefore, a short introduction is given in this section to the model of Hawaiian rift zones and the Cumbre Vieja rift zone which is based on the model for the 1949 eruption (Klügel 1997, Klügel et al., 2000).

Interdisciplinary studies at Hawaiian volcanoes, and especially at Kilauea, have revealed most of our present knowledge of the internal structure and dynamics of volcanic rift zones (e.g. Wright and Fiske, 1971; Garcia et al., 1989; Tilling and Dvorak, 1993; Yang et al., 1999). Hawaiian rift zones show either a triple star configuration like Mauna Kea or a two-arm configuration, such as is seen on Kilauea and Mauna Loa with their eastern and western rift arms (Fig. 5a). These rift arms are interconnected with a so-called summit reservoir or shallow magma chamber beneath a collapse caldera. The magmatic system of the Hawaiian volcanoes extends from the mantle where melting occurs at depth of at least 80 km (Putirka, 1997). From those depths the primary conduit delivers the melt to the deep magma chamber which begins to form during the pre-shield stage when the magma supply rate is still low (Clague and Dixon, 2000). Shallow subcaldera magma reservoirs at 2 - 6 km depth beneath the volcano's summit formed somewhat later when the magma supply rate increases (Fig. 5B). From the summit reservoir the magmas are injected laterally into the rift zones. Such a "rift-event" is associated with earthquakes and a summit collapse and can often (but not always) induce eruptions. It is supposed that about 50% of the magma can remain as intrusions within the rift zone (Dzurisin et al., 1984). After an eruption, when the magma supply rate decreases, the remaining magma is stored in isolated magma batches where melts can differentiate and then solidify or be erupted later (Wright and Fiske, 1971; Garcia et al 1989). Within the rift zone the compositions of the erupted lavas is strongly influenced by mixing of older and fresh magmas (Garcia et al., 1996) or by wall-rock assimilation during magma transport (Garcia et al., 1998). In addition to the subsurface rift zone (2 – 6 km depth) the Kilauea rift zones also comprise a deep rift system at depth of between 3 to 10 km. This deeper rift zone is composed of permanent magma bodies, crystal mush and cumulates (Ryan, 1988; Garcia et al., 1989; Delaney et al., 1990).

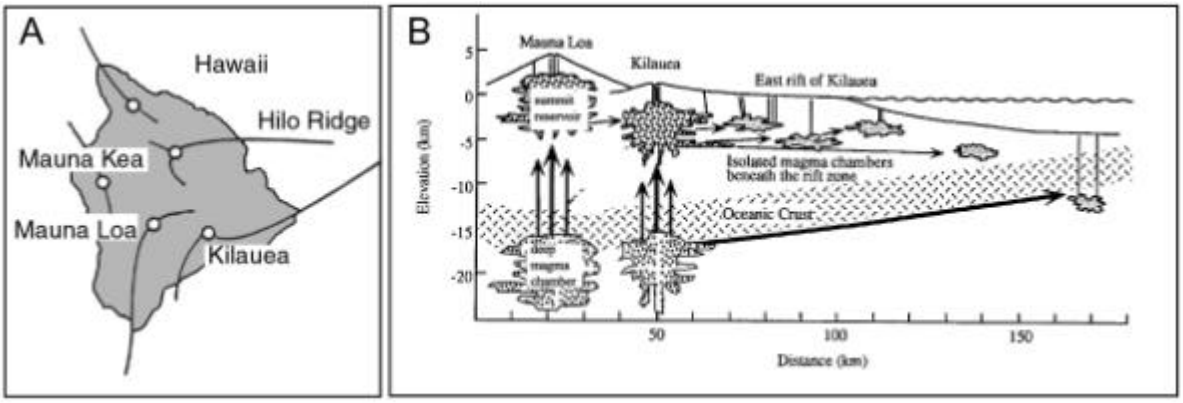

Fig. 5: (A) Volcanic rift zones on Big Island (Hawaii) (after Fiske and Jackson, 1972). Hawaiian volcanoes display a two- or three rift arm configuration. Each volcano edifice is characterized by a central volcano (white circle) underlain by summit reservoir from where rift zones emanate. (B) Inferred pathways (arrows) for magma ascent beneath Kilauea and Mauna Loa volcanoes (modified after Yang et al., 1999). At each volcano, a central conduits feeds the deep magma chamber close to the Moho and the summit reservoir at depths of 2 – 7 km. The summit reservoir can be single chamber or a group of interconnected pockets (Tilling and Dvorak, 1993). Magmas migrate laterally into rift zones from the summit reservoir. When magma the supply rate decreases, isolated magma chambers can form in rift zones. Magma can also migrate laterally at deeper levels, such as at the crust-mantle boundary (Garcia et al., 1995).

However, lateral movement of melts can also occur at deeper levels, as for example at the oceanic crust mantle boundary where abrupt density changes and subhorizontal layering can promote magma migration (Fig. 5B) (Garcia et al., 1995; Yang et al., 1999). According to this model, rift zone eruptions of Kilauea comprise three components: (i) primary magma from the mantle, (ii) magma from the shallow magma chamber and (iii) partly highly evolved magma from the rift zone (Fig. 6). The geochemical variations of these components can be large (e.g. Garcia et al., 1986). However, the variations of the erupted lavas are mostly minor because the different components are effectively mixed within the rift zone by a continuous supply of new magma. In particular mixing of new added magma pulses and older magma occurs within the deep rift zone and within the summit reservoir.

Model for the Cumbre Vieja rift zone based on the 1949 eruption

Klügel (1997) and Klügel et al. (2000) have described a model of the magma plumbing system for the 1949 Cumbre Vieja rift zone eruption. According to this model the magma supply system is characterized by three reservoirs: (i) a permanent reservoir within the upper mantle from where the magmas migrate upwards into (ii) the deep rift within the oceanic crust. From here they migrate further into (iii) the shallow rift within the volcanic edifice (Fig. 6). Within these stagnation levels assimilation, differentiation and mixing were identified as the most important magmatic processes. Inside the deep and the shallow rift, these processes occurred within years to months and months to days respectively. During the main

effusive phase magmas were transported directly from the upper mantle to surface within days to hours.

Klügel et al. (2000) have shown that magma batches can survive between eruptions in isolated or partly interconnected pockets within the mantle where melts can become more differentiated. This means that erupted magmas of one eruption are representing magma batches which have evolved independently and, therefore, cannot be related to one parental magma.

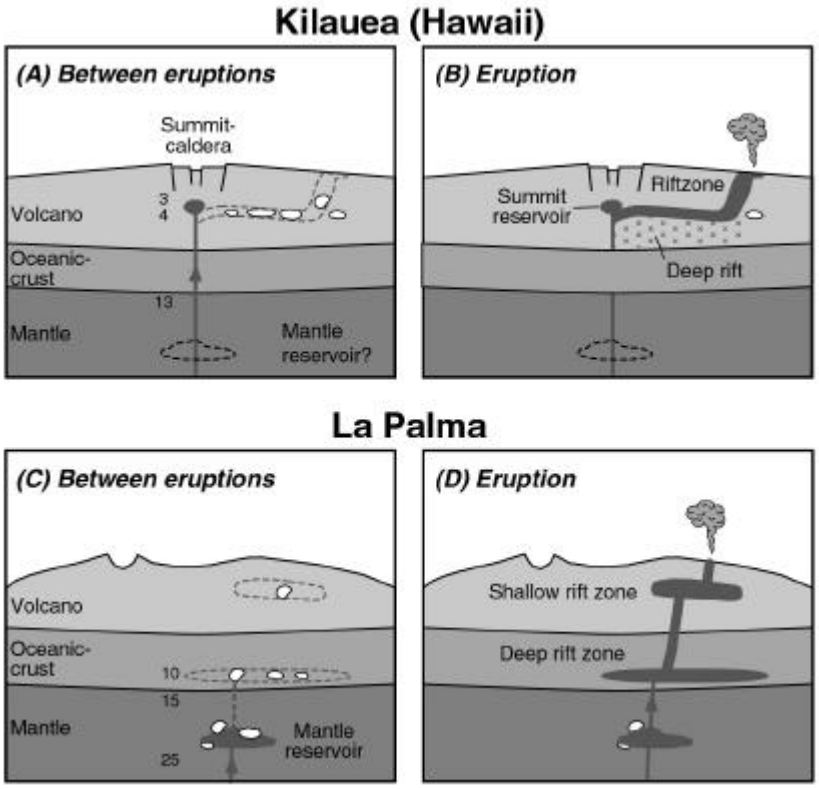

Fig. 6 Comparison of the magma plumbing system of Kilauea and the Cumbre Vieja before and after an eruption (after Klügel et al., 2000), numbers indicate depths in km; white pockets are filled with older, evolved magmas. (A) Between eruptions at Kilauea, a continuous supply of sub-crustal magmas enters the summit inflating the volcanic edifice (Wright and Fiske, 1971). (B) During an eruption magma is fed from below and from the summit reservoir into the rift zone, where it mixes and mingles with magma that has been stored and slightly differentiated. Eruptions occured at Kilauea with a frequency of years to tens of years. (C) Between eruptions at the Cumbre Vieja only little or no magma is fed into the volcanic edifice, which lacks a summit reservoir. (D) During Cumbre Vieja eruptions, magma is transported from mantle reservoirs through the deep and shallow rift system towards the surface. It may mixes with magmas that has been stored at differentiated at different stages. Eruptions occured at the Cumbre Vieja with a frequency of tens of years to hundred of years.

In contrast to Hawaiian rift zones, thermobarometric studies of the 1949 eruption of Cumbre Vieja have shown that this rift zone lacks both a summit caldera and a summit reservoir where mixing and homogenization of different magmas can occur (Klügel et al. 2000). Therefore, compositionally bimodal and multimodal eruptions are the norm. These involve distinct magma batches produced and evolved in the mantle and crust.

However, the existence of shallow magma chambers is not excluded categorically, but it is thought that if they had existed then they were only short-lived features during volcanic activity. The absence of a long-term summit reservoir at the Cumbre Vieja could be ascribed to the longer periods between the eruptions and the smaller volumes emitted per eruption. This can be related directly to the lower buoyancy flux and lower supply rate of basanitic melts as compared to Hawaiian volcanoes (Table 1). A simplified illustration comparing the magma plumbing systems of Kilauea and the Cumbre Vieja, based on studies of the 1949 eruption, is given in Figure 6.

Overview of research

The goal of this thesis is to improve our understanding of magma evolution processes and transport mechanisms at La Palma as a type example of an ocean island volcano in the North Atlantic. For this reason geochemical, thermobarometric and geochronolocical analyses have been carried out. The results are presented and discussed in four chapters. Chapters 2, 3 and 4 consist of individual papers which have been or will be submitted to peer-reviewed international scientific journals.

Chapter 2: ***Magma storage and underplating beneath Cumbre Vieja volcano, La Palma (Canary Islands),*** focuses on magma storage, plumbing and related intrusive island growth and underplating of magmatic material beneath the Cumbre Vieja rift zone. Fluid-inclusion barometry and clinopyroxene-melt thermobarometry were applied to phenocrysts and xenoliths from the volcano's subaerial ridge and submarine flanks in order to reconstruct levels of magma stagnation and fractionation. After adressing where, how and how much igneous material is stored beneath the volcano, the implications for the island's subaerial evolution and inferred uplift that may have affected flank instability are discussed. By using a simple model based on the cumulative volume of material added to the crust, uplift rates caused by underplating are estimated.

Chapter 3: ***Changing depths of magma fractionation and stagnation during the evolution of an oceanic island volcano: La Palma (Canary Islands)****.* This papers discusses the evolution of the magma plumbing system of a rift zone from its earliest stage until present and allows to discuss the question if, and how, the presently active Cumbre Vieja rift zone is connected to the old Taburiente shield volcano. Thermobarometric studies were carried out to constrain the temporal and spatial evolution of La Palma's magma plumbing system over the last 1.0 Ma at La Palma. Depths of magma fractionation and temporary stagnation during magma ascent were investigated using fluid inclusion as well as clinopyroxene-melt barometry and melt barometry. The data suggest that the old shield

volcano and the young Cumbre Vieja rift system are not fed by a common magma reservoir and therefore both systems represent two distinct volcanoes with separate magma plumbing systems.

Chapter 4: ***Petrogenesis and geochemical evolution of lavas from La Palma (Canary Islands): implications for plume-lithosphere interaction.*** This chapter presents a comprehensive geochemical data set of La Palma rocks aged from 1.0 Ma to present. In order to compare the geochemical evolution and sources of the different volcanic units major and trace element analyses of representative samples were carried out. Furthermore, Sr-Nd-Pb isotopic compositions were determined. Differences in the isotopic composition between the volcanic units are interpreted to reflect various contributions of a depleted component into the source. Trace-element modelling is applied to constrain the source and possible source variations of La Palma melts. Additionally, LA-ICP-MS studies of amphibole and phlogopite of dunite xenoliths and apatite-phenocrysts in tephriphonolitic lava were carried out in order to test if one of these mineral phases may have influenced the trace element signature of basaltic melts by assimilation.

Chapter 5: ***Geochronology***

Despite the enclosing and accurate age data of La Palma's extrusive and intrusive rocks there are still gaps in the existing geochronological data set. Lava flows erupted between the Cumbre Nueva collapse and the onset of volcanism at the Cumbre Vieja rift have not yet been dated. In order to address the question whether the apparent gap from 410 to 125 ka may correspond to a period of volcanic quiescence or merely reflects the fact that older rocks at the Cumbre Vieja are completely covered by younger lavas, samples from the Cumbre Nueva, Cumbre Vieja and the Bejenado volcano were dated and ages are presented in this chapter. Although rock samples were carefully prepared for the incremental $^{40}Ar/^{39}Ar$ dating method, only few samples reveal crystallization ages. These have been used to fill gaps in the existing data sets, e.g. to improve time resolution of critical segments in the stratigraphy.

References

Abdel-Monem, A., Watkins, N.D. and Gast, P.W., 1972. Potassium-argon ages, volcanic stratigraphy, and geomagnetic polarity history of the Canary Islands: Tenerife, La Palma and Hierro. American Journal of Science, 272: 805-825.

Ancochea, A. et al., 1994. Constructive and destructive episodes in the building of a young Oceanic Island, La Palma, Canary Islands, and genesis of the Caldera de Taburiente. Journal of Volcanology and Geothermal Research, 60: 243-262.

Anguita, F. and Hernán, F., 2000. The Canary Islands origin: a unifying model. Journal of Volcanology and Geothermal Research, 103: 1-26.

Arana, V., 1995. A field guide to the central volcanic complex of Tenerife. In: J. Marti and J. Mitjavila (Editors), Workshop on explosive eruptions in phonolitic magmas. IAVCEI Commision on Explosive Volcanism, Tenerife, pp. 3-17.

Canales, J.P. and Danobeitia, J.J., 1998. The Canary Island swell: a coherence analyses of bathymetry. Geophysical Journal International, 132: 479-488.

Caroff, M. Guillou, H., Lamiaux, M., Maury, R.C.,Guille, G., Cotten, J., 1999. Assimilation of ocean crust by hawaiitic and mugearitic magmas: an example from Eiao (Marquesas). Lithos, 46: 235-258.

Carracedo, J.C., 1994. The Canary Islands: an example of structural control on the growth of large ocean-island volcanoes. Journal of Volcanology and Geothermal Research, 60: 225-241.

Carracedo, J.C., 1999. Growth, structure, instability and collapse of Canarian volcanoes and comparisons with Hawaiian volcanoes. Journal of Volcanology and Geothermal Research, 94: 1-19.

Carracedo, J.C., Day, S.J., Guillou, H. and Gravestock, P., 1999. Later stages of volcanic evolution of La Palma, Canary Islands: Rift evolution, giant landslides, and the genesis of the Caldera de Taburiente. Geological Society of America Bulletin, 111(5): 755-768.

Carracedo, J.C., Badiola, E.R., Guillou, H., de La Nuez, J. and Pérez Torado, F.J., 2001. Geology and Volcanology of La Palma and El Hierro, Western Canaries. Estudios Geologicos, 57(5-6): 157-273.

Carracedo, J.C., Badiola, E.R. and Guillou, H., 2001b. Magna, Mapa Geológico De Espana (MAGNA) Sur De La Palma Hojas 1085 I-IV a 1087 I-II.

Clague, A.A., 1987. Hawaiian xenolith populations, magma supply rates, and development of magma chambers. Bulletin of Volcanology: 49: 577-587

Clague, A.A. and Dixon, J.E., 2000. Extrinsic controls on the evolution of Hawaiian ocean island volcanoes. Geochemistry Geophysics Geosystems, 1.

Class, C., Goldstein, S.L., Altherr, R. and Bachèlery, P., 1998. The process of plume-lithosphere interactions in the ocean basins - the case of Grande Comore. Journal of Petrology, 39(5): 881-903.

Day, S.J., Carracedo, J.C., Guillou, H. and Gravestock, P., 1999. Recent structural evolution of the Cumbre Vieja volcano, La Palma, Canary Islands: volcanic rift zone reconfiguration as a precursor to volcano flank instability? Journal of Volcanology and Geothermal Research, 94: 135-167.

Delaney, P.T., Fiske, R.S., Miklius, A., Okamura, A.T. and Sako, M.K., 1990. Deep magma body beneath the summit and rift zones of Kilauea Volcano, Hawaii. Science, 247: 1311-1316.

Dieterich, J.H., 1988. Growth and persistence of Hawaiian volcanic rift zones. Journal of Geophysical Research, 93(B5): 4258-4270.

Dzurisin, D., Koyanagi, R.Y. and English, T.T., 1984. Magma supply and storage at Kilauea volcano, Hawaii, 1956-1983. Journal of Volcanology and Geothermal Research, 21: 177-206.

Feigenson, M.D., Hofmann, A.W. and Spera, F.J., 1983. Case studies on the origin of basalts II. The transition from tholeiitic to alkalic volcanism on Kohala volcano, Hawaii. Contributions to Mineralogy and Petrology, 84: 390-405.

Fiske, R.S. and Jackson, E.D., 1972. Orientation and growth of Hawaiian volcanic rifts: the effect of regional structure and gravitational stresses. Proceedings of the Royal Society of London, A329: 299-326

Frey, F.A. et al., 1991. The evolution of Mauna Kea Volcano, Hawaii: petrogenesis of tholeiitic and alkalic basalts. Journal of Geophysical Research, 96 B: 14347-14375.

Garcia, M.O., Frey, F.A. and Grooms, D.G., 1986. Petrology of volcanic rocks from Kaula Island, Hawaii Implications for the origin of Hawaiian phonolites. Contibutions to mineralogy and petrology, 94: 461-471.

Garcia, M.O., Ho, R.A., Rhodes, J.M. and Wolfe, E.W., 1989. Petrologic constraints on rift-zone processes; results from episode 1 of the Puu Oo eruption of Kilauea Volcano, Hawaii. Bulletin of Volcanology, 52(2): 81-96.

Garcia, M.O., Hulsebosch, T.P. and M, R.J., 1995. Olivine-rich submarine basalts from the southwest rift zone of Mauna Loa volcano: implications for magmatic processes and geochemical evolution, Mauna Loa Revealed: Structure, Composition, History, and Hazards. Geophysical Monograph. American Geophysical Union, pp. 219-239.

Garcia, M.O., Rhodes, J.M., Trusdell, F.A. and Pietruszka, A.J., 1996. Petrology of lavas from the Puu Oo eruption of Kilauea Volcano: III. The Kupaianaha episode (1986-1992). Bulletin of Volcanology, 58: 359-379

Garcia, M.O., Ito, E., Eiler, J.M. and Pietruszka, A.J., 1998. Crustal contamination of Kilauea Volcano magmas revealed by oxygen isotope analyses of glass and olivine from Puu Oo eruption lavas. Journal of Petrology, 39(5): 803-817.

Gudmundsson, A., 1995. Infrastructure and mechanics of volcanic systems in Iceland. Journal of Volcanology and Geothermal Research, 64: 1-22.

Gudmundsson, A., 2000. Dynamics of volcanic systems in Iceland: Example of tectonism and volcanism at juxtaposed hot-spot and mid-ocean ridge systems. Annual Review of Earth and Planetary Science, 28: 107-140.

Guillou, H., Carracedo, J.C. and Day, S., 1998. Dating of the upper Pleistocene-Holocene activity of La Palma using the unspiked K-Ar technique. Journal of Volcanology and Geothermal Research, 86: 137-149.

Guillou, H., Carracedo, J.C. and Duncan, R., 2001. K-Ar, $^{40}Ar/^{39}Ar$ ages and magnetostratigraphy of Brunhes and Matuyama lava sequences from La Palma Island. Journal of Volcanology and Geothermal research, 86(1-4): 37-149.

Hansteen, T.H., Klügel, A. and Schmincke, H.U., 1998. Multi-stage magma ascent beneath the Canary Islands: evidence from fluid inclusions. Contributions to Mineralogy and Petrology, 132: 48-64.

Hardarson, B.S., Fitton, J.G., Ellam, R.M. and Pringle, M.S., 1997. Rift relocation; a geochemical and geochronological investigation of a palaeo-rift in Northwest Iceland. Earth and Planetary Science Letters, 153(3-4): 181-196.

Harris, C., Smith, H.S. and le Roex, A.P., 2000. Oxygen isotope composition of phenocrysts from Tristan da Cunha and Gough Island lavas: variation with fractional crystallization and evidence for assimilation. Contributions to Mineralogy and Petrology, 138: 164-175.

Hausen, H., 1969. Some contributions to the geology of La Palma. Comm. Phys. Math. Finn. Acad. Sci., 35: 1-140.

Hayes, D.E. and Rabinowitz, P.D., 1975. Mesozoic magnetic lineations and the magnetic quiet zone off northwest Africa. Earth and Planetary Science Letters, 28: 105-115.

Hoernle, K., Tilton, G. and Schmincke, H.U., 1993. Sr-Nd-Pb isotopic evolution of Gran Canaria: evidence for shallow enriched mantle beneath the Canary Islands. Earth and Planetary Science Letters. 106: 44-63

Hoernle, K.A., Zhang, Y.S. and Graham, D., 1995. Seismic and geochemical evidence for large-scale mantle upwelling beneath the eastern Atlantic and western and central Europe. Nature, 374: 34-39.

Hoernle, K., 1998. Trace element and Sr-Nd-Pb isotopic geochemistry of Jurassic ocean crust beneath Gran Canaria (Canary Islands): implications for the generation of OIB reservoirs and for crustal contamination of ascending OIB magmas. Journal of Petrology, 39(5): 859-880.

Hofmann, A.W., Feigenson, M.D. and Raczek, I., 1984. Case studies on the origin of basalt: III. Petrogenesis of the Mauna Ulu eruption, Kilauea, 1969-1971. Contributions to Mineralogy and Petrology, 88: 24-35.

Holik, J.S and Rabinowitz, P.D., 1991. ffects of Canary hotspot volcanism on structure of oceanic crust off Morocco. Journal of Geophysical Research. 96: 12039-12067

Klügel, A., 1997. Ascent rates of magmas and genesis, transport, and reactions of mantle and crustal xenoliths of the 1949 eruption on La Palma (Canary Islands). Ph.D. Thesis, Christian-Albrechts-Universität, Kiel.

Klügel, A., 1998. Reactions between mantle xenoliths and host magma beneath La Palma (Canary Islands): constraints on magma ascent rates and crustal reservoirs. Contributions to Mineralogy and Petrology, 131: 237-257.

Klügel, A., Hoernle, K.A., Schmincke, H.U. and White, J.D.L., 2000. The chemically zoned 1949 eruption on La Palma (Canary Islands): Petrologic evolution and magma supply dynamics of a rift-zone eruption. Journal of Geophysical Research, 105(B3): 5997-6016.

Masson, D.G., Watts, A.B., Gee, M.J.R., Urgeles, R., Mitchell, N.C., Le Bas, T. P. and Canals, M., 2002. Slope failures on the flanks of the western Canary Islands. Earth Science Review, 57: 1-35

Middlemost, E.A.K., 1972. Evolution of La Palma, Canary archipelago. Contributions to Mineralogy and Petrology, 36: 33-48.

Mitchell, N.C., Masson, D.G., Watts, A.B., Gee, M.J.R. and Urgeles, R., 2002. The morphology of the submarine flanks of volcanic ocean islands: A comparative study of the Canary and Hawaiian hotspot islands. Journal of Volcanolgy and Geothermal Research, 115: 83-107.

Morgan, W.J., 1983. Hotspot tracks and the early rifting of the Atlantic. Tectonophysics. 94: 123-139

Moore, J.G., Normark, W.R. and Holcomb, R.T., 1994. Giant Hawaiian landslides. Annual Reviews of Earth and Planetary Sciences, 122: 119-144.

Neumann, E.R., 1991. Ultramafic and mafic xenoliths from Hierro, Canary Islands: evidence for melt infiltration in the upper mantle. Contributions to Mineralogy and Petrology, 106: 236-252.

Neumann, E.R., Wulff-Pedersen, E., Johnsen, K., Andersen, T. and Krogh, E., 1995. Petrogenesis of spinel harzburgite and dunite suite xenoliths from Lanzarote, eastern Canary Islands: Implications for the upper mantle. Lithos, 35: 83-107.

Praegel, N.O., 1986. The petrology and geochemistry of Volcán Teneguía, La Palma, Canary Islands. Ph.D. Thesis, Univ. Copenhagen.

Putirka, K., 1997. Magma transport at Hawaii: Inferences based on igneous thermobarometry. Geology, 25(1): 69-72.

Roeser, H.A., 1982. Magnetic anomalies in the magnetic quiet zone off Morocco. In: U. Rad, K. Hinz, M. Sarnthein and E. Seibold (Editors), Geology of the northwest African continental margin. Springer, Berlin Heidelberg New York, pp. 61-68.

Ryan, M.P., 1988. The mechanics and three-dimensional internal structure of active magmatic systems: Kilauea volcano, Hawaii. Journal of Geophysical Research, 93(B5): 4213-4248.

Schmincke, H.U., 1976. Geology of the Canary Islands. In G. Kunkel (Editor), Biogeography and ecology of the Canary Islands. pp 67-184

Schmincke, H.U., 1982. Volcanic and chemical evolution of the Canary Islands. In U. von Rad, K. Hinz, M. Sarnthein and E. Seibold (Editors), Geology of the northwestern african continental margin, pp 3-20

Schmincke, H.U., Klügel, A., Hansteen, T.H., Hoernle, K. and Bogaard, P.v.d., 1998. Samples from the Jurassic ocean crust beneath Gran Canaria, La Palma and Lanzarote (Canary Islands). Earth and Planetary Science Letters, 163: 343-360.

Schmincke, H.U. and Sumita, M., 1998. Volcanic evolution of Gran Canaria reconstructed from apron sediments. Synthesis VICAP drilling project (ODP Leg 157), Proc. ODP, Sci. Results Leg 157. College Station, TX (Ocean Drilling Program).

Schwarz, S., Klügel, A. and Wohlgemuth-Ueberwasser, C., 2004. Melt extraction pathways and stagnation depths beneath the Madeira And Desertas rift zone (NE Atlantik) inferred from barometric studies. Contributions to Mineralogy and Petrology, 147: 228-240.

Simonsen, S.L., Neumann, E.-R. and Seim, K., 2000. Sr-Nd-Pb isotope and trace-element geochemistry evidence for a young HIMU source and assimilation at Tenerife (Canary Islands). Journal of Volcanology and Geothermal Research, 103: 299-312.

Sleep, N.H., 1990. Hotspots and mantle plumes: some phenomenology. Journal of Geophysical Research, 95(B5): 6715-6736.

Staudigel, H. and Schmincke, H.U., 1984. The Pliocene seamount series of La Palma / Canary Islands. Journal of Geophysical Research, 89(13): 11195-11215.

Staudigel, H., Feraud, G. and Giannerini, G, 1986. The history of intrusive activity on the Island of La Palma (Canary Islands). Journal of Volcanology and Geothermal Research, 27: 299-322

Tilling, R.I. and Dvorak, J.J., 1993. Anatomy of a basaltic volcano. Nature, 363: 125-133.
Triepold, S., 2003. Feldspar zonation, magma chamber dynamics and evolution of the Teide - Pico Viejo magmatic system (Tenerife). Diploma Thesis. Georg-August-Universität zu Göttingen
Verhoef, J., Collette, B.J., Dañobeitia, J.J., Roeser, H.A. and Roest, W.R., 1991. Magnetic anomalies off West-Africa (20-38° N). Mar Geophys Res, 13: 81-103.
Walker, G.P.L., 1987. The dike complex of Koolau volcano, Oahu: Internal structure of a Hawaiian rift zone. In: R.W. Decker, T.W. Wright and P.H. Stauffer (Editors), Volcanism in Hawaii. US Geol Surv Prof Paper 1350, pp. 961-993.
Walker, G.P.L., 1999. Volcanic rift zones and their intrusion swarms. Journal of Volcanology and Geothermal Research, 94: 21-34.
Walter, T.R. and Troll, V.R., 2003. Experiments on rift zone evolution in unstable volcanic edifices. Journal of Volcanology and Geothermal Research, 127: 107-120.
Watts, A.B., 1994. Crustal structure, gravity anomalies and flexure of the lithosphere in the vicinity of the Canary Islands. Geophysical Journal International, 119: 648-666.
Wolfe, E.W. et al., 1987. The Puu Oo eruption of Kilauea Volcano, episodes 1-20, January 3, 1983, to June 8, 1984. In: R.W. Decker, T.W. Wright and P.H. Stauffer (Editors), Volcanism in Hawaii. US Geol Surv Prof Paper 1350, pp. 471-508.
Wright, T.L. and Fiske, R.S., 1971. Origin of the differentiated and hybrid lavas of Kilauea volcano, Hawaii. Journal of Petrology, 12: 1-65.
Yang, H.-J., Frey, F.A., Clague, D.A. and Garcia, M.O., 1999. Mineral chemistry of submarine lavas from Hilo Ridge, Hawaii: implications for magmatic processes within Hawaiian rift zones. Contribution to Mineralogy and Petrology, 135: 355-372.

2. Magma storage and underplating beneath Cumbre Vieja volcano (separate Paper)

This chapter consists of an individual paper which has been submitted to “Earth and Planetary Science Letters” on July 15, 2004. The complete data not shown in this chapter are shown in the Appendix of this thesis.

Appendix A 2.1: Compositions of glasses analyzed for thermobarometry; Table 2 of the Background Dataset
Appendix A 2.2: Clinopyroxene compositions and calculated temperatures and pressures; Table 3 of the Background Dataset

Magma storage and underplating beneath Cumbre Vieja volcano, La Palma (Canary Islands)

Andreas Klügel[a,*], Thor H. Hansteen[b], Karsten Galipp[a]

Earth and Planetary Science Letters, Revised manuscript, 18 February 2005

[a] Universität Bremen, Fachbereich Geowissenschaften
Postfach 330440, D-28334 Bremen, Germany
Fax: +49-421-218-9460, e-mail: akluegel@uni-bremen.de

[b] IFM-GEOMAR, Leibniz-Institut für Meereswissenschaften
Wischhofstr. 1-3, D-24148 Kiel, Germany
Fax: +49-431-600-2924, e-mail: thansteen@ifm-geomar.de

[*] Corresponding author: Andreas Klügel (akluegel@uni-bremen.de)

Abstract

We have conducted a barometric study of basaltic lavas and mafic to ultramafic xenoliths from Cumbre Vieja volcano (La Palma) in order to reconstruct magma storage, plumbing and related intrusive island growth. The samples were collected both along the volcano's rift zone and from its subaerial and submarine flanks up to 30 km off the rift axis. Clinopyroxene-melt barometry of lavas yields a well-defined pressure range of 410-770 MPa (average 600 MPa) and shows no systematic variation with sample locality. This pressure range reflects a major fractionation level at ca. 15-26 km depth, within the uppermost mantle, where phenocrysts and melt last equilibrated. In contrast, microthermometry of CO_2-dominated fluid inclusions in phenocrysts and xenoliths gives pressure estimates of 240 to 470 MPa (average 330 MPa), within the lower oceanic crust. These pressures are interpreted to reflect an underplating zone at 7-14 km depth where ascending magmas become ponded prior to eruption and where passing magmas temporarily stagnate during eruption. The underplating zone is inferred to extend to a radius of ca. 30 km at least, and its depth appears to increase slightly with distance to the rift axis. Our data thus show a remarkable pressure bimodality for long-term and short-term storage of magma that appears to be characteristic for Cumbre Vieja. By using a simple model based on the cumulative volume of material added to the crust, we have estimated uplift rates of >0.5 m/ka due to underplating that occurs on the island scale. On a time-scale of some 10 ka, these uplift rates are of similar magnitude as global changes in sea-level. A second, more local mode of uplift and related faulting is caused by shallow intrusions into the volcanic edifice as is indicated by the highly irregular morphology of the Cumbre Vieja. We stress that intrusion-related uplift should be qualitatively considered when reconstructing the evolution of oceanic island volcanoes. Since most of the underplated material is inferred to consist of cumulate rocks being intimately mixed and juxtaposed with the lower oceanic crust and having similar densities, it is probably impossible to detect such an underplating zone seismically.

Keywords: La Palma; underplating; barometry; fluid inclusions; magma chambers

1. Introduction

Only a small fraction of magmas generated in Earth's mantle ever reaches the surface. When magma ascends through the lithosphere, it cools and may freeze if ascent rate or flow rate are not sufficiently high. After segregation from the melting region where porous flow along a melt network dominates, rapid and effective magma transport can occur along buoyancy-driven vertical hydrofractures (dikes) once a critical overpressure threshold has been reached [1]. Although this mode of dike propagation is self-propelling, magma ascent may cease temporarily or permanently at a level of neutral buoyancy (LNB) where magma density equals that of the host rock and buoyancy becomes zero [2, 3]. Near the LNB, dikes tend to accumulate and to spread laterally as dikes or sills [2]. Depending on the rate of magma supply and the rate of subsequently intruding dikes, these lateral intrusions may either solidify or may combine and ultimately result in the formation of magma chambers [4]. Once formed, a magma chamber or crystal mush zone provides an efficient magma trap to brake ascending dikes. Beneath continental areas, likely horizons to trap basaltic magmas are located near the Moho or within the crust. The accumulation of magma at the base of the crust is known as underplating and is a quantitatively important mechanism of crustal growth and evolution [5, 6].

For oceanic intraplate volcanoes, there is probably no LNB within the lower crust because the basaltic and gabbroic rocks are denser than basaltic magma. It could rather be located in the uppermost crust within sedimentary layers or within the volcanic edifices themselves. This is best exemplified at Kilauea volcano, Hawaii, where a LNB is inferred at 2 to 4 km beneath the surface as expressed by the depth of the shallow summit reservoir and the pathways of laterally propagating dikes at Kilauea's rift zones [3]. At most oceanic volcanoes, however, the relevance of a LNB is less clear and ascending magmas may become trapped for other reasons.

There is geological and geophysical evidence that magmatic underplating *sensu lato* is not restricted to continental regions but is also highly relevant in the evolution of oceanic intraplate volcanoes [7]. For example, the exposure of deep-water eruptive rocks and more than 1800 m of sills at the seamount complex of La Palma indicates a minimum uplift of 2200 m by intrusions during seamount building [8, 9]. Intrusive processes are the most plausible explanation for uplift on the kilometer-scale of sediments, lavas or gabbros from the oceanic crust now exposed at e.g. Fuerteventura (Canary Islands), Maio and Sáo Tiago (Cape Verde Islands) [10-12]. Petrological investigations suggest stagnation and ponding of ascending magmas at mantle and crustal depths [4, 13-17]. Seismic studies provide evidence for underplated bodies beneath the Hawaiian Islands [18, 19], the Marquesas Islands [20], La Réunion [21] and the Ninetyeast Ridge [22]. For the Canary Islands, the existence of

underplated material is strongly suggested by some geophysical data [14, 23, 24] although evidence for significant underplating is controversial [25]. Last but not least, the best petrological evidence for the significance of magma intrusion and accumulation beneath many volcanic islands is the ubiquitous occurrence of cumulate xenoliths and phenocryst-rich lavas [16, 26-32].

In this study, we investigate the depths at which ascending magmas stagnate and pond beneath the active Cumbre Vieja volcano on La Palma. We present new barometric data for xenoliths and lavas from the volcano's subaerial ridge and submarine flanks. After addressing the question of where, how and how much igneous material is stored beneath the volcano, we discuss the implications for the island's subaerial evolution and inferred uplift that may have affected flank stability.

2. Geological background

The Canary Islands form a chain of seven volcanic islands located off the northwestern African continental shelf (Fig. 1). All islands are underlain by Jurassic oceanic crust as indicated by mid-ocean ridge basalt (MORB) gabbro xenoliths occurring on Lanzarote, Gran Canaria, and La Palma [33, 34]. The age of the crust is bracketed by paleomagnetic anomalies S1 (175 Ma), between the easternmost islands and the African coast, and M25 (155 Ma) between La Palma and Hierro, which are the westernmost and youngest islands [35, 36]. An age progression of the islands' shield phases from west to east suggests that the archipelago formed by slow movement of the African plate over a hotspot [37-39].

The geology of La Palma is extensively described in [38] and references therein. Briefly summarized, the island consists of three main units: (1) the basal complex (3-4 Ma) which comprises a Pliocene seamount sequence and a plutonic complex that have been uplifted and tilted to their present position; (2) the older volcanic series (1.7 Ma to 410 ka) which includes the Taburiente shield volcano and the Bejenado edifice; and (3) the Cumbre Vieja series (>125 ka to present) which is confined to the southern half of the island (Fig. 1). Cumbre Vieja has been the most active volcano of the Canary Islands in historic times with eruptions recorded in the 15th century, 1585, 1646, 1677, 1712, 1949 and 1971. The north-south trending Cumbre Vieja ridge represents a volcanic rift zone with alignment of vents, fissures and faults along its crest [40, 41]. It consists dominantly of mafic lava flows, cinder cones and scattered phonolitic plugs. Lava compositions range from basanite to phonolite with titaniferous clinopyroxene, olivine and kaersutite as the major phenocryst phases in the mafic rocks. Most historic eruptions were chemically and mineralogically zoned, and xenoliths are ubiquitous in the final eruptive phase [27, 42, 43]. Xenolith types include

ultramafic cumulates (the most common type), MORB gabbros from the Jurassic ocean crust, alkalic gabbros, peridotites and various felsic fragments; particularly noteworthy is the occurrence of composite xenoliths (Fig. 2).

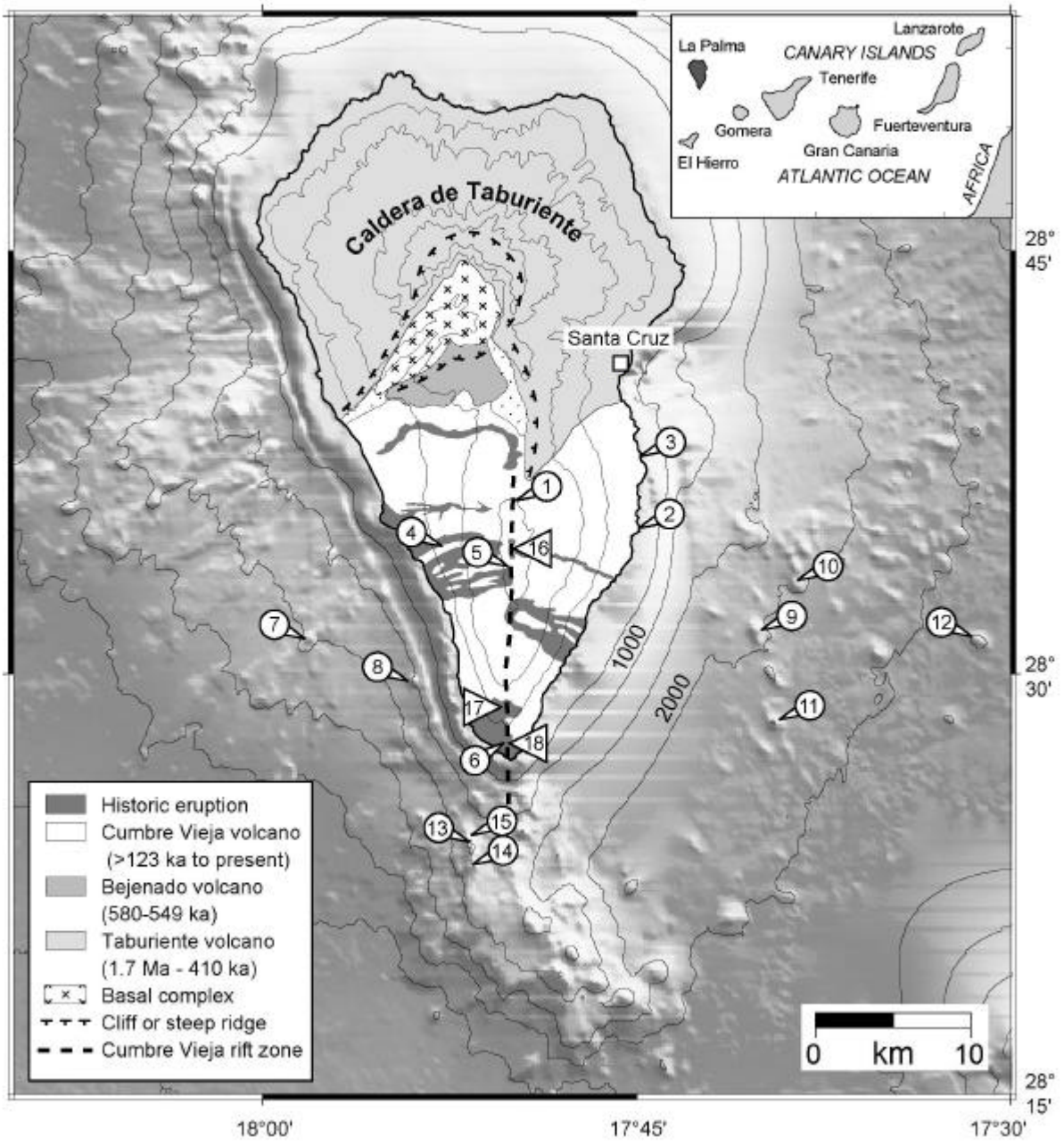

Fig. 1 Simplified geological map of La Palma, modified after [38, 61]. The detailed bathymetry is based on [74]. *Circles with arrows*: sample localities of this study; *triangles*: sample localities of published barometric data from the Cumbre Vieja [14, 47, 48, 56].

3. Samples and analytical methods

Representative samples from various Cumbre Vieja localities were selected for thermobarometric investigations. The samples include MORB gabbro xenoliths, ultramafic cumulate xenoliths, peridotite xenoliths and porphyric alkalic lavas (Table 1). Whereas the

ultramafic cumulates are cogenetic to Recent La Palma lavas, the MORB gabbros represent fragments of the Jurassic oceanic crust beneath La Palma as indicated by their mineralogical and chemical composition [27, 31, 34]. The sampling objective was to probe the ridge crest (three localities) as well as the subaerial flanks (three localities) and the submarine ridge and flanks (nine localities) (Fig. 1). The submarine samples were dredged during RV "Meteor" cruise M43/1 in 1998 [44] and RV "Poseidon" cruise POS270 in 2001. Each dredge haul sampled the flank of a single volcanic cone. The depths of the submarine samples range between 900 and 2600 m with the most distal sample being located 30 km off the Cumbre Vieja ridge axis.

Table 1: Sample localities and compositions

Sample	Loc#	Locality	Sample type	Method
HAT5-13-9-97	1	Pico Birigoyo, 1800 m asl	Cpx-kaersutitite xenolith	FI
HAT1-13-9-97	1	Pico Birigoyo, 1800 m asl	MORB gabbro xenolith	FI
HAT1-18-9-97	2	Mña. Goteras, 100 m asl	Cpx-kaersutitite xenolith	FI
HAT3-18-9-97	2	Mña. Goteras, 100 m asl	MORB gabbro xenolith	FI
HUS29192-4	3	Airport lava flow, 20 m asl	Amph-Ol-pyroxenite xenolith	FI
HUS29192-5	3	Airport lava flow, 20 m asl	MORB gabbro xenolith	FI
KLA1620	4	Volcán Jedey (1585 eruption), 760 m asl	Glassy basanite lapilli	CPM
KLA1653	5	Mña. Negra (1712 eruption), 1750 m asl	Glassy basanite lapilli	CPM
KLA1690	6	Teneguía (1971 eruption), 370 m asl	Glassy basanite lapilli	CPM
POS_155-1	7	submarine cone, 1470-1500 m bsl	Basanite lava	CPM
POS_164-7	8	submarine cone, 840-1200 m bsl	Tephrite lava	CPM
POS_165-3	9	submarine cone, 1550-1930 m bsl	Basanite lava	CPM
POS_166-3	10	submarine cone, 1640-2020 m bsl	Dunite xenolith fragments	FI
POS_169-1-9	11	submarine cone, 2200-2250 m bsl	Basanite lava	CPM
POS_170-1	12	submarine cone, 2500-2580 m bsl	Basanite lava	FI
POS_170-2	12	submarine cone, 2500-2580 m bsl	Basanite lava	CPM
M43_639-1	13	submarine cone, 870-1090 m bsl	Basanite lava	CPM
M43_658-2	14	submarine cone, 1110-1250 m bsl	Basanite lava	CPM
M43_660-2	15	submarine cone, 920-970 m bsl	Basanite lava	CPM
(earlier study)	16	Mña. Duraznero (1949 eruption), 1800 m asl	Basanite, various xenoliths	FI, CPM
(earlier study)	17	Volcán San Antonio, 610 m asl	Basanite, peridotite xenoliths	FI, CPM
(earlier study)	18	Teneguia (1971 eruption), 370 m asl	Peridotite xenoliths	FI

Loc#: locality number referring to symbols in Fig. 1.
asl: above sea level, bsl: below sea level.
FI: Fluid inclusion microthermometry, CPM: Clinopyroxene-melt thermobarometry

Geobarometric data were obtained by (1) thermobarometry of basalts using microprobe analyses of matrix glass and the rims of coexisting clinopyroxene phenocrysts, and (2) microthermometry of CO_2-rich fluid inclusions occurring in xenoliths and phenocrysts. These methods are inherently different: whereas the chemical thermobarometer is based on clinopyroxene-melt equilibria [45], fluid inclusions record the pressure of entrapment or re-equilibration through their density. Since there is petrographic evidence for magma mixing, no clinopyroxene core/whole rock pairs were used for thermobarometry. A description of the methods and the petrography of the samples are given in Appendix A and B, respectively.

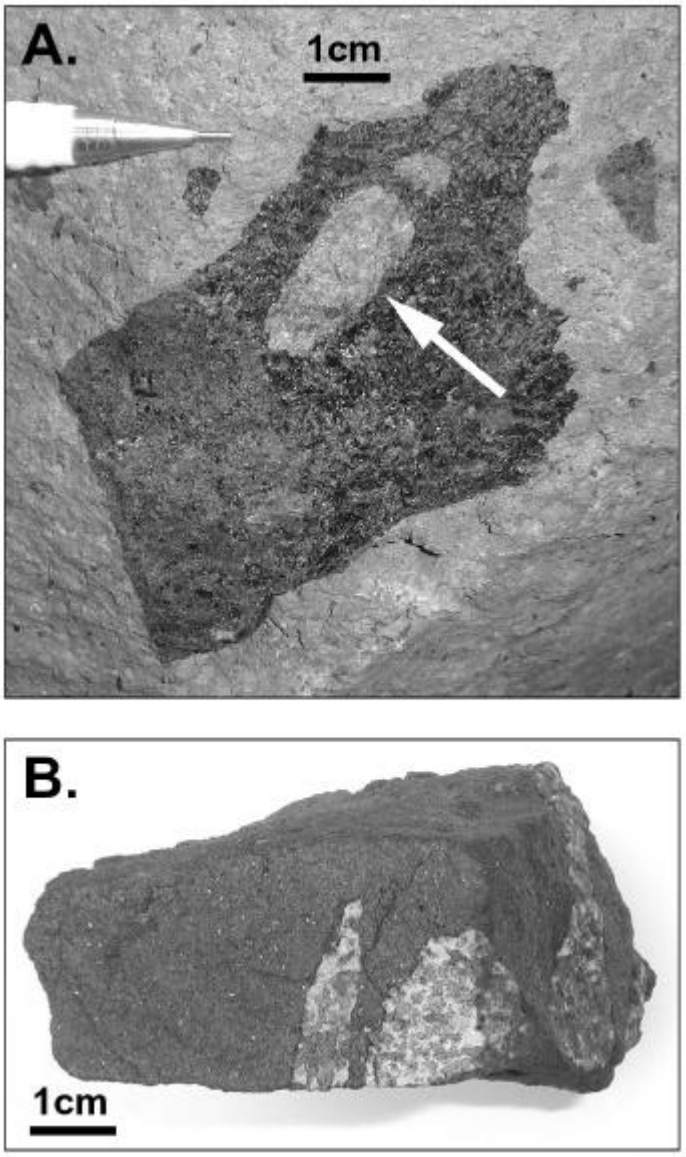

Fig. 2: A. Composite xenolith with peridotite fragment (*arrow*) embedded in ultramafic amphibole-rich cumulate. **B.** Composite xenolith with MORB gabbro fragments from the Jurassic oceanic crust and ultramafic amphibole-rich cumulate.

4. Results

4.1. Clinopyroxene-melt thermobarometry

Pressure (P) and temperature (T) of last equilibration between melt and the rims of euhedral clinopyroxene phenocrysts were calculated using the formulation of Putirka et al. [45]; the results are presented in Fig. 3 and in Tables 2 and 3 of the Background Dataset in Appendix C. As an independent consistency check, we compared the magnesium numbers (mg#) of clinopyroxene rims and melt and found that all were near chemical equilibrium [46]. Calculated pressures range from 410 to 770 MPa and approximate a Gaussian distribution with an average of 600 MPa and ? = 87 MPa, where individual samples show variations between 40 and 250 MPa. Corresponding temperatures range from 1100 to 1160 °C.

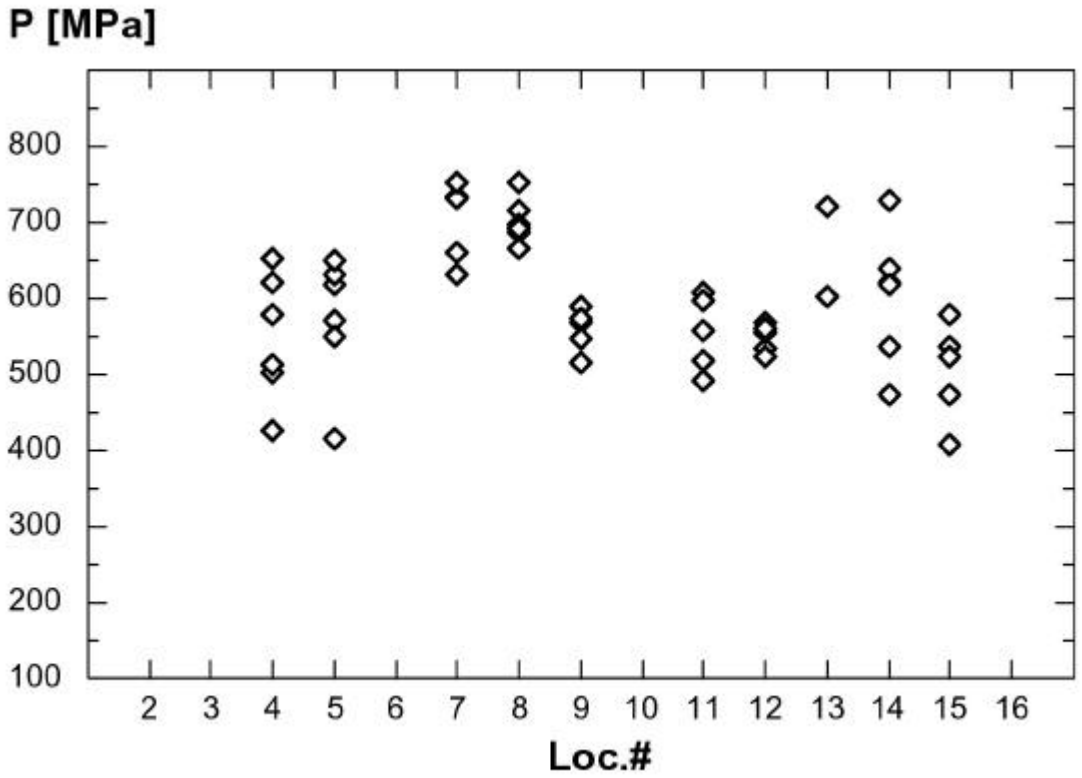

Fig. 3: Calculated pressures for subaerial and submarine samples from the Cumbre Vieja ridge based on clinopyroxene-melt equilibrium. Each data point represents a single clinopyroxene phenocryst. The locality number (Loc.#) refers to the sample localities indicated in Fig. 1 and Table 1.

Possible sources of error in the pressure determinations are the calibration of the thermobarometer and analytical errors. The barometer has a mean prediction uncertainty of ±140 MPa and apparently no systematic error [45]. The effect of analytical errors was assessed by using the standard deviations of the analyzed glasses and of augite standards analyzed along with the samples. An uncertainty of 1s for any of the measured elements results in a pressure uncertainty of 0 to 20 MPa (relative error is <5 % at 410 MPa and <3 % at 770 MPa); this leverage is largest for Mg and Na in glass and clinopyroxene analyses, respectively. We have also generated test data where an analytical uncertainty of max. ±3? was randomly imposed on all elements of a single glass or clinopyroxene analysis. Each data set yielded a symmetrical distribution of calculated pressures around the actual value; for example, a pressure of 620 MPa converted into 620 ± 40 MPa (±2s). Thus, errors in calculated pressures owing to analytical uncertainties are 1) smaller than the prediction error of the barometer, 2) smaller than the spread of our data, and 3) not systematically biased. We conclude, therefore, that our data shown in Fig. 3 reflect realistic pressures and note that the data spread partly reflects variable clinopyroxene compositions due to strong zonations near their rims.

The calculated pressures overlap well with published data for lavas from the summit and the southern end of the subaerial Cumbre Vieja ridge [47, 48]. Despite considerable

variations in pressures obtained for the different localities, Fig. 3 shows no systematic differences between the ridge crest and the distal submarine flanks. As the Moho beneath La Palma is probably located at 14-15 km depth corresponding to about 450 MPa [49], all but a few samples indicate final equilibration between melt and clinopyroxene phenocrysts within the uppermost mantle.

4.2. Microthermometry of fluid inclusions

Composition of fluid phases

All fluid inclusions froze to aggregates of solid CO_2 and vapour when cooled to -65 to -100 °C and produced no further visible phase changes during further cooling. Upon heating of the inclusions from about -190 °C, the following three phase transitions were observed: 1) initial melting (T_i) of CO_2 crystals between -57.6 and -56.3 °C, in most cases coinciding with 2) final melting of CO_2 (T_m) at -57.6 to -56.3 °C (CO_2 triple point at -56.6 °C), and 3) final homogenization into liquid (Th_l) at less than 31.1 °C. In most inclusions, fluid components other than CO_2 thus probably occur in amounts <1 mol% [50]. An exception is sample POS_170-1 where many inclusions showed a melting interval (T_m-T_i) of up to 2.1 °C and/or a depression of T_m down to -58.7 °C, which may reflect the presence of a few mol% of N_2, CH_4 or SO_2. Since small amounts of these components do not significantly affect the interpretation of entrapment conditions [50, 51], we have filtered out those inclusions with T_m < -57.5 °C (equivalent to about 5 mol% of N_2 or CH_4 [50]) and included the remaining data in the further evaluation. No inclusion studied gave evidence for the presence of H_2O although expected as a component in fluids exsolved from mafic melts. This "missing H_2O" indicates either diffusive hydrogen loss at high temperatures [52] or hydration reactions between fluid and host mineral [51, 53].

Homogenization temperatures and inclusion densities

In all xenolith samples, both texturally early and texturally late fluid inclusions show similar and well-defined ranges of homogenization temperatures. Most inclusions homogenized into the liquid phase between 26.1 and 31.0 °C corresponding to densities of 0.53 to 0.70 g cm^{-3} if a composition of pure CO_2 is assumed (Fig. 4). It is noteworthy that the data for MORB gabbro and ultramafic cumulate xenoliths overlap largely to completely. They also correspond strikingly well to those for peridotite, MORB gabbro and ultramafic cumulate xenoliths and phenocrysts from other subaerial Cumbre Vieja lavas [14, 54] (Fig. 4). By comparison, fluid inclusions in phenocrysts and xenoliths from submarine samples show only partial overlap with these data having a tendency to slightly lower homogenization temperatures (19.3 to 29.9 °C) and higher densities (0.59 to 0.78 g cm^{-3}).

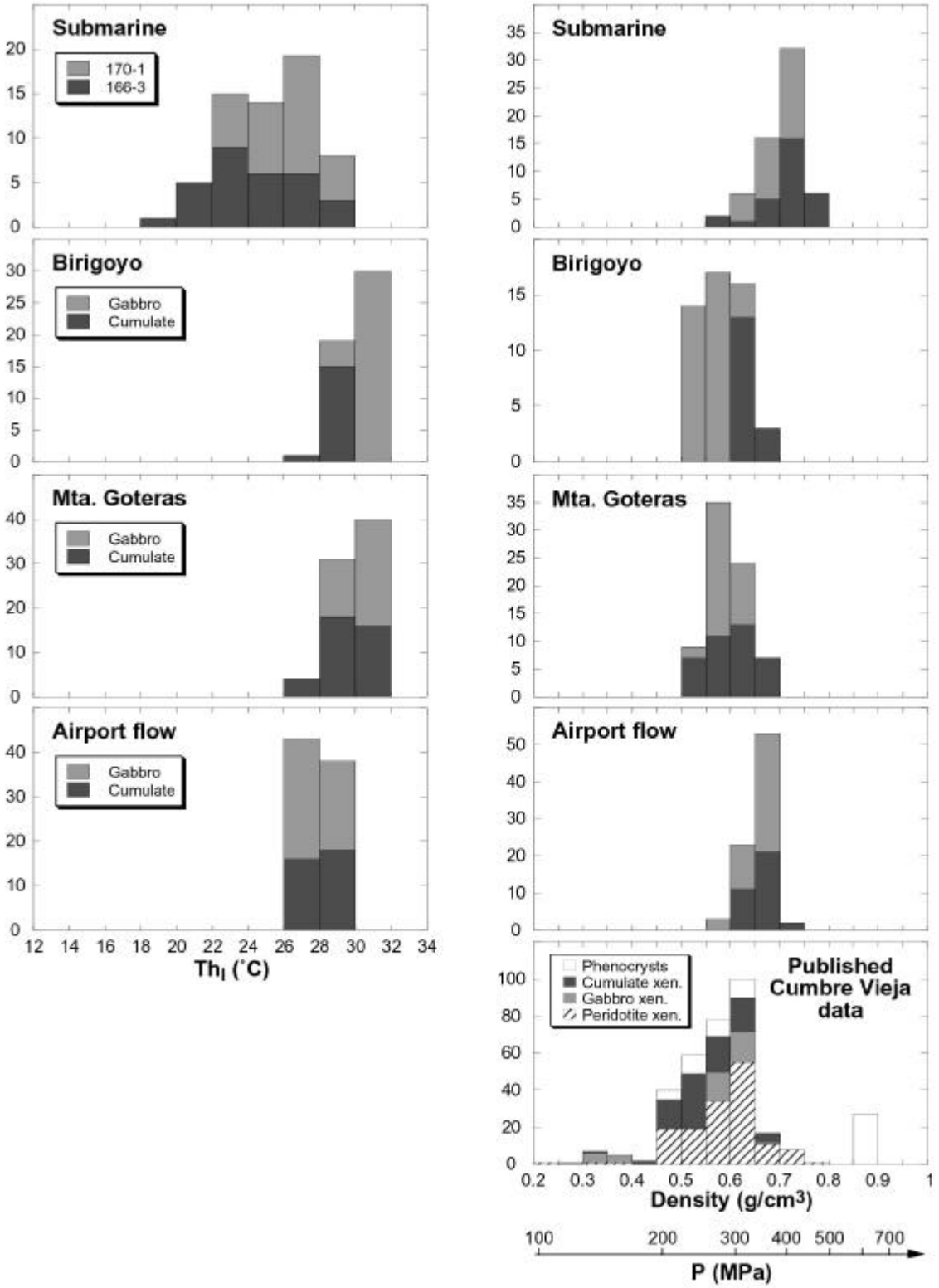

Fig. 4: Measured homogenisation temperatures (*left*) and calculated densities (*right*) of fluid inclusions in xenoliths and phenocrysts. All inclusions homogenized into the liquid phase. Densities were calculated after [75] assuming pure CO_2 composition, the pressure scale is based on a model temperature of 1150 °C. The new density data overlap well with published data for fluid inclusions in phenocrysts and xenoliths from the Cumbre Vieja [14, 54].

Pressure calculations

Pressures of formation or last re-equilibration of fluid inclusions were calculated from their densities using isochores for pure CO_2 [55]. A model temperature of 1150 °C was used according to the results of clinopyroxene-melt thermobarometry. Pressures range from 240 to 470 MPa (average 330 MPa) and show almost no overlap with those obtained by clinopyroxene-melt barometry. If the model temperature were higher by 50 °C, calculated pressures would increase only slightly to 250-490 MPa, respectively. The calculated pressures clearly represent *minimum* pressures of inclusion formation or re-equilibration since post-entrapment processes such as decrepitation or diffusion during magma ascent result in lower densities. If the entrained CO_2-dominated fluid has lost its former H_2O content (<10 mol% as an upper limit for fluids coexisting with basanitic melts at 1 GPa [56]) then the inclusion density after entrapment is reduced by <4.5% [57]. By using the isochores for the CO_2-H_2O system with X_{H2O} = 0.1 [55], the density range of 0.53 to 0.78 g cm^{-3} of this study would yield a corrected pressure range of 250-530 MPa, i.e. the pressures would increase by 10-60 MPa (4-13 %) which we consider as an upper limit of systematic error.

5. Discussion

5.1. Bimodality of calculated pressures

Probably the most striking feature of our data is the bimodality of pressure ranges indicated by clinopyroxene-melt barometry and fluid inclusions. This difference becomes even more evident when the data from this study and published data from the Cumbre Vieja are combined. The main peak of the fluid inclusion data shows an almost perfect Gaussian distribution with an average of 300 MPa and 95% of the data (average ± 2?) falling between 180 and 420 MPa. In contrast, the combined clinopyroxene-melt data indicate rather higher pressures with a 95% interval of 430-780 MPa and an average of 625 MPa (Fig. 5). Both data sets show a well-defined pressure range and only minor overlap, except for the subordinate maximum between 590 and 630 MPa indicated by fluid inclusions, which coincides with the average of the clinopyroxene-melt data. Although such bimodal pressure distribution could principally reflect a systematic error or "bias" between the two different methods rather than distinct pressure ranges, we consider the bimodality as realistic for the following reasons: (1) The potential systematic error for the fluid inclusion data is comparatively small. Even combining the corrections discussed above (model temperature too low by 50 °C and loss of 10 mol% of former H_2O), a rather extreme case, would increase the main pressure range to mere 260-550 MPa and would still yield a bimodal data set. (2) As discussed above, the cpx-melt thermobarometer contains no systematic error. (3) The Gaussian distribution of each data set indicates a combination of random variables rather

than sytematic bias. (4) The overlap of the two data sets around 600 MPa indicates that there is little systematic error between both barometric methods. In addition, it has been demonstrated that both methods can essentially yield overlapping data sets [13, 17].

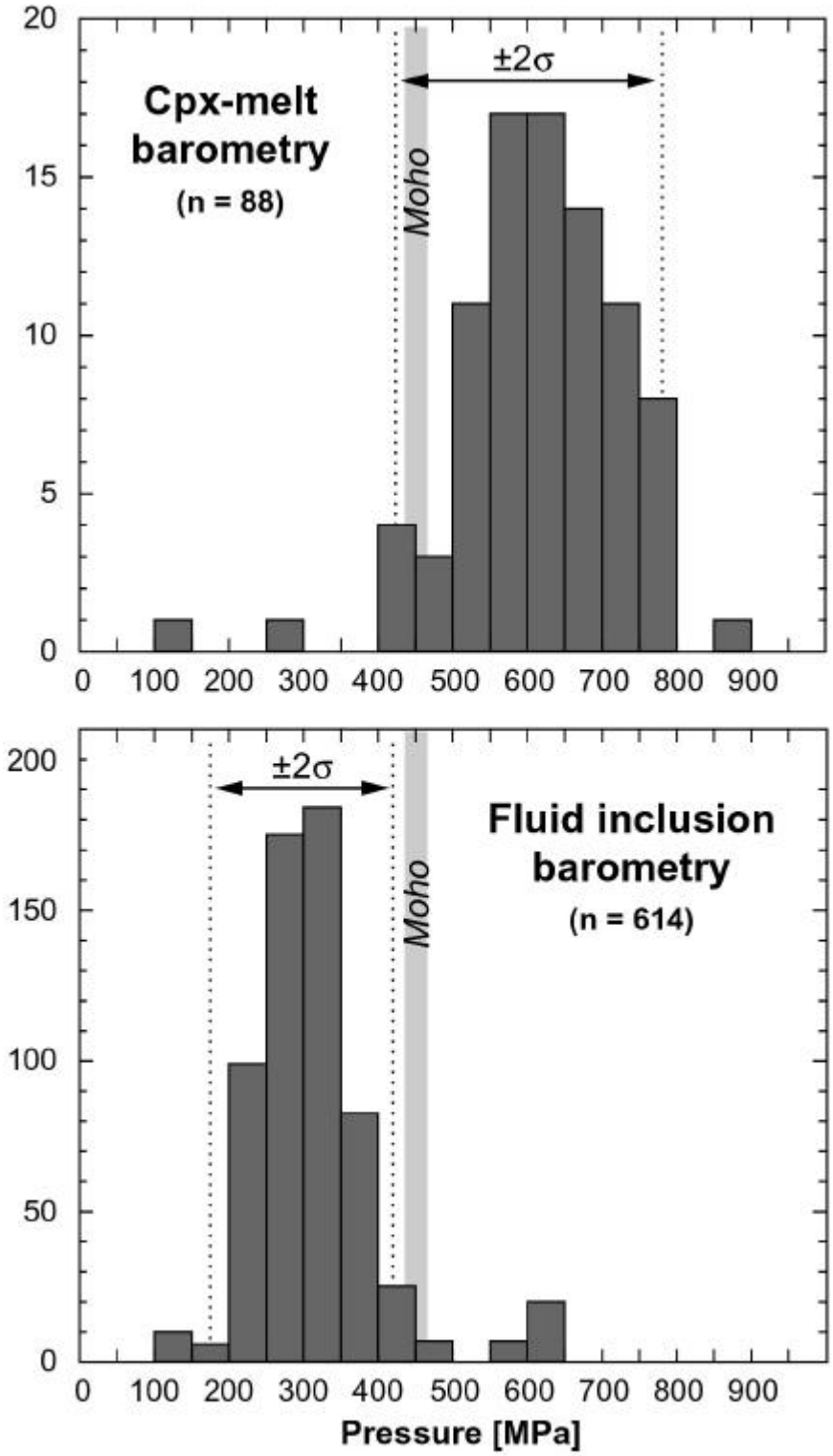

Fig. 5: Calculated pressures for subaerial and submarine samples from the Cumbre Vieja volcano as indicated by clinopyroxene-melt thermobarometry and fluid inclusion microthermometry. This compilation includes data from the present study and from [14, 47, 48, 54], n is total number of data. The intervals comprising 95% of the data (average ± 2 sigma) are indicated.

The general tendency for fluid inclusions to yield lower pressures than mineral-melt equilibria is in accordance with previous studies at different localities [13, 14, 17] but appears to be most pronounced at La Palma. This tendency is best explained by resetting of partially decrepitated inclusions during temporary stagnation of the ascending magma at shallower depths, which was too short to be reflected in the sluggish mineral-melt barometer. Re-equilibration of fluid inclusions can proceed within hours to days [58], whereas growth of a 5-10 µm wide clinopyroxene rim at equilibrium conditions, or diffusive re-equilibration along 5-10 µm width (the typical distance of our microprobe spots to the rim), needs months to years [15, 59].

5.2. Depths of magma fractionation

We interpret the range of 430-780 MPa (ca. 15-26 km depth) to reflect levels of major clinopyroxene (±olivine) crystallization within the uppermost mantle. There is also evidence for prior fractionation at deeper levels since the cores of some clinopyroxene phenocrysts indicate pressures of 800-1100 MPa [48]. The combined data indicate polybaric crystal fractionation with final equilibration between clinopyroxene and host melt occurring at 430-780 MPa. We note that the inferred fractionation depths are in accordance with clinopyroxene preceding plagioclase as the fractionating phase and with the paucity of plagioclase phenocrysts in Cumbre Vieja basalts.

Our data do not indicate any dependence of fractionation pressures on sample locality such as altitude or distance from the rift axis (Fig. 3). Some samples yield a considerable range of pressures, and calculated pressures vary strongly between different eruptions or localities. We thus propose that each eruption of the Cumbre Vieja is fed by relatively small ephemeral magma reservoirs in the uppermost mantle rather than by a single large magma chamber. This scenario is supported by 1) the rather limited volume of individual eruptions (ca. 0.01-0.03 km^3 as based on the time between historic eruptions and the long-term eruptive rate [60]); 2) the strong mineralogical and chemical zonation of many eruptions [42]; 3) the sudden change in composition during single eruptions precluding a large homogenizing reservoir; and 4) the petrologic indicators of magma mixing such as strongly zoned green-core clinopyroxenes in most samples studied [27, 48]. We visualize the magma chambers beneath the Cumbre Vieja as a plexus of interconnected dikes and magma pockets from which magma is periodically expelled and which crystallize completely or partly between eruptions (Fig. 6). The small reservoir size facilitates cooling and crystal fractionation which might explain why most basanites contain <9 wt% MgO [38, 42]. The proposed concept shows some resemblance to a magma mush column [61] but the depth interval of magma storage beneath Cumbre Vieja appears to be more confined. The discrete pressure distributions are similar to results e.g. from the Madeira and Aeolian islands [17, 62]

but contrast with findings at other localities where calculated depths are a continuum from the mantle to near the surface (e.g. [15, 63]).

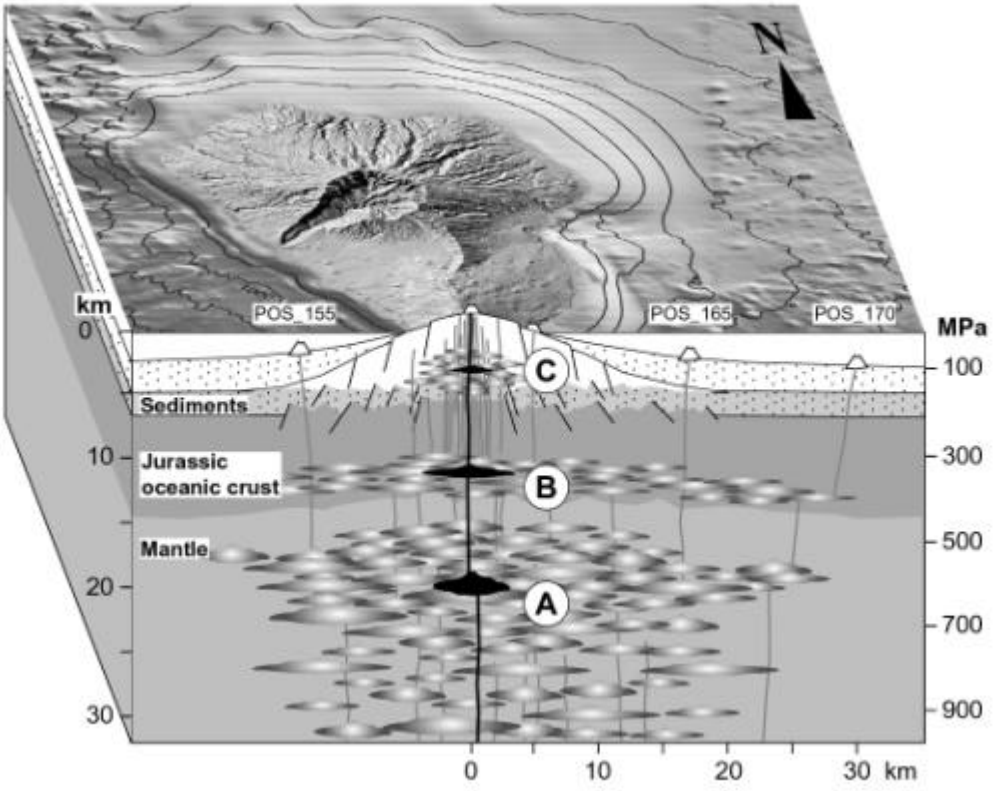

Fig. 6: Model of magma storage and fractionation beneath Cumbre Vieja volcano (no vertical exaggeration). The magma storage systems in the uppermost mantle and lower crust are visualized as a plexus of interconnected magma pockets and sills/dikes. They are illustrated by an arbitrary number of blobs, where the active part of the storage system during a single eruption is shown in *black* and the older, partially or completely crystallized parts in *gray gradients*. The igneous activity causes uplift of the volcano and underlying crust as is indicated by fault lines. Major storage levels are indicated: (A) major crystal fractionation level, (B) short-time stagnation / underplating, (C) shallow intrusive core complex as indicated by fluid inclusions in a few samples [14]. Some localities of submarine samples are marked.

5.3. Depths of temporary magma stagnation

The pressure range of 180-420 MPa (ca. 7-14 km depth) indicated by fluid inclusions coincides with the lower crust beneath the Cumbre Vieja and is interpreted as a major stagnation level for ascending magmas. Remarkably, this well-defined horizon is indicated by fluid inclusions in phenocrysts as well as in almost all xenoliths we have studied (Fig. 4). We suggest that the lower crust comprises cumulate rocks and sill-like pockets of crystal-rich mush that may solidify between successive magma batches (Fig. 6). These "sub-reservoirs" become filled prior to eruption but are not a locus of major crystal fractionation. They are also inferred to act as a "sediment trap" for dense mantle xenoliths that become re-mobilized during subsequent eruptions years to decades later [54, 64]. During eruption, the time of stagnation for passing magmas is probably on the order of hours to days as indicated by

diffusion calculations [48], which is long enough for fluid inclusions to re-equilibrate. Such intermediate stagnation levels appear to be a common feature of many basaltic volcanoes [14, 17, 62, 65].

The petrologic evidence supporting our interpretation is the abundance of MORB-gabbro xenoliths from the lower oceanic crust in some Cumbre Vieja lavas and pyroclastics [27, 31, 34]. All gabbros indicate strong magmatic overprinting by Recent magmas, and some are associated with ultramafic cumulates in composite xenoliths (Fig. 2). Because the gabbros typically occur in the terminal lavas of an eruption, their origin is best explained by wall-collapse of magma holding reservoirs following magma withdrawal and pressure release.

The inferred intrusion horizon within the lowermost crust was termed "deep rift system" in a previous study [48], but as it becomes clear that this horizon extends to 30 km off the rift axis at least (as indicated by submarine samples(POS_165 and POS_170), we propose to use the term "underplating zone" instead. The depth of the underplating zone shows no systematic variation along the rift axis but appears to increase for the more distal submarine samples (Fig. 4). The depths inferred for these samples are also underestimated since the lithostatic pressure at given depth increases from the distal island flanks towards its center. The Recent underplating zone thus appears to be slightly domed (Fig. 6), which would be expected if it began to form within the cold oceanic crust at relatively great depths and then progressed slowly upward beneath the island where magma supply was sufficient for the formation of an intrusive core complex.

To our knowledge there are no seismic data to confirm or reject the proposed underplating zone. We point out, however, that it may be impossible to detect this zone seismically as most of the underplated material is inferred to consist of cumulate rocks, with the possible exception of small melt or mush lenses beneath Cumbre Vieja (cf. Fig. 6). The mafic and ultramafic cumulates have densities similar to the lower oceanic crust or uppermost mantle in which they formed, and are intimately juxtaposed with it. We have measured the bulk densities of different xenoliths from the 1949 eruption (not corrected for microfractures formed during decompression) and found completely overlapping values for MORB gabbros (2.66-3.00 g/cm^3), mafic cumulates (2.63-2.91 g/cm^3) and ultramafic cumulates (2.74-3.21 g/cm^3); mantle peridotites gave 3.24-3.27 g/cm^3. These considerations show that underplating must not be ruled out only because seismic evidence is equivocal [25].

5.4. Calculation of uplift

Uplift is an inevitable consequence of the inferred underplating beneath Cumbre Vieja. Since observational data are lacking, we have estimated the intrusion-related uplift with a straightforward model under simplifying assumptions. Our calculations are based on the

cumulative thickness of astenospheric material added to the upper mantle and lower crust. We do not consider possible topographic swell, subsidence or isostasy because of lacking evidence for the relevance and magnitude of these effects. Isostatic uplift of La Palma owing to igneous material added to the mantle may be counterbalanced by the island's load onto the crust. Seismic data indicate that there is no flexural moat to the west and southwest of La Palma but rather a shallowing of the basement [49, 66]. This modest swell is in qualitative accordance with our model (Fig. 6) but could also result from a localized hotspot or from the flexural arch imposed by the load of Tenerife [25, 67]. Thus, isostasy is neglected in our calculations as isostatic equilibrium cannot be assessed.

We modelled the underplated igneous material as an oblate ellipsoid of fixed radius r and uniform growth, i.e., repeated magma intrusion increases the ellipsoid volume V and thickness $h = \mathbf{3V/(2\pi r^2)}$ (Fig. 7A). Uplift is thus maximum beneath the volcano center and thins out to its margins. The radius was set to 30 km (roughly corresponding to the 2500 m depth contour) which accounts for underplating beneath the entire volcano including the most distal sites sampled. The flux of underplated material was calculated using a growth rate of 1 km^3/ka for subaerial Cumbre Vieja volcano [68], which is a minimum value neglecting submarine growth. We assume a ratio of intrusive to extrusive volumes of 1:1 for the volcanic edifice (as inferred for the seamount series [8]) and of 3:1 for the entire magmatic system (based on estimates between 3:1 and 5:1 for oceanic hot spots [69]). These conservative estimates give an emplacement rate of 0.5 km^3/ka for intrusions within the edifice and 1 km^3/ka for intrusions beneath Cumbre Vieja causing uplift. The resulting increase in ellipsoid thickness, corresponding to the maximum uplift in the center of Cumbre Vieja, is 0.53 m/ka or a total of 65 m since 123 ka which is the age of the oldest lava flows dated [70]. If underplating were confined to an area outlining the subaerial volcano (radius = 15 km), then maximum uplift is four times higher equivalent to 2.1 m/ka (Fig. 7).

Although these estimates are rather crude, they show the dimension of uplift necessarily linked to Recent Cumbre Vieja volcanism. Our results are in agreement with an estimated minimum rate of uplift of 0.4-0.6 m/ka for northern La Palma as constrained by the present position of the Pliocene seamount series [9] and by an analysis of the deposition time and present height of conglomerates [71]. The calculations also show that uplift due to underplating and global changes in sea-level are of similar magnitude and therefore are competing over time (Fig. 7B). Direct measurements of uplift rates on La Palma are lacking, but based on our model and on eruption history [48] we infer that uplift is periodic rather than continuous. Uplift rates are probably highest prior to and during eruption when intrusive activity is strongest, and may turn into minor subsidence after eruption due to solidification and cooling of the intrusive bodies.

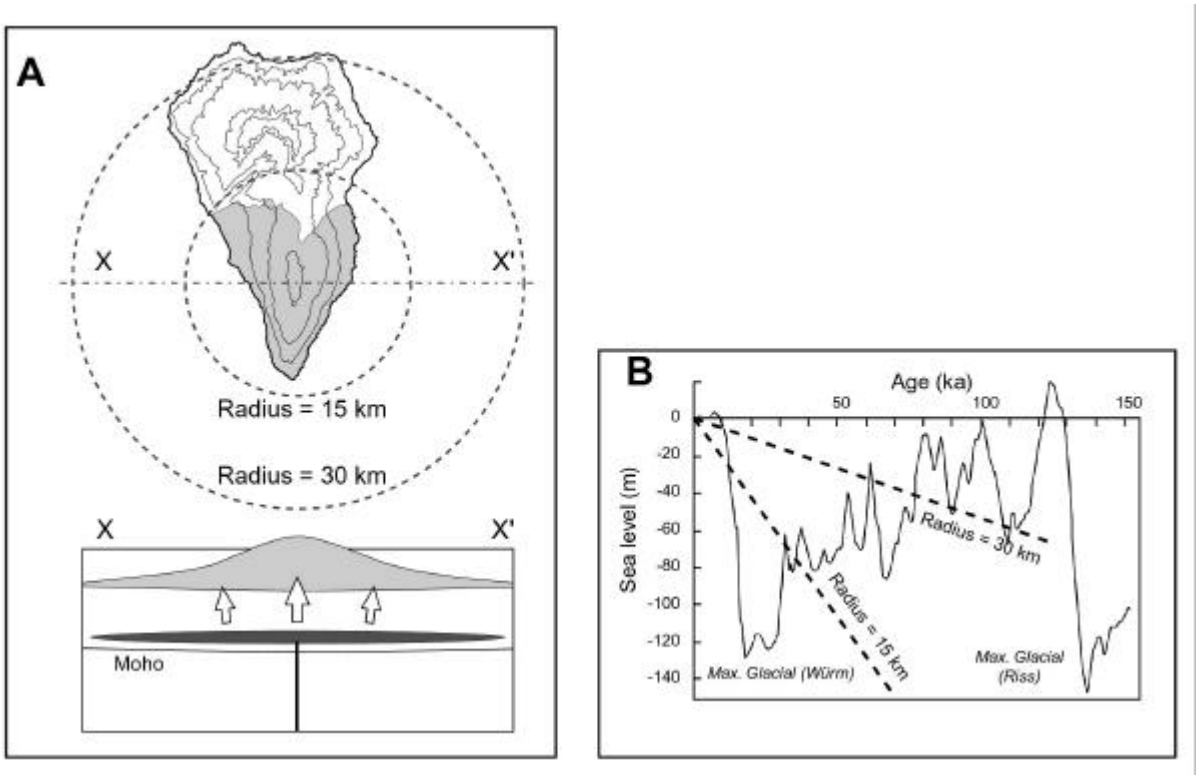

Fig. 7: A. The model to estimate the uplift of Cumbre Vieja volcano (shown in *light gray*) is based on an oblate ellipsoid of fixed radius representing the underplated igneous material (*dark gray*). Repeated magma intrusion increases the ellipsoid's thickness but not its radius. The radii of 30 km and 15 km correspond to underplating beneath the entire volcano (including the most distal sites sampled) and the subaerial Cumbre Vieja, respectively. **B.** Calculated maximum uplift (*dashed lines*) as compared to eustatic sea-level changes (*solid line*, redrawn after [70]). Uplift is calculated for a long-term intrusion rate at depth of 1 km^3/ka (see text for details).

5.5. Uplift modes and faulting at Cumbre Vieja

In the light of our data and field observations, it is worthwile to distinguish between two modes of uplift at La Palma: a more deep-seated uplift on the island scale due to underplating *sensu lato* and a more local uplift due to shallow intrusions. As suggested by our data and illustrated in Fig. 6, underplating is not confined to southern La Palma but should affect the entire island. This first mode of uplift thus provides a petrological and volcanological explanation for the inferred Recent rise of northern La Palma without invoking rather speculative regional tectonics [71]. Nevertheless, uplift is expected to be maximum at Cumbre Vieja, and this may be reflected by the conspicuous cliff line along its western coast: Cliff height is largest just beneath the volcano summit, the region of most volcanic output, and decreases to the north and to the south (Fig. 8). The maximum height of coastal cliffs at Cumbre Vieja even exceeds that at extinct Taburiente volcano in the north where marine erosion has lasted for a considerably longer period of time. It thus appears that uplift by prolonged underplating on the island scale results in some doming centered beneath the Cumbre Vieja.

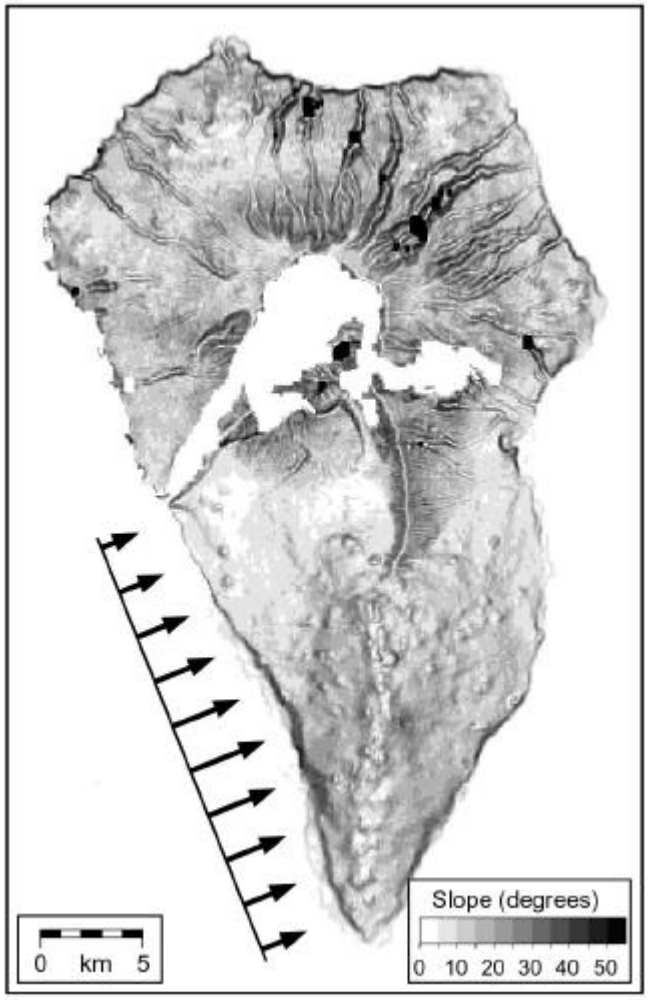

Fig. 8: Slope map of La Palma indicate steep coastal cliffs around the Cumbre Vieja that may be indicative of uplift. The west coast in particular shows that cliff height (indicated by length of *arrows*) is at maximum beneath the ridge crest and decreases to the north and to the south. Maps are based on digital elevation models from the SRTM (Shuttle Radar Topography Mission) global processor and distributed by the U.S. Geological Survey. Empty fields indicate areas of missing SRTM data.

The second, and more dramatic, form of uplift is caused by intrusions into the volcanic edifice. These include not only dikes centered near the rift axis but also shallow plutonic bodies, as is clearly evidenced by the ubiquitous occurrence of phonolite domes all over the Cumbre Vieja and by an intruding phonolite that bulged the flank during the 1585 eruption [38, 72]. We propose that such shallow intrusions are the most relevant mechanism to cause the remarkable topographical irregularities of the Cumbre Vieja ridge. The complex morphology was analyzed by previous workers and was ascribed to deep-reaching listric faults, induced by a strong magma bulge along a postulated N-S fault that reaches into the oceanic basement [71]. Whereas this is a basic concept, magma bulge is an inaccurate term as there is no evidence for any high-level magma chamber on La Palma or for a main N-S fault beneath the Cumbre Vieja. Field observations and petrological data rather point to a succession of smaller intrusions during the evolution of Cumbre Vieja that may be or may not be linked to individual eruptions. Each intrusive event contributes to local uplift and normal faulting, which is a potential cliff-forming mechanism. While accepting the proposed causal relation between falling sea-level and cliff formation about 30-20 ka ago [70], we suggest that underplating and local uplift are important mechanisms for the formation of fault scarps at Cumbre Vieja. The faults caused by shallow intrusions may result in local collapse but are

not necessarily deep-reaching to cause catastrophic giant landslides [72]. The flanks are probably stabilized by the large number of discordant shallow-level intrusions. Despite considerable uplift of the Cumbre Vieja during its evolution, the vertical movements have not been accompanied by any large-scale landslide on La Palma since about 560 ka [68, 73].

6. Conclusions

Geobarometric investigations of lavas and xenoliths from the subaerial ridge and submarine flanks of Cumbre Vieja volcano (La Palma) indicate three distinct pressure ranges of magmatic processes. These are (1) a major fractionation level within the uppermost mantle (430-780 MPa), (2) an underplating zone within the lowermost crust (180-420 MPa), and (3) shallow intrusion levels within the volcanic edifice. The underplating zone is not confined to the Cumbre Vieja but may extend to a radius of at least 30 km from the volcano summit.

Underplating and related intrusive activity result in an uplift on the island scale with an estimated rate of >0.5 m/ka beneath Cumbre Vieja. In long term this uplift is of similar magnitude as global changes in sea-level. Uplift on the island scale and local uplift due to shallow intrusions resulted in coastal cliffs, normal faults and a rather irregular topography of Cumbre Vieja. The steep volcano flanks are thus a cumulative result of volcanic rift zone activity, uplift through shallow intrusions and normal faulting.

The presence of intermediate stagnation levels for ascending magmas appears to be a common feature of basaltic volcanoes, as is shown by our and other studies. We emphasize, therefore, that intrusion-related uplift should be qualitatively considered when reconstructing volcano evolution at longer timescales.

Acknowledgements. We thank the captains, crews and Shipboard Scientific Parties of METEOR cruise M43/1 and POSEIDON cruise POS270 for their professional assistance and pleasant working atmosphere. D. Masson is thanked for kindly providing bathymetric data, S. Krastel for providing maps and helpful comments, M. Thöner and N. Stroncik for support of the EMP analyses, and H.-U. Schmincke, I. Grevemeyer and K. Hoernle for discussions. Fig. 8 was prepared using the freeware program MICRODEM by P. Guth. The constructive reviews by K. Putirka and M. Wilson helped improving the manuscript. Our studies were support by the Deutsche Forschungsgemeinschaft (DFG grants KL1313/3, KL1313/4, HA2100/5, HA2100/6 and HA2100/8).

Appendix A. Analytical methods

Electron microprobe (EMP) analyses were carried out on a Cameca SX-50 at IFM-GEOMAR in Kiel. Analytical conditions included a peak counting time of 20 s, an acceleration voltage of 15 kV and a focussed beam of 20 nA; for glass analyses a rastered beam (3x4 µm) of 10 nA was used to minimize alkali loss. The built-in PAP correction was applied for data reduction. Analytical precision and accuracy were controlled by regular analyses of reference samples Cr-augite, Kakanui augite, VG-2 glass and VG-A99 glass [74]. The averages of 5-25 analyses of each matrix glass and 2-15 analyses at the rims of euhedral clinopyroxenes were used for thermobarometric calculations.

Microthermometric measurements were performed on inclusions in clinopyroxene, olivine and apatite from xenoliths and in clinopyroxene phenocrysts from lavas using Linkam® THM 600 and Fluid Inc.® heating-cooling stages, which were calibrated using SYNFLINC® synthetic fluid inclusion standards. Accuracy was estimated at ±0.2 °C near the triple point of CO_2 (-56.6 °C); melting and homogenization temperatures were reproduced to better than ±0.2 °C. Densities of CO_2 were derived from measured homogenization temperatures [75]. Isochores in P-T space for the CO_2-dominated inclusions were calculated using the computer program FLINCOR [76] utilizing the Kerrick and Jacobs [55] equation of state for CO_2.

Appendix B. Sample descriptions

The investigated vesicular basanitic lavas and lapilli from Cumbre Vieja contain about 5-25 % of olivine and clinopyroxene phenocrysts in a glassy to tachylitic groundmass with clinopyroxene, olivine, Ti-magnetite and plagioclase. Brownish clinopyroxenes with green, partially resorbed cores are ubiquitous and suggest magma mixing prior to eruption [48]. Tephrites contain no olivine but kaersutitic amphibole. There is no apparent chemical or mineralogical difference between subaerial and submarine Cumbre Vieja lavas.

Ultramafic cumulate xenoliths: Olivine-bearing pyroxenites and kaersutitites are the most abundant xenolith types in La Palma lavas. The studied xenoliths consist of 5-50 modal percent titaniferous augite, 5-80 % kaersutite, 0-15 % olivine, 2-8 % Ti-magnetite, 1-10 % glass or or fine-grained aggregates, ± phlogopite ± apatite ± resorbed plagioclase ± hauyne. They typically show cumulus textures characterized by euhedral crystals of varying size, some being poicilitically enclosed by large anhedral kaersutite crystals. Locally, the xenolith textures are "open" due to an interconnected framework of glass. A more comprehensive description of this xenolith type is presented in [14, 27]. The investigated small dunite xenoliths contain minor clinopyroxene and may represent either fragments of the upper mantle or magmatic cumulates.

MORB-type gabbro xenoliths consist of 35-60 % plagioclase, 30-55 % augite, 0-10 % olivine, 0-5 % Fe-Ti oxides, 0-5 % orthopyroxene, and minor amphibole. All rocks contain variable amounts of glassy or microcrystalline mesostasis. Isotropic, medium- to coarse-grained gabbros having cumulus textures are most common. Many crystals show strong intracrystalline deformation or are replaced by less deformed subgrains. The textural features of the gabbros and the occurrence of numerous fluid, melt, and oxide inclusions are interpreted to reflect pervasive magmatic overprinting and partial melting. The gabbros resemble those described in earlier studies [14, 27, 31] and are interpreted as fragments of the Jurassic oceanic crust beneath La Palma.

Occurrence of fluid inclusions: CO_2-dominated fluid inclusions are common in olivine, clinopyroxene and plagioclase but comparatively rare in amphibole. They can be divided into 1) primary or texturally early inclusions occurring singly or in randomly orientated groups which do not form trails, and 2) texturally late inclusion trails reaching or crosscutting grain boundaries. Inclusion sizes range from <2 to 35 µm, and many show textural evidence of partial decrepitation. Many inclusions also contain brown to colorless glass, and in some cases oxides, in variable proportions. Texturally early fluid inclusions occurring in groups are commonly associated with numerous glass and oxide inclusions, irregularly orientated within large areas of individual crystals (see also [14]).

References

[1] A. Nicolas, A melt extraction model based on structural studies in mantle peridotites, J. Petrol. 27 (1986) 999-1022.

[2] J.R. Lister, R.C. Kerr, Fluid-mechanical models of crack propagation and their application to magma transport in dykes, J. Geophys. Res. 96(B6) (1991) 10049-10077.

[3] M.P. Ryan, Neutral buoyancy and the mechanical evolution of magmatic systems, in: B.O. Mysen (Ed.), Magmatic Processes: Physicochemical Principles, Spec. Publ. 1, The Geochemical Society, University Park, Pa., 1987, pp. 259-287.

[4] A. Gudmundsson, Infrastructure and mechanics of volcanic systems in Iceland, J. Volcanol. Geotherm. Res. 64 (1995) 1-22.

[5] K.G. Cox, Continental magmatic underplating, in: K.G. Cox, D. McKenzie, R.S. White (Eds.), Melting and Melt Movement in the Earth, Oxford University Presss, Oxford, 1993, pp. 155-166.

[6] J. Maclennan, B. Lovell, Control of regional sea level by surface uplift and subsidence caused by magmatic underplating of Earth's crust, Geology 30 (2002) 675-678.

[7] W.S. Holbrook, Underplating over hotspots, Nature 373 (1995) 559.

[8] H. Staudigel, H.U. Schmincke, The Pliocene seamount series of La Palma / Canary Islands, J. Geophys. Res. 89(13) (1984) 11195-11215.

[9] H. Staudigel, F. G, G. Giannerini, The history of intrusive activity on the Island of La Palma (Canary Islands), J. Volcanol. Geotherm. Res. 27 (1986) 299-322.

[10] C.J. Stillman, H. Furnes, M.J. LeBas, A.H.F. Robertson, J. Zielonka, The geological history of Maio, Cape Verde Islands, J Geol Soc 139 (1982) 347-361.

[11] A.H.F. Robertson, C.J. Stillman, Submarine volcanic and associated sedimentary rocks of the Fuerteventura basal complex, Canary Islands, Geol. Mag. 116 (1979) 203-214.

[12] M.J. Le Bas, L.C. Silva, A.H.F. Robertson, An oceanic carbonatite volcano on Santiago, Cape Verde Islands, Journal of the Geological Society of London 139 (1982) 659.

[13] I.K. Nikogosian, T. Elliott, J.L.R. Touret, Melt evolution beneath thick lithosphere: a magmatic inclusion study of La Palma, Canary Islands, Chem. Geol. 183 (2002) 169-193.

[14] T.H. Hansteen, A. Klügel, H.U. Schmincke, Multi-stage magma ascent beneath the Canary Islands: evidence from fluid inclusions, Contrib. Mineral. Petrol. 132 (1998) 48-64.

[15] K. Putirka, Magma transport at Hawaii: Inferences based on igneous thermobarometry, Geology 25(1) (1997) 69-72.

[16] M.O. Garcia, T. Hulsebosch, J.M. Rhodes, Olivine-rich submarine basalts from the southwest rift zone of Mauna Loa volcano: Implications for magmatic processes and geochemical evolution, in: J.M. Rhodes, J.P. Lockwood (Eds.), Mauna Loa revealed, Geophysical Monograph 92, American Geophysical Union, 1995
[17] S. Schwarz, A. Klügel, C. Wohlgemuth-Ueberwasser, Melt extraction pathways and stagnation depths beneath the Madeira and Desertas rift zones (NE Atlantic) inferred from barometric studies, Contrib. Mineral. Petrol. 147 (2004) 228-240.
[18] A.B. Watts, U.S. ten Brink, P. Buhl, T. Brocher, A multichannel seismic study of lithospheric flexure across the Hawaiian-Emperor seamount chain, Nature 315 (1985) 105-111.
[19] A.B. Watts, U.S. ten Brink, Crustal structure, flexure and subsidence history of the Hawaiian islands, J. Geophys. Res. 94 (1989) 10473-10500.
[20] D.W. Caress, M.K. McNutt, R.S. Detrick, J.C. Mutter, Seismic imaging of hotspot-related crustal underplating beneath the Marquesas Islands, Nature 373 (1995) 600-603.
[21] P. Charvis, A. Laesanpura, J. Gallart, A. Hirn, J.C. Lépine, B. de Voogd, T.A. Minshull, Y. Hello, B. Pontoise, Spatial distribution of hotspot material added to the lithosphere under La Réunion, from wide-angle seismic data, J. Geophys. Res. 104 (1999) 2875-2893.
[22] I. Grevemeyer, E.R. Flueh, C. Reichert, J. Bialas, D. Kläschen, C. Kopp, Crustal architecture and deep structure of the Ninetyeast Ridge hotspot trail from active-source ocean bottom seismology, Geophys. J. Int. 144 (2001) 414-431.
[23] J.J. Dañobeitia, J.P. Canales, Magmatic underplating in the Canary Archipelago, J. Volcanol. Geotherm. Res. 103 (2000) 27-41.
[24] S. Ye, J.P. Canales, R. Rihm, J.J. Dañobeitia, J. Gallart, A crustal transect through the northern and northeastern part of the volcanic edifice of Gran Canaria, Canary Islands, Journal of Geodynamics 28 (1999) 3-26.
[25] A.B. Watts, C. Peirce, J. Collier, R. Dalwood, J.P. Canales, T.J. Henstock, A seismic study of lithospheric flexure in the vicinity of Tenerife, Canary Islands, Earth Planet. Sci. Lett. 146 (1997) 431-447.
[26] E.R. Neumann, E. Wulff-Pedersen, S.L. Simonsen, N.J. Pearson, J. Martí, J. Mitjavila, Evidence for Fractional Crystallization of Periodically Refilled Magma Chambers in Tenerife, Canary Islands, J. Petrol. 40 (1999) 1089-1123.
[27] A. Klügel, H.U. Schmincke, J.D.L. White, K.A. Hoernle, Chronology and volcanology of the 1949 multi-vent rift-zone eruption on La Palma (Canary Islands), J. Volcanol. Geotherm. Res. 94 (1999) 267-282.
[28] D.A. Clague, W.A. Bohrson, Origin of xenoliths in the trachyte at Puu Waawaa, Hualalai Volcano, Hawaii, Contrib. Mineral. Petrol. 108 (1991) 439-452.
[29] R.V. Fodor, E.A. Rudeck, G.R. Bauer, Hawaiian magma-reservoir processes as inferred from the petrology of gabbro xenoliths in basalt, Kahoolawe Island, Bull. Volcanol. 55 (1993) 204-218.
[30] A. Gaffney, Environments of crystallization and compositional diversity of Mauna Loa xenoliths, J. Petrol. 43 (2002) 963-980.
[31] E.R. Neumann, V.B. Sørensen, S.L. Simonsen, K. Johnsen, Gabbroic xenoliths from La Palma, Tenerife and Lanzarote, Canary Islands: evidence for reactions between mafic alkaline Canary Islands melts and old oceanic crust, J. Volcanol. Geotherm. Res. 103 (2000) 313-342.
[32] G. Sen, Petrogenesis of spinel lherzolite and pyroxenite suite xenoliths from the Koolau shield, Oahu, Hawaii: Implications for petrology of the post-erosive lithosphere beneath Oahu, Contrib. Mineral. Petrol. 100 (1988) 61-91.
[33] K. Hoernle, Trace element and Sr-Nd-Pb isotopic geochemistry of Jurassic ocean crust beneath Gran Canaria (Canary Islands): implications for the generation of OIB reservoirs and for crustal contamination of ascending OIB magmas, J. Petrol. 39(5) (1998) 859-880.
[34] H.U. Schmincke, A. Klügel, T.H. Hansteen, K. Hoernle, P.v.d. Bogaard, Samples from the Jurassic ocean crust beneath Gran Canaria, La Palma and Lanzarote (Canary Islands), Earth Planet. Sci. Lett. 163 (1998) 343-360.
[35] H.A. Roeser, Magnetic anomalies in the magnetic quiet zone off Morocco, in: U. Rad, K. Hinz, M. Sarnthein, E. Seibold (Eds.), Geology of the Northwest African Continental Margin, Springer, Berlin Heidelberg New York, 1982, pp. 61-68.
[36] K.D. Klitgord, H. Schouten, Plate kinematics of the Central Atlantic, in: P.R. Vogt, B.E. Tucholke (Eds.), The geology of North America, Vol. M, The Western North Atlantic Region, Geological Society of America, 1986, pp. 351-378.
[37] H.U. Schmincke, Volcanic and chemical evolution of the Canary Islands, in: U. von Rad, K. Hinz, M. Sarnthein, E. Seibold (Eds.), Geology of the Northwest African Continental Margin, Springer, Berlin Heidelberg New York, 1982, pp. 3-20.
[38] J.C. Carracedo, E.R. Badiola, H. Guillou, J. de La Nuez, F.J. Pérez Torrado, Geology and volcanology of La Palma and El Hierro, Western Canaries, Estudios Geol. 57 (2001) 175-273.
[39] K. Hoernle, H.U. Schmincke, The role of partial melting in the 15-Ma geochemical evolution of Gran Canaria: a blob model for the Canary hotspot, J. Petrol. 34(3) (1993b) 599-626.
[40] J.C. Carracedo, The Canary Islands: an example of structural control on the growth of large ocean-island volcanoes, J. Volcanol. Geotherm. Res. 60 (1994) 225-241.
[41] E.A.K. Middlemost, Evolution of La Palma, Canary archipelago, Contrib. Mineral. Petrol. 36 (1972) 33-48.
[42] A. Hernandéz-Pacheco, M.C. Valls, The historic eruptions of La Palma Island (Canarias), Arquipelago, Rev. Univ. Azores, Ser. C. Nat. 3 (1982) 83-94.
[43] E. Ibarrola, Temporal modification of the basaltic materials from 1971 eruption of the Teneguía volcano (La Palma, Canary Islands), Estudios Geol., Vol. Teneguía (1974) 49-58.

[44] H.U. Schmincke, G. Graf, DECOS / OMEX II, Cruise No. 43, METEOR-Berichte, Universität Hamburg, 2000, pp. 99.
[45] K. Putirka, M. Johnson, R. Kinzler, J. Longhi, D. Walker, Thermobarometry of mafic igneous rocks based on clinopyroxene-liquid equilibria, 0-30 kbar, Contrib. Mineral. Petrol. 123 (1996) 92-108.
[46] J.M. Duke, Distribution of the period four transition elements among olivine, calcic clinopyroxene and mafic silicate liquid: experimental results, J. Petrol. 17 (1976) 499-521.
[47] A. Klügel, Prolonged reactions between harzburgite xenoliths and silica-undersaturated melt: implications for dissolution and Fe-Mg interdiffusion rates of orthopyroxene, Contrib. Mineral. Petrol. 141 (2001) 1-14.
[48] A. Klügel, K.A. Hoernle, H.U. Schmincke, J.D.L. White, The chemically zoned 1949 eruption on La Palma (Canary Islands): Petrologic evolution and magma supply dynamics of a rift-zone eruption, J. Geophys. Res. 105(B3) (2000) 5997-6016.
[49] C.R. Ranero, M. Torne, E. Banda, Gravity and multichannel seismic reflection constraints on the lithospheric structure of the Canary Swell, Mar. Geophys. Res. 17 (1995) 519-534.
[50] A.M. van den Kerkhof, Isochoric phase diagrams in the systems CO_2-CH_4 and CO_2-N_2: Application to fluid inclusions, Geochim. Cosmochim. Acta 54 (1990) 621-629.
[51] M.L. Frezzotti, T. Andersen, E.R. Neumann, S.L. Simonsen, Carbonatite melt–CO_2 fluid inclusions in mantle xenoliths from Tenerife, Canary Islands: a story of trapping, immiscibility and fluid–rock interaction in the upper mantle, Lithos 64 (2002) 77-96.
[52] R.J. Bakker, J.B.H. Jansen, Experimental post-entrapment water loss from synthetic CO_2-H_2O inclusions in natural quartz, Geochim. Cosmochim. Acta 55 (1991) 2215-2230.
[53] T. Andersen, E.R. Neumann, Fluid inclusions in mantle xenoliths, Lithos 55 (2001) 301-320.
[54] A. Klügel, T.H. Hansteen, H.U. Schmincke, Rates of magma ascent and depths of magma reservoirs beneath La Palma (Canary Islands), Terra Nova 9(3) (1997) 117-121.
[55] D.M. Kerrick, G.K. Jacobs, A modified Redlich-Kwong equation for H_2O, CO_2 and H_2O-CO_2 mixtures at elevated temperatures and pressures, Am. J. Sci. 281 (1981) 735-767.
[56] J.E. Dixon, D.A. Clague, P. Wallace, R. Poreda, Volatiles in alkalic basalts from the North Arch volcanic field, Hawaii: extensive degassing of deep submarine-erupted alkalic series lavas, J. Petrol. 38(7) (1997) 911-939.
[57] P.M. Sachs, T.H. Hansteen, Pleistocene underplating and metasomatism of the lower continental crust: a xenolith study, J. Petrol. 41 (2000) 331-356.
[58] B.J. Wanamaker, T.F. Wong, B. Evans, Decrepitation and crack healing of fluid inclusions in San Carlos olivine, J. Geophys. Res. 95(B10) (1990) 15623-15641.
[59] K.V. Cashman, Textural constraints on the kinetics of crystallization of igneous rocks, in: J. Nicholls, J.K. Russell (Eds.), Reviews in Mineralogy Vol. 24: Modern Methods of Igneous Petrology: Understanding Magmatic Processes 24, Min. Soc. Amer., 1990, pp. 259-314.
[60] A. Ancochea, F. Hernán, A. Cendrero, J.M. Cantagrel, J.M. Fúster, E. Ibarrola, J. Coello, Constructive and destructive episodes in the building of a young Oceanic Island, La Palma, Canary Islands, and genesis of the Caldera de Taburiente, J. Volcanol. Geotherm. Res. 60 (1994) 243-262.
[61] B.D. Marsh, Solidification fronts and magmatic evolution, Mineral. Mag. 60 (1995) 5-40.
[62] M.L. Frezzotti, A. Peccerillo, Fluid inclusion and petrological studies elucidate reconstruction of magma conduits, Eos Trans. Am. Geophys. Union 85 (2004) 157-163.
[63] K. Putirka, C.D. Condit, Cross section of a magma conduit system at the margin of the Colorado Plateau, Geology 31 (2003) 701-704.
[64] A. Klügel, Reactions between mantle xenoliths and host magma beneath La Palma (Canary Islands): constraints on magma ascent rates and crustal reservoirs, Contrib. Mineral. Petrol. 131 (1998) 237-257.
[65] C.S. Szabó, R.J. Bodnar, Changing magma ascent rates in the Nógrád-Gömör volcanic field, Northern Hungary / Southern Slovakia: Evidence from CO_2-rich fluid inclusions in metasomatized mantle xenoliths, Petrology 4 (1996) 240-249.
[66] E. Banda, C.R. Ranero, J.J. Danobeitia, A. Rivero, Seismic boundaries of the eastern Central Atlantic Mesozoic crust from multichannel seismic data, Geol. Soc. Am. Bull. 104 (1992) 1340-1349.
[67] R. Urgeles, M. Canals, J. Baraza, B. Alonso, Seismostratigraphy of the western flanks of El Hierro and La Palma (Canary Islands): a record of Canary Islands volcanism, Marine Geology 146 (1998) 225-241.
[68] J.C. Carracedo, S.J. Day, H. Guillou, P. Gravestock, Later stages of volcanic evolution of La Palma, Canary Islands: Rift evolution, giant landslides, and the genesis of the Caldera de Taburiente, Geol. Soc. Am. Bull. 111(5) (1999) 755-768.
[69] J.A. Crisp, Rates of magma emplacement and volcanic output, J. Volcanol. Geotherm. Res. 20 (1984) 177-211.
[70] H. Guillou, J.C. Carracedo, S. Day, Dating of the upper Pleistocene-Holocene activity of La Palma using the unspiked K-Ar technique, J. Volcanol. Geotherm. Res. 86 (1998) 137-149.
[71] A. Hildenbrand, P.Y. Gillot, V. Soler, P. Lahitte, Evidence for a persistence uplifting of La Palma (Canary Islands), inferred from morphological and radiometric data, Earth Planet. Sci. Lett. 210 (2003) 277-289.
[72] S.J. Day, J.C. Carracedo, H. Guillou, P. Gravestock, Recent structural evolution of the Cumbre Vieja volcano, La Palma, Canary Islands: volcanic rift zone reconfiguration as a precursor to volcano flank instability?, J. Volcanol. Geotherm. Res. 94 (1999) 135-167.
[73] R. Urgeles, D.G. Masson, M. Canals, A.B. Watts, T. Le Bas, Recurrent large-scale landsliding on the west flank of La Palma, Canary Islands, J. Geophys. Res. 104(B11) (1999) 25331-25348.
[74] E.J. Jarosewich, J.A. Nelen, J.A. Norberg, Reference samples for electron microprobe analysis, Geostand. Newslett. 4 (1980) 43-47, Correction Vol. 4, 257-258.

[75] S. Angus, B. Armstrong, K.M. de Reuck, V.V. Altunin, O.G. Gadetskii, G.A. Chapela, J.S. Rowlinson, International Tables of the Fluid State, Carbon dioxide, Pergamon Press, Oxford, 1976, 385 pp.
[76] P.E. Brown, FLINCOR: A fluid inclusion data reduction and exploration program (abstr), in: Second Biennial Pan-Am. Conf. Fluid Inclusions Prog. Abstr., 1989, pp. 14.
[77] D.G. Masson, A.B. Watts, M.J.R. Gee, R. Urgeles, N.C. Mitchell, T.P. Le Bas, M. Canals, Slope failures on the flanks of the western Canary Islands, Earth Sci Rev 57 (2002) 1-35.

3. Thermobarometry (separate paper)

This chapter consists of an individual paper which has been submitted to “Journal of Volcanology and Geothermal Research” on November 3, 2004. The complete data not presented in the paper are shown in the Appendix of the thesis.

Appendix A 3.1: Composition of clinopyroxene rims
Appendix A 3.2: Composition of glass and fused groundmass
Appendix A 3.3: Fluid inclusion data
Appendix A 3.4: Electron microprobe analyses of standards
Appendix A 5.1: Map of sample localities

Changing depths of magma fractionation and stagnation during the evolution of an oceanic island volcano: La Palma (Canary Islands)

Karsten Galipp[1)], Andreas Klügel[1)], Thor H. Hansteen[2)]

Submitted to Journal of Volcanology and Geothermal Research
Received 03.11.04

1) Universität Bremen, Fachbereich Geowissenschaften
Postfach 330440, D-28334 Bremen, Germany
Fax: +49-421-218-9460, e-mail: kgalipp@uni-bremen.de

2) IFM-GEOMAR, Leibniz-Institut für Meereswissenschaften
Wischhofstr. 1-3, D-24148 Kiel, Germany
Fax: +49-431-600-2924, e-mail: thansteen@ifm-geomar.de

Corresponding author: Karsten Galipp (kgalipp@uni-bremen.de)

Abstract

La Palma (Canary Islands) represents a hotspot island with an active rift zone, inferred to have formed during the last 800 ka following southward growth of the former radial-symmetrical stratovolcano Taburiente. Clinopyroxene-melt thermobarometry and microthermometry of fluid inclusions were applied to constrain magma pathways and major levels of magma stagnation and to determine a possible genetic relationship between Taburiente and the active rift zone (Cumbre Vieja). CO_2-dominated fluid inclusions in olivine and clinopyroxene in Taburiente dunites show frequency maxima at pressures of 0.40 - 0.60 GPa (10 - 17 km depth). Inclusion data of Cumbre Nueva ankaramites and Bejenado cumulates give pressure estimates of 0.25 - 0.45 GPa (8 - 14 km). In comparison, published data of fluid inclusions in Cumbre Vieja rocks yield a pronounced pressure estimate at 0.20 - 0.40 GPa (5 - 14 km) (Klügel et al., submitted) which partly overlaps with the Cumbre Nueva and Bejenado data but is shallower than that for Taburiente. Clinopyroxene-melt barometry of phenocryst rims and glassy groundmass yield pressures of 0.60 and 1.05 GPa (19 - 34 km; Taburiente) and 0.50 - 0.85 GPa (16 - 28 km; Cumbre Nueva, Bejenado). These pressure ranges partly overlap with that for Cumbre Vieja between 0.45 and 0.64 GPa (14 - 25 km) but has a tendency to higher pressures. The combined data indicate two separate magma stagnation levels beneath each volcanic phase: (1) a main fractionation level within the upper mantle which is common to all phases, and (2) intermittent stagnation close to the Moho for the Taburiente volcano and above the Moho for both the Cumbre Nueva and Cumbre Vieja. The observation that the present rift system and the early stages of the rift show different levels of fractionation within the mantle and magma stagnation within the crust, suggests that there is no common magma reservoir within in the crust feeding both the the fossile rift and the present rift system. Therefore we suggest that the present rift configuration does not reflect continuous growth of the Taburiente shield during the last 800 ka. We thus propose that Taburiente/Cumbre Nueva and Cumbre Vieja represent two distinct volcanoes with separate magma plumbing systems. This model is supported by the overall morphology and by compositional differences between the lavas.

Keywords: Canary Islands, thermobarometry, fluid inclusions, magma plumbing, rift zone

1. Introduction

Rift zones on ocean island volcanoes are elongated areas or morphological ridges along which volcanic and intrusive activity are concentrated. Being the locus of major volcano growth, they have a strong control on magmatic processes, rates and pathways of magma transport, and structure and stability of volcanic edifices (e.g. Walker, 1999). Petrological, geochemical and geophysical studies on rift zones such as on Hawaii (e.g. Eaton and Murata, 1960; Clague, 1987; Delaney et al., 1990; Duffield et al., 1982; Ryan, 1988; Garcia et al., 1996, 1998; Yang et al; 1999, Leslie et al., 2004), Iceland (Gudmundsson, 1998), the Canary Islands (Carracedo, 1994; Ablay et al., 1998; Klügel et al., 2000), Madeira (Geldmacher et al., 2000; Schwarz et al., 2004), Tahiti (Duncan et al.; 1994; Hildenbrand et al., 2004) and Réunion (Albarede et al., 1997) have provided insights into magma chamber processes and the evolution of rift systems. Most studies, however,are based on the eruptive sequence of a single eruption or a short period of activity (< 1000 a) (e.g. Elliot 1991; Klügel et al., 2000), or on the temporal change in compositions of erupted lavas. Our knowledge of the long-term temporal and spatial evolution of magma plumbing systems beneath rift zones at ocean islands is still limited.

Clearly, a study on the evolution of magmatic processes and magma plumbing systems beneath rift zones should cover a period spanning the entire evolution of the rift. La Palma is an ideal place for such a detailed study because it consists of an old radial shield volcano (Taburiente) that began to form a dominant rift at about 800 ka which ultimately resulted in the presently active, well-developed rift zone (Cumbre Vieja). The geochronological evolution of La Palma during the island's subaerial stage (since about 1.7 Ma) is well reconstructed by precise K-Ar and $^{40}Ar/^{39}Ar$ dating (Guillou et al., 1998, 2001). Little is known, however, about the petrological and geochemical evolution of the rift and about possible genetic relationships between the magmatic systems of the Cumbre Vieja and Taburiente.

We carried out thermobarometric investigations in order to constrain the temporal and spatial evolution of magma plumbing over the last 1.0 Ma at La Palma. The depths of magma fractionation and temporary stagnation during ascent were investigated using fluid inclusions as well as clinopyroxene-liquid barometry and melt barometry, which are suitable approaches to address this question (e.g. Roedder, 1983; De Vivo et al. 1988; Belkin and De Vivo, 1993; Szabo and Bodnar, 1996; Hansteen et al, 1998; Andersen and Neumann, 2001; Schwarz et al, 2004; Putirka et al., 1996; 2003; Yang et al., 1996). Our data provide some insight into the evolution of the magma plumbing system of a rift zone from its earliest stage until present and allows to discuss the question if, and how, the presently active rift zone is connected to the old shield volcano.

2. Geological setting

La Palma is the historically most active island of the Canary Archipelago, a 600 km long chain of seven volcanic islands off the coast of NW Africa (Fig. 1). Subaerial volcanic activity at the archipelago started more than 20 million years ago with the formation of the eastern islands Lanzarote and Fuertventura. All islands are underlain by Jurassic oceanic crust as is indicated by tholeiitic mid-ocean ridge basalt (MORB) gabbro xenoliths occurring on Gran Canaria, Lanzarote and La Palma (Hoernle, 1998; Schmincke et al., 1998). The age of the crust is bracketed by magnetic anomalies S1 (175 Ma) between the easternmost islands and the African coast, and M25 (155 Ma) between La Palma and El Hierro, which are the westernmost and youngest islands (Klitgord and Schouten, 1986). The Canary Islands are believed to result from volcanism above a hotspot that impinges beneath the slowly moving oceanic lithosphere (Morgan et al.; 1983; Holik et al.; 1991, Hoernle et al., 1991). The geology of the Canary Islands is summarized in Schmincke (1976, 1982) and Carracedo (1999). Tenerife, La Palma and El Hierro are presently in the shield-stage of growth, whereas Lanzarote, Fuerteventura, Gran Canaria and La Gomera are in the post-erosional stage of development.

The geological evolution of La Palma is discussed in Carracedo et al. (1999; 2001) and is briefly summarized here. As early recognized (Hausen, 1969; Middlemost, 1972; Abdel-Monem et al., 1972; Schmincke, 1976), the geology of La Palma can be divided into three major units (Fig. 1): (1) the older basal complex (ca. 4.0 to 3.0 Ma) which comprises a Pliocene seamount sequence and a plutonic complex, uplifted and tilted by intrusions coeval with the later subaerial activity (Staudigel and Schmincke, 1984); (2) the older volcanic series (1.7 to 0.5 Ma) which include the Garafia volcano, the Taburiente shield volcano, the Bejenado edifice, and the Cumbre Nueva series; and (3) the Cumbre Vieja series (125 ka to present) which is confined to the southern half of the island.

The first subaerial volcanism formed Garafia volcano (1.7 - 1.2 Ma) which overlies and mantles the uplifted seamount. Outcrops of Garafia volcano are limited to erosive windows at the north and southwest flanks of the northern shield. The Taburiente shield-volcano (1.2 - 0.4 Ma) forms the northern part of La Palma (Fig. 1; Ancochea et al., 1994, Guillou et al., 1998; 2001). From about 830 ka on, Taburiente volcano began to extend to the south along the Cumbre Nueva rift zone. This rift was partially destroyed by a giant lateral collapse at 560 ka resulting the present steep shape of the Cumbre Nueva ridge. Immediately after the collapse, a new episode of volcanic activity within the collapsed embayment produced the Bejenado volcano. The growth of this stratovolcano occurred rapidly from about 560 to 490 ka with little concomitant activity from Taburiente (Guillou et al., 1998; 2001).

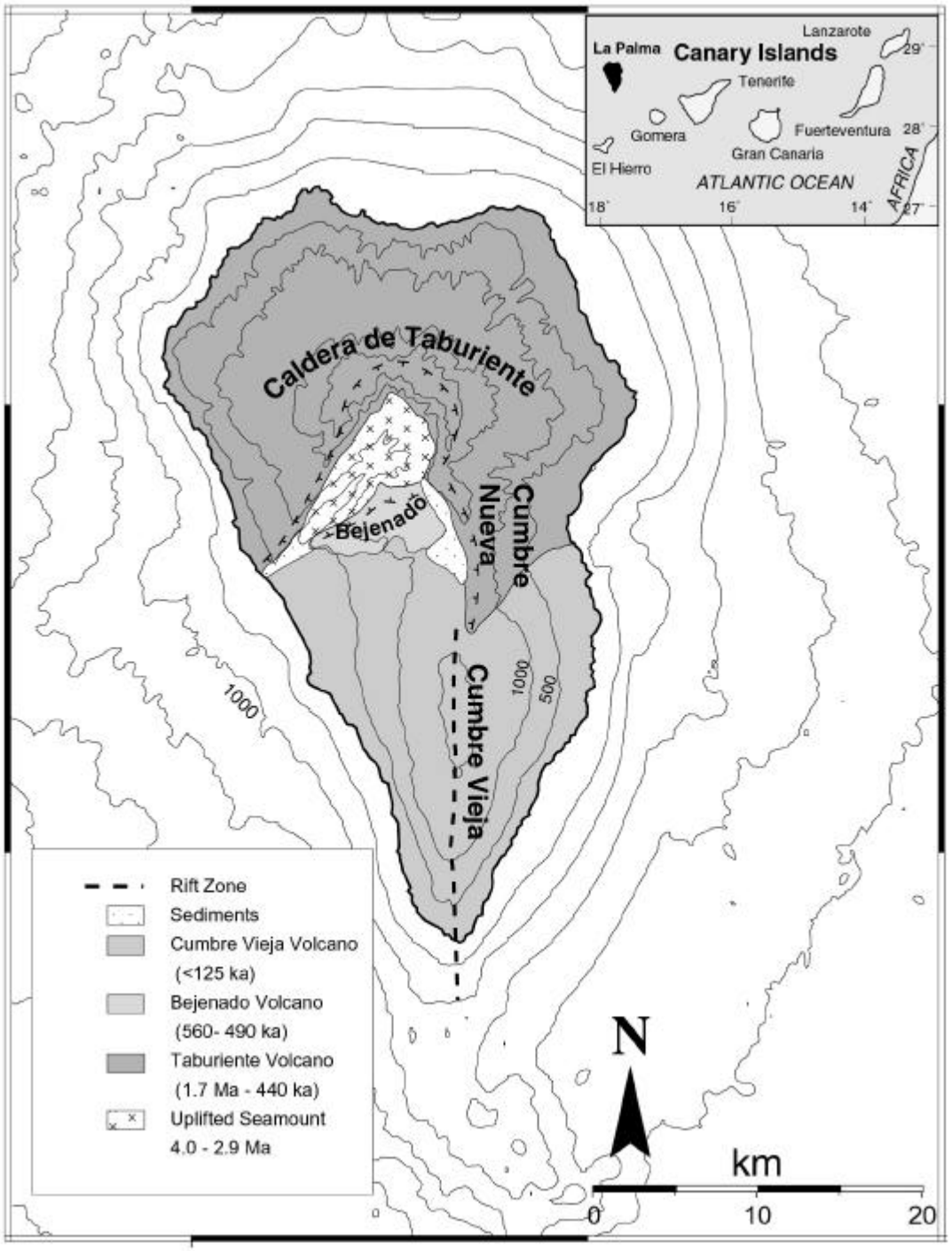

Fig. 1 Simplified geological map of La Palma (modified after Ancochea et al., 1994 and Carracedo et al., 1999). Age range of volcanic units are from Staudigel et al. (1986) and Guillou et al. (1998, 2001). Bathymetric data are partly based on D. G. Masson et al. (2002), compiled by S. Krastel, Universität Bremen.

After cessation of volcanism at Bejenado, the activity shifted to the south forming the Cumbre Vieja volcano from about 125 ka to present. The apparent gap from 400 to 125 ka separating the volcanism at Taburiente and Cumbre Vieja may correspond to a period of volcanic quiescence. A more likely explanation, however, is that volcanism continued but older rocks at Cumbre Vieja are completely covered by younger lavas.

Recent eruptive activity on La Palma is largely confined to the N-S trending Cumbre Vieja ridge forming a pronounced rift zone as indicated by the prominent north-south alignment of vents, fissures and faults (Middlemost, 1972; Carracedo, 1994). Morphologically, the Cumbre Vieja rests on the southern flank of the older Cumbre Nueva ridge and represents a separate volcanic edifice.

3. Petrography

La Palma is characterised by alkaline rocks ranging from basanites and alkali picrites to phonolites (Fig. 2) (Carracedo et al., 2001). Although the different geological units of La Palma essentially overlap in their bulk chemical compositions, we found significant petrographic differences (Table 1). Ankaramites occur commonly at Taburiente and Cumbre Nueva but are almost absent at Cumbre Vieja. More differentiated lavas (phonotephrites to phonolites) are far more abundant at Bejenado and Cumbre Vieja than at Taburiente and Cumbre Nueva, and phonolite plugs occur ubiquitiously and exclusively at Cumbre Vieja. Finally, green-core clinopyroxenes showing reverse zonation (Klügel et al., 2000) occur commonly in lavas from Bejenado and Cumbre Vieja but rarely in Taburiente samples. All these petrographic and lithologic characteristics suggest that there are significant differences in magma evolution of the different volcanoes.

Table 1 Comparison of lithological and petrographical characteristics of different geological units of La Palma

	Taburiente	**Cumbre Nueva**	**Bejenado**	**Cumbre Vieja**
ankaramites	occasional	common	none	none
xenoliths	rare (mafic and ultramafic cumulates)	rare (mafic and ultramafic cumulates)	occasional (mafic and ultramafic cumulates)	MORB-gabbros, mafic and ultramafic cumulates, peridodites, evolved rocks
differentiated lavas*	rare	none	common	common
phonolitic intrusions	none	none	none	common

*with amphibol- and greencore-clinopyroxenes

The investigated basanitic to alkalibasaltic lavas of Taburiente, Cumbre Nueva and Cumbre Vieja contain phenocrysts of olivine (0 - 30%), titaniferous augite (0 - 30%) (see Appendix 1). In some basalts amphibole and plagioclase represent minor microphenocryst phases. Olivine (0.4 - 4.5 mm long) is euhedral or rounded, partially resorbed and in some samples slightly to strongly altered. Clinopyroxenes (0.4 - 4.0 mm long) are optically zoned and in some ankaramites slightly to moderately resorbed. They occur as single crystals or form aggregates with olivines. Ti-magnetite is present in small amounts (< 2 vol. %, < 1 mm). The groundmass consists of olivine, clinopyroxene, plagioclase laths and Fe-Ti oxides.

The phonotephritic to phonolitic samples are aphyric to phyric and contain phenocrysts of plagioclase, clinopyroxene, magnetite and in most phonotephrites, olivine (see Appendix 1). One Bejenado sample (KLP 115) contains kaersutitic amphibole, hauyne and titanite as additional phenocryst phases. The groundmass of the differentiated rocks is composed of a fresh to altered glassy or trachytic matrix with plagioclase, clinopyroxene and Fe-Ti-oxides.

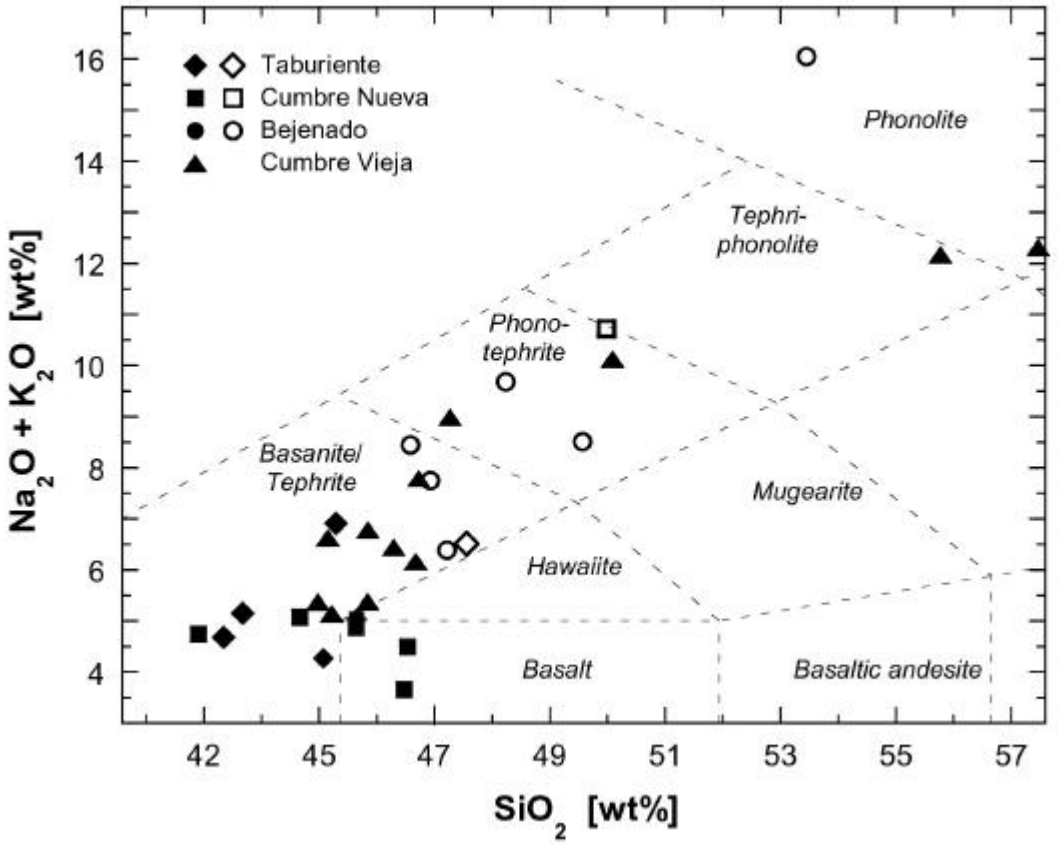

Fig. 2 Total alkali vs. silica diagram of samples used in this study, using the field boundaries of Le Maitre et al. (1989). Open symbols represent natural analyzed glass samples; closed symbols represent fused groundmass.

Petrography of fluid inclusions

Samples chosen for fluid inclusion studies are mafic and ultramafic xenoliths and ankaramitic lavas with olivine and clinopyroxene phenocrysts. Detailed petrographic descriptions of the xenoliths are given in Appendix 2. All analysed fluid inclusions are hosted by clinopyroxene or olivine. Inclusion range from <4 to 28 µm in size (longest dimension) with the majority around 5 - 10 µm, and show roundish or oval to negative-crystal shapes. Some inclusions contain brownish glass and in rare cases oxides in variable proportions. The fluid inclusions can be divided into two groups: (1) primary inclusions occurring singly or in randomly oriented groups, well removed from host grain boundaries; and (2) intracrystalline clusters and trails which rarely crosscut grain boundaries thus giving evidence of pseudosecondary origin. Some fluid inclusions show textures characteristic of partial decrepitation such as

microcracks radiating from inclusions. Since decrepitated inclusions do not give reliable density values they were not incorporated in our analyses.

4. Methods

Fluid inclusions were investigated in 100 µm doubly-polished plates from xenoliths and lavas. Microthermometric measurements were carried out at the Department of Geosciences, University of Bremen, using a Linkam® THMSG 600 heating-cooling stage, which was calibrated with SYNFLINC® synthetic fluid inclusion standards at -56.6 (CO_2) and -10.7 °C (H_2O - KCl with 19.6 wt. % KCl). Accuracy and precision of CO_2 triple point measurements are estimated at better than ± 0.2 °C, homogenization temperatures are reproducible to better than ± 0.2 °C. Fluid inclusion density was directly derived from the observed homogenization temperatures using the phase diagram of Angus (1976) and assuming pure CO_2 composition. Isochores were calculated using the Kerrick and Jacobs (1981) equation of state for the CO_2 - H_2O system using the FLINCOR computer program (Brown, 1989).

Major element analyses of minerals and glass were performed with a CAMECA SX-50 electron microprobe (EMP) at the IFM-GEOMAR research center in Kiel. Analytical conditions included a focussed beam with a current of 30 nA for olivine and 10 to 20 nA for other phases at an acceleration voltage of 15 kV. Glasses were analysed with a beam current of 8 nA and a defocussed beam of 10 µm. In glassy samples the melt composition was directly measured on the thin section. For samples containing no glass, the groundmass was separated, finely ground an then fused on an Ir-filament and quenched to glass under air at the Institute of Mineralogy at the University of Frankfurt. To determine average compositions, at least 13 points per glass sample and 4 points per clinopyroxene rim were analyzed.

5. Results

5.1. Fluid inclusion barometry

Composition of fluid inclusions

Upon cooling all fluids froze to a solid phase between -70 and -100 °C. During reheating, fluid inclusions showed a melting point between -58.2 and -56.1 °C (Tm) close to the triple point of CO_2 (-56.6 °C); only a few inclusions in a single sample showed a melting interval of 0.8 to 1.0 °C (Fig. 3). This indicates that most inclusions consist largely of pure CO_2. The lowering of the melting temperature could be attributed to the presence of minor additional components (e.g. N_2, CH_4 or SO_2) or to thermal gradients in the heating-cooling stage. As no further phase transitions were observed in the inclusions between -57 and -190 °C, neither N_2 nor CH_4 and SO_2 can be present in significant amounts (Burrus, 1981, Touret 1982; Van den Kerkhof 1988). We note that small amounts of CH_4 and/or N_2 (< about 5 mol %) do not

significantly affect the interpretation of trapping PT conditions of CO_2-inclusions (Van den Kerkhof, 1990). On further heating, the liquid + vapour phase assemblage in the inclusions homogenized into the liquid phase (Th_l) below the critical point of pure CO_2 (+31.1 °C). Homogenization into the vapour phase (Th_v) was not observed.

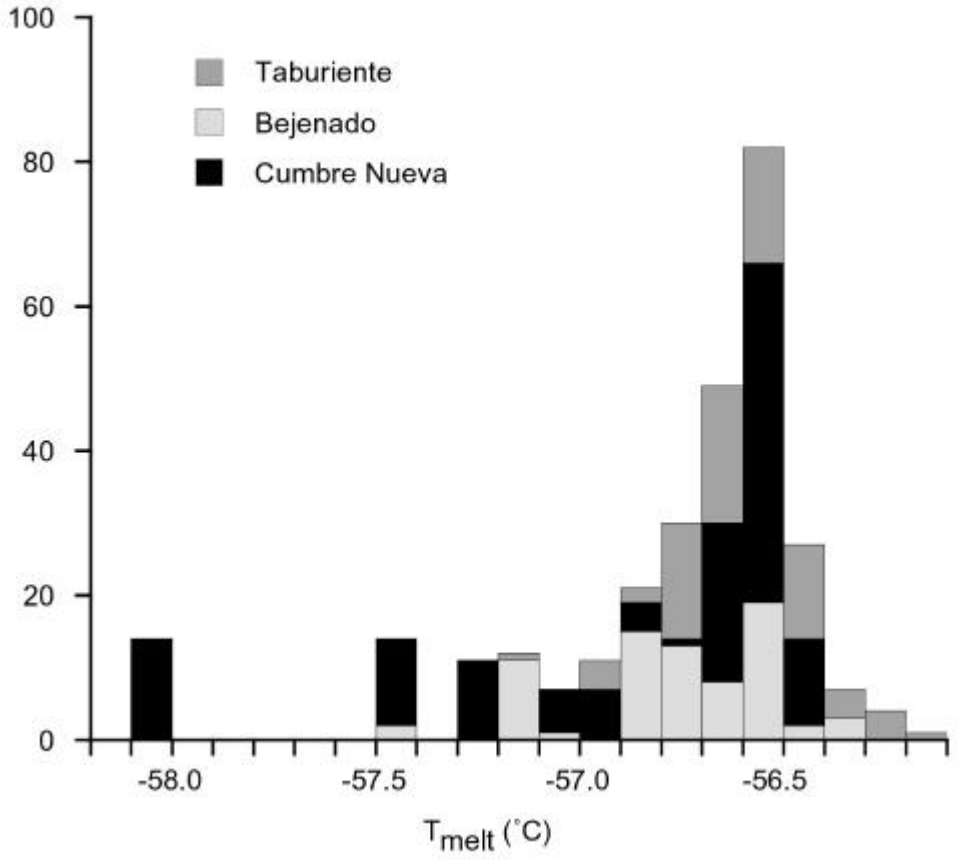

Fig. 3 Measured triple melting temperatures of fluid inclusions in phenocrysts and xenoliths from this study. Lowering of the melting temperature compared to that of pure CO_2 (-56.6 °C) may be attributed to to the minor presence of additional components (e.g. N_2, CH_4, SO_2).

Although H_2O is expected as a component in fluids exsolved from mafic melts (Dixon, 1997; Moore, et al., 1998) and in fluid inclusion in mantle xenoliths (Sachs and Hansteen, 2000), there is no evidence for the presence of H_2O in the investigated fluid inclusions. Either H_2O was removed from the inclusions by diffusive hydrogen loss at high temperatures (Bakker & Jansen, 1991), or H_2O was consumed by a reaction between the fluid and inclusion wall forming secondary minerals such as amphiboles, sheet silicates and carbonates (Andersen, 1984; Andersen & Neumann, 2001, Frezzotti et al, 2002). We did not find any sign of secondary products, although this may be related to small inclusion diameters (mostly <10 µm).

If we assumed that the fluid phase of the mafic melt was not pure CO_2 but had an $X(H_2O) = H_2O/(CO_2+H_2O)$ of 0.1, which is probably an upper limit for basaltic melts at 1.0 GPa (Roedder 1984; Dixon, 1997), actual fluid inclusion densities would be systematically 4.5 %

higher (cf. Sachs and Hansteen, 2000). Throughout this study we present uncorrected fluid densities as derived for pure CO_2-inclusions because we can nothing but guess the former H_2O content and thus introduce additional errors. The effect of former H_2O in the inclusions and related errors are considered in the discussion.

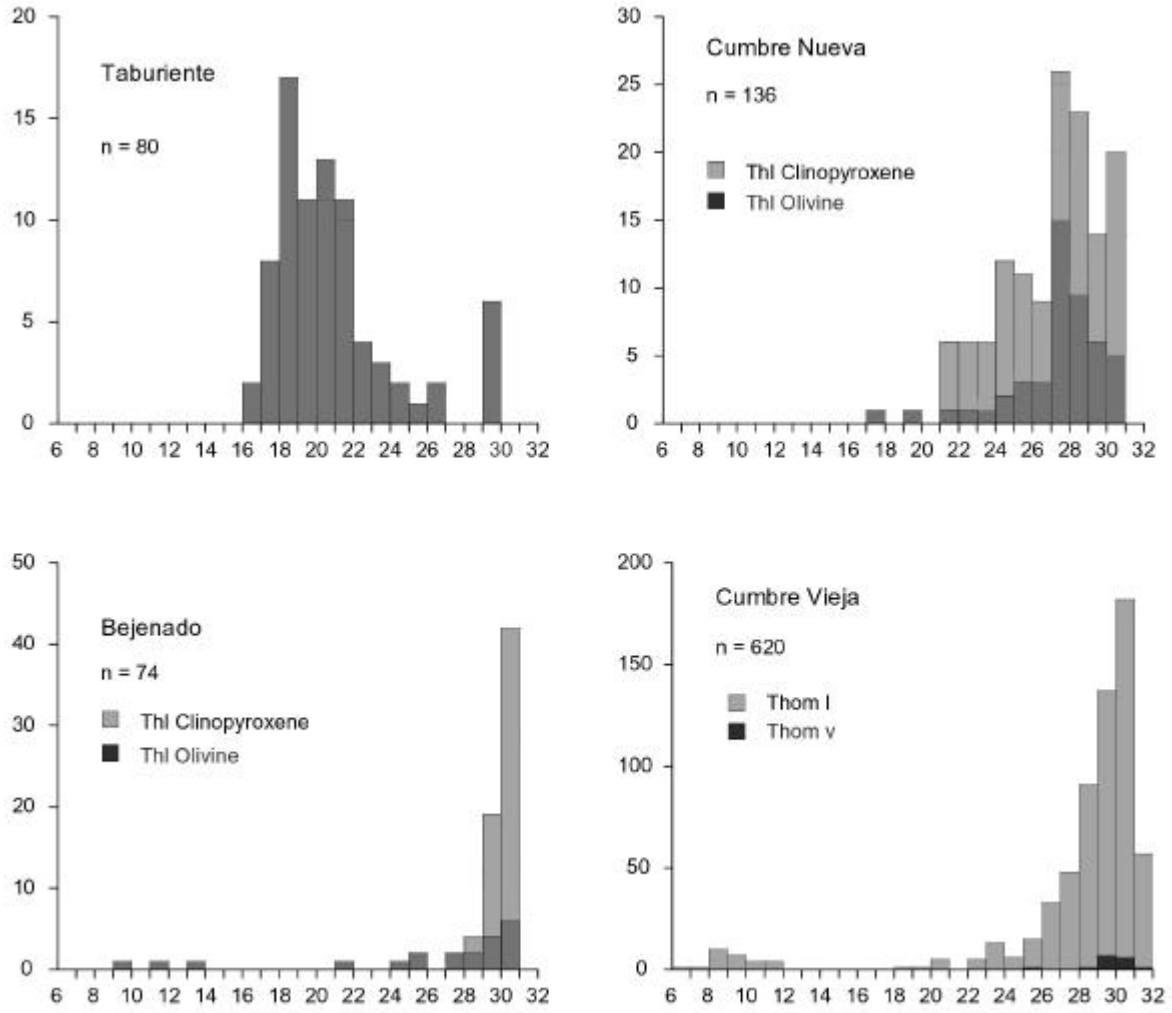

Fig. 4 Measured homogenisation temperatures of CO_2-dominated fluid inclusions in phenocrysts and xenoliths from La Palma. Data for the Cumbre Vieja are from Klügel et al. (1997, submitted) and Hansteen et al. (1998). Thl: homogenized into liquid, Thv: homogenized into vapour; n: number of inclusion studied

Homogenization temperatures and densities of fluid inclusions

The measured homogenization temperatures and melting points of all inclusions are presented in Fig. 3 and 4 and the resulting inclusion densities in Fig. 5. Inclusion densities and homogenization temperatures show distinct maxima in their frequency distributions.

Taburiente volcano: Fluid inclusions in olivines of two dunite xenoliths were investigated. Both primary and secondary inclusions of sample KLA 1-8-04 homogenized into liquid at 16.1 to 21.6 °C corresponding to densities between 0.81 and 0.75 g/cm^3. In sample KLA 1-8-03, all inclusions gave higher homogenization temperatures between 19.6 and 29.8 °C corresponding to densities of 0.77 to 0.59 g/cm^3. These ranges overlap with data of

Nikogosian et al. (2002) who carried out fluid inclusion studies in olivine-clinopyroxene phyric Taburiente lavas erupted at 700 ka.

Cumbre Nueva: Primary and secondary fluid inclusions in olivine and clinopyroxene phenocrysts in ankaramites yield Th_l ranging from 17.4 to 30.8 °C. Compared to samples from Taburiente, homogenization temperatures tend to higher values. One sample showed CO_2 melting intervals of -59.1 to -57.3 °C for a small number of inclusions indicating the presence of minor amounts of additional components such as N_2, CH_4 or SO_2, which were also found in some xenoliths from other Canary Islands e.g. Lanzarote (N_2, Andersen et al. 1995) and Tenerife (SO_2, Frezzotti et al., 2002). Homogenization temperatures of fluid inclusions in this sample tend to lower values (average 24.2 °C) than the four other Cumbre Nueva samples (averages between between 25.2 and 30.0 °C). In summary, the Cumbre Nueva inclusion data correspond to an average density of 0.67 g/cm^3 with 90% of the values fallingbetween 0.56 and 0.75 g/cm^3 (defined as 90% density interval).

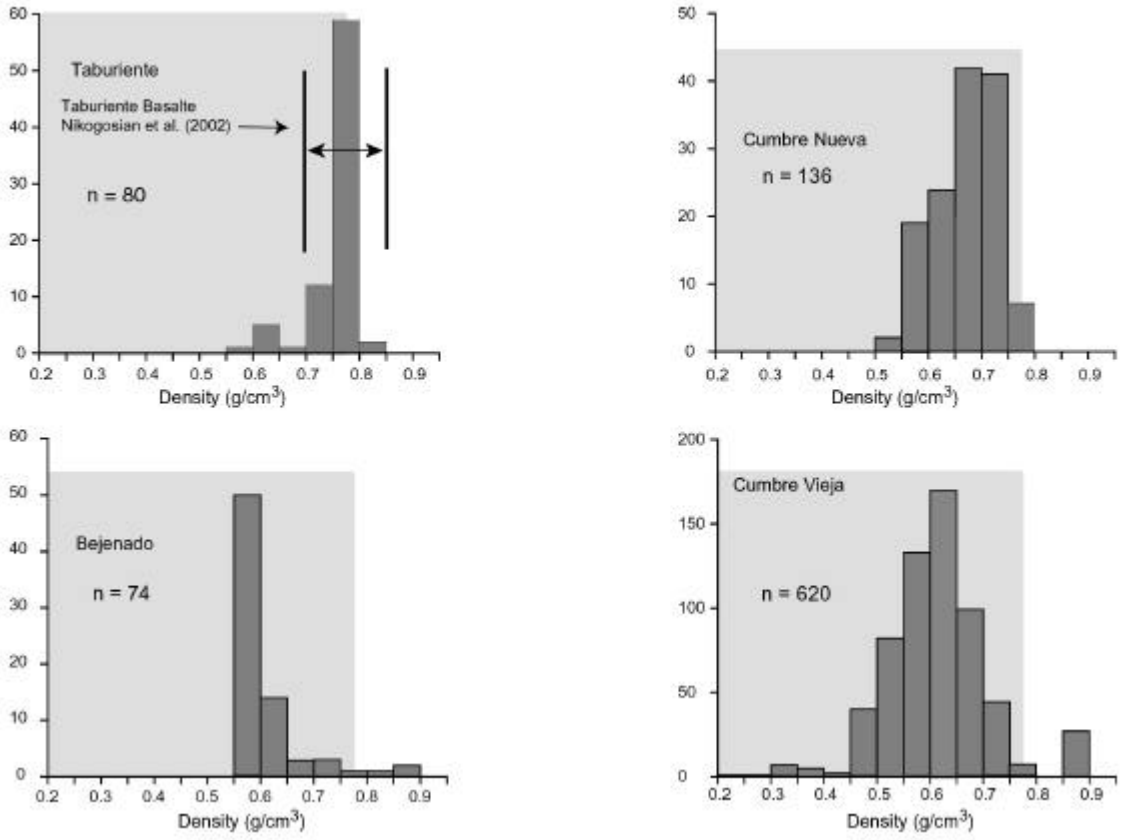

Fig. 5 Density distribution of CO_2-dominated fluid inclusions in phenocrysts and xenoliths studied. Densities were derived from measured homogenization temperatures after Angus et al. (1976). Grey field represent densities of fluid formation or re-equilibration in the crust; n: number of inclusion studied

Bejenado volcano: Primary and secondary fluid inclusions in olivines and clinopyroxenes from ultramafic cumulate xenoliths homogenized into the liquid phase between 21.6 °C and 30.5 °C and secondary fluid inclusions in basanite phenocrysts between 9.9 to 13.7 °C. Corresponding inclusion densities are 0.55 - 0.75 g/cm^3 and 0.83 - 0.86 g/cm^3, respectively, with a distinct frequency maximum between 0.71 and 0.56 g/cm^3. In contrast to fluid inclusion data from Taburiente and Cumbre Nueva the density distribution is assymmetric and non-Gaussian. Some fluid inclusions in Bejenado samples showed triple points at about -57.0 °C but no homogenization could be observed. We suspect that some of these inclusions homogenized into the vapour phase but could not be optically recognized.

Cumbre Vieja: CO_2 inclusions in olivine and clinopyroxene phenocrysts as well as in peridotite, ultramafic cumulate and MORB gabbro xenoliths were analyzed in earlier studies (Klügel et al., 1997; Hansteen et al., 1998; Klügel et al.,submitted). Inclusion densities in Cumbre Vieja samples define three distinct ranges: (1) 0.25 to 0.47 g/cm^3 indicated by some MORB-gabbro xenoliths, (2) 0.47 to 0.79 g/cm^3 which is the main range showing a Gaussian distribution, and (3) 0.85 to 0.88 g/cm^3 restricted to inclusions in olivine phenocrysts in basanites. Compared to olivine phenocrysts,
inclusions in clinopyroxenes have lower densities of 0.47 to 0.65 g/cm^3 and overlap with the main range for the different xenoliths types of the Cumbre Vieja.

Pressure of inclusion formation

Pressures of inclusion formation or re-equilibration corresponding to calculated densities were derived from isochores using the Kerrick and Jacobs (1981) equation of state for pure CO_2. We assumed a model temperature of 1150 °C based on clinopyroxene-melt-thermometry (see below). We note that variations in model temperature have only little effect on calculated pressures because the calculated CO_2-isochores have moderately positive slopes at high temperatures.

Generally, our calculated pressures represent minimum values because all post-entrapment processes tend to lower the inclusion densities. In particular, the former density may be reduced by H_2O removal through diffusion or in-situ hydration reactions. If the entrapped fluid had contained a maximum H_2O fraction of 10 % for all inclusions, isochores for the system CO_2-H_2O rather than for pure CO_2 would result (Kerrick and Jacobs, 1981). For an inclusion density range between 0.25 and 0.89 g/cm^3 as observed in La Palma samples, the resulting pressures would increase from 0.09 - 0.65 (pure CO_2) to 0.09 - 0.81 GPa ($H_2O/(H_2O+CO_2)$ = 0.1), i.e. by 0 to 24%. As outlined above, however, we present only uncorrected data calculated for pure CO_2.

Fluid inclusion densities of Taburiente samples yield pressures between 0.52 and 0.32 GPa with a distinct peak around 0.50 GPa (Fig. 5, Fig. 6). The calculated pressures overlap with the Moho, which is interpreted to be located at 14-15 km depth beneath the western Canary Islands (Banda et al., 1981, Ranero et al., 1995).

Compared to Taburiente, fluid inclusion data from Cumbre Nueva generally give lower pressures between 0.20 GPa and 0.50 GPa (average 0.35 GPa) *w*ith 90% of the data points falling between 0.25 and 0.45 GPa. Fluid inclusion densities from Bejenado yield pressures ranging from 0.20 to 0.60 GPa with a distinct maximum at 0.20 to 0.30 GPa. The pressures thus overlap with those inferred for Taburiente and Cumbre Nueva but show different frequency distribution: whereas the maximum for Bejenado is around 0.25 to 0.30 GPa, those for Taburiente and Cumbre Nueva are around 0.40 to 0.50 and 0.25 to 0.45 GPa, respectively.

Densities indicated by fluid inclusions in different rocks from Cumbre Vieja yield three pressure ranges: (1) 0.10 to 0.15 GPa interpreted to reflect shallow crustal reservoirs, (2) a dominant pressure range from 0.20 to 0.42 GPa (average 0.30 GPa), and (3) 0.60 to 0.65 GPa indicated by fluid inclusions in olivine phenocrysts from a historic basanite.

Clinopyroxene-melt thermobarometry

Temperatures and pressures of clinopyroxene crystallization were determined using the two clinopyroxene-melt thermobarometers of Putirka et al. (1996; 2003), hereafter refered to as PT96 and PT03, repectively. These are based on the exchange of jadeite/diopside/hedenbergite components between clinopyroxene and melt at equilibrium conditions. The two thermobarometers differ in the composition of the melts used for their calibration. The first model (PT96) was calibrated on dry basaltic and basanitic liquids and is more suited for basaltic compositions. The second model (PT03) was calibrated on basaltic to trachyandesitic melts and can be applied to a wider range of dry and hydrous compositions (basalts - dacites). According to Putirka et al. (2003), the mean prediction errors for both thermobarometers are $\pm$ 33 K and $\pm$ 0.17 GPa.

Clinopyroxene compositions were determined by analyzing 3 to 14 points at the rims of euhedral phenocrysts and averaging the values for each crystal. Clinopyroxenes showing sector zoning were avoided. As an independent check whether the measured clinopyroxene rim compositions are in equilibrium with the corresponding glass compositions, the empirical relation after Duke (1976) was applied:

$$\log(Fe_{tot}/Mg)_{cpx} = -0.564 + 0.755*\log (Fe_{tot}/Mg)_{liq}$$

If the discrepancy between measured and calculated $\log(Fe_{tot}/Mg)_{cpx}$ was significant for a single rim analysis or an entire crystal, the data were discarded in our study.

Pressures obtained with PT96 generally yield slightly higher pressure ranges than the newer PT03 formulation (0 - 0.15 GPa, Table 2), but the differences between both thermobarometers are still within the mean prediction error of ± 0.17 GPa. We therefore use the Putirka et al. (2003) formulation throughout our study in order to obtain a better intercomparability between basalts and more evolved La Palma samples. Likewise, the published data for the samples from Cumbre Vieja (Klügel et al., submitted) were recalculated in the present study. Tephriphonolitic (KLP 38) and phonolitic glass samples (KLP 115) show quite high deviations between both thermobarometers of 0.18 GPa and 0.47 GPa, respectively. This could be ascribed to their glass compositions, which are highly evolved, alkalic and far outside the calibration range, as well as to the high acmite ($NaFe^{3+}Si_2O_6$) content of the clinopyroxene phenocrysts. Acmite is a common component in clinopyroxenes of evolved alkalic melts and is not considered by the thermodynamic model of Putirka et al. (1996; 2003), as this assigns all Na to the jadeite component.

Calculated pressures

Taburiente Volcano: The samples from Taburiente yield pressures between 0.60 and 1.04 GPa (Fig. 6). This pressure range partly overlaps with data of Nikogosian et al. (2002) who applied the geothermobarometer of Putirka et al. (1996) to melt inclusions and their host clinopyroxenes from olivine-clinopyroxene-phyric Taburiente lavas. Pressure data from these samples lie between 0.94 and 1.14 GPa and thus tend to slightly higher values, probably because the isolated melt inclusions represent a previous stage of melt composition in equilibrium with clinopyroxene phenocrysts at deeper mantle levels.

Cumbre Nueva: Cumbre Nueva samples give a pressure range between 0.47 and 0.84 GPa (Fig. 6) with a frequency maximum at 0.60 to 0.75 GPa. Exception is sample KLP 35 indicating pressures between 1.10 and 1.17 GPa clearly above those of all other Cumbre Nueva samples. Petrographic observations of this sample give no indication of disequilibrium between clinopyroxene rims and melt, and equilibrium is also confirmed by the evaluation after Duke (1976) showing no inconsistency between measured and predicted $\log(Fe_{tot}/Mg)_{cpx}$.

The tephriphonolitic sample KLP 38 was considered in our study despite its highly evolved glass composition, because the pressure calculations for this sample (0.47 to 0.6 GPa) are within the range of other Cumbre Nueva samples.

Bejenado Volcano: Basanitic to phonotephritic samples from Bejenado yield a well-defined pressure range between 0.50 GPa and 0.78 GPa with a conspicuous peak around 0.60 GPa (Fig. 6). Pressures for phonolite KLP 115 were also tentatively calculated because Ablay et al. (1998) found that the Putirka et al. (1996) model could be used to constrain shallow fractionation levels for evolved rocks. Using the PT03 model, our data indicate a pressure

range for this sample of about 1.09 - 1.36 GPa. This pressures range for phonolites from Bejenado appears rather unlikely because it would imply that they evolved at deeper levels than the coeval basanites. More realistic results were obtained with the PT96 model which yields a pressure range from 0.51 - 0.95 GPa completely overlapping the range for other Bejenado samples. Given that the results of both barometers for this sample are very different and that the PT96 model is not calibrated for phonolites, pressure estimates after PT96 are considered as very approximate and are not incorporated in Fig. 6 and 7.

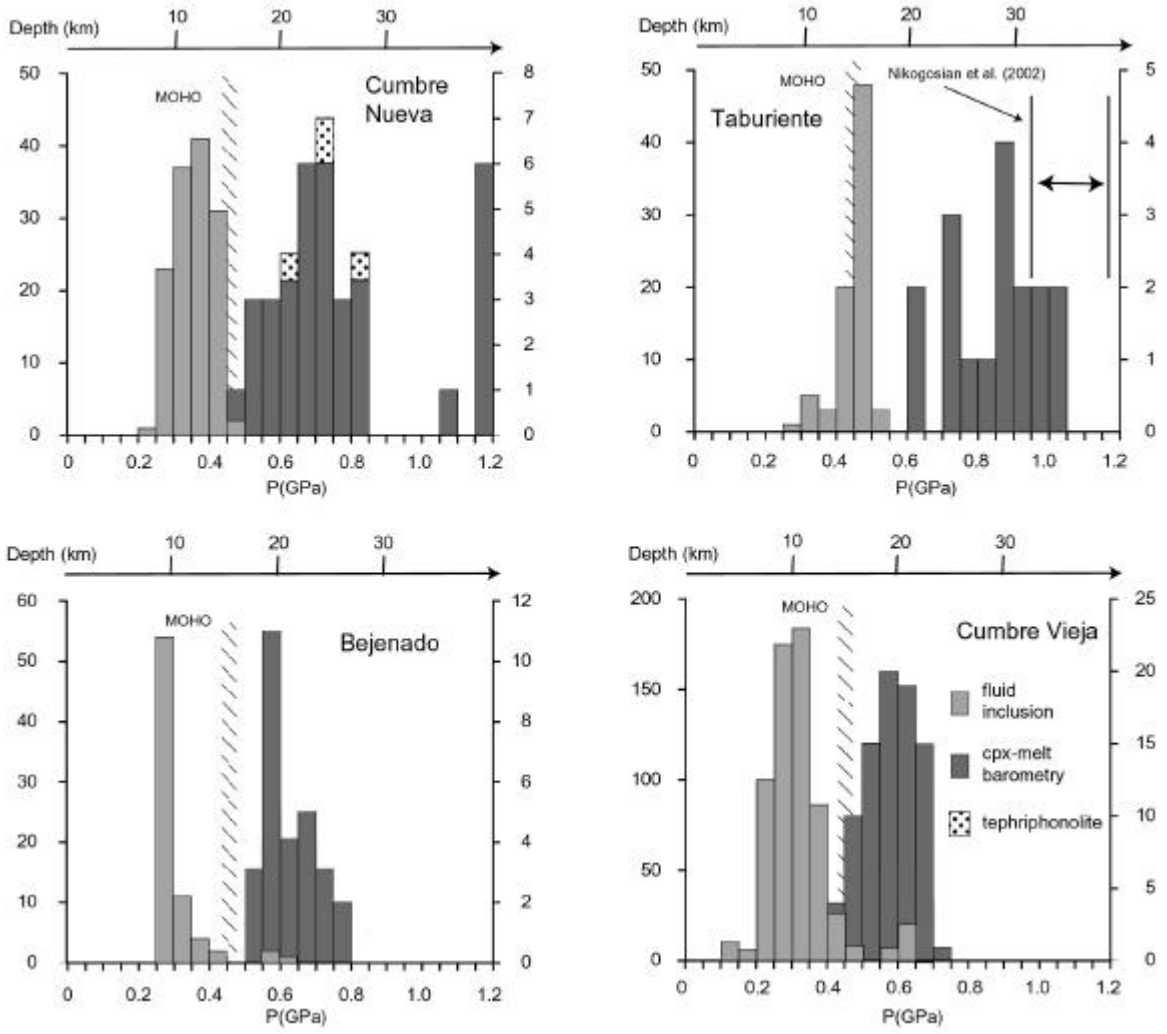

Fig. 6 Calculated pressures of clinopyroxene phenocrysts in rocks from La Palma samples infered by clinopyroxene-melt thermobarometry together with pressures of fluid inclusion formation. Each value (right ordinate) represents the pressure derived for a single clinopyroxene phenocryst using its average rim composition. Pressures of fluid inclusion formation were calculated for a model temperature of 1150 °C and pure CO_2 using the Kerrick and Jacobs (1981) equation of state. Data for Cumbre Vieja from Klügel et al. (submitted), and references therein. Depth of Moho after Ranero (1995). Dotted bars represent values of tephriphonolitic sample (KLP 38).

Cumbre Vieja: Clinopyroxene-melt thermobarometry applied to Cumbre Vieja samples yield pressures between 0.36 GPa and 0.73 GPa (summarized in Klügel et al., submitted) with a

near-Gaussian distribution and a frequency maximum at 0.45 GPa to 0.7 GPa. Compared to data from Taburiente, Cumbre Nueva and Bejenado, the Cumbre Vieja samples have a tendency to lower pressures.

Calculated temperatures

Temperatures calculated by clinopyroxene-melt thermobarometry range from 1110 °C to 1230 °C for basanites and 1020 °C to 1150 °C for tephrites and phonotephrites. For the phonolites KLP 115 and KLP 38 we obtain temperatures of 850 °C to 1040 °C and 1030 °C to 1130 °C respectively.

As an independent test of the data, calculated temperatures were compared to those derived from olivine-liquid equilibria (Table 2) (Roeder and Emslie, 1970; Roeder, 1974, Ford et al., 1983, Putirka, 1997). In general there is a good agreement between the clinopyroxene-liquid and olivine-liquid temperatures, the maximum difference being less than 80 °C.

5.3. Melt barometry

The pressures calculated by PT96 and PT03 were compared with pressure estimates using the empirical equation of Yang et al. (1996). This equation calculates temperature, Al, Ca, and Mg molar fraction of the melt as functions of Si, Fe, Na, Ti and K molar fractions and pressure. The Yang et al. (1996) model is appropriate for basaltic melts which are olivine-, plagioclase- and augite-saturated. All samples chosen for application of this barometer contain olivine, clinopyroxene and feldspar as phenocrysts or microphenocrysts. Samples with MgO < 4.3 wt% were not considered, because these samples are out of the calibration range of the Yang et al. (1996) equation.

It should be noted that the Yang et al. (1996) formulation was calibrated for mid-ocean ridge basalt (MORB) and not for silica-undersaturated alkalic basalts. Therefore pressure estimates for La Palma samples after the Yang et al. (1996) equation can be regarded as very approximate. In general, the data overlap only partly with the clinopyroxene-melt barometer data and indicate an overall decrease in pressure estimates from Taburiente (0.70 - 0.90 GPa) and Cumbre Nueva (0.40 - 0.90 GPa) to Cumbre Vieja (0.30 - 0.50 GPa) (Table 2). For Bejenado, pressures were not calculated because all samples were too low in MgO.

6. Discussion

6.1. Post-entrapment modification of fluid inclusions

Most fluid inclusion densities observed in xenoliths and phenocrysts do not reflect the original pressures and temperatures of inclusion formation. Fluid inclusions typically suffer post-entrapment modifications during magma ascent such as decrepititation and re-equilibration (e.g. Roedder, 1984; Hansteen et al., 1998; Andersen and Neumann, 2001) in response to

Table 2 Calculated temperatures and pressures of crystallization, obtained by geothermometers and geobarometers by (1) Putirka et al. (1996), (2) Putirka et al. (2003), (3) Putirka (1997), (4) Roeder (1974), (5) Roeder and Emslie (1970), (6) Ford et al. (1983) and (7) Yang et al. (1996). Samples in italic were analyzed by fusing the groundmass.

	Temperature (°C)						Pressure (GPa)		
Sample	(1) cpx-melt	(2) cpx-melt	(3) ol-melt	(4) ol-melt	(5) ol-melt	(6) ol-melt	(1) cpx-melt	(2) cpx-melt	(7) ol-plag-aug-melt
Taburiente									
KLP 66	1146	1130					0.70	0.6	
KLP 61	1172 - 1189	1179 - 1189	1225	1183	1188	1174	0.81 – 1.06	0.85 – 1.02	0.90
KLP 76	1144 - 1159	1126 - 1143	1189	1126	1134	1150	0.67 – 0.82	0.65 – 0.77	
KLP 63	1170 - 1174	1168 - 1173	1219	1176	1181	1172	0.86 – 0.89	0.88 – 0.90	
KLP 69									0.70
KLP 73									0.90
KLP 77	1200 - 1220	1210 - 1230	1238	1226	1238	1226	0.71 – 0.95	0.86 – 1.04	
Cumbre Nueva									
KLP 19	1158 - 1169	1152 - 1164	1192	1149	1157	1142	0.70 – 0.83	0.71 – 0.81	0.70
KLP 41	1149 - 1170	1138 - 1159	1184	1145	1155	1140	0.51 – 0.72	0.56 – 0.75	0.70
KLP 38	1110 - 1128	1035 - 1042					0.60 – 0.90	0.47 – 0.60	
KLP 80	1160 - 1171	1166 - 1177	1193	1161	1173	1150	0.56 – 0.69	0.55 – 0.65	0.40
KLP 35	1205 - 1212	1213 - 1218	1244	1210	1214	1206	1.05 – 1.17	1.10 – 1.17	0.90
KLP 89	1151 - 1169	1147 - 1165	1194	1158	1168	1152	0.52 – 0.72	0.58 – 0.73	0.70
KLP 103	1204 - 1212	1226 - 1234	1234	1216	1231	1210	0.76 – 0.87	0.76 – 0.84	
Bejenado								0.60 – 0.63	
KLP 112	1114 - 1123	1081 - 1091	1145	1054	1061	1098	0.66 – 0.77	0.60 – 0.68	
KLP 113	1137 - 1142	1107 - 1112	1168	1076	1084	1110	0.85 – 0.91	0.73 – 0.78	
KLP 106	1143 - 1148	1124 - 1130	1161	1087	1097	1100	0.74 – 0.80	064 – 0.69	
KLP 6	1100 - 1108	1054 - 1063					0.60 – 0.69	0.55 – 0.61	
KLP 6A	1106 – 1115	1056 – 1065					0.57 – 0.70	0.50 – 0.60	
KLP 115*	*1007 – 1040*	*846 - 867*					*0.51 – 0.95*	*1.09 – 1.36*	
Cumbre Vieja									
POS 169-9	1127 - 1137	1113 - 1121	1139	1077	1087	1102	0.49 – 0.60	0.47 – 0.56	0.50
POS 170-2	1123 - 1127	1108 - 1113	1143	1075	1084	1114	0.52 – 0.57	0.52 – 0.55	0.50
POS 155-1	1131 - 1135	1105 - 1113	1139	1055	1064	1124	0.63 – 0.73	0.58 – 0.67	0.40
POS 164-	1121 - 1128	1059 - 1065					0.67 – 0.75	0.60 – 0.66	
POS 165-3	1128 - 1135	1117 - 1125	1135	1070	1079	1104	0.52 – 0.59	0.48 – 0.53	0.40
M43 658-2	1138 - 1150	1151 - 1163	1155	1120	1130	1122	0.41 – 0.54	0.38 – 0.48	0.30
M43 660-2	1130 - 1153	1140 - 1163	1151	1109	1119	1116	0.38 – 0.64	0.36 – 0.56	0.30
M43 639-1	1149 - 1158	1157 - 1164	1160	1113	1123	1116	0.62 – 0.73	0.57 – 0.65	0.50
KLA 1507	1116 - 1142	1109 - 1132	1165	1107	1115	1120	0.44 – 0.77	0.45 – 0.69	
KLA 1502	1085 -1122	1018 - 1046					0.28 – 0.75	0.37 – 0.70	
KLA 1620	1109 - 1130	1080 - 1090					0.42 – 0.65	0.44 – 0.61	
KLA 1653	1098 - 1119	1062 - 1082					0.42 – 0.65	0.44 – 0.61	
KLA 1690	1126 - 1142	1130 - 1146					0.58 – 0.77	0.54 – 0.68	
KLA 1646	1105 - 1133	1069 - 1092					0.51 – 0.86	0.48 – 0.73	

*Pressure and temperature calculations are considered as unrealistic because sample is highly evolved

changing pressure and temperature. Both processes readjust the internal pressure of the fluid inclusions towards the new ambient conditions. Another process which can modify inclusion densities is non-decrepitative CO_2 leakage by diffusion along dislocations in host minerals. This process can occur within days, even when no decrepitation is visible (Wanamaker and Evans, 1989; Wanamaker et al. 1990). Different densities of fluid inclusions in coexisting clinopyroxenes and olivines may result because leakage occurs more readily in clinopyroxene due to its better cleavage, as was shown for a historic Cumbre Vieja basanite (Hansteen et al., 1998).

Non-decrepitative CO_2 leakage by diffusion along dislocations in olivine and clinopyroxene is unlikely to have occurrred in our samples because (i) the density histograms (Fig. 5) show tight density distributions (cf. Viti and Frezzotti, 2000) and (ii) fluid inclusions in olivines and clinopyroxenes have largely overlapping densities.

6.2 Depths of magma stagnation and fractionation

A conspicuous feature of our data set is that clinopyroxene-melt barometry and fluid inclusion barometry show two well-defined pressure ranges, and minor overlap, at all studied volcanic edificies (Fig. 6). The fluid inclusion data largely indicate pressures above or close to the Moho, whereas clinopyroxene-melt data yield rather higher pressures within the upper mantle. Although such bimodal pressure distribution may suggest a systematic bias between both methods used, we note that the obtained pressures are realistic because the systematic error for fluid inclusion data is minor (see section 4) and would not affect the bimodality observed. Furthermore, previous studies have shown that both methods can actually yield overlapping data sets (Nikogosian et al., 2002; Schwarz et al., 2004).

Pressures obtained by clinopyroxene-melt barometry and melt barometry are interpreted as major levels of crystal fractionation. Since our pressure calculations reflect the last equilibration conditions of clinopyroxene phenocrysts prior to eruption, we do not preclude fractionation at deeper levels. Fluid inclusion data, in contrast, place constraints on the pressures at which they were entrapped or re-equilibrated during crystal growth or crack healing (Roedder and Bodnar, 1980; Roedder 1984). We interpret the pressures derived from fluid inclusion barometry as levels of magma stagnation, degassing and crystal fractionation at a corresponding range of depths. Since fluid inclusion densities can rapidly reequilibrate during magma ascent, the densities indicate depths of temporary magma stagnation (Frezzotti et al., 1992; Szabo and Bodnar, 1996; Hansteen et al., 1998) at shallower depths which was too short for the rather sluggish clinopyroxene-melt barometer to re-equilibrate. A similar model of fractionation in the upper mantle and short-term stagnation of ascending magmas in the lower crust was developed for the rift systems of Madeira archipelago (Schwarz et al., 2004).

During the early phase of subaerial volcanic activity of La Palma, the ascending magmas stagnated and differentiated to varying extents in the upper mantle beneath Taburiente. Our data suggest that tha last - if not major - fractionation occurred at depths between 19 - 34 km as indicated by clinopyroxene-melt barometry. This range largely overlaps with the depth range (32 - 39 km) of Nikogosian et al. (2002) (Fig. 6, Fig. 7). During ascent to the surface, magmas stagnated temporarily at 10 - 17 km depth as deduced by fluid inclusion data. This range overlaps with an inferred Moho depth of 14 - 15 km beneath the western Canary Islands (Banda et al., 1981, Ranero et al., 1995).

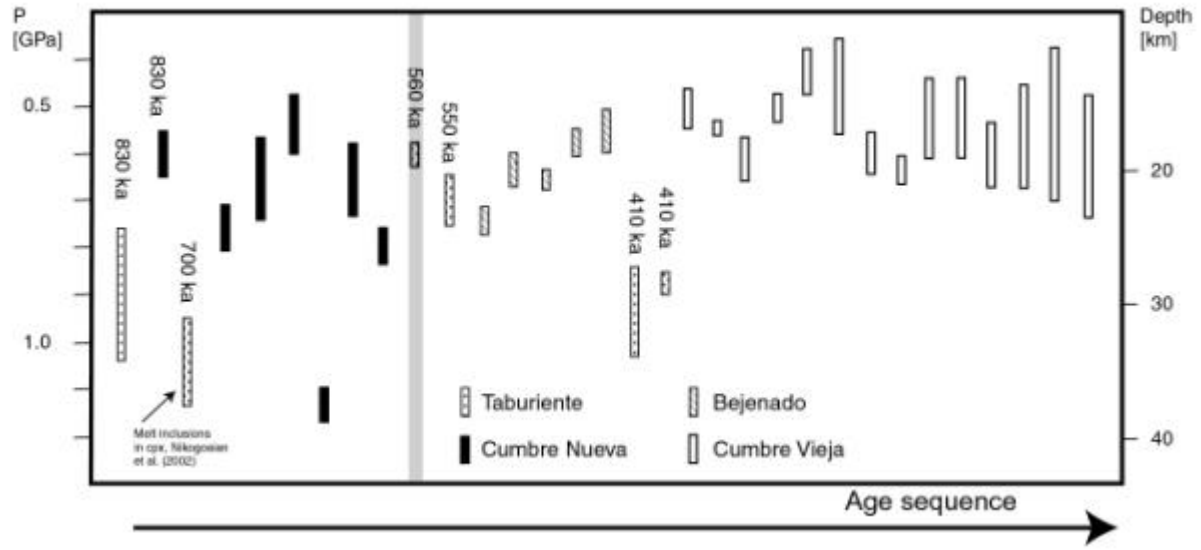

Fig. 7 Pressures calculated by clinopyroxene-melt thermobarometry arranged in sequential order. Each line represents the calculated pressure range for all analyzed phenocrysts of a single sample. Grey bar marks Cumbre Nueva collapse at about 560 ka. Sample ages are from Guillou et al. (1998, 2001) and Cumbre Vieja data are from Klügel et al. (submitted) and references therein. Undated samples are arranged in stratigraphical order based on field observations

During the evolution of the Cumbre Nueva rift zone from 800 ka until 560 ka, fractionation levels shifted slightly to shallower depths between 16 and 28 km (Fig. 6, Fig. 7). Fluid inclusion data for Cumbre Nueva ankaramites indicate that temporary stagnation levels for ascending magmas also became shallower, between 8 and 14 km. The magmas thus ponded no longer at the Moho but more within the lowermust crust.

For Bejenado, which was formed immediately after the Cumbre Nueva collapse (560 ka), the inferred fractionation levels were located in the uppermost mantle at 16 to 26 km depth and overlap with those for Cumbre Nueva. Still, some coeval Taburiente lavas fractionated at larger depths (Fig. 7). Fluid inclusions in ultramafic cumulates suggest that temporary stagnation levels for ascending Bejenado magmas were located within the lower crust at 8 to 14 km depth, which correspond with those beneath Cumbre Nueva but show a shift in frequency distribution towards shallower depths (Fig. 6).

After termination of volcanic activity at Taburiente around 410 ka, eruptions took place exclusively at the Cumbre Vieja rift from 125 ka to present. The final fractionation levels of magmas erupted at Cumbre Vieja are located at of 15 to 26 km depth, which overlaps well with the corresponding range for Cumbre Nueva with a slight tendency to shallower depths. Temporary magma stagnation levels derived from fluid inclusion densities exist at 7 to 14 km depth and also show perfect overlap with the respective Cumbre Nueva data (Fig. 6).

6.3 Is the Cumbre Vieja a separate volcanic system?

Since this study is concerned with the evolution of the magma plumbing systems of La Palma since 1.0 Ma, the spatial arrangement of the volcanoes must be taken into account. Based on models for other oceanic island volcanoes, three basic scenarios are envisioned (Fig. 8): Taburiente/Cumbre Nueva and Cumbre Vieja represent one single volcanic system with a central volcano from where magmas migrate laterally into the rift zone either within the crust (Model A) or within the upper mantle (Model B), or Taburiente/Cumbre Nueva and Cumbre Vieja represent two separate volcanic systems with independent magma plumbing systems (Model C).

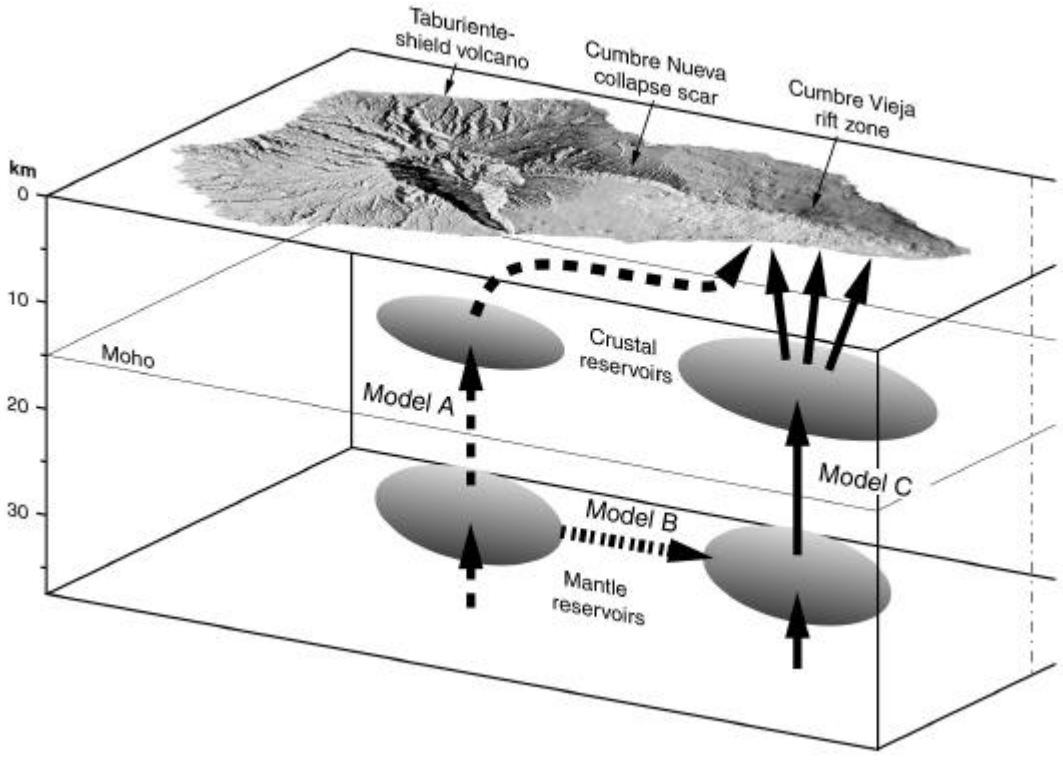

Fig. 8 Schematic illustration of different end-member models for magma ascent beneath Cumbre Vieja. A: Magmas ascend beneath Taburiente and lateral move laterally within the crust (dashed line). Model B: Magmas ascend beneath Taburiente and move laterally within the uppermost mantle (dotted line). Model C: The Cumbre Vieja rift represent a separate volcano with its own magma plumbing system independent of Taburiente (solid line).

Models A and B are typical of oceanic island volcanoes such as at Hawaii (Kilauea, Mauna Loa: e.g. Fiske and Jackson, 1972) or the Canary Islands (Tenerife; Carracedo, 1994). Their rift systems are characterised by a multiple rift arm configuration and a central volcano. The rift zones are fed by lateral injections from a shallow magma chamber beneath the central volcano mostly along dikes (e.g. Ryan, 1988, Garcia et al., 1995; Yang et al., 1999). For La Palma, Carracedo et al. (2001) also postulate a triaxial rift arm configuration with Taburiente representing a central volcano that developed two subordinate rift arms to the northwest and northeast and a major rift arm (the Cumbre Nueva and the younger Cumbre Vieja rifts) to the south.

Cumbre Vieja is closely interconnected with Taburiente and Cumbre Nueva

The following observations are in accordance with hypotheses A and B (Fig. 8) which call for an interconnection between the Taburiente/Cumbre Nueva and Cumbre Vieja volcanic systems:

(1) Temporary magma stagnation levels within the lowermost crust for Cumbre Vieja (7 - 14 km) inferred from fluid inclusion studies show a strong overlap with those of Cumbre Nueva (8 - 14 km; Fig. 5, Fig. 6). This may suggest that both rift systems shared a common magma reservoir. Alternatively, magma could have been transported laterally at those depths, possibly along the oceanic crust-mantle boundary. Such a scenario is mechanically plausible and has been proposed for Hawaiian rift zones (Garcia et al.; 1995; Yang et al., 1999).

(2) Although Taburiente/Cumbre Nueva and Cumbre Vieja were not contemporaneously active, the inferred fractionation levels of both volcanic edifices overlap between 16 and 24 km which may reflect a common system of magma reservoirs during the last 1000 ka.

(3) Seismic precursors of some historical eruptions appear to have migrated from the southern rim of the Caldera de Taburiente to the south of the island (Klügel et al., 1999). Such propagation of seismicity could indicate that magmas first ascended beneath Taburiente and then moved southward into the Cumbre Vieja edifice.

(4) The occurrence of syenitic xenoliths in Cumbre Vieja lavas (Klügel et al., 1999) may indicate that magma ascended beneath Taburiente and moved laterally southwards within the crust (Fig. 8, Model A). These xenoliths may represent fragments from the basal complex underlying Taburiente, where the only outcrops of syenites on La Palma are exposed (Staudigel and Schmincke, 1984).

(5) On the basis of analogue gelatin experiments, Walter and Troll (2003) confirm the hypothesis of Carracedo et al. (2001) that the structures of rift zones on La Palma developed early in the island's history and express a strong genetic connection between the Taburiente and Cumbre Vieja volcanoes. Their hypothesis suggests that volcanism at Cumbre Vieja is

closely related to that at Taburiente and Cumbre Nueva through a common magma plumbing system (Fig. 9, Model A and B).

Cumbre Vieja is an independent volcanic edifice

In contrast, the following observations rather support Model C (Fig. 8) regarding Taburiente and Cumbre Vieja as two distinct volcanoes.

(1) The exposed contact between the Cumbre Nueva and the Cumbre Vieja is characterised by a morphological unconformity where the southern part of the Cumbre Nueva is buried by the younger Cumbre Vieja lavas that form an individual edifice. Such an unconformity is typical of two overlapping volcanoes but less so of Cumbre Vieja being the continuation of Taburiente/Cumbre Nueva.

(2) After eruptions ended at Taburiente around 410 ka, volcanic activity on La Palma was completely confined to Cumbre Vieja and no eruptions occurred between both volcanoes. This observation is hard to reconcile with lateral movement of magma from Taburiente to the south, since in this case eruptions along both Cumbre Nueva and Cumbre Vieja would be expected.

(3) Our observation of systematic lithological differences between samples from Taburiente/Cumbre Nueva and those from Cumbre Vieja suggests different magma evolution (see section 3, Table 1). Most noteworthy are the common occurrence of phonolitic lavas and intrusions, the absence of ankaramites, and the abundance of mantle and crustal xenoliths at Cumbre Vieja. These differences may indicate different depths and timescales of fractionation and stagnation during ascent of Taburiente and Cumbre Vieja magmas, which is best explained by distinct magma transport systems.

(4) Although the last fractionation levels of lavas erupted at Cumbre Vieja indicated by clinopyroxene-melt equilibria) overlap partly with those of Taburiente and Cumbre Nueva (Fig. 6, Fig. 7), it is difficult to envisage a common, widespread magma reservoir at these depths. Such a large reservoir would homogenize distinct magma batches entering it, which is not in accordance with petrographical and geochemical data (Klügel et al., 2000). The alternative would be lateral magma transport within the upper mantle, but this is possible only where an appropiate stress field exists or where the horizontal compressive stress is higher than the vertical stress so that horizontal intrusions may form (Gudmundsson, 1990; 1995). Since both possibilities appear rather unlikely for the mantle beneath La Palma, the magmas should rise subvertically in accordance with Model C.

After considering all arguments discussed above, we favour Model C where the Cumbre Vieja is a volcanic edifice on its own with a magma plumbing system different from those of Taburiente/Cumbre Nueva and Bejenado. The present morphology is thus the result of two

overlapping major volcanic edifices rather than southward growth of Taburiente shield volcano.

6.4 Evolution of the magma plumbing system

Our model illustrated in Fig. 9 shows the evolution of magma plumbing beneath La Palma from 1.0 Ma to presentbased on our thermobarometric data. During all volcanic phases, two distinct storage systems characterize the magma pathways: (1) a system of prolonged storage within the upper mantle and (2) a system of short-term stagnation within the crust above or close to the Moho. Our data indicate that both the mantle and crustal storage systems show an upward migration from 1.0 Ma to present.

During southward growth of Taburiente along the Cumbre Nueva erift zone since 800 ka, the shift of the magma plumbing system to shallower depths is most evident (Fig. 7 and 9). We suggest that this trend is analogous to the progressive evolution of magma-storage systems to shallower depths proposed for Hawaiian volcanoes (Clague, 1987). These volcanoes pass through sequences of four eruptive stages characterized by distinct lava types and magma supply rates which are a function of the proximity to the center of the hotspot. When the magma supply rate and heat transfer are high during the tholeiitic shield stage, Hawaiian volcanoes build up rift zones and magma chambers form at shallower depths (Clague and Dixon, 2000). Certainly, the model for Hawaiian volcanoes is not directly transferable to La Palma because magma supply rates differ by up to two orders of magnitude (Moore and Clague, 1992; Carracedo et al., 1999) and are not high enough for La Palma to develop and maintain a long-lived shallow magma chamber, a characteristic feature of Hawaiian volcanoes. Nevertheless, the analogy of reservoirs migrating to shallower depths with time is remarkable.

Bejenado volcano (560 - 490 ka) also shows a shift of magma storage zones to slightly shallower levels as compared to Taburiente and Cumbre Nueva (Fig. 9C). This is in accordance with our petrological data and field observations indicating a change in fractionation conditions beneath Bejenado (Table 1), where the arrival of plagioclase phenocrysts, the absence of ankaramites and the increasing occurrence of differentiated rocks are particularly noteworthy. It seems that the differentiated rocks of Bejenado evolved in the mantle rather than the crust, because our approximate pressure estimates of phonolitic sample KLP 115 are between 0.51 and 0.95 GPa. It is thus likely that magma was stored in isolated magma “batches” in the uppermost mantle with residence times long enough to fractionate phonolites. This is in contrast with the neighboring island of Tenerife where phonolitic rocks evolved in long-term crustal reservoirs during times of limited mafic magma supply (Ablay et al., 1998). The tendency at Bejenado towards more differentiated magmas may also indicate increasing solidification of reservoirs as magma supply rates decrease (cf.

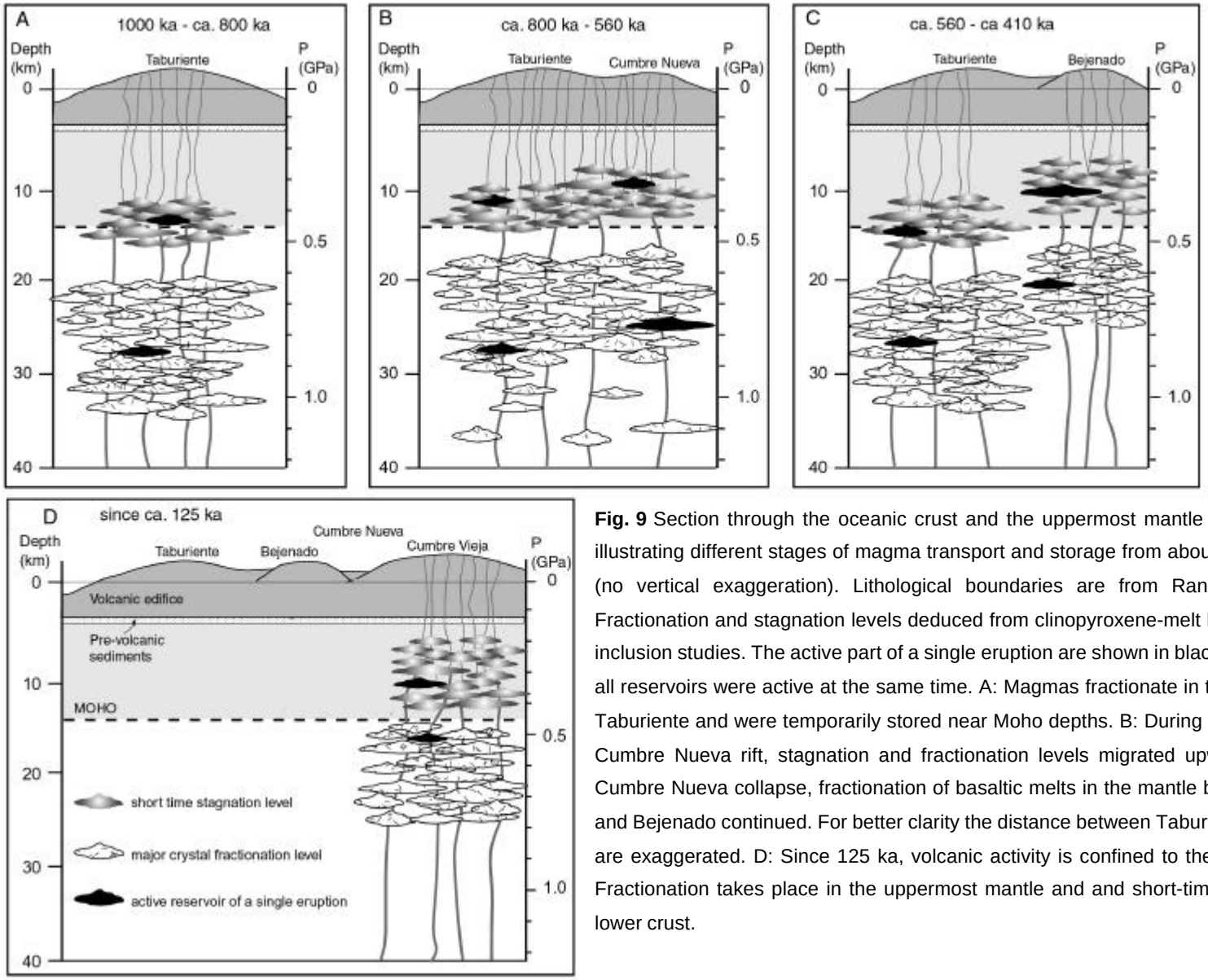

Fig. 9 Section through the oceanic crust and the uppermost mantle beneath La Palma illustrating different stages of magma transport and storage from about 1.0 Ma to present (no vertical exaggeration). Lithological boundaries are from Ranero et al. (1995). Fractionation and stagnation levels deduced from clinopyroxene-melt barometry and fluid inclusion studies. The active part of a single eruption are shown in black, meaning that not all reservoirs were active at the same time. A: Magmas fractionate in the mantle beneath Taburiente and were temporarily stored near Moho depths. B: During the evolution of the Cumbre Nueva rift, stagnation and fractionation levels migrated upwards C: After the Cumbre Nueva collapse, fractionation of basaltic melts in the mantle beneath Taburiente and Bejenado continued. For better clarity the distance between Taburiente and Bejenado are exaggerated. D: Since 125 ka, volcanic activity is confined to the Cumbre Vieja rift. Fractionation takes place in the uppermost mantle and and short-time stagnation in the lower crust.

Clague and Dixon, 2000). Likewise, the terminal eruptions (~410 ka) of Taburiente are also characterized by accumulation of more differentiated lavas (Carracedo et al., 2001) as magma supply rates decreased. Fractionation levels during the final activity at Taburiente, however, are significantly deeper than those of Bejenado (Fig. 7), which indicates that both volcanoes had distinct plumbing systems despite their very close proximity. This observation illustrates the fundamental modifactions of the magmatic system beneath Taburiente after the Cumbre Nueva collapse and during the evolution of Bejenado.

During the activity of Cumbre Vieja from 125 ka to present, our data indicate that the magma storage zones in the uppermost mantle (15 - 26 km) and within the crust (7 - 14 km) have become again shallower than during the older volcanic phases (Fig. 6 and 9D). In particular, a major stagnation level had developed within the gabbroic oceanic crust, which is consistent with the abundance of tholeiitic MORB gabbro xenoliths in many Cumbre Vieja lavas (Klügel et al., submitted). Whether this increasing importance of magma stagnation in the lower crust is related to the increasing occurrence of phonolites at Cumbre Vieja is plausible but still speculative, as the depths of phonolite formation are not yet known.

It is remarkable that the trend of stagnation and fractionation levels to migrate to shallower depths continues from 1 Ma to present even though Cumbre Vieja is located south of the older volcanoes and most likely represents a distinct volcano. The question arises, then, what has induced the gradual upward migration of the magma plumbing systems at La Palma. Possible explanations include changing levels of neutral buoyancy, of a stress barrier, of the brittle-ductile boundary or of a freezing horizon. Since a level of neutral buoyancy is not expected at depths of more than a few kilometers, we argue that the levels of magma stagnation are controlled by thermomechanical properties of the mantle and lower crust (cf. Clague and Dixon, 2000). These properties change during a volcano's long-term evolution through heating of the upper lithosphere by the plume and ascending melts, through metasomatic reactions modifying the composition and physical properties of mantle rocks, and through the introduction of fluids and melts in wall-rock. Another potentially effective process is stoping, i.e. engulfment of pieces of brittle wall rocks by magma. Evidence for magma emplacement by stoping could lie in the abundance of crustal and mantle xenoliths in Cumbre Vieja lavas. Although we don't know the relative importance of these processes during the evolution of La Palma, our data clearly indicate that they result in a net upward migration of magma holding reservoirs over time.

7. Conclusions

(1) Clinopyroxene-melt barometry and fluid inclusion studies provide insights into the magma plumbing systems of La Palma during its evolution from the Taburiente shield volcano to the present Cumbre Vieja rift. In all volcanic phases of La Palma we can identify

two distinct depth ranges of magma stagnation: (i) major fractionation levels in the upper mantle, and (ii) temporary stagnation levels in the lower crust close to the Moho.

(2) Our thermobarometric data yield a migration of inferred fractionation and stagnation levels to shallower depths from the earlier Taburiente shield volcano to the presently active Cumbre Vieja rift zone during the last 1.0 Ma.

(3) Our data suggest that the old Taburiente/Cumbre Nueva (>1.0 Ma to 410 ka) and young Cumbre Vieja (>125 ka to recent) volcanic systems are not fed by a common magma reservoir. Therefore we propose that both systems are not only spatially separated but also represent two distinct volcanoes with separate magma plumbing systems.

(4) None of the La Palma volcanoes shows any indicators of a high-level magma reservoir feeding the rift zones. This is an important difference to Hawaiian rift zones which are characterized by shallow subcaldera magma chambers from where rift zones emanate. The plumbing systems of La Palma rather show many similarities to those of Madeira Archipelago.

Acknowledgements. We gratefully acknowledge Director Félix Manuel Medina and the staff from the Unidad de Medio Ambiente and the Parque Nacional Caldera de Taburiente for their support during our field studies on La Palma and for permission to take samples. M. Thöner and B. Rajes are gratefully acknowledged for their help with sample preparation and/or analytical support. The paper strongly benefited from discussions with K. Hoernle and S. Schwarz. K. Freitag helped to improve the English of the manuscript. We also thank H. Guillou and J.C. Carracedo for providing us with details of sample locations. This study was supported by the Deutsche Forschungsgemeinschaft (DFG grant KL1313/4).

Appendix 1: Samples studied

Listed below are the sample locations and estimated phenocryst portions for basanitic to phonolitic lavas and xenoliths of this study.

Localities are grouped according to age and geological unit. Where possible to determine age and stratigraphic positions, the samples within each group are sorted by decreasing age. Samples from Cumbre Vieja are described in Klügel et al. (submitted) and references therein. Ages are taken from Guillou et al. (1998, 2001). cpx = clinopyroxene, ol = olivine, fsp = feldspar, amph = amphibole; cmp = clinopyroxene-melt barometry, Fl = fluid inclusion

Taburiente

Sample Number	UTM coordinates Altitude	Location	Age (ka)	Rock type	Phenocrysts	Applied method
KLP 61	209200/3181640 230 m	Playa de la Veta	410 ± 80	Basanite	cpx 10 %; ol 2%	cmp
KLP 63	209200/3181640 230 m	Playa de la Veta	410 ± 80	Basanite	cpx 2 %, ol 2%	cmp
KLP 66	206600/3184580 190 m	Puerto de Punta Gorda	563 ± 8	Basanite (lapilli)	Microphenocrysts of ol and cpx in vitreous matrix	cmp
KLP 73	233314/3181370 90 m	Coast of Puntallana (Pta. Salinas)	560 ± 8	Basanite	Microphenocrysts of ol and cpx	cmp
KLP 76	227805/3193540 m	Piscina de la Fajada	549 ± 12	Basanite	ol and cpx > 1 %	cmp
KLP 77	219932/319275260 m	La Fajana Barranco de los Hombres	833 ± 14	Basanite	ol and cpx > 1 %	cmp
KLP 69	220657/3185249 2210 m	Camino de Tamagantera	1080 ± 40	Basanite	ol 2 %, cpx 2 %	cmp
KLA 1-8-03	221800/3178700 450 m	Barranco de Angustias		Dunite	ol 100%	Fl
KLA 1-8-04	221800/3178700 450 m	Barranco de Angustias		Dunite	ol 100%	Fl

Cumbre Nueva

Sample Number	UTM coordinates Altitude	Location	Age (ka)	Rock type	Phenocrysts	Applied method
KLP 19	223409/3174371190 m	Camino Ermita La Pena	647 ± 10	Basanite	cpx 2 %, ol 1%	cmp
KLP 35	224111/3169291220 m	Eastern flank of Cumbre Nueva		Basanite	cpx 2 %, ol 2 %	cmp
KLP 38	222869/3170011177 m	Western flank of Cumbre Nueva		Phonotephrite (dyke)	Microphenocrysts of fsp and cpx in vitreous matrix	cmp
KLP 41	224111/3169291220 m	Western flank of Cumbre Nueva		Basalt	cpx 1 %, ol 1 %	cmp
KLP 89	223390/3170671060 m	Western flank of Cumbre Nueva		Basalt	ol 1 %, cpx 3 %	cmp
KLP 103	223375/3171461040 m	Western flank of Cumbre Nueva		Basalt	ol + cpx < 1 %	cmp
KLP 80	223520/3172481057 m	Western flank of Cumbre Nueva	834 ± 12	Basalt	ol 5 %, cpx 20 %	cmp
KLP 22	223559/3174391290 m	Camino Ermita La Pena		Ankaramite	cpx 30 %, ol 10 %	cmp, Fl
KLP 88	223214/3170351080 m	Western flank of Cumbre Nueva		Ankaramite (dyke)	cpx 30 %, ol 20 %	cmp, Fl
KLP 37	222869/3170011177 m	Western flank of Cumbre Nueva		Ankaramite	cpx 30 %, ol 30 %	cmp, Fl
KLP 26	223880/3174411420 m	Top of Cumbre Nueva ridge		Ankaramite	cpx 40 %, ol 10 %	cmp, Fl
KLP 84	223274/3172291032 m	Western flank of Cumbre Nueva		Basalt	cpx 15 %, ol 15 %	cmp, Fl

Bejenado

Sample Number	UTM coordinates Altitude	Location	Age (ka)	Rock type	Phenocrysts	Applied method
KLP 112	221485/317488 985 m	Road at southern flank		Basanite	cpx 25 %, ol 25 %, fsp 1 % in vitreous matrix	cmp, Fl
KLP 113	221225/317406 860 m	Road at southern flank		Basanite	cpx 30 %, ol 10 %, fsp 1 % in vitreous matrix	cmp
KLP 106	221297/317533 1090 m	Road at southern flank		Phonotephrite	cpx 15 %, ol 15 %, fsp 10% in vitreous matrix	cmp
KLP 6	219484/317679 1685 m	Trail to summit		Phonotephrite	cpx 8 %, ol 3 %, fsp 10 %, in vitreous matrix	cmp
KLP 6A	219484/317679 1685 m	Trail to summit		Tephrite	cpx 10 %, ol 3 %, fsp 15 % in vitreous matrix	cmp
KLP 115	220825/317578 1210	Road at southern flank		Phonolite	cpx 10 %, amph 10%, hauyne < 1 %, titanite < 1 % in vitreous matrix	cmp
KLP 6B	219484/3176791 1685 m	Summit		Pyroxenite	cpx 40%, amph 25, fsp 20%, ol 15%	Fl
KLP 216	216034/3175176 553 m	Western flank of Bejenado		Pyroxenite	cpx 70%, ol 30%	Fl
KLP 218	216627/3174620 523 m	Western flank of Bejenado		Pyroxenite	cpx 70%, ol 30%	Fl
KLP 218 A	216627/3174620 52 3m	Western flank of Bejenado		Pyroxenite	cpx 70%, ol 30%	Fl

Appendix 2

Xenolith petrography

KLA 1-8-04 and *KLA 1-8-03*: Dunites in a basanitic host lava from Barranco de las Angustias. The xenoliths consist of almost 100 % olivine up to 4.5 mm in size showing abundant fluid inclusions. Some grains are partly serpentinized. Olivines are subhedral to anhedral with inequigranular size distributions and interlobate grain boundaries. Intracrystalline deformation of some olivine grains is indicated by kink-bands. Host lava consists of a groundmass of clinopyroxenes, olivines, plagioclase laths and opaques and few olivine phenocrysts.

KLP 6B: Kaersutite-bearing pyroxenite from the summit of Pico Bejenado consisting of clinopyroxene (~40%), kaersutitic amphibole (~25%), feldspar (~20%) and olivine (~15%). Apatite, biotite and opaques are present as minor phases. Clinopyroxenes and olivines are commonly rimmed by kaersutite and/or biotite and contain patchy areas of clinopyroxene intergrown with amphibole or biotite. Locally, amphibole appears to have grown at the expense of clinopyroxene. Olivine appears as rounded grains poikilitically enclosed by clinopyroxenes and kaersutite which indicates a cumulate origin. Minerals are euhedral to subhedral and range in size from about 0.2 mm to 5 mm, and show only few fluid inclusions. Host lava shows a microlitic flow texture with aligned feldspar laths and kaersutite phenocrysts.

KLP 218, 218A, KLP 216: Olivine-bearing pyroxenites from Pico Bejenado consisting of clinopyroxene (~70 %), olivine (~30%) and minor amounts of opaques. A mixture of fine-grained interstitial opaques and brownish microlites occur throughout the xenoliths. Olivines

from 0.3 to 3 mm in size show curvlinear grain boundaries. Unzoned, subhedral to anhedral clinopyroxenes up to 5 mm in size give evidence of an adcumulate origin. Fluid inclusions are abundant in both mineral types.

References

Abdel-Monem, A., Watkins, N.D. and Gast, P.W., 1972. Potassium-argon ages, volcanic stratigraphy, and geomagnetic polarity history of the Canary Islands: Tenerife, La Palma and Hierro. American Journal of Science, 272: 805-825.

Ablay, G.J., Caroll, M.R., Palmer, M.R., Martí, J. and Sparks, S.J., 1998. Basanite-Phonolite Leneages of the Teide-Pico Viejo Volcanic Complex, Tenerife, Canary Islands. Journal of Petrology, 39(5): 905-936.

Albarède, F. et al., 1997. The geochemical regimes of Piton de la Fournaise Volcano (Réunion) during the last 530 000 years. Journal of Petrology, 38(2): 171-201.

Ancochea, A. et al., 1994. Constructive and destructive episodes in the building of a young Oceanic Island, La Palma, Canary Islands, and genesis of the Caldera de Taburiente. Journal of Volcanology and Geothermal Research, 60: 243-262.

Andersen, T., Burke, E.A.J. and Neumann, E.R., 1995. Nitrogen-rich fluid in the upper mantle: fluid inclusions in spinel dunite from Lanzarote, Canary Islands. Contributions to Mineralogy and Petrology, 120: 20-28.

Andersen, T. and Neumann, E.-R., 2001. Fluid inclusions in mantle xenoliths. Lithos, 55: 301-302.

Andersen, T., O'Reilly, S.Y. and Griffin, W.L., 1984. The trapped fluid phase in upper mantle xenoliths from Victoria, Australia: implications for mantle metasomatism. Contributions to Mineralogy and Petrology, 88: 72-85.

Angus, S. et al., 1976. International Tables of the Fluid State, Carbon dioxide, 3. Pergamon Press, Oxford, 385 pp.

Bakker, R.J. and Jansen, J.B.H., 1991. Experimental post-entrapment water-loss from synthetic CO2-H2O inclusions in natural quartz. Geochimica et Cosmochimica Acta, 55(8): 2215-2230.

Banda, E., Dañobeitia, J.J., Surinach, E. and Ansorge, J., 1981. Features of crustal structure under the Canary Islands. Earth and Planetary Science Letters, 55: 11-24.

Belkin, H.E. and De Vivo, 1993. Fluid inclusion studies of ejected nodules from plinian eruptions of Mt. Somma-Vesuvius. Journal of Volcanology and Geothermal Research, 58: 89-100.

Brown, P.E., 1989. FLINCOR: A fluid inclusion data reduction and exploration program (abstr), Second Biennial Pan-Am Conf Fluid Inclusions Prog Abstr, pp. 14.

Burruss, R.C., 1981. Analysis of phase equilibria in C-O-H-S fluid inclusions. In: L.S. Hollister and M.L. Crawford (Editors), Short course in fluid inclusions: applications to petrology. (Short course handbook vol 6). Mineral. Assoc. Can., pp. 101-137.

Carracedo, J.C., 1994. The Canary Islands: an example of structural control on the growth of large ocean-island volcanoes. Journal of Volcanology and Geothermal Research, 60: 225-241.

Carracedo, J.C., 1999. Growth, structure, instability and collapse of Canarian volcanoes and comparisons with Hawaiian volcanoes. Journal of Volcanology and Geothermal Research, 94: 1-19.

Carracedo, J.C., Badiola, E.R., Guillou, H., de La Nuez, J. and Pérez Torado, F.J., 2001. Geology and Volcanology of La Palma and El Hierro, Western Canaries. Estudios Geologicos, 57(5-6): 157-273.

Carracedo, J.C., Day, S.J., Guillou, H. and Gravestock, P., 1999. Later stages of volcanic evolution of La Palma, Canary Islands: Rift evolution, giant landslides, and the genesis of the Caldera de Taburiente. Geological Society of America Bulletin, 111(5): 755-768.

Clague, A.A. and Dixon, J.E., 2000. Extrinsic controls on the evolution of Hawaiian ocean island volcanoes. Geochemistry Geophysics Geosystems, 1.

Clague, D.A., 1987. Hawaiian xenolith populations, magma supply rates, and development of magma chambers. Bulletin of Volcanology, 49: 577-587.

De Vivo, B., Frezzotti, M.L., Lima, A. and Trigila, R., 1988. Spinel lherzolite nodules from Oahu island (Hawaii): a fluid inclusion study. Bulletin Minéralogique, 111: 307-319.

Delaney, P.T., Fiske, R.S., Miklius, A., Okamura, A.T. and Sako, M.K., 1990. Deep magma body beneath the summit and rift zones of Kilauea Volcano, Hawaii. Science, 247: 1311-1316.

Dixon, J.E., 1997. Degassing of alkalic basalts. American Mineralogist, 82: 368-378.

Duffield, W.A., Christiansen, R., L, Koyanagi, R.Y. and Peterson, D.W., 1982. Storage, migration and eruption of magma at Kilauea Volcano, Hawaii, 1971-1972. Journal of Volcanology and Geothermal Research, 13(3-4): 273-307.

Duke, J.M., 1976. Distribution of the period four transition elements among olivine, calcic clinopyroxene and mafic silicate liquid: experimental results. Journal of Petrology, 17: 499-521.

Duncan, R.A., Fisk, M.R., White, W.M. and Nielsen, R.L., 1994. Tahiti: geochemical evolution of a Prench Polynesian volcano. Journal of Geophysical Research, 99B: 24341-24357.

Eaton, J.P. and Murata, K.J., 1960. How volcanoes grow. Science, 132: 925-938.

Elliott, T.R., 1991. Element Fractionation in the Petrogenesis of Ocean Island Basalts. Ph.D. Thesis, The Open University, Milton Keynes.

Fiske, R.S. and Jackson, E.D., 1972. Orientation and growth of Hawaiian volcanic rifts: the effect of regional structure and gravitational stresses. Proceedings of the Royal Society of London, A 329: 299-326.

Ford, C.E., Russell, D.G., Craven, J.A. and Fisk, M.R., 1983. Olivine-liquid equilibria: Temperature, pressure and composition dependence of the crystal/liquid cation partition coefficients for Mg, Fe^{2+}, Ca and Mn. Journal of Petrology, 24(3): 256-265.

Frezzotti, M.L., Andersen, T., Neumann, E.-R. and Simonsen, S.L., 2002. Carbonatite melt CO_2 fluid inclusions in mantle xenoliths from Tenerife, Canary Island: a story of trapping, immiscibility and fluid-rock interaction in the upper mantle. Lithos, 64: 77-96.

Frezzotti, M.L., Burke, E.A.J., De Vivo, B. and Villa, I.M., 1992. Mantle fluids in pyroxenite nodules from Salt Lake Crater (Oahu, Hawai). European Journal of Mineralogy, 4: 1137-1153.

Garcia, M.O., Hulsebosch, T.P. and M, R.J., 1995. Olivine-rich submarine basalts from the southwest rift zone of Mauna Loa volcano: implications for magmatic processes and geochemical evolution, Mauna Loa Revealed: Structure, Composition, History, and Hazards. Geophysical Monograph. American Geophysical Union, pp. 219-239.

Garcia, M.O., Ito, E., Eiler, J.M. and Pietruszka, A.J., 1998. Crustal contamination of Kilauea Volcano magmas revealed by oxygen isotope analyses of glass and olivine from Puu Oo eruption lavas. Journal of Petrology, 39(5): 803-817.

Garcia, M.O., Rhodes, J.M., Trusdell, F.A. and Pietruszka, A.J., 1996. Petrology of lavas from the Puu Oo eruption of Kilauea Volcano: III. The Kupaianaha episode (1986-1992). Bulletin of Volcanology, 58: 359-379.

Geldmacher, J. and Hoernle, K.A., 2000. The 72 Ma geochemical evolution of the Madeira hotspot (eastern North Atlantic): recycling of Paleozoic (500 Ma) oceanic lithosphere. Earth and Planetary Science Letters, 183: 73-92.

Gudmundsson, A., 1990. Emplacement of dikes, sills and crustal magma chambers at divergent plate boundaries. Tectonophysics, 176: 257-275.

Gudmundsson, A., 1995. The geometry and growth of dykes. In: G. Baer and A. Heimann (Editors), Physics and Chemistry of Dykes. Balkema, Rotterdam, Brookfield, pp. 23-34.

Gudmundsson, A., 1998. Magma chambers modeled as cavities explain the formation of rift zone central volcanoes and their eruption and intrusion statistics. Journal of Geophysical Research, 103(B4): 7401-7412.

Guillou, H., Carracedo, J.C. and Day, S., 1998. Dating of the upper Pleistocene-Holocene activity of La Palma using the unspiked K-Ar technique. Journal of Volcanology and Geothermal Research, 86: 137-149.

Guillou, H., Carracedo, J.C. and Duncan, R., 2001. K-Ar, $^{40}Ar/^{39}Ar$ ages and magnetostratigraphy of Brunhes and Matuyama lava sequences from La Palma Island. Journal of Volcanology and Geothermal research, 86(1-4): 37-149.

Hansteen, T.H., Klügel, A. and Schmincke, H.U., 1998. Multi-stage magma ascent beneath the Canary Islands: evidence from fluid inclusions. Contributions to Mineralogy and Petrology, 132: 48-64.

Hausen, H., 1969. Some contributions to the geology of La Palma. Comm. Phys. Math. Finn. Acad. Sci., 35: 1-140.

Hildenbrand, A., Gillot, P.-Y. and Le Roy, I., 2004. Volcano-tectonic and geochemical evolution of an oceanic intra-plate volcano: Tahiti-Nui (French Polynesia). Earth and Planetary Science Letters, 217: 349-365.

Hoernle, K., 1998. Trace element and Sr-Nd-Pb isotopic geochemistry of Jurassic ocean crust beneath Gran Canaria (Canary Islands): implications for the generation of OIB reservoirs and for crustal contamination of ascending OIB magmas. Journal of Petrology, 39(5): 859-880.

Hoernle, K., Tilton, G. and Schmincke, H.U., 1991. Sr-Nd-Pb isotopic evolution of Gran Canaria: evidence for shallow enriched mantle beneath the Canary Islands. Earth and Planetary Science Letters, 106: 44-63.

Holik, J.S. and Rabinowitz, P.D., 1991. Effects of Canary hotspot volcanism on structure of oceanic crust off Morocco. Journal of Geophysical Research, 96: 12039-12067.

Kerkhof, A.M., van den, 1988. The system CO2-CH4-N2 in fluid inclusions: theoretical modelling and geological applications. Free University Press, Free University in Amsterdam, 206 pp.

Kerkhof, A.M., van den, 1990. Isochoric phase diagrams in the systems CO_2-CH_2 and CO_2-N_2: Application to fluid inclusions. Geochimica et Cosmochimica Acta, 54: 621-629.

Kerrick, D.M. and Jacobs, G.K., 1981. A modified Redlich.Kwong equation for H_2O, CO_2 and H_2O-CO_2 mixtures at elevated temperatures and pressures. American Journal of Sciences, 281: 735-767

Klitgord, K.D. and Schouten, H., 1986. Plate kinematics of the Central Atlantic. In: P.R. Vogt and B.E. Tucholke (Editors), The geology of North America, Vol. M, The Western North Atlantic Region. Geological Society of America, pp. 351-378.

Klügel, A., Hansteen, T.H. and Galipp, K., submitted. Magma storage and underplating beneath Cumbre Vieja volcano, La Palma (Canary Islands). Earth and Planetary Science Letters.

Klügel, A., Hansteen, T.H. and Schmincke, H.U., 1997. Rates of magma ascent and depths of magma reservoirs beneath La Palma (Canary Islands). Terra Nova, 9(3): 117-121.

Klügel, A., Hoernle, K.A., Schmincke, H.U. and White, J.D.L., 2000. The chemically zoned 1949 eruption on La Palma (Canary Islands): Petrologic evolution and magma supply dynamics of a rift-zone eruption. Journal of Geophysical Research, 105(B3): 5997-6016.

Klügel, A., Schmincke, H.U., White, J.D.L. and Hoernle, K.A., 1999. Chronology and volcanology of the 1949 multi-vent rift-zone eruption on La Palma (Canary Islands). Journal of Volcanology and Geothermal Research, 94: 267-282.

Le Maitre, R.W. et al., 1989. A Classification of Igneous Rocks and Glossary of Terms - Recommendations of the International Union of Geological Sciences Subcommission on the Systematics of Igneous Rocks. Blackwell Scientific Publications, Oxford, 193 pp.

Leslie, S., Moore, G. and Morgan, J., 2004. Internal structure of Puna Ridge: evolution of the submarine east rift zone of Kilauea Volcano. Journal of Volcanology and Geothermal Research, 129(237-259).

Masson, D.G. et al., 2002. Slope failures on the flanks of the western Canary Islands. Earth Science Review, 57: 1-35.
Middlemost, E.A.K., 1972. Evolution of La Palma, Canary archipelago. Contributions to Mineralogy and Petrology, 36: 33-48.
Moore, G., Vennemann, T. and Carmichael, I.S.E., 1998. An empirical model for the solubilty of H_2O in magmas to 3 kilobars. American Mineralogist, 83: 36-42.
Moore, J.G. and Clague, D.A., 1992. Growth of the Island of Hawaii. Geological Society of America Bulletin, 104: 1471-1484.
Morgan, W.J., 1983. Hotspot tracks and the early rifting of the Atlantic. Tectonophysics, 94: 123-139.
Nikogosian, I.K., Elliott, T. and Touret, J.L.R., 2002. Melt evolution beneath thick lithosphere: a magmatic inclusion study of La Palma, Canary Island. Chemical Geology, 183: 169-193.
Putirka, K., 1997. Magma transport at Hawaii: Inferences based on igneous thermobarometry. Geology, 25(1): 69-72.
Putirka, K., Johnson, M., Kinzler, R., Longhi, J. and Walker, D., 1996. Thermobarometry of mafic igneous rocks based on clinopyroxene-liquid equilibria, 0-30 kbar. Contributions to Mineralogy and Petrology, 123: 92-108.
Putirka, K.D., Mikaelian, H., Ryerson, F. and Shawa, H., 2003. New clinopyroxene-liquid thermobarometers for mafic evolved, and volatile-bearing lava compositions, with applications to lavas from Tibet and the Snake River Plain, Idaho. American Mineralogist, 88(10): 1542-1554.
Ranero, C.R., Torne, M. and Banda, E., 1995. Gravity and multichannel seismic reflection constraints on the lithospheric structure of the Canary Swell. Marine Geophysical Researches, 17: 519-534.
Roedder, E., 1983. Geobarometry of ultramafic xenoliths from Loihi Seamount, Hawaii, on the basis of CO2 inclusions in olivine. Earth and Planetary Science Letters, 66(369-379).
Roedder, E., 1984. Fluid inclusions, 12. Mineralogical Society of America, Washington, 644 pp.
Roedder, E. and Bodnar, R.J., 1980. Geologic pressure determinations from fluid inclusion studies. Annual Rev Earth Planet Sci, 8: 263-301.
Roeder, P.L., 1974. Activity of iron and olivine solubility in basaltic liquids. Earth and Planetary Science Letters, 23: 397-410.
Roeder, P.L. and Emslie, R.F., 1970. Olivine-liquid equilibrium. Contributions to Mineralogy and Petrology, 29: 275-289.
Ryan, M.P., 1988. The mechanics and three-dimensional internal structure of active magmatic systems: Kilauea volcano, Hawaii. Journal of Geophysical Research, 93(B5): 4213-4248.
Sachs, P.M. and Hansteen, T.H., 2000. Pleistocene underplating and metasomatism of the lower continental crust: a xenolith study. Journal of Petrology, 41: 331-356.
Schmincke, H.U., 1982. Volcanic and chemical evolution of the Canary Islands. In: U. von Rad, K. Hinz, M. Sarnthein and E. Seibold (Editors), Geology of the northwestern african continental margin. Springer, Berlin Heidelberg New York, pp. 3-20.
Schmincke, H.U., Klügel, A., Hansteen, T.H., Hoernle, K. and Bogaard, P.v.d., 1998. Samples from the Jurassic ocean crust beneath Gran Canaria, La Palma and Lanzarote (Canary Islands). Earth and Planetary Science Letters, 163: 343-360.
Schmincke, H.U. and Staudigel, H., 1976. Pillow lavas on eastern Atlantic islands. Bull. Soc. Geol. France, 18: 870-883.
Schwarz, S., Klügel, A. and Wohlgemuth-Ueberwasser, C., 2004. Melt extraction pathways and stagnation depths beneath the Madeira And Desertas rift zone (NE Atlantik) inferred from barometric studies. Contributions to Mineralogy and Petrology, 147: 228-240.
Staudigel, H., Feraud, G. and Giannerini, G., 1986. The history of intrusive activity on the Island of La Palma (Canary Islands). Journal of Volcanology and Geothermal Research, 27: 299-322.
Staudigel, H. and Schmincke, H.U., 1984. The Pliocene seamount series of La Palma / Canary Islands. Journal of Geophysical Research, 89(13): 11195-11215.
Szabó, C.S. and Bodnar, R.J., 1996. Changing magma ascent rates in the Nógrád-Gömör volcanic field, Northern Hungary / Southern Slovakia: Evidence from CO_2-rich fluid inclusions in metasomatized mantle xenoliths. Petrology, 4: 240-249.
Touret, J.L.R., 1982. An empirical phase diagram for a part of the system N_2-CO_2 system at low temperature. Chemical Geology, 37: 49-58.
Viti, C. and Frezzotti, M.-L., 2000. Re-equilibration of glass and CO_2 inclusions in xenoliths olivine: A TEM study. American Mineralogist, 85: 1390-1396.
Walker, G.P.L., 1999. Volcanic rift zones and their intrusion swarms. Journal of Volcanology and Geothermal Research, 94: 21-34.
Walter, T.R. and Troll, V.R., 2003. Experiments on rift zone evolution in unstable volcanic edifices. Journal of Volcanology and Geothermal Research, 127: 107-120.
Wanamaker, B.J. and Evans, B., 1989. Mechanical re-equilibration of fluid inclusions in San Carlos olivine by power-law creep. Contributions to Mineralogy and Petrology, 102: 102-111.
Wanamaker, B.J., Wong, T.F. and Evans, B., 1990. Decrepitation and crack healing of fluid inclusions in San Carlos olivine. Journal of Geophysical Research, 95(B10): 15623-15641.
Yang, H.-J., Frey, F.A., Clague, D.A. and Garcia, M.O., 1999. Mineral chemistry of submarine lavas from Hilo Ridge, Hawaii: implications for magmatic processes within Hawaiian rift zones. Contribution to Mineralogy and Petrology, 135: 355-372.
Yang, H.-J., Kinzler, R.J. and Grove, T.L., 1996. Experiments and models of anhydrous, basaltic olivine-plagioclase-augite saturated melts from 0.001 to 10 kbar. Contributions to Mineralogy and Petrology, 124: 1-18.

4. Geochemistry (separate paper)

This chapter consists of an individual paper which will be submitted to “Chemical Geology” in August 05. Samples from the Cumbre Vieja in this chapter are denoted as CV and TSJ. TSJ -samples were taken and analyzed by T.S. Johansen. In the submitted paper this distinction will be abandoned. The complete data not presented in the paper are shown in the Appendix of the thesis.

Appendix A 4.1: Sample list and sample localities
Appendix A 4.2: Composition of fractionation-corrected lavas
Appendix A 4.3: XRF analyses of international standards
Appendix A 4.4: ICP-MS analyses of USGS reference standard material
Appendix A 4.5: Sr-Nd-Pb isotope analyses of standard material
Appendix A 4.6: Melting model
Appendix A 5.2: Map of sample localities

Petrogenesis and geochemical evolution of lavas from La Palma (Canary Islands): implications for plume-lithosphere interaction

Karsten Galipp[1)*], Andreas Klügel[1)], Tor S. Johansen[2)], F. Hauff[2)], K. Hoernle[2)]

For submission to Chemical Geology

1) Universität Bremen, Fachbereich Geowissenschaften
Postfach 330440, D-28334 Bremen, Germany
Fax: +49-421-218-9460, e-mail: kgalipp@uni-bremen.de

2) IFM-GEOMAR, Leibniz-Institut für Meereswissenschaften
Wischhofstr. 1-3, D-24148 Kiel, Germany
Fax: +49-431-600-2924

*Corresponding author: kgalipp@uni-bremen.de

Abstract

Major and trace element and Sr-Nd-Pb isotopic compositions are presented for alkaline basaltic rocks from La Palma (Canary Islands). In the last 1.0 Ma subaerial volcanic activity at La Palma was confined to three volcanoes: (1) the extinct Taburiente shield volcano with the Cumbre Nueva rift zone, (2) the extinct Bejenado volcano and (3) the presently active Cumbre Vieja rift zone. Cumbre Vieja rocks are systematically more enriched in incompatible elements including P, Sr, Th, U, Nb and LREE, and show larger La/Yb (27.1 - 49.1) and Sm/Yb (4.6 - 7.3) than rocks from the older volcanoes (La/Yb = 19.1 - 37.2; Sm/Yb = 3.7 - 6.3). Slight concave-upward REE patterns, negative K anomalies as well as relative depletion in Rb and Ba on mantle-normalized diagrams of fractionation-corrected La Palma basalts require the presence of residual amphibole in their melting region. It is suggested that this amphibole is of metasomatic origin as a consequence of earlier infiltrating plume melts penetrating the colder lithosphere at its base. Forward modelling of trace element compositions as a function of source composition and degree of melting indicates that they cannot be generated by a single-stage melting process of an amphibole-bearing garnet peridotite or any other plausible source. The high Nb/U ratios above the global OIB range (47 ± 10) of many Taburiente and Bejenado lavas require addition of up to ~20% of amphibole to the partial melts. This amphibole was probably formed as metasomatic veins by earlier plume melts passing through the cold lithosphere. In contrast, the high Sm/Yb and La/Yb ratios and high P, Th, U and REE contents of Cumbre Vieja lavas require addition of ~1% apatite rather than amphibole. The apatite may derive from cumulates of older Cumbre Vieja melts or may be of metasomatic origin. Sr, Nd and Pb isotopic ratios for the older Taburiente and Bejenado volcanoes show considerable variability ($^{87}Sr/^{86}Sr$ = 0.703001 - 0.703110, $^{143}Nd/^{144}Nd$ = 0.512880 - 0.512971, $^{206}Pb/^{204}Pb$ = 19.142 - 19.947, $^{207}Pb/^{204}Pb$ = 15.544 - 15.639; $^{208}Pb/^{204}Pb$ = 38.829 - 39.758), whereas the range for Cumbre Vieja is rather limited ($^{87}Sr/^{86}Sr$ = 0.703087 - 0.703169, $^{143}Nd/^{144}Nd$ = 0.512888 - 0.512901, $^{206}Pb/^{204}Pb$ = 19.497 - 19.715, $^{207}Pb/^{204}Pb$ = 15.609 - 15.888; $^{208}Pb/^{204}Pb$ = 39.159 - 39.488) and has a tendency to more depleted compositions than Taburiente. Much of the isotope variations can be explained by binary mixing between an enriched HIMU-type plume component and a more depleted lithospheric component. Our combined data indicate no progressive geochemical evolution of La Palma magmas but a compositional break between Taburiente volcanism in the north and Cumbre Vieja volcanism in the south. This suggests that the active Cumbre Vieja rift zone and the extinct volcanoes represent distinct volcanic systems rather than a progressively evolving volcano.

Keywords: Canary Islands, La Palma, plume, metasomatism, assimilation

1. Introduction

The chemical composition of lavas from oceanic island volcanoes results from the superposition of various processes during their genesis: variation of source compositions, entrainment of surrounding asthenosphere as a plume rises through the mantle, fractionation between partial melts and residual minerals, reactions between lithospheric mantle and ascending partial melts, magma mixing, shallow level assimilation, and crystal fractionation before eruption. Recently there has been increased recognition of the significance of lithospheric contributions to final lava compositions (e.g. Hoernle et al., 1991; Dupuy et al., 1993; Class et al., 1997). Although most oceanic island basalts (OIB) are believed to derive from plumes originating at deep thermal boundary layers (Morgan, 1972), contamination by metasomatized oceanic lithosphere may contribute to their geochemical characters (e.g. Class et al., 1998; Jörgensen and Holm, 2002). However, the involvement of the lithospheric mantle and the crust to plume derived melts has not been satisfactorily evaluated and is still a matter of debate (Frey et al., 1990, Class and Goldstein, 1997; Späth et al., 1996). In order to address this issue we have embarked on a comprehensive geochemical study of La Palma (Canary Islands) and show how interaction of plume-derived melts with the metasomatized lithosphere has influenced their trace element signature. We also present a model for the geochemical evolution of La Palma in space and time from the early subaerial shield stage to the presently active rift zone (Cumbre Vieja) and discuss the question if and how the geochemical evolution of La Palma magmas is related to the rift zone evolution. La Palma is an ideal place for such a study because the island illustrates well the development from the late seamount stage to a radial shield volcano to a pronounced rift zone accompanied by continuous growth to the south. The subaerial geochronological evolution of La Palma since about 1.7 Ma is well reconstructed by precise K-Ar and $^{40}Ar/^{39}Ar$ dating (Guillou et al., 1998, 2001), and a large set of major and trace element compositions of La Palma rocks is presented in Sigmarsson et al. (1992), Marcantonio et al. (1995), Hilton et al. (2000), Klügel et al. (2000) and Carracedo et al. (2001). Little is known, however, about systematic geochemical variations during the evolution of the island and about possible genetic relationships between the magmatic systems of the former Taburiente shield volcano and the recent Cumbre Vieja rift system.

The aims of the paper are (1) to place constraints on the composition of the mantle source beneath La Palma; (2) to explore systematic temporal and spatial geochemical variations of the magmas during the evolution from the radial shield volcano to the presently active rift zone. We present major and trace element and Sr, Nd and Pb isotope data of selected basaltic rocks from the different volcanic phases of La Palma providing a comprehensive picture of geochemical variations in space and time over the last 1.0 Ma. The observed trace element variations of differentiation-corrected lavas were reproduced by forward-modelling of

melting and assimilation processes. We also carried out LA-ICP-MS analyses of apatite phenocrysts and of amphibole and phlogopite from metasomatized mantle peridotites in order to test if assimilation of these mineral phases may have influenced the trace element composition of basaltic melts as they traverse the lithosphere.

2. Geological setting

The Canary Archipelago is a 600 km long chain of seven volcanic islands off the coast of NW Africa (Fig. 1). Magmatic activity started more than 20 million years ago with the formation of the eastern islands Lanzarote and Fuerteventura. All islands are underlain by Jurassic oceanic crust as is indicated by tholeiitic MORB-type gabbro xenoliths occurring on Gran Canaria, Lanzarote and La Palma (Hoernle, 1998; Schmincke et al., 1998). The age of the crust is bracketed by magnetic anomalies S1 (175 Ma) between the easternmost islands and the African coast, and M25 (155 Ma) between La Palma and El Hierro, which are the westernmost and youngest islands (Klitgord and Schouten, 1986). The Canary Islands are believed to result from volcanism above a mantle plume that impinges beneath the slowly moving oceanic lithosphere (Morgan et al., 1983; Holik and Rabinowitz, 1991; Hoernle et al., 1991). Summaries of the geology of the Canary Islands are given by Schmincke (1976, 1982) and Carracedo (1999). Together with El Hierro, La Palma represents the current locus of hotspot magmatism (Holik and Rabinowitz, 1991). Tenerife, La Palma and El Hierro are the only Canary islands at present in the shield-stage of growth, whereas Lanzarote, Fuerteventura, Gran Canaria and La Gomera are already in the post-erosional stage of development (Carracedo, 1999).

The geological evolution of La Palma is presented in Ancochea et al. (1994) and Carracedo et al. (1999, 2001) and is briefly discussed here. As recognized by early workers (Hausen, 1969; Middlemost, 1972; Schmincke, 1976), the geology of La Palma can be divided into three major units (Fig. 1): (1) the basal complex (ca. 3.0 to 4.0 Ma) comprising a Pliocene seamount sequence and a plutonic complex, uplifted and tilted by intrusions coeval with the later subaerial activity (Staudigel and Schmincke, 1984); (2) the older volcanic series (1.7 to 0.4 Ma) which include the Garafia volcano, the Taburiente shield volcano, the Bejenado edifice, and the Cumbre Nueva series; and (3) the Cumbre Vieja series (125 ka to present) which is confined to the southern half of the island.

The earliest subaerial volcanism formed Garafia volcano (1.7 - 1.2 Ma), which overlies and mantles the uplifted seamount. Outcrops of Garafia volcano are limited to erosive windows at the north and southwest flanks of the northern shield. The Taburiente shield volcano forms the northern part of La Palma (Fig. 1) and developed from about 1.2 Ma until 0.4 Ma (Guillou et al., 1998; 2001). From about 830 ka, Taburiente began to extend to the south forming the Cumbre Nueva rift zone. The Cumbre Nueva ridge was destroyed by a giant lateral collapse

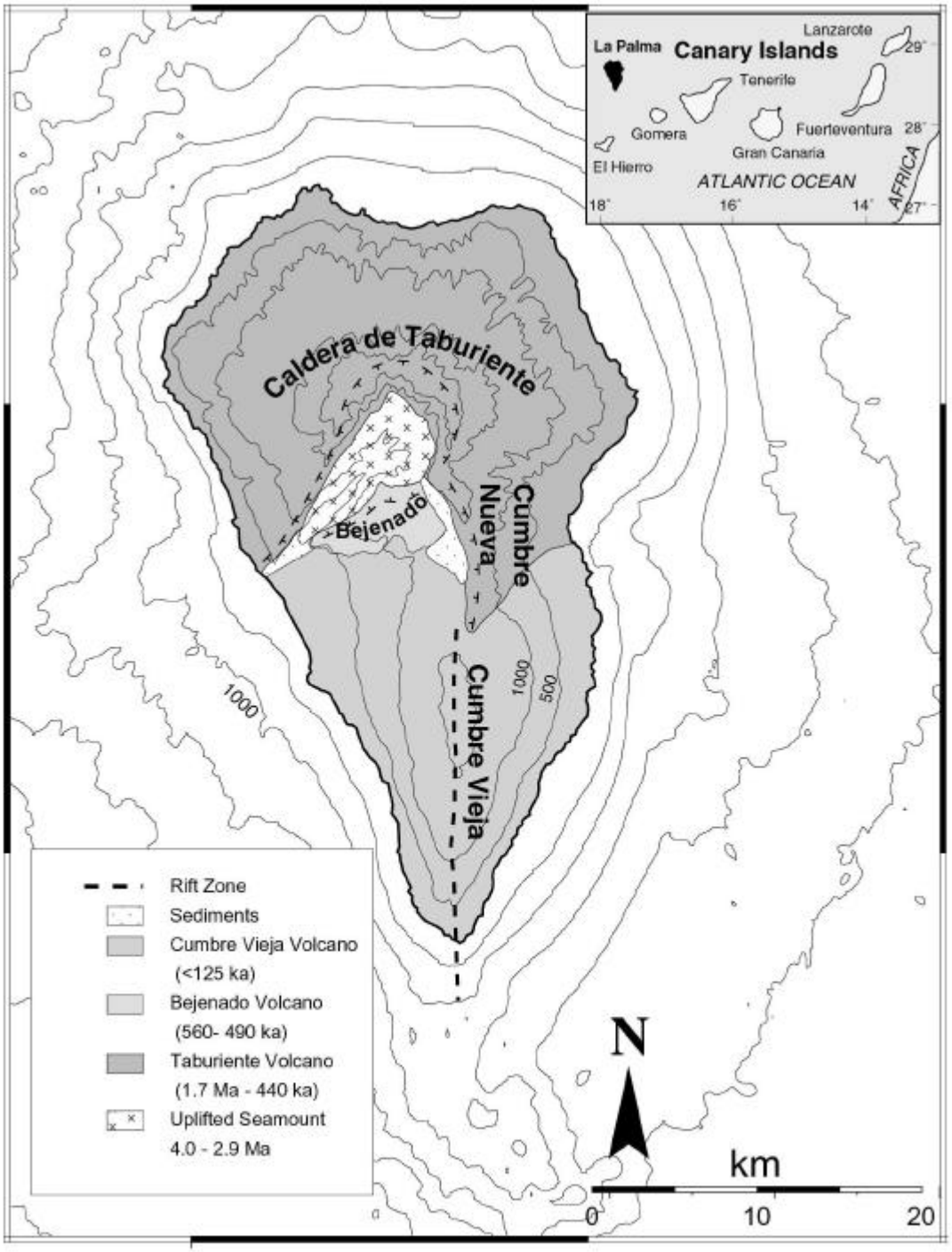

Fig. 1: Simplified geological map of La Palma (modified after Ancochea et al., 1994 and Carracedo et al., 1999). Age range of volcanic units are from Staudigel et al. (1986), and Guillou et al. (1998, 2001). Bathymetric data based on D. G. Masson, Southampton Oceanography Center, compiled by S. Krastel, Universität Bremen.

at 560 ka. Immediately after the collapse, a new episode of volcanic activity within the collapsed embayment produced Bejenado volcano. The growth of this stratovolcano occurred rapidly from about 560 to 490 ka (Guillou et al., 1998; 2001) with little concomitant activity from Taburiente.

After cessation of volcanism at Bejenado, activity shifted to the south forming Cumbre Vieja volcano from about 125 ka to present. Morphologically, the Cumbre Vieja rests on the

southern flank of the older Cumbre Nueva ridge and represents a separate volcanic edifice. The apparent gap from 400 to 125 ka separating the volcanism at Taburiente, Cumbre Nueva and Bejenado (hereafter termed as pre-CV) from Cumbre Vieja volcanism (hereafter termed as CV) is not a period of volcanic quiescence but merely reflects older CV rocks being completely covered by younger lavas. The Cumbre Vieja ridge is a well-developed north-south-trending rift zone as indicated by alignment of abundant cinder cones and fissures along its crest. The submarine southern extension of the rift zone becomes somewhat diffuse and grades into a seamount east of the rift axis, which morphologically represents a comparatively old structure (Schmincke and Graf, 2000; Gee et al., 2001).

3 Petrography

La Palma is characterized by alkaline rocks ranging from basanites and alkali picrites to phonolites (Fig. 2) (Middlemost, 1972; Carracedo et al., 2001). Although the different geological units of La Palma essentially overlap in their compositions, systematic petrographic differences are observed (Galipp et al., submitted): (1) Ankaramites occur commonly at Taburiente and Cumbre Nueva but are absent at Cumbre Vieja; (2) differentiated lavas (phonotephrites to phonolites) are far more abundant at Bejenado and Cumbre Vieja than at Taburiente and Cumbre Nueva; and (3) green-core clinopyroxenes are ubiquitous in lavas from Cumbre Vieja but are almost absent in the other series. Mafic La Palma rocks show phenocrysts of olivine + clinopyroxene; plagioclase occurs only in some Bejenado rocks. Olivines (0.4 - 4.5 mm long) are euhedral to subhedral, partially resorbed, and in some samples slightly to strongly altered. Clinopyroxenes (0.4 - 4.0 mm long) are optically zoned and in some samples slightly to moderately resorbed. They occur as single crystals or form glomerocrysts with olivines. Olivine and clinopyroxene phenocrysts occur almost in equal proportions in mafic samples each with up to 20 vol%. Ti-magnetite is present in small amounts (< 2 vol. %, < 1 mm). Olivine xenocrysts with deformation lamellae and clinopyroxene xenocrysts are common. The groundmass consists of olivine, clinopyroxene, plagioclase laths and Fe-Ti oxides. Thermobarometric studies show that major crystal fractionation occurs within the upper mantle and not at crustal levels (Klügel et al., 2000; Nikogosian et al., 2002; Galipp et al., submitted).

Xenoliths are common in CV lavas but comparatively rare in the older units. They include (1) ultramafic cumulates containing highly variable proportions of kaersutitic amphibole, clinopyroxene, olivine, Fe-Ti-oxides, and apatite; (2) MORB-type gabbros from the Jurassic oceanic crust, (3) mafic cognate cumulates containing plagioclase, kaersutitic amphibole, clinopyroxene, Fe-Ti-oxides, apatite, ± hauyne, ± titanite; (4) harzburgite and dunite mantle xenoliths which in some cases contain amphibole and phlogopite (Wulff-Pedersen et al.,

1996, 1999; Klügel, 1998), and (5) various types of fragments from evolved rocks (Klügel et al., 1999).

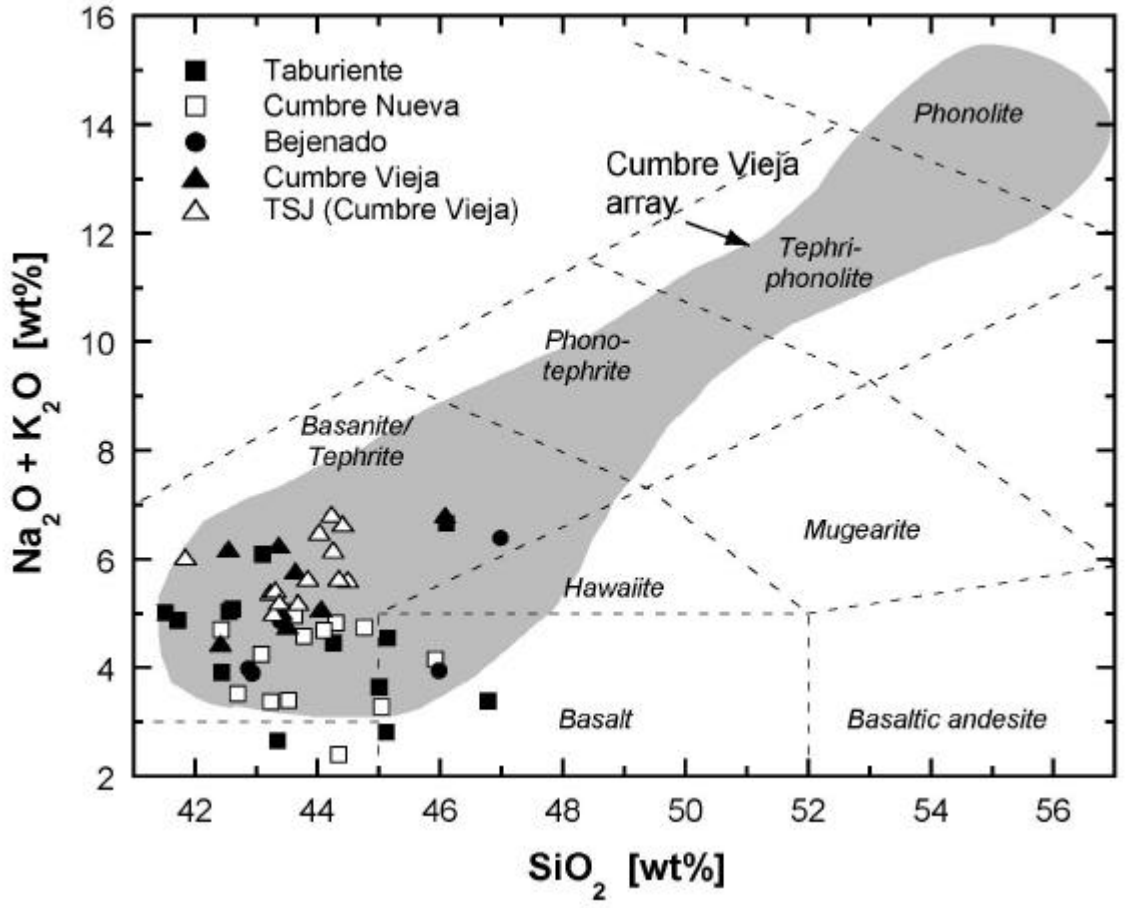

Fig. 2: Total alkali vs. silica diagram of mafic samples from La Palma, using the field boundaries of Le Maitre et al. (1989). Grey field for the active Cumbre Vieja rift zone is based on data from Hernandéz-Pacheco and Valls (1982), Hernandéz-Pacheco and De la Nuez (1983), Elliot (1991) and Klügel et al. (2000). TSJ samples are samples from different historic and prehistoric eruptions at the Cumbre Vieja.

4 Analytical Methods

Major and trace elements

After removing the weathered parts from each sample, the rocks were crushed, washed in distilled water in an ultrasonic bath and ground to fine powder in an agate mill. Samples with altered rims or vesicles filled with secondary minerals were hand-picked under a binocular microscope. Whole-rock major element compositions (SiO_2, Al_2O_3, TiO_2, Fe_2O_3, MgO, MnO, CaO, Na_2O, K_2O, and P_2O_5) and some trace elements (V, Cr, Zn) were determined at IFM-GEOMAR by X-ray fluorescence (XRF) on fused beads using a Philips X'Unique PW 1480 equipped with a Rh-tube and calibrated with international standards. H_2O and CO_2 were analyzed with an infrared photometer (Rosemount CSA 5003). All other trace elements were determined by inductively coupled plasma-mass spectrometry (ICP-MS) at the Department of Geosciences, University of Bremen, from mixed acid (HF-HCl-HNO_3) pressure digests

prepared at 210 °C with a MLS Ethos microwave. About 50 mg of sample material were digested and the analyte solutions were spiked with 1 ng/ml indium as internal standard. The final dilution factor was 1:5000 corresponding to 0.2 mg/ml of total dissolved solid. The analyses were carried out on a ThermoFinnigan Element2 with the resolution being set to high (10000) for the rare earth elements and Hf, medium (4000) for the transition metals, and low (300) for all other elements. External precision as determined by repeated analyses of standard reference materials is better than 7% for most elements, and is better than 11% for duplicate digestions of samples except for Tl, Hf and Pb (up to 15*%).* The accuracy of standard reference materials BHVO-2 and BCR-2, measured along with the samples, is better than 10 % except for Cu (up to 16%) with respect to the USGS reference values.

Sr-Nd-Pb isotopes

Samples were leached in 6N HCL for 1h at 120 °C. About 100 mg of rock powder or rock chips were dissolved in Teflon beakers using a HF-HNO_3 mixture. Sr, Nd and Pb ion chromatography followed closely the procedure outlined in Hoernle and Tilton (1991). The average Pb procedural blanks ranged between 20 and 60 pg Pb and thus are considered insignificant for the sample sizes. Samples were split after the final clean-up in order to obtain a load of 50-100ng Pb on the filament. Pb isotope ratios were measured in static mode on a Finnigan MAT262-RPQ^{2+} thermal ionization mass spectrometer (TIMS) at IFM-GEOMAR. Measured values for NBS981 (N = 60) and 2sigma external errors are $^{206}Pb/^{204}Pb$ = 16.900 ± 0.007, $^{207}Pb/^{204}Pb$ =15.437 ±- 0.008, and $^{208}Pb/^{204}Pb$ = 36.527 ± 0.027 corresponding to an external reproducibility of 0.019%/amu. The measured Pb isotopic ratios were normalized to the NBS981 values given by Todt et al. (1996). Replicate analyses of samples were carried out on 14 out of 28 and lie within 0.01 ± 0.006 %/amu.

Sr and Nd isotope measurements were carried out on a ThermoFinnigan TRITON TIMS operating in static mode and Sr and Nd isotope ratios being normalized within run to $^{86}Sr/^{88}Sr$ = 0.1194 and $^{146}Nd/^{144}Nd$ = 0.7219, respectively. Over two periods of analyses, NBS987 along with external 2 sigma errors gave $^{87}Sr/^{86}Sr$ = 0.710274+/- 0.000009 (n = 13) and $^{87}Sr/^{86}Sr$ = 0.71025646 +/- 0.000005 (n = 16). Sr isotope data measured in the latter period are normalized to the NBS987 data of the first period. La Jolla gave $^{143}Nd/^{144}Nd$ = 0.511848 ± 0.000005 (n = 12) and our in-house Nd monitor SPEX gave $^{143}Nd/^{144}Nd$ = 0.511712 ± 0.000006 (n = 20).

Mineral trace elements

Trace element in minerals were analysed by a laser ablation ICP-MS using a Finnigan UV LaserProbe (wavelenght 266 nm) coupled to a ThermoFinnigan Element2 at the Department of Geosciences, University of Bremen. Helium was used as sample gas in the ablation cell

(0.4 l/min) and Argon was subsequently added (0.8 l/min) to the gas flow. Analytical conditions included a laser energy of 0.8 mJ, pulse rate of 5 Hz, beam diameter of 50 µm, blank duration prior to ablation of 15-20 s, and signal duration of 40-45 s following a pre-ablation period of ca. 5 s. Isotopes were analyzed with five samples at each peak's flat top and a total dwell time of 25 ms per isotope. NIST612 (Pearce et al., 1997) and NIST610 (Rocholl et al., 2000) glasses were used for external single-point calibration using as internal standard ^{29}Si for phlogopite and amphibole and ^{43}Ca for apatite. External precision as determined by replicate analyses of USGS glasses BCR-2G and BHVO-2G is 3-10 %. The accuracy of BCR-2G analysed along with the samples is typically 5-10% for most elements with respect to the values given by Gao et al. (2002) but reached 20% in a few cases.

5 Whole-rock and mineral chemistry

5.1 Major and trace elements

Major and trace element analyses of representative samples from all investigated units are listed in Table 1. Mafic La Palma samples generally show negative correlations of MgO with Al_2O_3, alkalies and P_2O_5, and positive correlations with Ni, Cr, Co, and Sc (Fig. 3). These variations are consistent with fractionation of clinopyroxene, olivine and minor Ti-magnetite which are also the main phenocrysts phases observed. Fractionation of magnetite appears to be subordinate based on the negative correlation between TiO_2 and MgO, and decreasing CaO/Al_2O_3 with decreasing MgO rules out significant involvement of feldspar. We note that even the most primitive La Palma lavas have undergone significant fractionation as is indicated by their comparatively low MgO, Ni and Cr concentrations. More evolved La Palma rocks (MgO <6%) show good negative correlations between MgO and incompatible trace elements (Carracedo et al., 2001). In the mafic rocks of the present study, however, these correlations are only moderate to weak (Fig. 4) indicating significant influence of processes other than crystal fractionation. Concentrations of incompatible elements are highly variable in all units, and positive correlations of K, Rb, Ba, Pb with immobile elements such as Nb, Ti, Zr for La Palma samples in general indicate that alteration has not destroyed the primary signature of these elements.

Although the compositions of Cumbre Vieja and pre-CV (Taburiente, Cumbre Nueva and Bejenado) samples essentially overlap, there are some systematic differences between both groups. At given MgO, Cumbre Vieja lavas have significantly higher alkalies, P_2O_5 and incompatible trace elements than pre-CV lavas and have a tendency to higher Al_2O_3. The overall difference in trace element concentrations between CV and pre-CV samples is largest for the highly incompatible elements (e.g. Th: 6 - 15 ppm vs. 2 - 8 ppm) and becomes smaller for less incompatible elements such as Sr (1025 - 1575 vs. 438 - 1057 ppm), Y (27 - 42 vs. 18 - 35 ppm) and Yb (1.4 - 2.9 vs. 2.0 - 3.1 ppm). Ratios of incompatible elements to U or Th in primitive La Palma samples (MgO > 6 wt%) show large variations (e.g. Nb/U = 21.6 - 87.6,

Table 1: Major and trace element concentrations of La Palma lavas

Sample:	KLP19 C.N.	KLP22 C.N.	KLP23 C.N.	KLP24 C.N.	KLP 27 C.N.	KLP35 C.N.	KLP36 C.N.	KLP37 C.N.	KLP39 C.N.	KLP41 C.N.	KLP80 C.N.	KLP87 C.N.	KLP85 C.N.	KLP88 C.N.
SiO_2	43.60	43.24	44.31	43.63	46.49	42.43	43.08	44.35	43.53	43.79	45.92	44.28	44.11	42.70
TiO_2	4.00	3.37	3.69	3.76	3.01	3.86	3.70	2.44	3.24	3.62	3.21	4.02	3.94	3.68
Al_2O_3	15.17	11.57	14.51	13.48	17.59	13.56	13.73	9.13	12.16	14.77	13.76	15.37	14.51	11.51
Fe_2O_3T	14.43	13.80	14.04	14.22	11.05	14.65	14.49	13.26	14.57	12.91	13.09	13.88	13.94	15.17
MnO	0.18	0.18	0.18	0.18	0.21	0.19	0.18	0.17	0.18	0.18	0.17	0.19	0.18	0.18
MgO	6.32	10.53	7.08	7.47	3.92	8.02	7.85	15.89	10.88	7.51	7.31	5.74	6.78	10.83
CaO	10.60	12.90	11.02	10.94	8.99	12.14	11.28	11.65	11.74	10.45	11.37	10.32	10.82	12.06
Na_2O	3.45	2.81	3.55	3.53	5.31	3.30	3.07	1.64	2.35	3.00	2.88	3.68	3.21	2.45
K_2O	1.58	0.56	1.27	1.42	2.20	1.40	1.18	0.76	1.04	1.58	1.27	1.81	1.47	1.07
P_2O_5	0.79	0.54	0.68	0.81	1.07	0.85	0.67	0.37	0.49	0.74	0.66	0.73	0.65	0.55
Sum	100.45	99.82	100.63	99.76	100.18	100.75	99.57	100.04	100.47	99.89	99.92	100.30	99.92	100.51
mg#	46.5	60.2	50.0	51.0	41.3	52.0	51.8	70.4	59.7	53.5	52.5	45.0	49.1	58.6
Fr. cor.	20.0	10.0	20.0	12.0	n.d.	18.0	10.0	0.0	13.0	15.0	16.0	n.d.	19.0	9.0
Li	7.70	5.75	n.d.	9.03	n.d.	n.d.	n.d.	5.35	n.d.	n.d.	n.d.	n.d.	n.d.	n.d.
Sc	25.6	42.0	30.1	32.8	7.0	25.4	28.2	45.6	33.5	20.9	21.3	16.8	21.7	37.7
V	434	386	348	384	199	362	357	310	332	306	275	358	349	384
Cr	145	535	181	262	18	201	275	1066	426	285	196	18	146	503
Co	50.3	61.7	47.8	58.0	21.5	47.9	52.9	82.9	56.8	41.3	43.5	40.6	44.4	65.4
Ni	91.9	190.4	77.9	119.3	3.6	97.1	136.1	468.8	172.5	106.5	104.0	41.1	79.6	204.9
Cu	72.1	104.5	69.2	117.6	12.5	124.7	102.0	86.8	77.6	53.6	105.7	64.5	98.2	114.6
Zn	132.0	106.1	122.9	138.4	128.4	110.3	124.6	96.2	99.4	107.4	112.9	122.9	120.5	112.7
Ga	25.5	19.0	21.8	22.7	23.5	21.5	22.4	14.6	16.7	19.5	22.1	23.7	23.0	20.1
Rb	40.10	57.37	32.36	41.12	46.9	32.6	26.1	20.2	22.7	34.2	25.7	36.6	31.5	23.8
Sr	1057	724	762	1018	1159	855	853	525	555	901	817	888	793	629
Y	31.4	24.5	26.7	31.7	34.1	27.4	25.5	22.5	21.1	27.7	23.8	27.3	26.3	23.9
Zr	323	253	320	374	411	285	273	182	198	311	242	345	401	230
Nb	83.3	53.7	67.8	77.9	101.2	74.8	60.5	38.0	41.2	70.3	58.3	78.8	68.6	50.2
Cs	0.52	0.39	0.41	0.39	0.64	0.39	0.42	0.24	0.27	0.57	0.42	0.53	0.73	0.30
Ba	499	348	383	395	680	537	403	214	271	470	416	495	572	317
La	56.3	42.9	50.8	62.2	70.9	58.9	50.5	37.5	35.6	59.5	43.3	54.1	48.1	41.7
Ce	111.3	86.3	109.5	124.0	147.9	122.4	104.7	67.4	76.0	129.0	89.8	114.9	101.6	89.6
Pr	12.8	10.6	12.6	14.8	17.3	15.0	12.5	8.7	9.1	14.6	10.9	13.5	12.3	10.6
Nd	51.1	43.9	53.3	57.2	71.9	63.9	51.7	33.9	38.4	60.1	44.0	55.9	51.0	45.8
Sm	10.3	8.8	10.2	11.0	13.7	12.6	10.1	6.5	7.2	10.9	9.0	10.7	10.2	9.0
Eu	2.95	2.71	3.11	3.35	4.16	3.63	3.17	1.98	2.28	3.26	2.97	3.29	3.11	2.89
Gd	8.57	7.80	8.35	9.09	11.06	10.05	8.81	5.84	6.26	8.38	7.86	8.73	8.56	7.72
Tb	1.11	1.04	1.09	1.17	1.46	1.34	1.13	0.76	0.89	1.18	1.05	1.17	1.15	1.04
Dy	6.06	5.67	6.17	6.78	8.38	7.51	6.11	4.50	4.97	6.54	5.84	6.36	6.29	5.75
Ho	1.08	1.04	1.04	1.12	1.46	1.25	1.01	0.80	0.91	1.19	1.02	1.18	1.14	0.99
Er	2.53	2.46	2.84	2.56	3.68	3.26	2.67	2.00	2.27	3.11	2.48	2.96	3.01	2.44
Tm	0.32	0.31	0.34	0.31	0.49	0.42	0.32	0.26	0.32	0.38	0.31	0.40	0.38	0.32
Yb	2.06	1.88	2.25	1.79	2.90	2.35	1.90	1.49	1.82	2.41	1.81	2.31	2.24	1.82
Lu	0.28	0.26	0.30	0.24	0.44	0.34	0.25	0.22	0.24	0.35	0.25	0.32	0.33	0.26
Hf	6.35	6.47	7.58	7.03	9.35	7.82	6.85	4.04	5.39	7.70	6.06	7.99	9.80	6.10
Ta	3.94	3.43	4.30	4.38	6.64	4.99	3.83	2.25	2.71	4.47	3.87	5.31	4.61	3.29
Pb	2.46	2.79	2.97	2.94	5.46	4.37	2.97	1.45	2.23	3.60	3.12	4.12	3.83	2.54
Th	4.57	4.08	5.09	4.67	7.14	5.94	4.88	2.28	3.17	5.66	4.32	5.35	4.48	3.90
U	1.07	0.91	1.33	1.25	1.85	1.31	1.18	0.60	0.73	1.38	1.01	1.35	1.20	0.94

Major elements (wt%) and Cr, V, Zn determined by XRF; trace elements (ppm) determined by ICP-MS; mg# = molar Mg/(Mg+Fetot)*100; Fr. cor. = (wt%) olivine and clinopyroxene fractionation correction required to reach partial melting curve of a mantle lherzolite; C.N. Cumbre Nueva; T. Taburiente; B. Bejenado; C.V. Cumbre Vieja; n.d. not determined

Table 1 (continued)

Sample:	KLP89 C.N.	KLP103 C.N.	KLP59 T.	KLP61 T.	KLP63 T.	KLP64 T.	KLP65 T.	KLP67 T.	KLP72 T.	KLP73 T.	KLP75 T.	KLP77 T.	KLP207 T.
SiO_2	44.77	45.04	46.11	42.44	42.62	40.83	41.73	41.52	43.35	42.56	43.11	44.26	45.12
TiO_2	3.48	2.83	3.38	3.72	4.03	4.24	4.13	3.86	3.26	3.92	3.77	3.74	2.18
Al_2O_3	15.05	11.90	17.26	12.68	14.62	14.73	14.44	13.79	11.36	13.24	14.97	13.51	9.82
Fe_2O_3T	13.85	13.83	11.82	14.73	15.08	14.97	15.28	15.17	13.98	14.69	14.16	13.63	12.61
MnO	0.18	0.17	0.19	0.18	0.19	0.19	0.18	0.18	0.17	0.18	0.20	0.18	0.17
MgO	6.65	10.72	4.43	9.35	6.80	6.79	6.84	7.24	11.35	7.93	5.99	8.29	15.20
CaO	10.50	11.59	9.32	11.98	10.81	11.08	11.84	12.17	13.38	11.79	10.71	11.47	12.15
Na2O	3.38	2.51	4.77	3.28	4.14	3.50	3.48	3.98	1.97	4.21	4.99	3.04	2.03
K_2O	1.36	0.77	1.89	0.64	0.94	1.71	1.39	1.03	0.68	0.83	1.10	1.42	0.78
P_2O_5	0.69	0.52	0.94	0.58	0.73	1.09	0.79	0.82	0.41	0.69	0.87	0.59	0.30
Sum	100.19	100.21	100.43	99.84	100.27	99.44	100.42	100.06	100.02	100.39	100.22	100.42	100.69
mg#	48.8	60.6	42.6	55.7	47.2	47.3	47.0	48.6	61.7	51.7	45.6	54.7	70.5
Fr. cor.	16.0	5.0	n.d.	21.0	29.0	n.d.	26.0	25.0	17.0	16.0	32.0	16.0	2.0
Li	n.d.	n.d.	n.d.	6.73	n.d.	n.d.	n.d.	n.d.	5.25	n.d.	n.d.	n.d.	4.62
Sc	25.3	29.1	9.8	36.9	21.6	18.3	26.7	30.3	43.6	27.7	17.4	26.7	49.8
V	336	292	217	395	349	366	413	419	359	398	317	358	300
Cr	105	534	2	155	61	16	56	91	453	223	27	248	966
Co	45.7	55.5	23.7	60.8	44.3	42.7	48.6	54.8	59.2	51.4	39.1	48.6	77.8
Ni	88.4	240.7	2.9	97.3	48.6	29.2	58.0	62.6	145.8	106.2	35.4	114.4	395.7
Cu	88.5	100.1	13.8	62.2	73.2	46.9	89.9	56.7	42.8	53.8	67.7	93.1	85.9
Zn	125.3	110.2	115.4	112.4	113.9	124.3	124.0	125.0	94.7	115.6	121.7	104.0	89.0
Ga	22.3	19.4	22.5	19.7	22.5	22.4	22.5	21.8	16.4	22.8	23.5	21.4	13.9
Rb	33.3	14.9	37.5	13.0	22.3	33.2	30.2	14.2	25.6	7.2	14.1	27.9	22.6
Sr	819	612	1055	718	841	1000	872	865	607	848	998	725	439
Y	29.1	22.8	30.0	25.4	27.1	30.4	28.0	27.3	21.2	26.5	29.9	26.0	18.7
Zr	288	195	337	254	292	323	262	264	192	348	394	283	158
Nb	74.3	50.3	83.9	52.7	65.6	75.7	66.8	64.0	37.9	79.0	94.0	61.0	41.8
Cs	0.33	0.17	0.43	0.36	0.45	0.43	0.37	0.40	0.33	0.49	0.64	0.31	0.19
Ba	403	313	600	348	487	547	466	423	249	492	641	427	211
La	63.5	39.1	68.9	44.2	53.1	57.4	56.9	56.8	34.3	56.3	74.0	41.2	32.5
Ce	126.9	81.6	139.5	92.1	110.4	124.7	120.9	118.0	70.1	119.8	147.8	88.4	62.7
Pr	13.9	9.8	16.8	11.3	13.5	15.4	14.1	13.5	8.7	14.1	17.7	11.1	7.3
Nd	54.3	41.6	67.0	45.5	57.4	59.8	58.3	54.9	35.8	52.3	70.8	47.5	27.9
Sm	9.8	8.2	12.7	9.1	11.3	12.2	11.0	9.8	7.4	10.7	13.8	9.7	5.4
Eu	2.99	2.54	3.85	2.89	3.38	3.90	3.47	3.09	2.36	3.31	4.00	3.06	1.67
Gd	8.41	7.44	10.33	8.16	9.54	10.68	9.70	8.44	6.85	9.02	10.78	7.86	4.91
Tb	1.10	0.99	1.39	1.12	1.29	1.39	1.24	1.08	0.94	1.15	1.44	1.11	0.66
Dy	6.08	5.50	7.95	6.05	7.10	7.27	7.06	5.94	5.10	6.37	8.09	6.27	4.01
Ho	1.12	0.94	1.36	1.06	1.28	1.27	1.21	1.04	0.92	1.11	1.44	1.12	0.73
Er	2.80	2.43	3.54	2.65	3.24	3.08	2.91	2.56	2.29	2.63	3.41	2.79	1.88
Tm	0.38	0.30	0.48	0.34	0.42	0.39	0.37	0.32	0.29	0.36	0.46	0.36	0.24
Yb	2.27	1.75	2.80	2.02	2.38	2.14	2.19	1.93	1.70	1.88	2.77	2.07	1.44
Lu	0.29	0.25	0.39	0.28	0.35	0.30	0.29	0.26	0.25	0.26	0.38	0.30	0.20
Hf	6.74	5.23	8.63	6.30	7.93	7.26	6.84	6.01	5.34	7.97	10.29	7.11	3.66
Ta	4.32	3.21	5.62	3.33	4.53	4.84	4.27	3.65	2.49	4.91	6.43	4.10	2.42
Pb	3.06	1.84	5.09	2.74	4.44	3.36	3.27	2.77	1.87	4.14	5.63	3.86	1.39
Th	5.97	3.99	7.08	3.90	5.54	5.60	5.47	4.88	3.19	6.73	8.41	4.29	2.50
U	1.47	0.93	1.65	0.83	1.21	1.24	1.28	1.26	0.75	1.31	1.79	1.06	0.62

Table 1 (continued)

Sample:	KLP208 T.	KLP209 T.	KLP221 T.	KLP105 B.	KLP106* B.	KLP114 B.	KLP205 B.	KLP217 B.	KLP47 C.V.	KLP48 C.V.	KLP51 C.V.	KLP52 C.V.	KLP82 C.V.
SiO_2	45.00	46.78	45.15	43.39	46.98	42.93	42.87	45.98	43.65	43.51	42.55	45.44	46.08
TiO_2	3.03	3.03	3.38	3.49	4.09	3.23	3.30	3.17	3.71	3.42	3.54	3.20	2.83
Al_2O_3	11.96	12.55	13.94	13.60	16.83	11.94	12.20	13.90	16.07	12.43	14.21	16.77	15.03
Fe_2O_3T	13.38	13.31	13.37	13.94	11.01	13.61	13.69	14.42	12.44	13.47	13.16	10.97	11.70
MnO	0.17	0.16	0.18	0.18	0.19	0.17	0.17	0.17	0.21	0.18	0.19	0.20	0.18
MgO	10.73	9.21	8.43	9.31	3.99	11.84	11.66	7.76	4.88	10.47	7.37	4.39	7.25
CaO	11.07	11.12	10.61	10.48	9.72	11.12	11.26	10.19	10.30	11.20	10.89	9.36	9.11
Na_2O	2.53	2.69	3.19	3.47	4.12	3.03	3.10	3.06	5.12	3.28	4.30	5.80	4.76
K_2O	1.11	0.69	1.36	1.39	2.26	0.87	0.88	0.89	2.28	1.48	1.89	2.42	2.05
P_2O_5	0.43	0.49	0.67	0.66	0.77	0.59	0.60	0.52	1.09	0.76	0.86	0.96	0.66
Sum	99.77	100.33	100.62	100.27	99.96	99.70	100.11	100.33	100.16	100.61	99.35	99.94	100.05
mg#	61.4	57.8	55.5	57.0	41.8	63.3	62.8	51.6	43.7	60.6	52.6	44.2	55.1
Fr. cor.	0.0	0.0	10.0	7.0	n.d.	3.0	0.0	4.0	n.d.	8.0	22.0	n.d.	8.0
Li	6.92	6.25	8.15	n.d.	n.d.	n.d.	7.86	7.29	n.d.	n.d.	n.d.	n.d.	n.d.
Sc	37.0	39.5	33.6	22.5	16.9	24.7	31.6	30.7	13.6	28.1	26.9	15.4	20.5
V	339	323	372	332	306	294	360	329	243	314	323	286	274
Cr	696	482	341	350	175	523	606	218	14	601	216	26	261
Co	64.4	58.7	55.1	53.7	46.2	54.8	66.7	59.4	26.5	53.8	42.5	30.6	43.4
Ni	285.9	245.3	150.5	195.0	129.2	290.6	331.7	182.2	19.2	210.4	76.1	24.4	143.9
Cu	124.6	102.8	85.3	93.5	101.1	74.7	106.1	108.7	41.6	97.7	83.2	47.4	66.5
Zn	103.6	110.2	112.1	120.2	119.1	98.7	113.8	116.9	105.7	106.1	111.8	129.3	127.1
Ga	18.1	19.4	19.1	21.4	22.2	18.2	20.1	20.3	19.2	18.7	20.2	23.6	24.2
Rb	27.7	11.9	43.2	28.7	37.4	22.6	34.2	17.9	49.5	34.4	47.1	62.0	62.9
Sr	584	579	897	894	895	742	844	617	1229	935	1106	1576	1121
Y	24.4	29.1	28.5	22.8	25.5	20.3	23.5	28.1	31.2	27.2	29.8	37.2	28.2
Zr	241	235	365	268	295	224	266	210	361	285	345	476	400
Nb	51.1	42.0	64.4	89.7	99.3	66.4	73.8	41.0	108.3	79.9	95.1	126.6	122.0
Cs	0.24	0.03	0.35	0.76	0.61	0.68	0.60	0.07	0.62	0.46	0.61	0.83	0.71
Ba	264	211	351	513	600	429	403	249	649	516	620	865	731
La	39.5	40.8	69.1	46.2	57.9	42.3	44.0	38.9	100.8	81.1	89.5	125.9	111.9
Ce	78.4	81.4	141.0	95.3	109.9	89.1	87.3	78.8	201.5	161.8	179.8	236.4	186.4
Pr	9.4	9.7	15.7	11.1	13.5	10.5	10.6	9.5	21.2	17.4	19.7	24.4	18.4
Nd	37.2	37.4	57.2	47.4	56.5	44.5	42.0	37.5	83.3	68.0	77.4	93.1	66.0
Sm	7.6	7.9	9.5	9.1	10.5	8.9	8.5	7.8	13.6	11.7	13.1	15.2	10.8
Eu	2.28	2.53	2.92	2.82	3.18	2.65	2.66	2.51	3.96	3.47	3.93	4.46	3.19
Gd	6.55	7.33	7.56	7.70	8.99	7.28	7.20	7.21	10.88	9.08	9.94	11.72	8.78
Tb	0.88	0.97	1.02	1.00	1.13	0.98	0.91	0.97	1.34	1.21	1.28	1.50	1.15
Dy	5.09	6.05	5.83	5.33	6.20	5.15	5.15	5.87	7.39	6.71	7.11	8.01	6.08
Ho	0.90	1.07	1.05	0.91	1.02	0.88	0.87	1.05	1.33	1.23	1.28	1.37	1.08
Er	2.28	2.59	2.59	2.21	2.75	2.10	2.05	2.59	3.25	2.96	3.32	3.78	2.69
Tm	0.28	0.31	0.33	0.27	0.33	0.26	0.25	0.33	0.42	0.36	0.41	0.45	0.35
Yb	1.63	1.89	1.86	1.73	1.86	1.51	1.43	1.85	2.36	2.22	2.56	2.81	2.28
Lu	0.23	0.26	0.28	0.21	0.26	0.19	0.20	0.26	0.37	0.34	0.35	0.41	0.32
Hf	5.03	5.04	7.08	6.20	6.96	6.31	5.47	4.68	8.64	7.24	8.69	9.46	8.30
Ta	2.95	2.35	3.62	5.10	6.14	4.23	3.96	2.39	6.57	4.81	5.46	6.98	5.86
Pb	1.68	1.22	2.39	2.43	3.11	2.26	1.75	1.47	5.54	3.80	4.90	7.22	7.44
Th	3.09	2.68	4.70	4.57	5.76	4.63	3.36	2.45	10.43	8.98	9.39	15.54	14.74
U	0.84	0.69	1.30	1.16	1.45	1.06	0.84	0.55	2.80	2.36	2.46	4.03	5.65

*major elements analyzed by electron microprobe

Table 1 (continued)

Sample:	KLP92	KLP93	KLA1-2-10*	KLA1-5-07*	KLA1-5-13*	TLP 23-1	TLP 25-1	TLP 38-1	TLP 43-1	TLP 50-2
	C.V.	C.V.	C.V.	C.V.	C.V.	C.V.	C.V.	C.V.	C.V.	C.V.
SiO_2	43.37	43.64	44.06	43.41	42.42	41.85	43.84	44.23	43.29	44.49
TiO_2	3.47	3.53	3.39	3.46	3.40	3.60	3.64	3.54	3.66	3.68
Al_2O_3	14.72	14.25	13.76	13.64	11.77	11.93	13.83	15.35	13.08	14.46
Fe_2O_3T	12.76	12.98	13.61	13.62	13.57	14.20	13.89	13.34	14.10	13.68
MnO	0.19	0.19	0.20	0.20	0.19	0.20	0.19	0.20	0.19	0.19
MgO	7.17	7.58	8.23	7.97	11.76	10.05	7.85	6.54	8.55	7.14
CaO	10.84	11.58	10.53	10.63	10.64	12.15	11.36	10.09	12.39	11.03
Na_2O	4.35	4.46	3.77	3.76	3.06	4.25	3.88	4.73	3.46	3.83
K_2O	1.91	1.32	1.32	1.26	1.39	1.79	1.77	2.09	1.55	1.79
P_2O_5	0.84	0.86	0.69	0.72	0.69	1.13	0.88	0.97	0.87	0.83
Sum	100.02	100.78	99.56	98.67	98.90	101.16	101.14	101.09	101.15	101.12
mg#	52.7	53.6	54.5	53.7	63.2	58.4	52.8	49.3	54.6	50.8
Fr. cor.	17.0	16.0	21.0	n.d.	2.0	9.0	15.0	21.0	15.0	17.0
Li	n.d.	n.d.	n.d.	n.d.	n.d.	n.d.	n.d.	n.d.	n.d.	n.d.
Sc	26.7	29.3	n.d.	n.d.	n.d.	23.5	25.2	20.0	30.0	24.7
V	342	346	n.d.	n.d.	n.d.	324	331	297	343	313
Cr	194	262	n.d.	n.d.	n.d.	455	305	136	365	281
Co	43.6	46.3	n.d.	n.d.	n.d.	53.3	49.0	41.3	49.3	44.8
Ni	90.6	101.0	n.d.	n.d.	n.d.	188.9	109.1	69.3	124.2	93.2
Cu	87.9	56.1	n.d.	n.d.	n.d.	96.9	97.1	57.9	114.1	90.9
Zn	116.1	122.5	n.d.	n.d.	n.d.	124.9	121.5	121.2	108.3	116.9
Ga	21.8	21.5	24.3	27.6	23.5	22.6	22.5	23.8	21.2	22.9
Rb	49.2	33.7	31.4	33.5	37.8	45.7	42.5	56.6	37.0	43.2
Sr	1199	1193	1049	1150	1047	1431	1267	1501	1183	1228
Y	32.1	32.3	33.9	38.1	32.8	33.9	35.7	41.0	33.6	35.4
Zr	328	325	307	331	305	380	344	426	304	358
Nb	96.4	94.0	70.8	77.9	78.2	123.8	101.3	116.1	89.3	105.8
Cs	0.62	0.53	0.38	0.38	0.44	0.54	0.48	0.64	0.47	0.45
Ba	698	664	446	452	506	713	642	738	558	596
La	92.2	95.0	64.3	66.8	68.0	98.6	101.6	111.5	89.0	82.6
Ce	176.0	181.1	126.5	131.3	128.4	185.4	188.7	208.2	167.3	159.1
Pr	18.9	19.7	14.8	15.6	14.7	21.0	20.9	23.0	18.2	18.0
Nd	72.3	75.1	57.2	60.3	55.2	80.5	75.2	83.1	70.2	67.4
Sm	12.0	13.1	10.7	11.3	10.2	14.9	13.3	14.8	12.5	12.2
Eu	3.64	3.77	3.25	3.41	3.02	4.32	4.04	4.55	3.96	3.88
Gd	9.67	10.26	9.49	9.92	8.81	11.81	11.49	12.37	11.16	10.97
Tb	1.30	1.31	1.27	1.33	1.18	1.51	1.50	1.61	1.39	1.40
Dy	6.80	6.98	6.41	6.74	5.90	7.53	7.78	8.75	7.50	7.61
Ho	1.27	1.22	1.14	1.19	1.04	1.27	1.41	1.50	1.30	1.33
Er	3.03	3.07	2.87	2.98	2.66	3.18	3.46	3.88	3.25	3.42
Tm	0.39	0.39	0.36	0.36	0.33	0.41	0.46	0.52	0.45	0.45
Yb	2.42	2.25	2.19	2.22	2.05	2.04	2.51	3.02	2.29	2.50
Lu	0.35	0.31	0.30	0.31	0.28	0.27	0.32	0.39	0.31	0.31
Hf	7.31	7.29	6.66	6.79	6.27	8.08	7.32	8.35	6.56	7.05
Ta	5.32	5.25	3.92	4.10	3.97	7.63	6.59	7.34	5.84	6.87
Pb	4.76	4.87	3.51	3.90	2.99	3.75	4.55	5.06	2.57	4.30
Th	9.93	10.29	6.11	6.45	7.42	9.37	9.55	10.34	8.42	7.65
U	2.65	2.61	1.69	1.73	1.91	2.80	2.56	2.92	2.23	2.02

*Analyses are taken from Klügel et al. (2000)

Table 1 (continued)

Sample:	TLP 58-1 C.V.	TLP 64-1 C.V.	TLP 79-1 C.V.	TLP 15-1 C.V.	TLP 17-1 C.V.	TLP 76-1 C.V.	TLP 111-1 C.V.	TLP 44-1 C.V.	TLP 36-1 C.V.
SiO_2	44.25	44.41	43.68	44.03	44.35	43.24	43.23	43.31	43.38
TiO_2	3.68	3.62	3.66	3.67	3.31	3.74	3.75	3.77	3.43
Al_2O_3	14.51	15.27	14.18	14.92	14.66	13.58	13.43	13.45	13.89
Fe_2O_3T	13.67	13.35	14.50	13.60	13.43	13.99	14.25	14.04	13.96
MnO	0.21	0.20	0.19	0.20	0.20	0.19	0.19	0.19	0.20
MgO	7.04	6.10	7.75	6.69	7.45	7.98	8.29	7.82	8.68
CaO	10.66	10.41	11.17	10.46	11.15	12.10	11.70	12.22	11.36
Na2O	4.21	4.56	3.77	4.48	3.95	3.77	3.74	3.80	3.68
K2O	1.96	2.08	1.43	2.02	1.70	1.61	1.64	1.63	1.53
P_2O_5	0.92	1.07	0.87	1.03	0.90	0.94	0.93	0.91	1.04
Sum	101.12	101.09	101.19	101.11	101.10	101.14	101.17	101.15	101.14
mg#	50.5	47.5	51.4	49.4	52.4	53.1	53.5	52.5	55.2
Fr. cor.	16.0	24.0	17.0	20.0	17.0	17.0	17.0	17.0	16.0
Li	n.d.	n.d.	n.d.	n.d.	n.d.	n.d.	n.d.	n.d.	n.d.
Sc	21.5	20.9	25.9	22.9	25.1	27.3	26.4	30.2	25.0
V	302	295	313	318	318	332	312	376	323
Cr	258	151	231	228	283	297	343	282	310
Co	44.3	37.4	47.1	43.2	45.6	46.6	46.2	49.5	49.6
Ni	95.6	56.4	99.0	73.8	97.5	104.6	107.3	101.9	131.5
Cu	73.8	70.8	97.9	78.6	85.7	112.2	96.0	104.7	80.7
Zn	120.3	117.9	111.0	122.8	108.8	110.1	109.8	120.7	118.0
Ga	23.4	23.6	22.2	24.1	21.4	21.7	21.3	21.3	20.0
Rb	48.6	51.5	30.3	51.8	41.7	37.5	39.2	39.3	32.4
Sr	1271	1345	1033	1329	1025	1216	1166	1287	1227
Y	37.3	36.5	31.7	37.3	33.7	33.8	32.6	34.4	34.0
Zr	396	389	304	384	340	313	307	343	315
Nb	112.9	110.6	76.7	110.9	93.8	90.6	91.6	100.3	91.5
Cs	0.55	0.55	0.34	0.54	0.47	0.41	0.44	0.44	0.39
Ba	652	661	464	649	545	585	583	608	569
La	94.4	84.7	74.1	91.7	74.6	89.3	87.7	99.0	92.6
Ce	183.1	170.3	153.4	172.5	146.9	177.9	174.6	186.8	178.5
Pr	20.4	18.8	17.3	19.6	16.7	19.5	19.0	20.9	20.2
Nd	79.2	74.6	69.1	72.9	66.0	76.2	73.6	79.4	78.7
Sm	14.4	13.9	12.5	13.7	12.6	13.4	13.8	13.7	14.3
Eu	4.41	4.23	3.90	4.16	3.47	4.01	4.03	3.93	4.06
Gd	12.21	11.47	10.64	11.51	9.76	10.80	11.07	11.86	11.84
Tb	1.57	1.51	1.37	1.51	1.33	1.42	1.46	1.45	1.47
Dy	8.48	7.96	7.29	7.96	7.03	7.59	7.83	7.94	8.23
Ho	1.47	1.41	1.27	1.38	1.28	1.32	1.32	1.33	1.39
Er	3.69	3.70	3.21	3.58	3.43	3.45	3.41	3.25	3.46
Tm	0.48	0.50	0.41	0.48	0.48	0.48	0.47	0.42	0.45
Yb	2.72	2.73	2.31	2.58	2.72	2.44	2.53	2.36	2.59
Lu	0.35	0.37	0.29	0.34	0.36	0.32	0.33	0.34	0.36
Hf	8.55	8.01	6.72	7.85	6.85	6.92	7.21	7.68	7.17
Ta	7.76	7.06	5.08	6.84	6.29	5.90	6.20	5.05	4.78
Pb	5.12	5.16	3.33	5.49	5.57	3.77	4.34	3.74	3.89
Th	8.54	8.01	5.99	8.12	8.05	8.80	7.87	10.04	8.71
U	2.32	2.70	1.79	2.57	2.12	2.35	2.21	2.48	1.88

K/U = 3014 - 13557, Zr/U = 71 - 386) and form inverse correlations with U. Because these correlations also exist with Th as denominator, they are not caused by alteration and mobilization. The pre-CV samples show the highest of these ratios and in particular have Nb/U ratios partly above the global OIB range of 47 ± 10 (Hofmann et al., 1986), whereas Nb/U of CV samples is around the global range (Fig. 5).

On incompatible element diagrams, primitive samples from La Palma show features characteristic of HIMU-type basalts (HIMU = high μ = high $^{238}U/^{204}Pb$) including relative enrichment in Nb and Ta and pronounced K and Pb troughs (Fig. 6), as well as high Ce/Pb (11.3 - 68.6) and Nd/Pb (8.9 - 30.6) but relatively low K/Nb (87 - 210), Ba/Nb (5.0 - 8.3) and La/Nb (0.51 - 1.07) (cf. Weaver, 1991). Fig. 6 also illustrates the progressive enrichment of CV samples compared to pre-CV samples with decreasing compatibility. Chondrite-normalized REE patterns of all studied rocks show no Eu anomalies and steep negative slopes (Fig. 7) consistent with residual garnet in the mantle source. Remarkably, La/Yb (27.1 - 49.1) and Sm/Yb (4.6 - 7.3) ratios of Cumbre Vieja lavas are higher than those of most other OIB worldwide (Table 2) as shown by a comparison with the GeoRock database (Max-Planck-Institut für Geochemie, Mainz, Germany).

Despite some systematic differences between pre-CV and CV rocks, there is no progressive change in the geochemical composition of La Palma lavas during the last 1.1 Ma. This is

Table 2: La/Yb and Sm/Yb ratios in La Palma mafic samples (this study, Klügel et al, 2000; Carracedo et al, 2001) and other OIB. Only samples with MgO > 6 wt% were incorporated.

	La/Yb (range)	La/Yb (average)	Sm/Yb (range)	Sm/Yb (average)
Taburiente	19.1 – 37.2	24.4	3.7 – 6.4	4.9
Cumbre Nueva	19.5 - 34.7	25.4	4.0 – 6.2	4.8
Bejenado	21.1 – 30.8	26.7	4.2 – 5.3	5.5
Cumbre Vieja	27.1 - 49.1	37.0	4.6 – 7.3	5.6
Gran Canaria[1]	13.9 – 56.5	29.3	4.1 - 9.4	6.1
Tenerife[2,3]	11.5 – 33.5	23.9	2.4 – 6.5	4.8
Hawaii[4,5,6,7,8]	4.7 – 60.8	20.7	2.6 – 12.8	4.7
Madeira[9,10]	3.3 – 30.1	16.7	1.3– 5.2	3.8
Cape Verde[11,12,13]	14.8 – 38.0	26.9	3.7 – 6.5	5.3
Reunion[14,15]	6.3 – 18.6	10.5	2.4 – 4.0	3.1
Comore[16,17]	10.3 – 53.3	25.2	2.2 – 4.5	3.5
St. Helena[18,19]	3.0 – 20.6	16.5	1.1 – 4.6	3.7

1 Hoernle et al., 1993; 2, Thirlwall et al., (2000), 3 Neumann et al (1999), 4 Frey et al, (1990), 5 Frey et al, (1991), 6 Jackson et al., (1999), 7 Sims et al., (1999), 8 Clague et al. (1982), 9 Geldmacher et al. (2000), 10 Schwarz et al., 2005, 11 Gerlach et al. (1988), 12 Davies et al. (1989), 13 Jorgensen and Holm (2002), 14 Fisk et al. (1988), 15 Fretzdorff and Haase (2002), 16 Deniel (1998), 17 Class and Goldstein (1997), 18 Chaffey et al. (1989), 19 Asavin et al. (1997)

shown by plots of trace element ratios of dated or age-constrained samples versus age (Fig. 8). All trace element or isotope ratios examined by us showed no correlation with age but rather an irregular scatter, which is beyond analytical error in most cases. The data variation over a short period such as the Bejenado phase (560 - 490 ka) can be as large as that for the entire pre-CV period since 1.1 Ma. Although it is possible that a gradual change in

composition occurred during the pre-CV to CV transition from 400 - 125 ka not covered by any sample, the overall data spread renders this possibility rather unlikely.

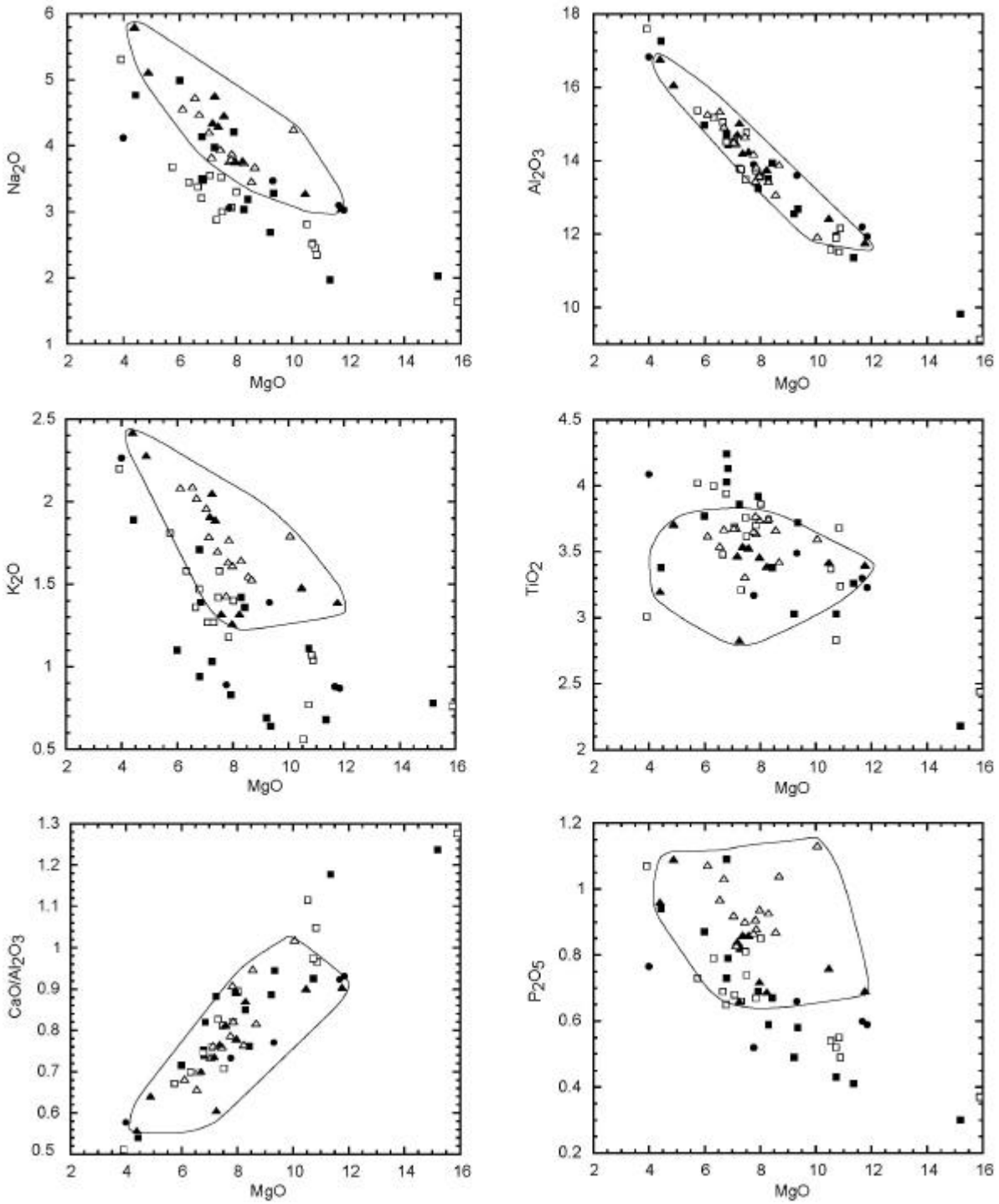

Fig. 3: Selected major element (wt%) variations versus MgO (wt%) for mafic samples from La Palma. Field for CV samples are highlighted. Symbols as in Fig. 2. At given MgO, CV samples have higher Na_2O, K_2O and P_2O_5 than samples from the older units.

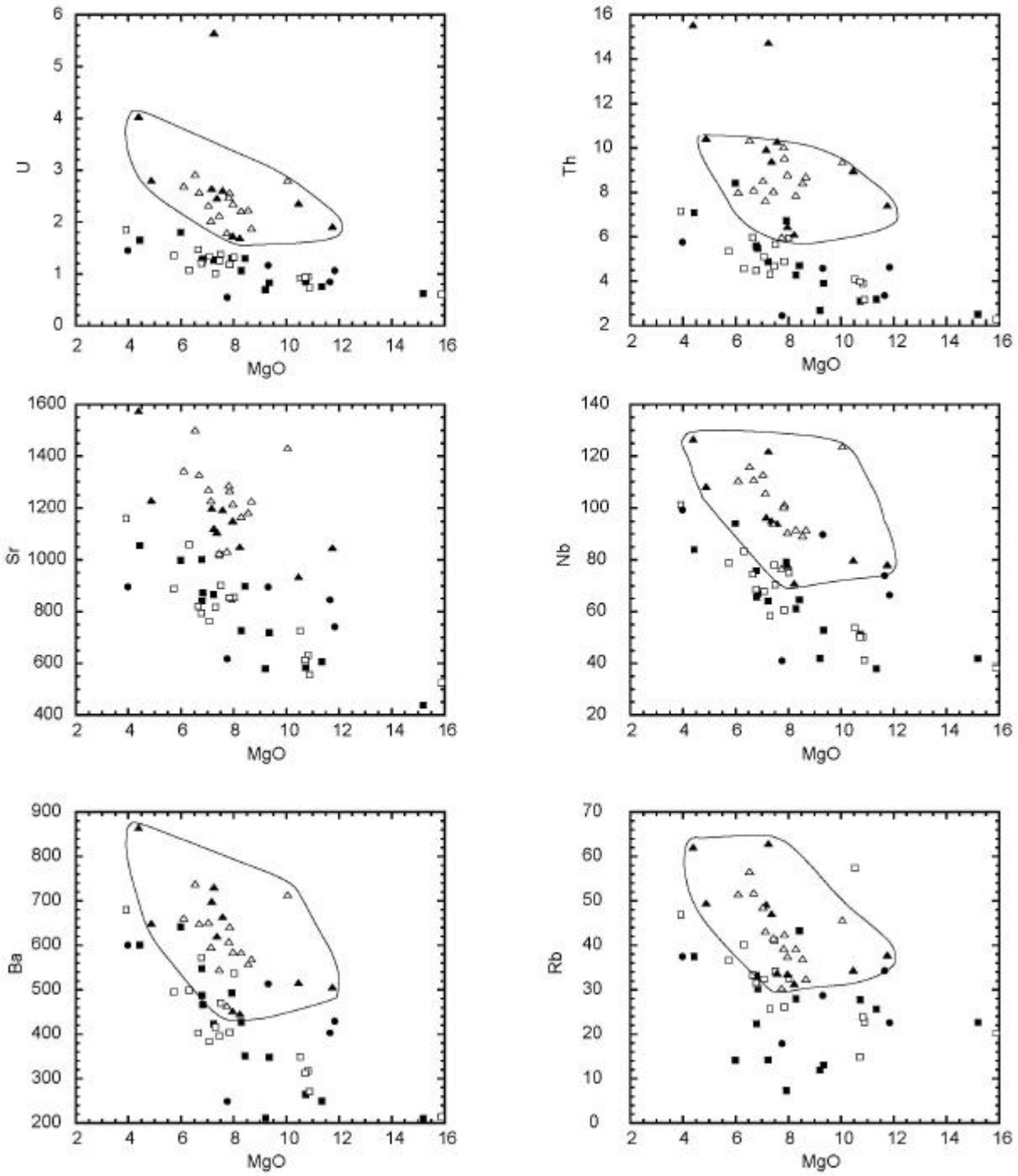

Fig. 4: Selected trace element (ppm) variations versus MgO (wt%) for mafic samples from La Palma. Symbols as in Fig. 2.

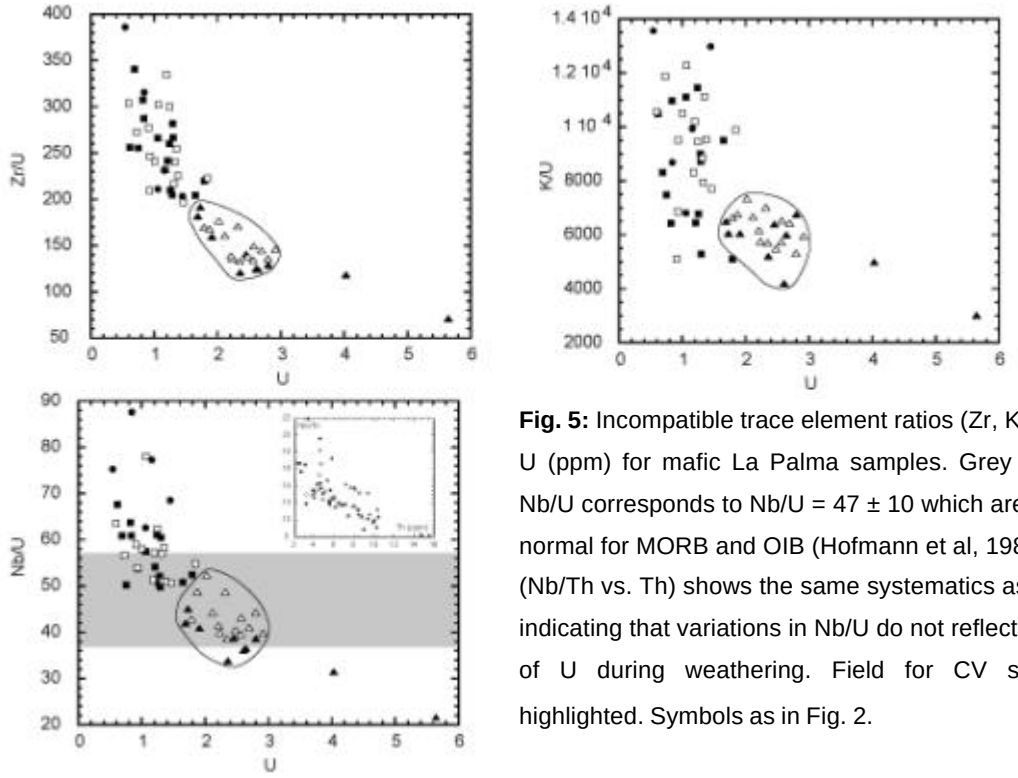

Fig. 5: Incompatible trace element ratios (Zr, K, Nb) versus U (ppm) for mafic La Palma samples. Grey rectangle of Nb/U corresponds to Nb/U = 47 ± 10 which are considered normal for MORB and OIB (Hofmann et al, 1986) The inset (Nb/Th vs. Th) shows the same systematics as Nb/U vs. U indicating that variations in Nb/U do not reflect mobilization of U during weathering. Field for CV samples are highlighted. Symbols as in Fig. 2.

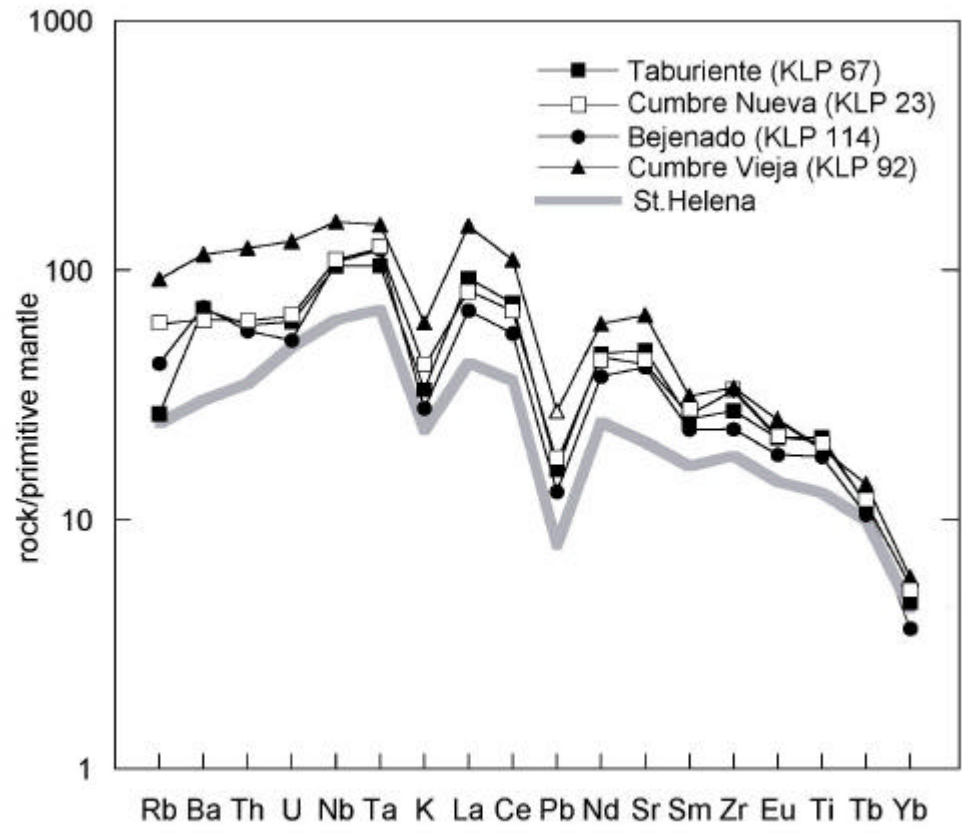

Fig. 6: Incompatible trace element concentrations normalized to primitive mantle values after Hofmann (1988) of representative primitive La Palma samples for each volcanic phase compared with HIMU basanite from St. Helena (sample 68 from Chaffey et al., 1989).

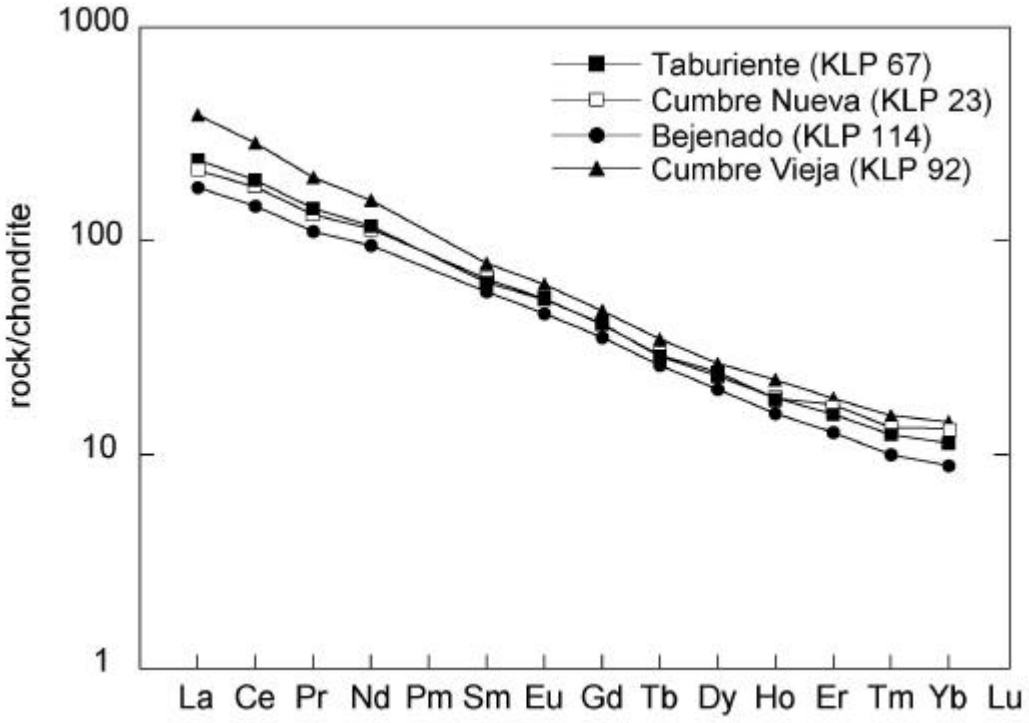

Fig. 7: Chondrite-normalized REE patterns of selected primitive La Palma samples for each volcanic phase. Normalizing values after Sun and McDonough (1989*)*

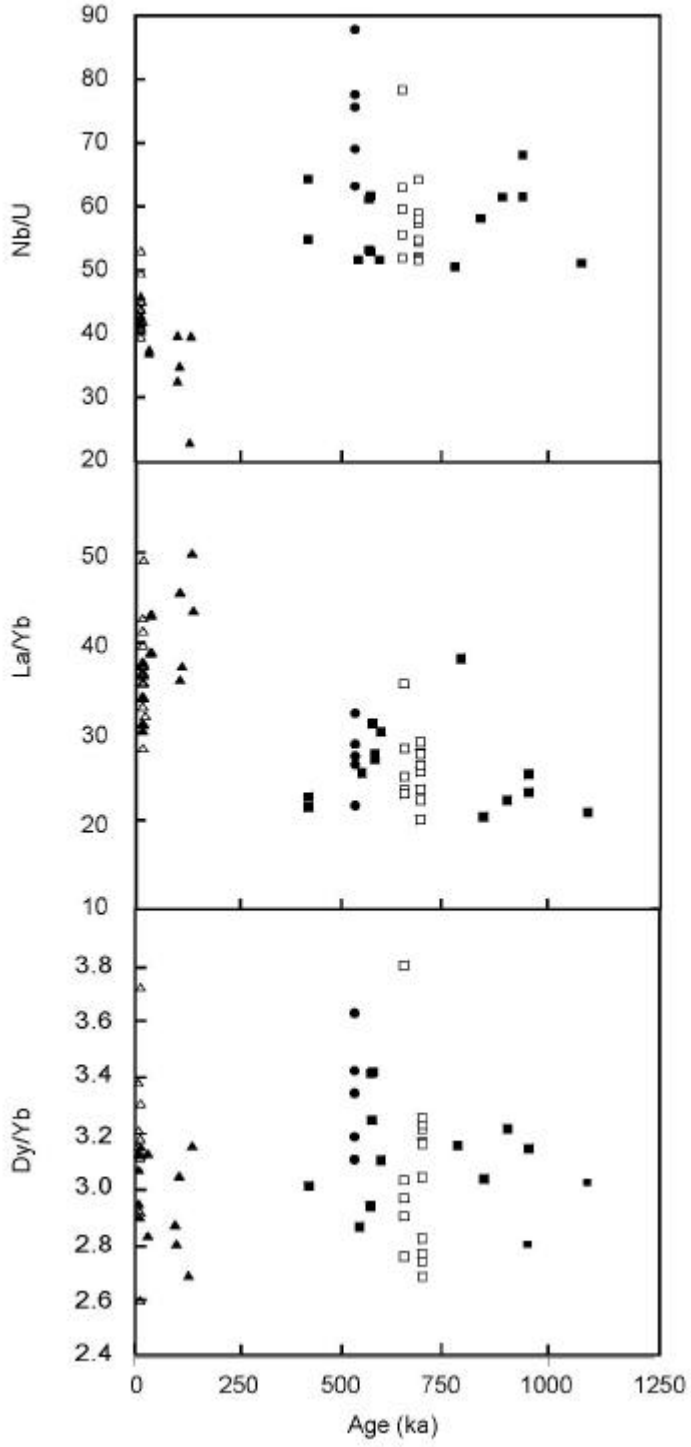

Fig. 8: Temporal variations of selected trace element ratios of dated or age-constrained samples (ages from Guillou et al., 1998, 2001 and Carracedo et al., 2001).symbols as in Fig. 2

5.2 Sr-Nd-Pb isotopes

Sr, Nd and Pb isotope ratios of representative samples from all units are presented in Table 3. As shown in Figs. 9 and 10, Cumbre Vieja rocks display a rather limited range in isotopic compositions ($^{87}Sr/^{86}Sr$ = 0.703087 - 0.703169, $^{143}Nd/^{144}Nd$ = 0.512888 - 0.512901, $^{206}Pb/^{204}Pb$ = 19.497 - 19.715, $^{207}Pb/^{204}Pb$ = 15.609 - 15.888; $^{208}Pb/^{204}Pb$ = 39.159 - 39.488). Only a few samples (KLP 82, KLA 1512, KLA 1514) have increased $^{87}Sr/^{86}Sr$ ratios plotting off the overall trend, which may be attributed to the involvement of seawater or alteration. Our data for Taburiente and Cumbre Nueva rocks show a small range only for $^{87}Sr/^{86}Sr$

(0.703017 - 0.703110) but are variable in $^{143}Nd/^{144}Nd$ (0.512880 - 0.512938) and highly variable in their Pb isotopic ratios ($^{206}Pb/^{204}Pb$ = 19.286 - 19.947, $^{207}Pb/^{204}Pb$ = 15.556 - 15.639, $^{208}Pb/^{204}Pb$ = 38.942 - 39.758), which becomes even more pronounced when additional data from detailed stratigraphic sections are included (B. Nelson, unpublished data, 2004). Generally, Taburiente and Cumbre Nueva rocks have a tendency to more radiogenic Pb compositions than Cumbre Vieja rocks, which was also observed in a previous study (Marcantonio at al., 1995). Bejenado volcano is somewhat exceptional as it has the largest Sr-Nd-Pb isotopic variability of all investigated units, even though it represents by far the shortest growth period and smallest spatial extent (see Fig. 1). Bejenado samples include the isotopically most depleted rocks of this study and extend well towards the fields for the most enriched La Palma rocks (Fig. 9, 10). Among all of our samples, the least radiogenic Pb and Sr and the most radiogenic Nd composition is shown by a group of four samples (KLP 105, KLP 106, KLP 114, KLP 205) hereafter termed LPbB ($^{87}Sr/^{86}Sr$ = 0.703001 - 0.703021; $^{143}Nd/^{144}Nd$ = 0.512945 - 0.512971; $^{206}Pb/^{204}Pb$ = 19.142 - 19.182; $^{207}Pb/^{204}Pb$ = 15.544 - 15.557; $^{208}Pb/^{204}Pb$ = 38.829 - 38.902).

In the $^{208}Pb/^{204}$ vs. $^{206}Pb/^{204}Pb$ correlation diagram, the points for all La Palma samples define a good linear array parallel to and slightly above the Northern Hemisphere Reference Line (NHRL) of Hart (1984), whereas in the $^{207}Pb/^{204}Pb$ vs. $^{206}Pb/^{204}Pb$ diagram the linear array is parallel to and below the NHRL (Fig. 9). As expected, $^{143}Nd/^{144}Nd$ correlates negatively with $^{206}Pb/^{204}Pb$ and positively with $^{87}Sr/^{86}Sr$ although the correlations are less well defined than for the Pb isotope diagrams (Figs. 9 and 10). Most of the data variation is consistent with mixing between two isotopically distinct sources involved in the formation of La Palma magmas. The most depleted isotopic composition (Sr / Nd / Pb = 0.702987 / 0.512971 / 19.142) is best represented by sample KLP205 from Bejenado plotting towards the DMM component (depleted MORB mantle); the most enriched of our samples (Sr / Nd / Pb = 0.703110 / 0.512880 / 19.942) is KLP41 from Cumbre Nueva plotting towards the HIMU component of Zindler and Hart (1986). However, the scatter of the data beyond analytical error and the lack of an unequivocal trend line in the $^{143}Nd/^{144}Nd$ diagrams of Figs. 9 and 10 cannot be explained by binary mixing alone and indicates additional processes controlling the isotopic composition of La Palma magmas.

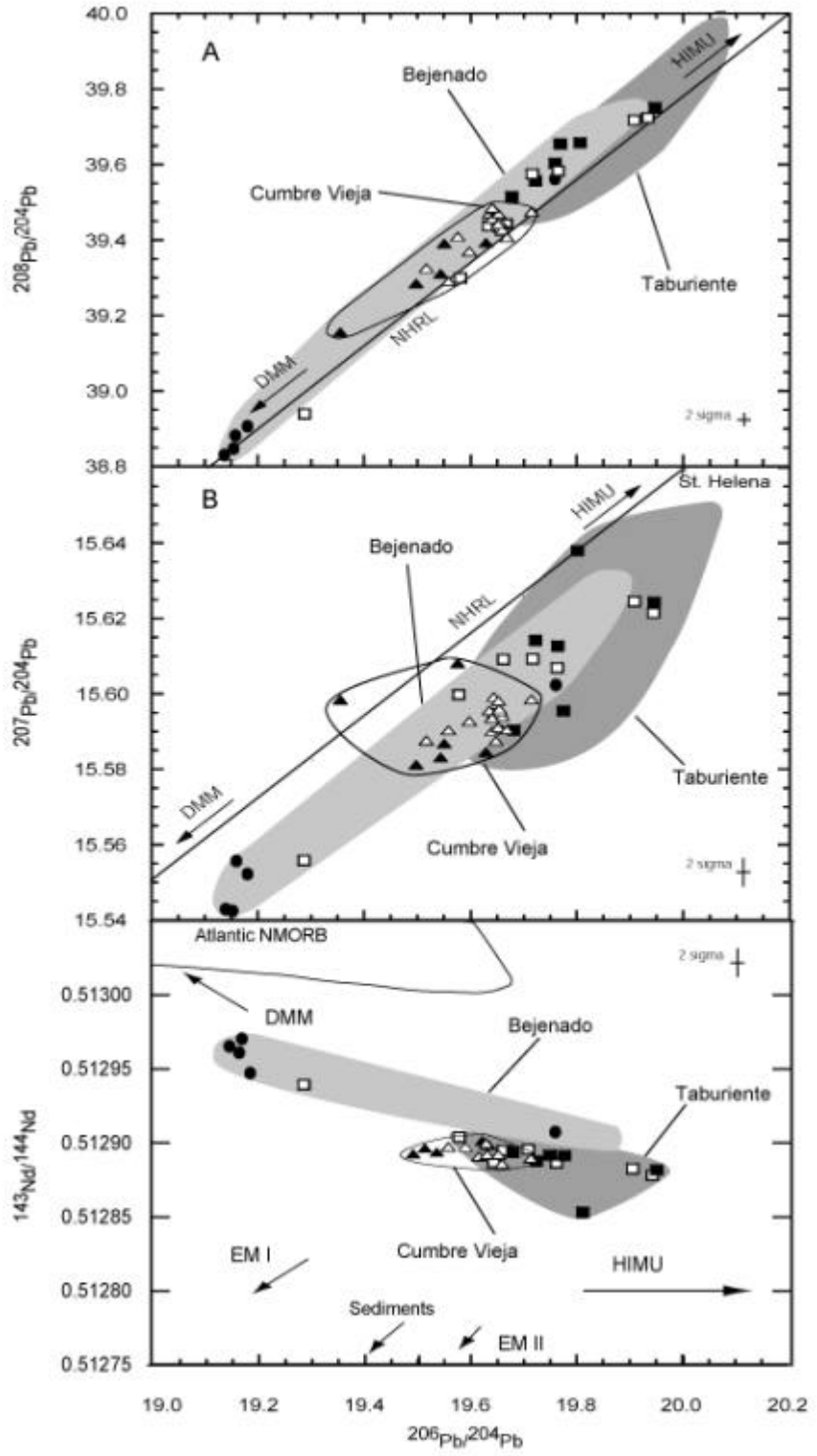

Fig. 9: Pb isotope correlation diagrams for representative La Palma samples. Grey fields indicate the range for Taburiente and Bejenado. Field for Bejenado includes data from Nelson et al. (unpublished data, 2004) and field for Taburiente includes data from Marcantonio et al., (1995) and Nelson et al. (unpublished data, 2004). Symbols as in Fig. 2. (a) $^{208}Pb/^{204}Pb$ vs. $^{206}Pb/^{204}Pb$ correlation diagram. Northern hemisphere reference line (NHRL) after Hart (1984). (b) $^{207}Pb/^{204}Pb$ vs. $^{206}Pb/^{204}Pb$ correlation diagram with NHRL after Hart (1984). (c) $^{144}Nd/^{143}Nd$ vs. $^{206}Pb/^{204}Pb$ correlation diagram for La Palma samples. Mantle end-member after composition are taken from Hart (1988). Array for Atlantic NMORB is based on data from Dupré and Allègre (1980), Ito et al., (1987) and Cohen and O'Nions (1982).

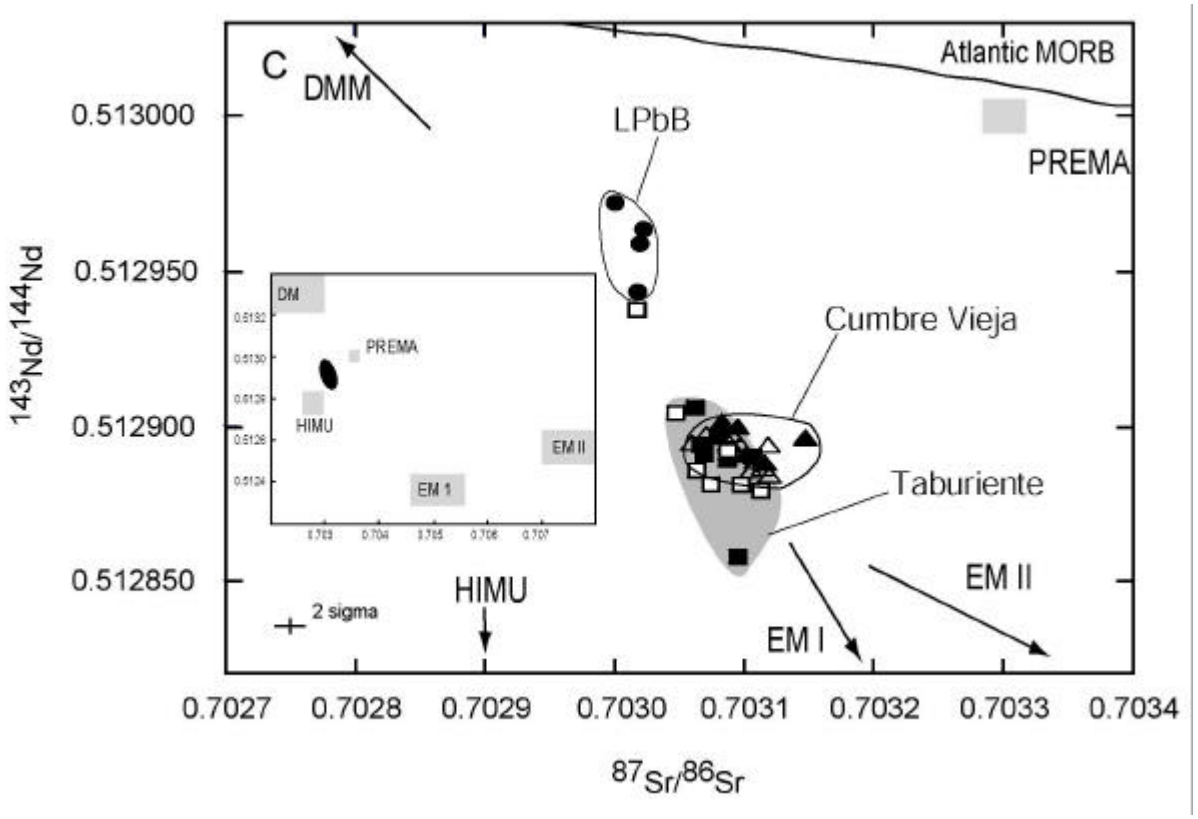

Fig. 10: $^{87}Sr/^{86}Sr$ vs. $^{144}Nd/^{143}Nd$ correlation diagram. Endmember values and PREMA (prevalent mantle) in the inset are taken from Hart (1988). Array for Atlantic NMORB is based on data from Dupré and Allègre (1980), Ito et al., (1987) and Cohen and O'Nions (1982). LPbB samples are the most depleted having the lowest radiogenic $^{87}Sr/^{86}Sr$ ratios (0.7030010 - 0.7030207) and highest $^{144}Nd/^{144}Nd$ (0.512945 - 0.512971). Symbols as in Fig. 2

Table 3: Sr-Nd-Pb isotope analyses from La Palma lavas

Sample No.	Age*	$^{87}Sr/^{86}Sr$	2sigma	$^{143}Nd/^{144}Nd$	2sigma	$^{206}Pb/^{204}Pb$	2sigma	$^{207}Pb/^{204}Pb$	2sigma	$^{208}Pb/^{204}Pb$	2sigma
Taburiente											
KLP59	533 ± 8	0.703072	0.000002	0.512892	0.000003	19.760	0.001	15.614	0.001	39.614	0.003
KLP63	410 ± 80	0.703078	0.000003	0.512889	0.000003	19.722	0.001	15.614	0.001	39.567	0.002
KLP65	563 ± 8	0.703080	0.000003	0.512892	0.000003	19.679	0.001	15.590	0.001	39.518	0.003
KLP67	585 ± 10	0.703080	0.000003	0.512890	0.000002	19.773	0.001	15.596	0.001	39.657	0.002
KLP73	560 ± 8	0.703098	0.000003	0.512881	0.000002	19.947	0.001	15.624	0.001	39.758	0.002
KLP77	833 ± 14	0.703095	0.000004	0.512858	0.000003	19.805	0.002	15.639	0.002	39.667	0.006
Cumbre Nueva											
KLP19	647 ± 10	0.703056	0.000002	0.512896	0.000003	19.663	0.001	15.608	0.001	39.451	0.002
KLP23		0.703066	0.000003	0.512886	0.000002	19.644	0.001	15.595	0.001	39.457	0.002
KLP27		0.703058	0.000002	0.512896	0.000004	19.717	0.001	15.609	0.001	39.571	0.002
KLP35		0.703091	0.000002	0.512885	0.000003	19.765	0.001	15.606	0.001	39.581	0.002
KLP41		0.703110	0.000002	0.512880	0.000002	19.942	0.002	15.622	0.002	39.726	0.004
KLP80	834 ± 12	0.703047	0.000002	0.512903	0.000003	19.577	0.002	15.600	0.001	39.308	0.004
KLP87		0.703075	0.000002	0.512882	0.000002	19.911	0.001	15.626	0.001	39.717	0.003
KLP103		0.703017	0.000003	0.512938	0.000002	19.286	0.002	15.556	0.001	38.942	0.003
Bejenado											
KLP105_Chips		0.702987	0.000004	0.512962	0.000002	19.157	0.002	15.542	0.001	38.849	0.003
KLP106		0.703006	0.000003	0.512953	0.000003	19.182	0.001	15.553	0.001	38.902	0.002
KLP114		0.703021	0.000003	0.512964	0.000002	19.142	0.002	15.544	0.002	38.829	0.004
KLP205_Chips		0.703001	0.000002	0.512971	0.000002	19.164	0.001	15.557	0.001	38.883	0.002
KLP217_Chips		0.703061	0.000002	0.512906	0.000002	19.762	0.001	15.603	0.001	39.567	0.002
Cumbre Vieja											
KLP47_Chips	123 ± 3	0.703083	0.000002	0.512901	0.000002	19.629	0.0007	15.585	0.001	39.396	0.002
KLP52	90 ± 3	0.703087	0.000003	0.512901	0.000003	19.544	0.0004	15.584	0.000	39.313	0.001
KLP82	120 ± 3	0.703141	0.000003	0.512892	0.000002	19.497	0.0005	15.582	0.000	39.288	0.001
KLP92	20± 2	0.703098	0.000003	0.512900	0.000002	19.550	0.0006	15.587	0.001	39.394	0.002
TLP19-2		0.703125	0.000003	0.512896	0.000002	19.648	0.0006	15.588	0.001	39.438	0.002
TLP23-1		0.703088	0.000003	0.512899	0.000002	19.558	0.0006	15.591	0.001	39.294	0.002
TLP25-1	1677 A.D.	0.703099	0.000003	0.512892	0.000002	19.636	0.0006	15.594	0.001	39.426	0.002
TLP38-1		0.703117	0.000003	0.512887	0.000002	19.660	0.0006	15.596	0.001	39.472	0.002
TLP43-1	1646 A.D.	0.703108	0.000003	0.512891	0.000002	19.641	0.0006	15.600	0.001	39.439	0.002

*****Sample ages from pre-historic eruptions are taken from Guillou et al. (1998, 2001)

Table 3 (continued)

Sample No.	Age*	$^{87}Sr/^{86}Sr$	2sigma	$^{143}Nd/^{144}Nd$	2sigma	$^{206}Pb/^{204}Pb$	2sigma	$^{207}Pb/^{204}Pb$	2sigma	$^{208}Pb/^{204}Pb$	2sigma
Cumbre Vieja											
TLP46-1		0.703129	0.000002	0.512895	0.000003	19.656	0.001	15.595	0.000	38.464	0.001
TLP50-1	1585 A.D.	0.703095	0.000003	0.512892	0.000007	19.655	0.001	15.594	0.001	38.448	0.002
TLP50-2	1585 A.D.	0.703082	0.000003	0.512898	0.000008	19.644	0.001	15.591	0.001	38.415	0.003
TLP51-2	1585 A.D.	0.703099	0.000003	0.512893	0.000004	19.660	0.001	15.599	0.001	38.468	0.002
TLP51-3	1585 A.D.	0.703076	0.000003	0.512897	0.000002	19.653	0.001	15.592	0.001	39.426	0.002
TLP58-1	1480 A.D.	0.703107	0.000003	0.512891	0.000002	19.652	0.002	15.599	0.002	39.454	0.005
TLP64-1		0.703102	0.000003	0.512891	0.000003	19.715	0.002	15.599	0.002	39.478	0.004
TLP69-1		0.703082	0.000002	0.512898	0.000003	19.641	0.001	15.596	0.001	39.411	0.003
TLP79-1	1971 A.D.	0.703118	0.000004	0.512896	0.000003	19.598	0.002	15.593	0.001	39.373	0.004
TLP116-1		0.703118	0.000003	0.512896	0.000003	19.669	0.001	15.599	0.001	39.488	0.003
KLA1-5-07	1949 A.D.	0.703114	0.000004	0.512890	0.000002	19.354	0.001	15.599	0.001	39.159	0.003
KLA1-2-10	1949 A.D.	0.703169	0.000002	0.512890	0.000003	19.516	0.001	15.599	0.000	39.329	0.001
KLA1-5-13	1949 A.D	0.703167	0.000002	0.512888	0.000002	19.576	0.004	15.609	0.003	39.412	0.008

5.3 Mineral chemistry

Amphibole and phlogopite are common metasomatic phases in peridotitic mantle xenoliths from Cumbre Vieja volcano (Wulff-Pedersen et al., 1996). We have analyzed amphiboles and phlogopites in veins of a dunite xenolith (sample KLA1362) and isolated phlogopite grains in another dunite (KLA1374) for their trace element composition. Both xenoliths derive from the 1949 eruption on the Cumbre Vieja and are described in detail in Klügel (1998). Amphiboles are titaniferous pargasites to kaersutites with a wide compositional range for both major and trace elements (Table 4). Their trace-element characteristics and concentrations resemble those of pre-CV lavas except for strongly negative Th and U and negative Zr anomalies. Phlogopites are also highly variable in composition but are important sites only for K, Rb, Ba, Nb and Ta as compared to La Palma lavas.

Apatite commonly occurs as inclusions and/or phenocrysts up to 1 mm in size in cumulate xenoliths and evolved lavas from Cumbre Vieja. We have analyzed apatite phenocrysts from a prehistoric tephriphonolitic lava (sample KLA1721). Their trace element compositions are highly variable and, compared to La Palma lavas, are highly enriched in Sr, Y, REE, Th and U (Table 4). They also overlap the compositional range for magmatic and metasomatic apatites in peridotite xenoliths from different localities (O'Reilly and Griffin , 2000).

Table 4: Major and trace element concentrations of amphibole, apatite and phlogopite used in the model calculations (N = number of grains analyzed)

Sample	*KLA 1-3-62*			KLA1-7-21			KLA 1-3-62/KLA1-3-74		
Mineral	Amphibole			Apatite			Phlogopite		
	N = 10			N = 4			N = 4		
	min.	max.	ave.	min.	max.	ave.	min.	max.	ave.
SiO_2	41.00	44.46	42.82	0.35	0.48	0.43	39.01	40.23	39.75
TiO_2	2.15	5.09	3.44	-	-	-	2.36	3.10	2.68
Al_2O_3	12.29	13.34	12.51	0.00	0.02	0.01	15.39	16.29	15.79
FeOt	4.33	4.62	4.49	-	-	-	4.58	4.93	4.79
MnO	0.00	0.05	0.03	0.06	0.19	0.11	0.00	0.04	0.02
MgO	16.13	18.63	17.40	-	-	-	22.52	23.48	23.12
CaO	11.96	12.51	12.35	54.23	55.14	54.47	0.00	0.00	0.00
Na_2O	2.77	3.13	2.95	0.15	0.22	0.20	1.59	1.74	1.65
K_2O	0.91	1.27	1.07	-	-	-	7.92	7.62	7.77
Cr_2O_3	0.96	1.73	1.24	-	-	-	0.00	0.04	0.02
P_2O_5	-	-	-	40.99	43.16	41.57	0.00	0.05	0.02
Cl	-	-	-	0.10	0.16	0.14	0.03	0.05	0.04
F	0.09	0.17	0.13	2.07	3.06	2.47	0.33	0.41	0.36
Total	98.26	99.52	98.99	99.44	101.04	100.63	95.41	96.55	96.01
	N = 8			N = 2			N = 8		
Rb	4.25	14.36	7.43	0.00	0.35	0.14	241	349	306
Sr	1001	1268	1152	3016	4740	3885	61.3	290	142
Y	21.8	28.4	24.7	193	407	3295	0.00	0.19	0.07
Zr	97.2	179	146	9.38	13.7	14.6	9.3	56.0	19.57
Nb	65.3	117.3	89.2	0.26	0.55	0.39	61.2	295	197
Ba	333	820	506	31.4	84.1	56.8	958	6272	2763
La	23.1	43.2	31.0	1080	5009	2863	0.04	0.24	0.09
Ce	75.3	132.4	98.4	1874	6122	3872	0.00	0.49	0.10
Pr	15.95	110.07	13.02	210	498	345	0.00	0.07	0.02
Nd	49.3	66.5	56.2	805	1478	1154	0.00	0.44	0.7
Sm	9.78	12.9	11.3	124	184	154	<LLD	<LLD	<LLD
Eu	3.37	4.37	3.69	33.7	47.3	40.4	0.03	0.20	0.11
Gd	7.67	9.82	8.63	86.6	116	106	<LLD	<LLD	<LLD
Tb	0.92	1.31	1.11	10.1	15.1	12.8	<LLD	<LLD	<LLD
Dy	5.58	7.06	6.22	45.6	79.0	62.8	<LLD	<LLD	<LLD
Ho	0.91	1.19	1.04	7.4	14.1	11.0	<LLD	<LLD	<LLD
Er	2.05	2.88	2.44	14.7	33.4	24.7	<LLD	<LLD	<LLD
Tm	0.24	0.33	0.29	1.68	4.39	3.0	<LLD	<LLD	<LLD
Yb	1.54	2.25	1.90	8.94	27.0	17.8	<LLD	<LLD	<LLD
Lu	0.15	0.29	0.24	1.2	3.68	2.25	<LLD	<LLD	<LLD
Hf	3.45	5.16	4.41	0.00	0.07	0.09	0.29	0.92	0.54
Ta	3.39	5.86	4.68	<LLD	<LLD	>LLD	1.53	8.90	4.58
Pb	0.25	1.16	0.59	1.35	3.69	2.59	0.67	1.63	1.10
Th	0.21	1.07	0.37	24.1	139	67.4	<LLD	<LLD	<LLD
U	0.04	0.32	0.10	4.8	27.7	13.8	0.01	0.08	0.03

Major elements (wt%) determined by electron microprobe; trace elements (ppm) determined by LA-ICP-MS; LLD = lower limit of detection

6. Discussion

We have shown that volcanic rocks from the Recent Cumbre Vieja rift zone are more enriched in highly incompatible elements than those from the older Taburiente/Cumbre Nueva and Bejenado volcanoes. The systematic geochemical differences between both groups and the lack of a progressive geochemical evolution over time suggests that the older volcanoes in the north and the younger Cumbre Vieja in the south represent distinct volcanic systems rather than a progressively evolving volcano. By evaluating the isotope data and the trace element characteristics, we compare the two volcanic groups in order to investigate if,

and how, the source composition and and melting conditions have changed during the last 1.0 Ma. In particular, we concentrate on the possible contribution of additional (metasomatic) mineral phases within the oceanic lithosphere to magmatism.

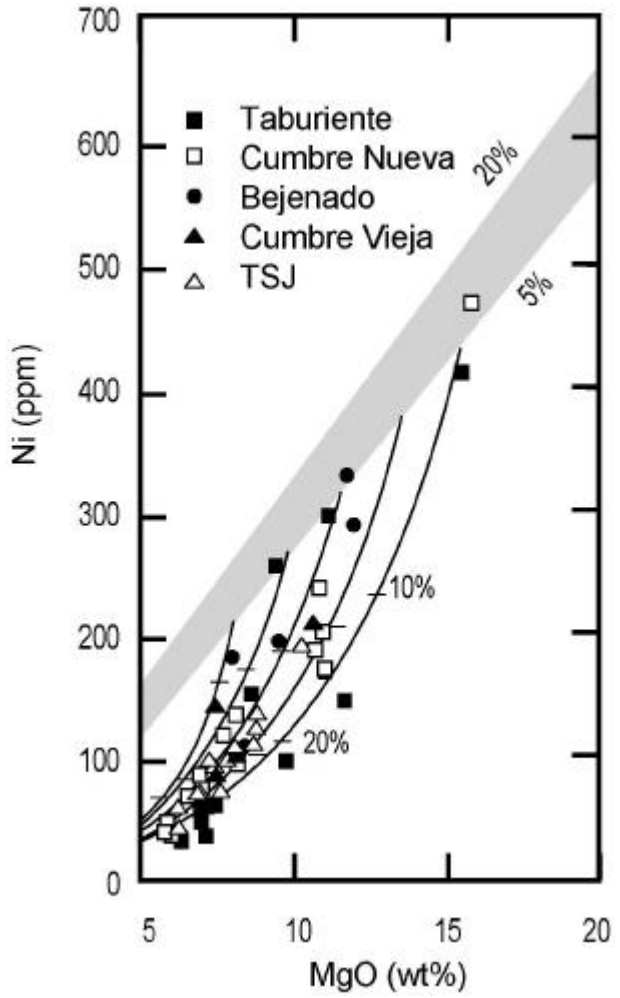

Fig. 11: Ni-MgO relationships for crystallization models of inferred La Palma parental liquids (>MgO 6%). Shaded field indicates range of batch partial melts of a fertile peridotite (Sato 1977; Hart and Davis, 1978). Possible crystallization trajectories are shown for liquids starting on the 5% melting curve. Calculations used partition coefficient of Ni between olivine and melt after Hart and Davis (1978) and between clinopyroxene and melt after Green (1994); Mg#(cpx) = 1.028*Mg#(ol) after Irving and Price (1981). Numbers at cross ticks show the amount of total olivine and clinopyroxene crystallized.

6.1 Melting models

Composition of primary melts

The occurrence of porphyritic rocks and differentiated lavas and the comparatively low Mg number of most basalts indicate that significant crystal fractionation is common beneath La Palma. This process needs to be corrected in order to estimate the compositions of primary melts, to place constraints on the mineralogical and chemical compositions of the mantle source beneath La Palma, and to investigate melting processes. In the following, we used data of relatively primitive samples (MgO > 6 wt%) and normalized them by correcting for olivine and clinopyroxene fractionation, which are the dominant phenocryst phases. This was done by adding equilibrium olivine and clinopyroxene in equal proportions to bulk-rock compositions until the Ni and MgO contents reached those of partial melts of a residual mantle lherzolite (Fig. 11; Sato, 1977; Hart and Davis, 1978). On average, 12-16 % fractionation of olivine and clinopyroxene for Taburiente, Cumbre Nueva and Cumbre Vieja lavas and 5-6 % for Bejenado lavas were estimated by this procedure (Fig. 11, Table 1).

Calculations using Rayleigh fractionation rather than equilibrium crystallization would result in slightly higher amounts of fractionation by about ~3 to 8%. Trace element concentrations in the fractionation-corrected lavas were calculated using the equilibrium-crystallization equation of Shaw (1970) yielding our best estimates for the compositions of the respective primary melts. As a second step, we aimed to reconstruct these compositions in a forward-modelling approach based on non-modal batch melting for variable degrees of melting and variable source mineralogy (see Table 5 and 6 for the partition coefficients and source parameters). The aim of these calculations was to constrain the source mineralogy and to test whether variable degrees of partial melting or variable source composition are capable of generating the overall range of trace element compositions observed for the full suite of La Palma lavas.

Evidence for an amphibole-bearing mantle source

The identification of hydrous phases in the mantle source beneath La Palma has important implications for melting processes and the depth of magma generation. The negative K anomalies (Fig. 6), relative depletion in Rb and Ba and slight concave REE patterns of primitive La Palma basalts strongly suggest that amphibole and/or phlogopite are involved in their petrogenesis (e.g. Mertes and Schmincke, 1985; Wilson and Downes, 1991; Späth et al., 2001). This is consistent with the observed buffering of K and Ti: Both elements behave incompatibly during partial melting of a dry lherzolite and when plotted against another incompatible element such as La, should display a positive correlation for a cogenetic suite of lavas produced by variable degrees of partial melting. This is not the case for La Palma lavas, which show relatively constant concentrations of K and Ti over a considerable range of La abundances (Fig. 12). These relations clearly require a residual K- and Ti-bearing phase buffering these elements during partial melting, where the low K-concentrations point to amphibole rather than phlogopite.

This interpretation is supported by the distribution of Nb, Ba and Rb in the La Palma samples (Fig. 13). Nb is slightly incompatible in both amphibole and phlogopite, whereas Ba and Rb are moderately incompatible in amphibole but compatible in phlogopite (Table 5). We compared the sample compositions to calculated variations of Nb, Rb, and Ba for variable degrees of batch melting of an amphibole-bearing and a phlogopite-bearing mantle source (for details of melting models, see Appendix A4.6). As a potential source composition we used a mixture of primitive mantle (PM) and oceanic crust (N-MORB) in proportion of 85:15 as inferred from He-Pb and Os-Pb systematics of La Palma lavas (Marcantonio et al., 1995; Hilton et al, 2000). On a diagram of Nb vs. Ba, most La Palma samples plot near the melting curve of an amphibole lherzolite. Their relatively high Ba concentrations are entirely

Table 5: Mineral melt partition coefficient used for petrogenetic modelling

	Olivine	Orthopyroxene	Clinopyroxene	Amphibole	Phlogopite	Garnet
K	0.0000[2]	0.0000[2]	0.001[1]	1.36[3]	1.5[1]	0.013[1]
Ti	0.015[1]	0.086[1]	0.4[1]	0.95[1]	0.98[1]	0.6[1]
Rb	0.0003[1]	0.0002[1]	0.0004[1]	0.3[1]	5.8[1]	0.0002[1]
Sr	0.0000[1]	0.0007[1]	0.091[1]	0.27[1]	0.044[1]	0.0007[1]
Zr	0.001[1]	0.012[1]	0.26[1]	0.25[1]	0.13[1]	0.2[1]
Nb	0.0001[2]	0.003[1]	0.0089[1]	0.2[3]	0.14[1]	0.01[1]
Ba	0.0000[1]	0.0000[1]	0.0003[1]	0.5[1]	2.9[1]	0.0001[1]
La	0.0002[1]	0.0031[1]	0.054[1]	0.075[1]	0.003[1]	0.0007[1]
Ce	0.0001[1]	0.0021[1]	0.086[1]	0.11[1]	0.021[1]	0.0026[1]
Nd	0.0003[1]	0.0023[1]	0.19[1]	0.23[1]	0.0063[1]	0.027[1]
Sm	0.0009[1]	0.0037[1]	0.27[1]	0.32[1]	0.0059[1]	0.22[1]
Eu	0.0005[1]	0.009[1]	0.43[1]	0.52[1]	0.031[1]	0.61[1]
Gd	0.0011[1]	0.0065[1]	0.44[1]	0.53[1]	0.0082[1]	1.2[1]
Dy	0.0027[1]	0.011[1]	0.44[1]	0.5[1]	0.026[1]	2.0[1]
Ho	0.01[1]	0.016[1]	0.4[1]	0.5[1]	0.03[1]	2.5[1]
Er	0.0109[1]	0.021[1]	0.39[1]	0.46[1]	0.03[1]	3.3[1]
Yb	0.0240[1]	0.038[1]	0.43[1]	0.5[1]	0.03[1]	5.0[1]
Th	0.0001[4]	0.0001[4]	0.0021[1]	0.5[5]		0.0021[1]
U	0.002[5]	0.0000[1]	0.04[5]	0.1[5]	0.0003[1]	0.011[1]
Pb	0.0003[1]	0.0014[1]	0.0075[1]	0.019[1]	0.0043[1]	0.0003[1]

1 Halliday et al. (1995), 2 Kelemen et al. (1993), 3 Dalpé and Baker (1994), 4 McKenzie and O'Nions (1991), 5 Rollinson (1993) and references therein,

Table 6: Starting and melt modes used in melt models

	amphibole-bearing lherzolite		phlogopite-bearing lherzolite	
	source mode	melt mode	source mode	melt mode
	Xi	Pi	Xi	Pi
ol	0.53	0.05	0.053	0.05
opx	0.22	0.054	0.22	0.054
cpx	0.15	0.33	0.15	0.33
amph	0.05	0.5		
phlog			0.05	0.5
grt	0.05	0.066	0.05	0.066

ol, olivine, opx, orthopyroxene; cpx, clinopyroxene; amph, amphibole; phlog, phlogopite, grt; garnet.
Sources after Späth et al. (2001) and references therein.

inconsistent with partial melting of a phlogopite-bearing source, for which the Ba concentrations would be buffered. Likewise, on a Nb vs. Rb diagram, the La Palma samples roughly follow the curve for amphibole-lherzolite melting but plot well off the phlogopite-lherzolite curve. We obtain the same conclusion when fractional rather than batch melting is used for the calculations or when the source composition is varied.

We also compared the compositions of fractionation-corrected La Palma samples to calculated partial melts of amphibole- and phlogopite-bearing sources on the base of multielement diagrams (Fig. 14). It is obvious that an amphibole-bearing source is required to produce melts that resemble La Palma lavas. The relations shown in Figs. 13 and 14 suggest low melting degrees for La Palma melts, in the order of 1 to 6%, which is consistent with the melt types produced in melting experiments on depleted and enriched lherzolites (Jaques and Green, 1980). The apparent melting degree for CV melts, however, appears unrealistically low and may rather indicate a more enriched source to cause the high concentrations of incompatible trace elements observed.

The inferred amphibole in the mantle source can be present either as a residual mantle phase during partial melting or as a metasomatic phase interacting with ascending mantle melts. Neither amphibole nor phlogopite, however, are stable at temperatures present in astenospheric mantle plumes (McKenzie and Bickle, 1988; Class and Goldstein, 1997). The upper temperature limit for amphibole depends on source composition, especially total alkali content (Niida and Green, 1999), but no experimental studies have demonstrated amphibole stability at asthenospheric temperatures (Tp ˜ 1300 °C) even in alkali-rich peridotites. Therefore, the evidence for amphibole in the source of La Palma lavas suggests that melt generation occurred at least partly within the cooler lithospheric mantle where this phase is stable.

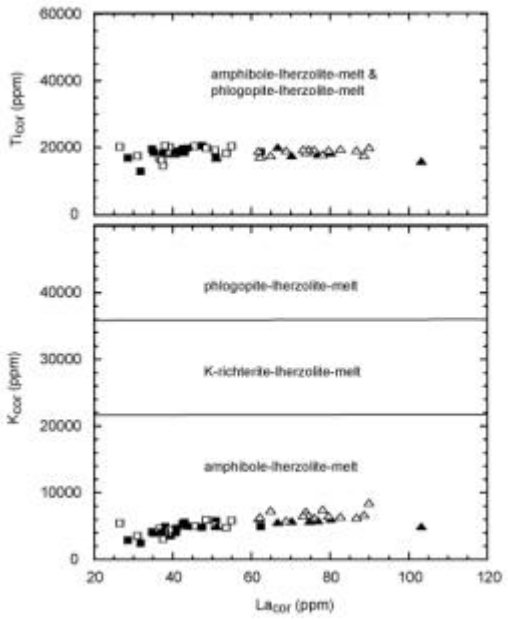

Fig. 12: Correlation diagrams of K and Ti vs. La for fractionation-corrected La Palma samples (MgO > 6 wt%). Symbols as in Fig. 2. Fields for partial melts from amphibole- and phlogopite-bearing lherzolites are from Späth et al. (2001). All La Palma samples plot within the fields for amphibole-bearing lherzolites and show no or only minor correlation of K and Ti with La indicating that these elements are buffered by a K- and Ti-rich mantle phase.

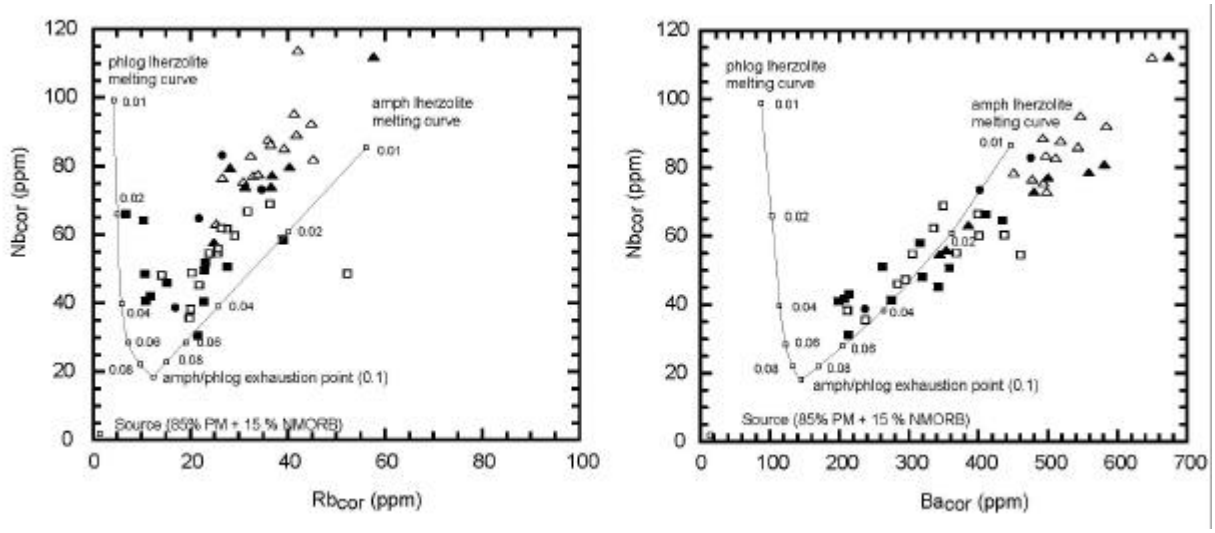

Fig. 13: Correlation diagrams of Nb vs. Rb and Nb vs. Ba for fractionation-corrected La Palma lavas (>MgO 6%). Symbols as in Fig. 2. The two curves in each plot represent calculated trajectories for non-modal batch melting of amphibole- and phlogopite bearing lherzolite sources, respectively. Small numbers indicate degree of partial melting which was varied from 0.01 to 0.1 (amphibole and phlogopite exhaustion point). Source mineralogy, melt proportions and partition coefficients are given in Tables 5 and 6. Source is composed of concentrations 85% primitive mantle + 15 % NMORB after Hofmann (1988).

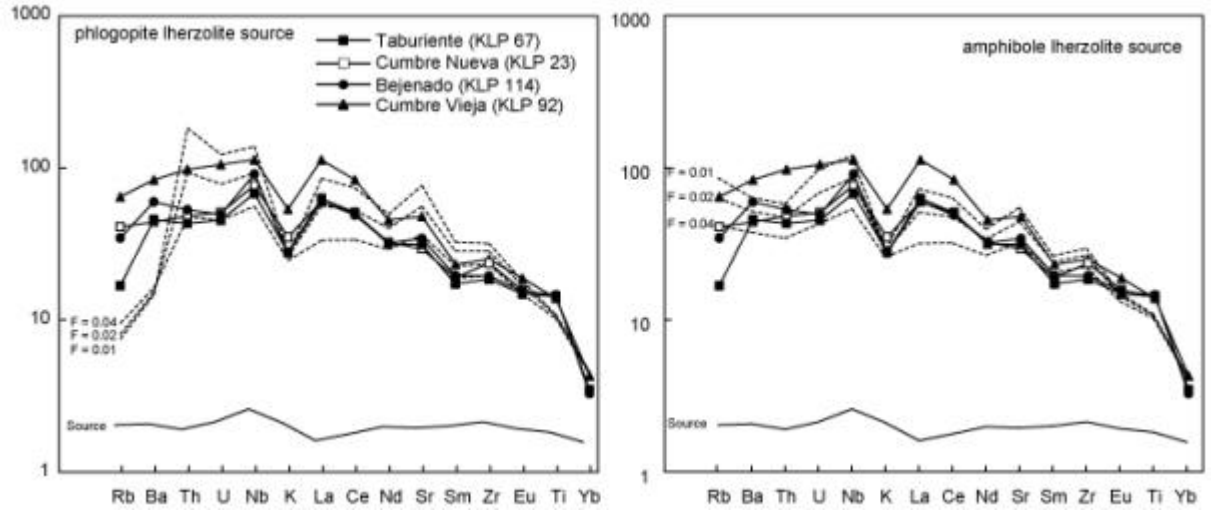

Fig. 14: Incompatible element diagrams for calculated non-modal batch melts (dashed lines), of different degrees of melting of an amphibole-lherzolite and a phlogopite-lherzolite source normalized to primitive mantle after Hofmann (1988) and compared to fractionation-corrected representative La Palma samples. The source composition are the same as in Fig. 13 and source mineralogy, melt proportions and partition coefficients are listed in Tables 5 and 6.

Addition of amphibole in pre-CV melts

Variations in the ratios (Nb, Zr, K)/U provide additional insights into the processes of magma generation beneath La Palma. Cumbre Vieja lavas have limited Nb/U ratios mostly within the global MORB and OIB range of 47 ± 10 (Hofmann et al., 1986), whereas the older pre-CV samples show larger variations and ratios between 50 and 88 (Fig. 5). Melting of an amphibol-bearing source alone cannot account for the high Nb/U ratios of pre-CV lavas

because the Nb/U ratio is largely buffered during melting. Lundstrom et al. (2003) suggested that elevated Nb/U ratios of Canary Islands basalts can be best explained by lithospheric contamination, possibly through melting of amphibole veins in the mantle as based on trace element characteristics. Phlogopite has high Nb contents and could also account for increased Nb/U ratios (Table 4), but bulk assimilation of phlogopite is unlikely as it would cause high Rb contents of the pre-CV lavas, opposite to what is observed (Fig. 13). If the high Nb/U of the pre-CV lavas derives from contamination with amphibole, than this must have occurred by some type of bulk dissolution since partial (incongruent) melting of amphibole cannot significantly increase Nb/U of the melts for any realistic pair of partition coefficients. Nevertheless, residual amphibole is required in a preceding stage of melt generation to buffer K and Ti (Fig. 12) and to account for the trace element systematics discussed above.

We tested our hypothesis of this rather complicated scenario by a simple forward modelling approach. We used the same amphibole-bearing garnet lherzolite as in the preceding section for the starting source composition (Table 5, Fig. 13) and calculated the compositions of non-modal batch melts for variable degrees of melting; we note that models for fractional melting yielded qualitatively similar results. To these melts we added variable amounts of amphibole of a composition found in metasomatized mantle xenoliths from La Palma (Table 4). Figure 15A compares fractionation-corrected La Palma lavas to calculated trajectories for different degrees of batch melting of different source compositions: (I) primitive mantle (PM), (II) a mixture of 85 % PM and 15 % NMORB (see section above), and (III) 85 % PM and 15 % NMORB plus subsequent amphibole assimilation. Clearly, partial melting of any amphibole-bearing source alone cannot fractionate Nb and U to produce the observed range of Nb/U of the pre-CV lavas. The high Nb/U ratios can only be generated if up to 20 % of amphibole is added to the melt; this value reduces to 15 % if we use the maximum instead of the average Nb/U of the amphibole analyses (Table 4). We also varied the partition coefficients in our calculations over a wide range (Nb: $Kd^{amph/liq}$ = 0.08-0.8; U: $Kd^{phlog/liq}$ = 0.0012-0.15) but this affected the Nb/U ratios and U concentrations only slightly at very low degrees of melting and still required up to 20% of amphibole addition. We also tested our scenario by comparing other trace element as well as major element compositions of representative pre-CV lavas to model melts formed by batch melting plus 20% amphibole addition (Fig. 16A). In general, there is good qualitative agreement between calculated model melts and observed pre-CV compositions except for Rb in some samples (Fig 16A). Apart from the simplicity of our model, the deviations may be due to poorly constrained mineral compositions, partition coefficients, and by a possible minor role of metasomatic phlogopite in the lithospheric mantle (Wulff-Pedersen et al., 1996; Klügel, 1998).

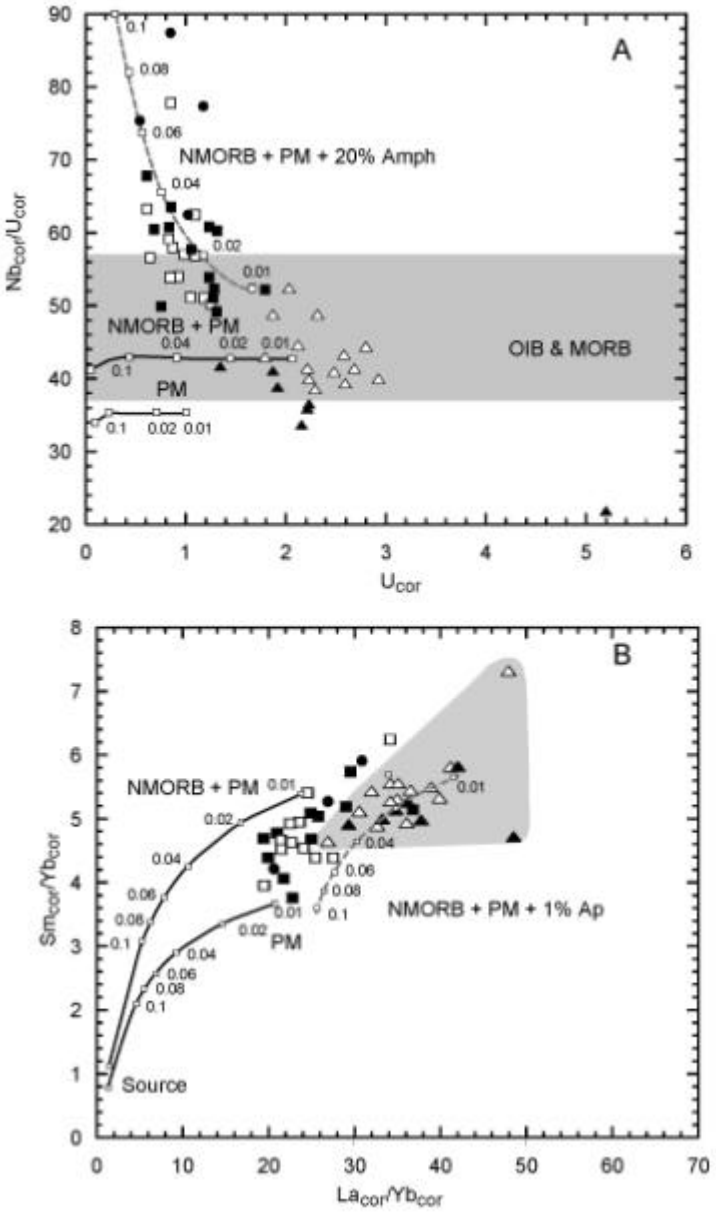

Fig. 15: Correlation diagram of fractionation-corrected primitive La Palma lavas (MgO > 6%). Also shown are calculated melting trajectories of non-modal batch-melting of the following source composition: (i) primitive mantle (PM), (ii) 85% PM + 15% NMORB, (iii) 85% PM + 15% NMORB mineral and subsequent mineral assimilation (grey dashed line). Mineral compositions are given in Table 4 and mineralogy of the source with residual amphibole, melting proportions and Kd are listed in Table 5 and 6. Symbols as in Figure 2. (A) Nb/U vs. U. Grey field of Nb/U corresponds to Nb/U = 47 ± 10 which is the global average for MORB and OIB (Hofmann et al, 1986). Trajectories with amphibole assimilation were calculated by adding of 20 % amphibole to the calculated melt at each degree of melting (F = 0.01 to 0.1). (B) Sm/Yb vs La/Yb. Grey field represents the observed range in Cumbre Vieja samples. Trajectories with apatite assimilation were calculated by adding of 1 % apatite to the calculated melt at each degree of melting (F = 0.01 to 0.1).

Addition of apatite in Cumbre Vieja melts

In the previous section we have shown that pre-CV lavas must have assimilated amphibole during their ascent through the lithosphere to explain their high Nb/U ratios. This is not the case for the younger CV lavas, which show normal Nb/U but are enriched in some

incompatible elements (P, Sr, Th, U, LREE) relative to pre-CV lavas (Figs. 4, 5, 6). These systematic differences between CV and pre-CV lavas cannot be explained by crystal fractionation but must have deeper roots. Our melting models for potential source compositions show that the strong enrichment of the light relative to the heavy REE and high concentrations of Th and U in many CV lavas cannot be produced by an amphibole-bearing garnet lherzolite and/or eclogite even at low degrees of melting. The association of selective enrichment in P, Sr, Th, U and LREE is a fingerprint of apatite (Irving and Frey, 1984; Yaxley and Kamenetsky, 1999; O'Reilly et al., 1991; O'Reilly and Griffin, 2000), a phase which occurs ubiquitously as inclusions and as phenocrysts in cumulate xenoliths and evolved lavas from Cumbre Vieja. We thus propose that the relative enrichment of incompatible elements in CV lavas is related to assimilation of apatite, as was already assumed for some historic CV lavas in a previous study (Elliott, 1991). Our data do not indicate where this assimilation occurs, but we will discuss the different possibilities below.

In order to constrain the amount of apatite assimilation, we used the same approach and source parameters as in the preceding section but with subsequent apatite instead of amphibole addition. For representative apatite compositions we used those from Table 4, which partly resemble metasomatic apatites in peridotite xenoliths from different localities (O'Reilly and Griffin, 2000). Without apatite addition, no calculated melting curve for a source of NMORB + PM in variable proportions overlaps the array for CV samples even for low degrees of melting (Fig. 15B). Also a larger amount of garnet within the source cannot produce the high La/Yb and Sm/Yb ratios observed in most CV lavas, as does no other plausible OIB source (subducted bulk oceanic crust + ambient mantle in various proportions) using data from Stracke et al. (2003). We obtain the high Sm/Yb and La/Yb ratios of CV lavas only if ~1% of apatite is added to a low-degree partial melt (Fig. 15B). In contrast, Elliot (1991) proposed assimilation of <1% of monazite to explain the high P, Th, U and LREE signature of some historic CV basanites. Since no monazite has been found in any La Palma rocks so far, we consider apatite addition as the more plausible explanation. Our preferred melting model with assimilation of ~1% of apatite is also qualitatively consistent with the contents of other trace elements and P in CV lavas (Fig. 16B) with the possible exception of Ba, Th and U. These differences, however, are readily explained by poorly constrained compositions of the apatites and by the simplicity of our model.

In summary, we conclude that any plausible source for La Palma melts must contain residual amphibole during melting. The high Nb/U ratios of pre-CV melts additionally require that some amphibole is bulk assimilated by the melts en route through the lithosphere, whereas the high P, Sr, Th, U and LREE contents of most CV melts require assimilation of apatite. Our calculations clearly represent only approximations to actual processes and the results depend on the melting models and the assumed source and mineral compositions, which

can be estimated at best. In spite of these uncertainties, our main conclusions on the roles of amphibole and apatite appear robust because they hold even for considerable variations of the model parameters in the calculations.

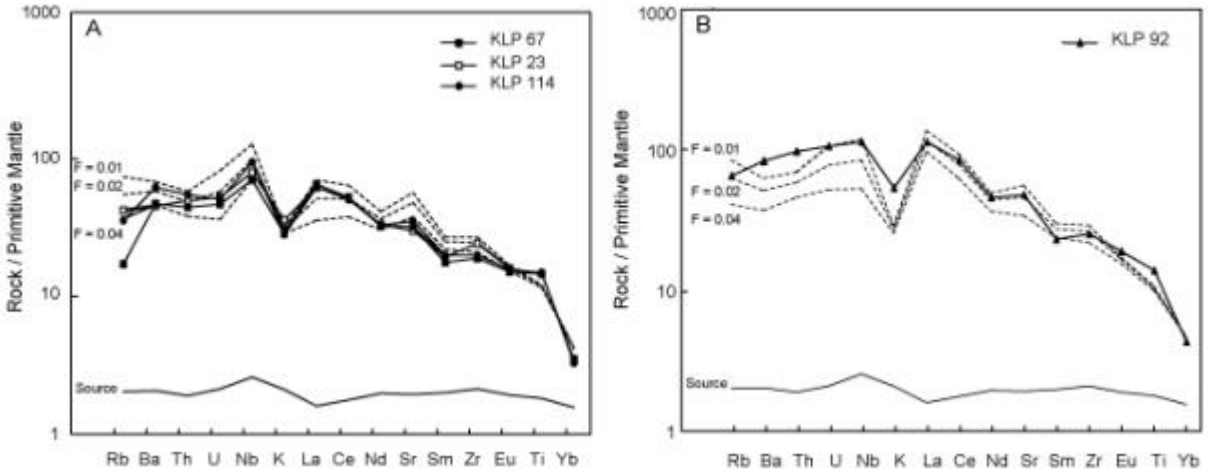

Fig. 16: (A) Incompatible element diagrams normalized to primitive mantle (Hofmann 1988) for non-modal batch melting of an amphibole-bearing lherzolite (85% PM + 15% NMORB) at variable melting degrees (F = 0.01 to 0.4) plus assimilation of 20% amphibole (dashed lines). For comparison average compositions of representative fractionation-corrected primitive pre-CV lavas are shown. Source mineralogy, melting proportions and Kd are listed in Tables 5 and 6 and mineral compositions are given in Table 4. (B) Incompatible element diagrams normalized to primitive mantle (Hofmann 1988) for non-modal batch melting of an amphibole-bearing lherzolite (85% PM + 15% NMORB) at variable melting degrees (F = 0.01 to 0.4) plus assimilation of 1% apatite (dashed lines). For comparison average composition of a representative fractionation-corrected primitive CV lava (MgO > 6%) is shown.

6.2 Interaction between plume and lithosphere

In the previous paragraph we have investigated the trace element characteristics of La Palma lavas to place constraints on mineral phases involved in melt generation. We will now discuss the isotopic composition in terms of mantle components and present a model of plume-lithosphere interaction to explain the observed geochemical variations.

It is remarkable that the combined Sr, Nd and Pb isotope data show large overlap of the different La Palma units but no gradual evolution over time: The older pre-CV rocks in the northern half of La Palma define the most enriched as well as the most depleted components, whereas the Recent CV rocks in the southern half have intermediate compositions and show a much smaller isotopic variability (Figs. 9 and 10). This is unlike the situation at e.g. Madeira Archipelago, where a progressive depletion of Sr-Nd-Pb isotope compositions with decreasing age can be observed (Geldmacher and Hoernle, 2000). However, if the somewhat exceptional Bejenado phase is not considered, then there is a clear tendency for Cumbre Vieja towards more depleted Nd and Pb isotope compositions than Taburiente/Cumbre Nueva (except for one sample, Fig. 9). This may indicate a shift from an early predominance of an enriched source component to a late predominance of a more depleted component, but still our data do not indicate a progressive depletion. Even

without Bejenado, the isotopic variability is much larger for pre-CV rocks than for CV rocks. This cannot be explained by the comparatively small age range of the Cumbre Vieja (125 ka) because Taburiente and Bejenado volcanoes show large isotopic variabilities also at shorter time scales (Fig. 9; B. Nelson, unpubl. data, 2004). It is rather suggestive to relate this difference to the inferred addition of amphibole in the lithosphere as discussed above.

Both the role of amphibole in melt generation beneath La Palma and the apparent binary mixing between an isotopically more enriched and a more depleted component are consistent with a model of plume-lithosphere interaction proposed for other OIB (Class and Goldstein, 1997; Class et al, 1998; Claude-Ivanaj et al., 1998; Deniel, 1998; Jörgensen et al., 2002). This scenario implies that the enriched component is from the plume and the depleted component is from the lower lithosphere, and requires mixing of HIMU-like plume melts with melts of the depleted lithosphere. This model suggests that the base of the lithosphere is metasomatized by plume-derived melts and/or fluids with HIMU-like signatures of an upwelling mantle plume.

Comparison of the stability field of amphibole with typical asthenosphere and plume adiabats have shown that amphibole is thermal unstable in the asthenospheric mantle and thermal mantle plumes (Class and Goldstein, 1997). Therefore, direct melting of hot asthenospheric mantle material is excluded. Hot plume material may have provided the fluids that metasomatized the lithosphere resulting in the formation of amphibole-bearing assemblages within the lower lithosphere. These amphibole-bearing assemblages were then partially molten by conductive heating of the plume and mixed with primary melts from the asthenosphere (plume source) which shifts the isotopic composition of the erupted lavas towards a more depleted signature. In the case of La Palma it is proposed that lavas with a isotopically more depleted character represent melts with a stronger contribution of the lithosphere whereas melts with a more enriched character are less diluted by lithospheric melts.

6.3 Evolution of volcanism at La Palma in space and time

Based on the combined geological and geochemical data discussed in the previous sections, we propose a model of the evolution of volcanism at La Palma (Fig. 17). A hot rising blob from the upwelling Canary Plume may have caused the onset of magmatism (Hoernle and Schmincke, 1993). The seamount stage at La Palma probably began more than 10 Ma ago when the rising blob impinged on the old, refractory and cold lithosphere (Fig. 17A). Fluids and volatile-rich melts derived from the plume advanced ahead and infiltrated the lithosphere. This resulted in modal metasomatism by crystallisation of high Nb/U amphibole deposited in veins or as an interstitial phase within the lithospheric mantle (Lundstrom et al., 2003). During this stage, only few melts passed through the cold lithosphere without freezing

and became erupted. We suspect that these deep-sea lavas have no sign of residual amphibole in their source, but this cannot be tested as they are overlain by the later volcanic edifices and not accessible for sampling. Metasomatism by plume-derived melts also caused formation of amphibole-rich assemblages at the base of the lithosphere at this stage. This results in a drastic lowering of the solidus compared with the anhydrous lithospheric mantle making the metasomatized regions susceptible to melting by conductive heating by the plume itself or by plume-derived melts (Class et al., 1998). The resulting lithospheric mantle source has isotopic compositions intermediate between the depleted lithospheric mantle and the enriched plume.

During the time of subaerial Taburiente and Cumbre Nueva volcanism, the plume has heated, penetrated and thinned the lithosphere and continued to form amphibole-bearing assemblages at its leading edge, within the garnet stability field (Fig. 17B). Near the plume center, partial melts of the metasomatized lithosphere were produced and mixed with plume melts. This resulted in the geochemical fingerprints of residual amphibole in the source of the La Palma melts, such as buffering of K and Ti as discussed above. When passing through the metasomatized lithosphere, the ascending melts caused melting of amphibole-bearing veins formed during the earlier seamount stage (Fig. 17A). The net result is an increase in Nb/U of many pre-CV lavas and also a high variability in their isotopic composition because of strongly varying proportions of the different components involved in their generation (depleted lithospheric mantle, metasomatic amphibole, enriched plume melts).

After the Cumbre Nueva collapse (~560 ka) a new episode of volcanic activity within the collapsed embayment produced the rapidly growing Bejenado volcano (560 to 490 ka). Despite its short growth period, Bejenado shows exceptional Sr-Nd-Pb isotopic variability and includes the isotopically most depleted rocks of all La Palma units (Figs. 9 and 10). We speculate that the isotopic characteristics of Bejenado are related to changes of the local stress field and of the magma plumbing system after the Cumbre Nueva collapse. Evidence for such changes is given by thermobarometric data indicating a shift of magma storage reservoirs to shallower depths, and by petrological observations such as the increased occurrence of plagioclase phenocrysts and differentiated rocks as compared to Taburiente and Cumbre Nueva (Galipp et al., submitted). The depleted lavas of Bejenado (LPbB group) could thus reflect assimilation of depleted crustal or upper mantle material because of a re-organizing magma plumbing system, although such assimilation is not indicated by geochemical data. Alternatively, the occurrence of depleted lavas could be related to a change in plume dynamics or termination of the plume pulse (blob) beneath northern La Palma. This scenario is consistent with the decline of volcanic activity at Taburiente after the Bejenado phase and its complete termination at 410 ka (Guillou et al., 2001).

After cessation of eruptions at Taburiente, volcanic activity shifted further south and was confined to the Cumbre Vieja. This shift cannot simply be explained by plate motion as the NE-oriented motion vector would have caused migration to the SW rather than to the S (Geldmacher et al., 2001). It is however possible that a new blob rose south of Taburiente and caused the volcanism at CV since >125 ka to present. Alternatively, the migration of volcanic activity to the south and formation of the Cumbre Vieja rift zone may have been causally linked to the Cumbre Nueva collapse through the changed gravitative stress field (Walter and Troll, 2003).

As for the pre-CV lavas, the compositions of the CV lavas require residual amphibole within the mantle source. We thus conclude that their melts were produced in a similar way, by formation of amphibole-rich assemblages at the lithospheric base at the leading edge of the plume pulse and their subsequent melting near the plume center. However, the "normal" Nb/U ratios of CV lavas (Fig. 5) rule out addition of significant amounts of amphibole during their ascent through the lithosphere. Either the lithosphere beneath southern La Palma was not metasomatized during the earlier stages and amphibole-bearing veins were never present, or these veins were largely to completely consumed by pre-CV melts. Both scenarios are not distinguishable from each other by our data. The smaller isotopic variability and tendency to more depleted compositions of CV lavas compared to Taburiente/Cumbre Nueva lavas is also consistent with the absence of amphibole veins as potential assimilants for CV melts.

We have shown above that trace element patterns of most CV lavas require bulk assimilation of apatite rather than amphibole, but the question about the origin of this apatite remains. Elliott (1991) suggested that contamination of historic CV basanites with monazite and/or apatite occurs in a long-lived, stratified magma chamber where basaltic melts are overlain by a lens of evolved (phonolitic) melts. Within the evolved layer, apatite or monazite crystallizes, settles down and becomes dissolved generating melts enriched in P, Th, U, and LREE. There is, however, no petrological or geochemical evidence for the presence of a large zoned magma reservoir beneath the Cumbre Vieja but rather for relatively small ephemeral reservoirs in the uppermost mantle (Klügel et al., 2005). In addition, phonolites from the Cumbre Vieja contain relatively few small apatites that probably cannot settle in the viscous melts.

Another possibility is that earlier metasomatic processes within the lithosphere produced apatite that during later stages was assimilated by ascending melts. Until now, metasomatized mantle xenoliths containing significant amounts of apatite have not been reported from the Cumbre Vieja (Wulff-Pedersen et al., 1996; Vannucci et al., 1998; Klügel, 1998; Wulff-Pedersen et al., 1999). Previous studies, however, have shown that apatite imparts distinctive geochemical imprints that can be recognized despite the absence of

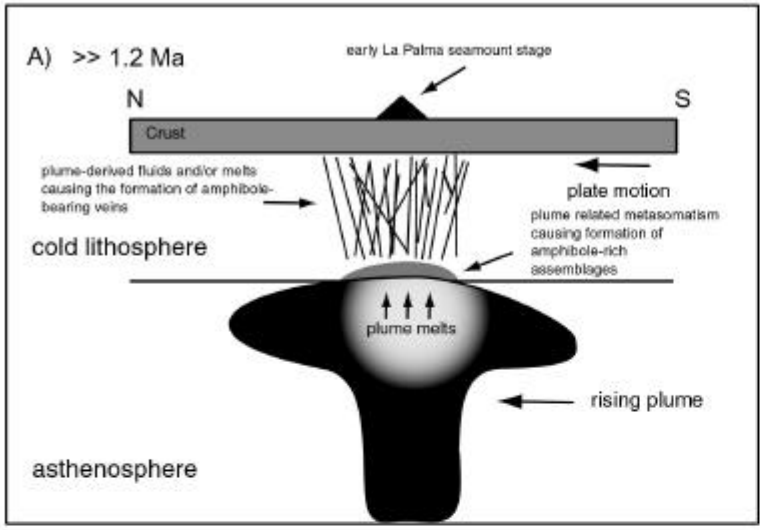

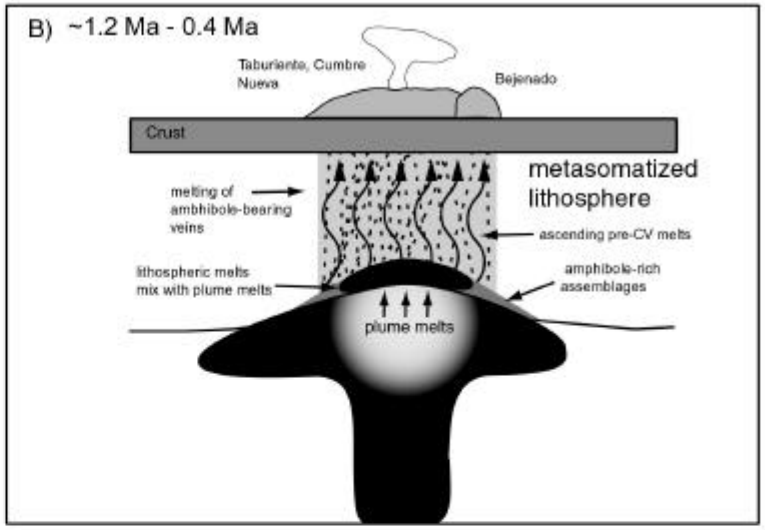

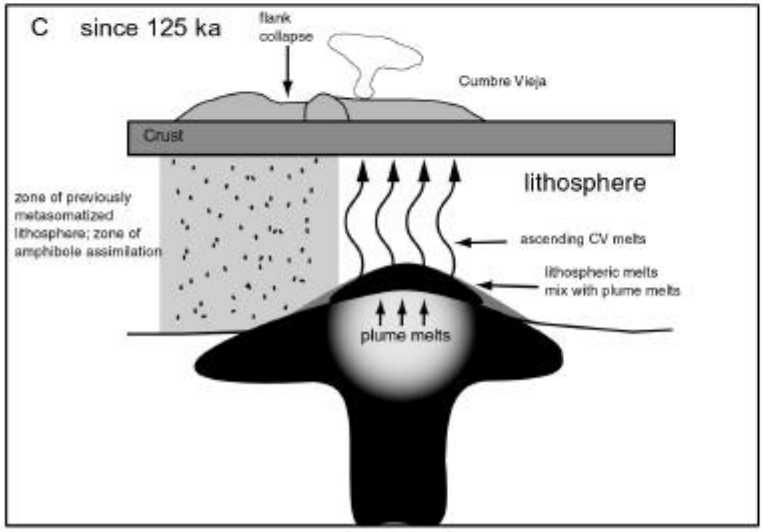

Fig. 17: Schematic model showing the process of plume-lithosphere interaction beneath La Palma. (A) During the seamount stage volatiles and/or melts advancing ahead of an upwelling mantle plume heat and metasomatize the old refractory pre-metasomatic lithosphere and cause the formation of amphibole-bearing veins within the thick cold lithosphere and amphibole-bearing assemblages at the base of the lithosphere. (B) Upon continued ascent the plume penetrates and thins the lithosphere and continued to form amphibole-bearing assemblages at its leading edge. Near the plume center, partial melts of the metasomatized lithosphere were produced and mixed with plume melts. When passing through the metasomatized lithosphere, the ascending Taburiente, Cumbre Nueva and Bejenado melts caused melting of amphibole-bearing veins formed during the earlier seamount stage. (C) As for the pre-CV lavas, the compositions of the CV lavas require residual amphibole within the mantle source. It is concluded that CV melts were produced in a similar way as pre-CV melts, by formation of amphibole-rich assemblages at the lithospheric base at the leading edge of the plume pulse and their subsequent melting near the plume center. Nb/U ratios of CV lavas do not reflect melting of amphibole-bearing veins during their ascent through the lithosphere. Either the amphibole-bearing veins were almost completely molten by pre-CV melts or these veins were never present beneath CV.

samples containing this phase (e.g. O'Reilly, 1987, Ionov et al., 1993, Hauri et al., 1993; O'Reilly and Zhang, 1995). We also point out that the La Palma mantle xenoliths do not represent the lower lithosphere where melt transport is dominated by porous flow and assimilation is most effective. The problem for La Palma is that we cannot provide a plausible mechanism or metasomatic agent that introduced apatite only beneath Cumbre Vieja but not beneath Taburiente.

Alternatively, addition of apatite to CV melts may have occurred within the lower crust or uppermost mantle by assimilation of cumulates or evolved rocks, which are common apatite-bearing rocks found at the Cumbre Vieja. This possibility, however, requires preferred assimilation of apatite but only small amounts of other mineral phases, because no bulk assimilation of any CV rock known to us would yield the required increase in P, Sr, Th, U and REE. Such a scenario is hard to envisage, although it is conceivable that apatite phenocrysts in cumulates or crystal mush zones become preferentially molten by hot basaltic magmas. Irrespective of the actual mechanism, apatite assimilation must occur in the upper mantle where the magmas differentiate. It does not occur in the crust which is passed by most erupted magmas in a relatively short time (Klügel et al., 2000, 2005) so that large-scale assimilation cannot take place. We prefer this model of apatite addition as it is supported by petrological and petrographic data and does not require exotic metasomatism. In addition, the small isotopic variability of CV rocks is consistent with the assimilated apatite being derived from CV magmas and thus having the same isotopic composition. Still we cannot rule out that metasomatic apatite also plays an important role.

7. Conclusions

1. Trace element systematics of both older and Recent La Palma lavas require the presence of residual amphibole in their melting region. This amphibole must be present in the lithospheric mantle because it is not stable in the asthenosphere. Following models for other OIB, we suggest that this amphibole is of metasomatic origin as a consequence of infiltrating melts and/or fluids from the plume.

2. The trace element characteristics of pre-CV and CV lavas cannot be generated by single-stage partial melting of an amphibole-bearing garnet peridotite or any other plausible source. Model calculations reveal that the high Nb/U ratios of many pre-CV lavas require addition of up to ~20% of amphibole to the partial melts, whereas the high Sm/Yb and La/Yb ratios and high P, Th and U contents of CV lavas require addition of ~1% apatite.

3. Much of the isotopic variations of La Palma samples can be explained by mixing of two mantle components in variable proportions: a more enriched HIMU-type component derived from the inferred plume beneath La Palma, and a more depleted component from the refractory oceanic lithosphere.

4. Plume-lithosphere interaction offers an explanation for both the binary mixing trends and the involvement of residual amphibole in melt genesis. La Palma magmas represent mixing between plume melts and melts from the amphibole-metasomatized base of the lithosphere in variable proportions. The large isotopic variability of pre-CV melts compared to CV melts and their increased Nb/U ratios are consistent with assimilation of metasomatic amphibole veins during their ascent. These veins were generated during the early stages of La Palma magmatism.

5. Our data indicate no progressive geochemical evolution of La Palma magmas over time but a compositional break between Taburiente volcanism in the north and Cumbre Vieja volcanism in the south. This suggests that Cumbre Vieja and the older volcanoes represent distinct volcanic systems rather than a progressively evolving volcano.

Acknowledgements. We gratefully acknowledge the staff from the Unidad de Medio Ambiente and the Parque Nacional Caldera de Taburiente for their support during our field studies on La Palma and for permission to take samples. Dagmar Rau, Silke Hauff, Imme Martelock and Heike Anders are gratefully acknowledged for their help with sample preparation and analytical support. The paper strongly benefited from discussions with Thor H. Hansteen and S. Schwarz. We also thank H. Guillou and J.C. Carracedo for providing us with details of sample locations and B. Nelson for his isotopic data. This study was supported by the Deutsche Forschungsgemeinschaft (DFG grant KL1313/4).

References

Ancochea, A. et al., 1994. Constructive and destructive episodes in the building of a young Oceanic Island, La Palma, Canary Islands, and genesis of the Caldera de Taburiente. Journal of Volcanology and Geothermal Research, 60: 243-262.

Asavin, A.M., Kogarko, L.N., Kryuchkova, O.I., Tyurin, D.A. and Kolesov, G.M., 1997. The Grand Canary, Saint Helena, and Tristan da Cunha oceanic islands; variations of trace element partition coefficients in pyroxene-melt equilibria during alkaline magma evolution. Geokhimiya., 5: 479-487.

Carracedo, J.C., 1999. Growth, structure, instability and collapse of Canarian volcanoes and comparisons with Hawaiian volcanoes. Journal of Volcanology and Geothermal Research, 94: 1-19.

Carracedo, J.C., Badiola, E.R., Guillou, H., de La Nuez, J. and Pérez Torado, F.J., 2001. Geology and Volcanology of La Palma and El Hierro, Western Canaries. Estudios Geologicos, 57(5-6): 157-273.

Carracedo, J.C., Day, S.J., Guillou, H. and Gravestock, P., 1999. Later stages of volcanic evolution of La Palma, Canary Islands: Rift evolution, giant landslides, and the genesis of the Caldera de Taburiente. Geological Society of America Bulletin, 111(5): 755-768.

Chaffey, D.J., Cliff, R.A. and Wilson, B.M., 1989. Characterization of the St Helena magma source. In: A.D. Saunders and M.J. Norry (Editors), Magmatism in the Ocean Basins. Geological Society Special Publication No. 42, pp. 257-276.

Clague, D.A. and Frey, F.A., 1982. Petrology and trace element geochemistry of the Honolulu Volcanics: Implications for the oceanic mantle below Hawaii. Journal of Petrology, 23(4): 447-504.

Class, C. and Goldstein, S.L., 1997. Plume-lithosphere interactions in the ocean basins: constraints from the source mineralogy. Earth and Planetary Science Letters, 150: 245-260.

Class, C., Goldstein, S.L., Altherr, R. and Bachèlery, P., 1998. The process of plume-lithosphere interactions in the ocean basins - the case of Grande Comore. Journal of Petrology, 39(5): 881-903.

Claude-Ivanaj, C., Bourdon, B. and Allègre, C.J., 1998. Ra-Th-Sr isotope systematics in Grande Comore Island: a case study of plume-lithosphere interaction. Earth and Planetary Science Letter, 164: 99-117.

Cohen, R.S. and O'Nions, R.K., 1982. The lead, neodymium and strontium isotopic structure of ocean ridge basalts. Journal of Petrology, 23(3): 299-324.

Dalpe, C. and Baker, D.R., 1994. Partition coefficients for rare-earth elements between calcic amphibole and Ti-rich basanitic glass at 1.5 Gpa, 1100 degrees C. Mineralogical Magazine, 58A: 207-208.

Deniel, C., 1998. Geochemical and isotopic (Sr, Nd, Pb) evidence for plume-lithosphere interactions in the genesis of Grande Comore magmas (indian Ocean). Chemical Geology, 144: 281-303.

Dupré, B. and Allègre, C.J., 1980. Pb-Sr-Nd isotopic correlation and the chemistry of the North Atlantic mantle. Nature, 286: 17-22.

Dupuy, C., Vidal, P., Maury, R.C. and Guille, G., 1993. Basalts from Mururoa, Fangataufa and Gambier Islands (French Polynesia): geochemical dependence on the age of the lithosphere. Earth and Planetary Science Letters, 117: 89-100.

Elliott, T.R., 1991. Element Fractionation in the Petrogenesis of Ocean Island Basalts. Ph.D. Thesis, The Open University, Milton Keynes.

Fretzdorff, S. and Haase, K.M., 2002. Geochemistry and petrology of lavas from the submarine flanks of Réunion Island (western Indian Ocean): implications for magma genesis and the mantle source. Mineralogy and Petrology, 75: 153-184.

Frey, F. et al., 1990. Evolution of Mauna Kea vlcano, Hawaii: petrologic and geochemical constraints on postshield volcanism. Journal of Geophysical Research, 95(B): 1271-1300.

Frey, F.A. et al., 1991. The evolution of Mauna Kea Volcano, Hawaii: petrogenesis of tholeiitic and alkalic basalts. Journal of Geophysical Research, 96 B: 14347-14375.

Galipp, K., Klügel, A. and Hansteen, T.H.. Changing depths of magma fractionation and stagnation during the evolution of an oceanic island volcano: La Palma (Canary Islands). Journal of Volcanology and Geothermal Research, submitted

Gao, S et al., 2000. Determination of forty-two major and trace elements in USGS and NIST SRM glasses by laser ablation-inductively coupled plasma-mass spectrometry. Geostandards Newsletters, 26: 181-196

Gee, M.J.R., Masson, D.G., Watts, A.B. and Mitchell, N.C., 2001. Offshore continuation of volcanic rift zones, El Hierro, Canary Islands. Journal of Volcanology and Geothermal Research, 105: 107-119.

Geldmacher, J., Hoernle, K., van den Bogaard, P., Zankl, G. and Garbe-Schönberg, D., 2001. Earlier history of the $\geq$ 70-Ma-old Canary hotspot based on the temporal and geochemical evolution of the Selvagen Archipelago and neighboring seamounts in the eastern North Atlantic. Journal of Volcanology and Geothermal Research, 111: 55-87.

Geldmacher, J. and Hoernle, K.A., 2000. The 72 Ma geochemical evolution of the Madeira hotspot (eastern North Atlantic): recycling of Paleozoic (500 Ma) oceanic lithosphere. Earth and Planetary Science Letters, 183: 73-92.

Gerlach, D.C., Cliff, R.A., Davies, G.R., Norry, M. and Hodgson, N., 1988. Magma sources of the Cape Verdes Archipelago; isotopic and trace element constraints. Geochimica et Cosmochimica Acta, 52(12): 2979-2992.

Green, T.H., 1994. Experimental studies of trace-element partitioning applicable to igneous petrogenesis - Sedona 16 years later. Chemical Geology, 117: 1-36.

Guillou, H., Carracedo, J.C. and Day, S., 1998. Dating of the upper Pleistocene-Holocene activity of La Palma using the unspiked K-Ar technique. Journal of Volcanology and Geothermal Research, 86: 137-149.

Guillou, H., Carracedo, J.C. and Duncan, R., 2001. K-Ar, $^{40}Ar/^{39}Ar$ ages and magnetostratigraphy of Brunhes and Matuyama lava sequences from La Palma Island. Journal of Volcanology and Geothermal research, 86(1-4): 37-149.

Halliday, A.N. et al., 1995. Incompatible trace elements in OIB and MORB and source enrichment in sub-oceanic mantle. Earth and Planetary Science Letters, 133: 379-395.

Hart, S.R., 1984. A large-scale isotope anomaly in the southern hemisphere mantle. Nature, 309: 753-757.

Hart, S.R. and Davis, K.E., 1978. Nickel partitioning between olivine and silicate melt. Earth and Planetary Science Letters, 40: 203-219.

Hauri, E.H., Shimuzu, N., Dieu, J.J. and Hart, S.R., 1993. Evidence for hotspot-related carbonatite metasomatism in the oceanic upper mantle. Nature, 365: 221-265.

Hausen, H., 1969. Some contributions to the geology of La Palma. Comm. Phys. Math. Finn. Acad. Sci., 35: 1-140.

Hernandéz-Pacheco, A. and De la Nuez, J., 1983. Las extrusiones sálicas del Sur de la Isla de La Palma (Canarias). Estud. Geol., 39: 3-30.

Hernandéz-Pacheco, A. and Valls, M.C., 1982. The historic eruptions of La Palma Island (Canarias). Arquipelago, Rev. Univ. Azores, Ser. C. Nat., 3: 83-94.

Hilton, D.R., Macpherson, C.G. and Elliott, T.R., 2000. Helium isotope ratios in mafic phenocrysts and geothermal fluids from La Palma, the Canary Islands (Spain): implications for HIMU mantle sources. Geochimica et Cosmochimica Acta, 64: 2119-2132.

Hoernle, K., 1998. Trace element and Sr-Nd-Pb isotopic geochemistry of Jurassic ocean crust beneath Gran Canaria (Canary Islands): implications for the generation of OIB reservoirs and for crustal contamination of ascending OIB magmas. Journal of Petrology, 39(5): 859-880.

Hoernle, K. and Schmincke, H.U., 1993. The role of partial melting in the 15-Ma geochemical evolution of Gran Canaria: a blob model for the Canary hotspot. Journal of Petrology, 34(3): 599-626.

Hoernle, K., Tilton, G. and Schmincke, H.U., 1991. Sr-Nd-Pb isotopic evolution of Gran Canaria: evidence for shallow enriched mantle beneath the Canary Islands. Earth and Planetary Science Letters, 106: 44-63.

Hoernle, K.A. and Tilton, G.R., 1991. Sr-Nd-Pb isotope data for Fuerteventura (Canary Islands) basal complex and subaerial volcanics: applications to magma genesis and evolution. Schweiz. Mineral. Petrogr. Mitt., 71: 5-21.

Hofmann, A.W., 1988. Chemical differentiation of the Earth: the relationship between mantle, continental crust, and oceanic crust. Earth and Planetary Science Letters, 90: 297-314.

Hofmann, A.W., Jochum, K.P., Seufert, M. and White, W.M., 1986. Nb and Pb in oceanic basalts: New constraints on mantle evolution. Earth and Planetary Science Letters, 79: 33-45.

Holik, J.S. and Rabinowitz, P.D., 1991. Effects of Canary hotspot volcanism on structure of oceanic crust off Morocco. Journal of Geophysical Research, 96: 12039-12067.
Ionov, D.A., Dupuy, C., O'Reilly, S.Y., Kopylova, M.G. and Genshaft, Y.S., 1993. Carbonated peridotite xenoliths from Spitsbergen: implications for trace element signature of mantle carbonate metasomatism. Earth and Planetary Science Letters, 119: 283-297.
Irving, A.J. and Frey, F.A., 1984. Trace element abundances in megacrysts and their host basalts: Constraints on partition coefficients and megacryst genesis. Geochimica et Cosmochimica Acta, 48: 1201-1221.
Ito, E., White, W.M. and Goepel, C., 1987. The O, Sr, Nd and Pb isotope geochemistry of MORB. Chemical Geology, 62(3-4): 157-76.
Jackson, M.C., A, F.F., Garcia, M.O. and Wilmoth, R.A., 1999. Geology and geochemistry of basaltic lava flows and dikes from the Trans-Koolau Tunnel, Oahu, Hawaii. Bulletin of Volcanology, 60: 381-401.
Jaques, A.L. and Green, D.H., 1980. Anhydrous melting of peridotite at 0-15 kb pressure and the genesis of tholeiitic basalts. Contibution to Mineralogy and Petrology, 73: 287-310.
Jörgensen, J.O. and Holm, P.M., 2002. Temporal variation and carbonatite contamination in primitive ocean island volcanics from Sao Vicente, Cape Verde Islands. Chemical Geology, 192: 249-267.
Kelemen, P.B., Shimizu, N. and Dunn, T., 1993. Relative depletion of niobium in some arc magmas and the continental crust: partitioning of K, Nb, La and Ce during melt/rock interaction in the upper mantle. Earth and Planetary Science Letters, 120(111-134).
Klitgord, K.D. and Schouten, H., 1986. Plate kinematics of the Central Atlantic. In: P.R. Vogt and B.E. Tucholke (Editors), The geology of North America, Vol. M, The Western North Atlantic Region. Geological Society of America, pp. 351-378.
Klügel, A., 1998. Reactions between mantle xenoliths and host magma beneath La Palma (Canary Islands): constraints on magma ascent rates and crustal reservoirs. Contributions to Mineralogy and Petrology, 131: 237-257.
Klügel, A., Hansteen, T.H. and Galipp, K.G., 2005. Magma storage and underplating beneath Cumbre Vieja volcano, La Palma (Canary Islands). Earth and Planetary Science Letters, in press
Klügel, A., Hoernle, K.A., Schmincke, H.U. and White, J.D.L., 2000. The chemically zoned 1949 eruption on La Palma (Canary Islands): Petrologic evolution and magma supply dynamics of a rift-zone eruption. Journal of Geophysical Research, 105(B3): 5997-6016.
LaTourette, T., Hervig, R.L. and Holloway, J.R., 1995. Trace element partitioning between amphibole, phlogopite and basanite melt. Earth and Planetary Science Letters, 135: 13-30.
Le Maitre, R.W. et al., 1989. A Classification of Igneous Rocks and Glossary of Terms - Recommendations of the International Union of Geological Sciences Subcommission on the Systematics of Igneous Rocks. Blackwell Scientific Publications, Oxford, 193 pp.
Lundstrom, C.C., Hoernle, K. and Gill, J., 2003. U-series disequilibria in volcanic rocks from the Canary Islands: Plume versus lithospheric melting. Geochimica et Cosmochimica Acta, 67(21): 4153-4177.
Marcantonio, F., Zindler, A., Elliott, T. and Staudigel, H., 1995. Os isotope systematics of La Palma, Canary Islands: Evidence for recycled crust in the mantle source of HIMU ocean islands. Earth and Planetary Science Letters, 133: 397-410.
McKenzie, D. and Bickle, M.J., 1988. The volume and composition of melt generated by extension of the lithosphere. Journal of Petrology.
McKenzie, D. and O'Nions, R.K., 1991. Partial Melt Distributions from inversion of rare earth elements. Journal of Petrology, 32(5): 1021-1091.
Mertes, H. and Schmincke, H.U., 1985. Mafic potassic lavas of the Quaternary West Eifel volcanic field. Contributions to Mineralogy and Petrology, 89: 330-345.
Middlemost, E.A.K., 1972. Evolution of La Palma, Canary archipelago. Contributions to Mineralogy and Petrology, 36: 33-48.
Morgan, W.J., 1972. Plate motions and deep mantle convection. Geol. Soc. Am. Mem., 132: 7-22.
Morgan, W.J., 1983. Hotspot tracks and the early rifting of the Atlantic. Tectonophysics, 94: 123-139.
Neumann, E.-R. et al., 1999. Evidence for Fractional Crystallization of Peridocally Refilled Magma Chambers in Tenerife, Canary Islands. Journal of Petrology, 40: 1089-1123.
Niida, K. and Green, D.H., 1999. Stability and chemical composition of pargasitic amphibole in MORB pyrolite under upper mantle conditions. Contributions to Mineralogy and Petrology, 135: 18-40.
Nikogosian, I.K., Elliott, T. and Touret, J.L.R., 2002. Melt evolution beneath thick lithosphere: a magmatic inclusion study of La Palma, Canary Island. Chemical Geology, 183: 169-193.
O'Reilly, S.Y. and Griffin, W.L., 2000. Apatite in the mantle: implications for metasomatic processes and high heat production in Phanerozoic mantle. Lithos, 53: 217-232.
O'Reilly, S.Y., Griffin, W.L. and Ryan, C.G., 1991. Residence of trace elements in metasomatized spinel lherzolite inxenoliths: a proton-microprobe study. Contributions to Mineralogy and Petrology, 109: 98-113.
O'Reilly, S.Y. and Zhang, M., 1995. Geochemical characteristics of lava-field basalts from eastern Australia and inferred sources: connection with subcontinenetal mantle? Contributions to Mineralogy and Petrology, 121: 148-170.
O'Reilly, Y., 1987. Volatile-rich mantle beneath eastern Australia. In: P.H. Nixon (Editor), Mantle Xenoliths. Wiley, Chichester, pp. 661-670.
Pearce, N.J.G. et al., 1997. A compilation of new and published major and trace element data for NIST SRM 610 and NIST SRM 612 glass reference materials. Geostandards Newsletter, 21: 115-144.
Rollinson, H., 1993. Using geochemical data. Longman, Essex, 352 pp.
Sato, H., 1977. Nickel content of basaltic magmas; identification of primary magmas and a measure of the degree of olivine fractionation. Lithos, 10(2): 113-120.

Schmincke, H.U., 1976. Geology of the Canary Islands. In: G. Kunkel (Editor), Biogeography and ecology of the Canary Islands. Junk BV, The Hague, pp. 67-184.

Schmincke, H.U., 1982. Volcanic and chemical evolution of the Canary Islands. In: U. von Rad, K. Hinz, M. Sarnthein and E. Seibold (Editors), Geology of the northwestern african continental margin. Springer, Berlin Heidelberg New York, pp. 3-20.

Schmincke, H.U., Klügel, A., Hansteen, T.H., Hoernle, K. and Bogaard, P.v.d., 1998. Samples from the Jurassic ocean crust beneath Gran Canaria, La Palma and Lanzarote (Canary Islands). Earth and Planetary Science Letters, 163: 343-360.

Schmincke, H.-U. and Graf, G., 2000. DECOS / OMEX II, Cruise No. 43 No. 00-2 - METEOR-Berichte, Universität Hamburg, Hamburg.

Schwarz, S., Klügel, A., van den Boogard, P. and Geldmacher, J., 2005. Internal structure and evolution of a volcanic rift system in the eastern North Atlantic: the Desertas rift zone, Madeira Archepilago. Journal of Volcanology and Geothermal Research, 141: 123-155.

Shaw, D.M., 1970. Trace element fractionation during anatexis. Geochimica et Cosmochimica Acta, 34: 237-243.

Sigmarsson, O., Condomines, M. and Ibarrola, E., 1992. 238U-230Th radioactive disequilibra in historic lavas from the Canary Islands and genetic implications. Journal of Volcanology and Geothermal Research, 54: 145-156.

Sims, K.W.W. et al., 1999. Porosity of the melting zone and variations in the solid mantle upwelling rate beneath Hawaii; inferences from 238U- 230Th-226Ra and 235U-231) Pa disequilibria. Geochimica et Cosmochimica Acta, 63(23-24): 4119-4138.

Späth, A., Le Roex, A.P. and Duncan, R.A., 1996. The geochemistry of lavas from the Comores Archepilago, Western Indian Ocean: petrogenesis and mantle source characteristics. Journal of Petrology, 37(4): 961-991

Späth, A., Le Roex, A.P. and Opiy-Akech, N., 2001. Plume-lithosphere interaction and the origin of continental rift-related alkaline volcanism - the Chyuli Hills Volcanic Province, southern Kenya. Journal of Petrology, 42(4): 765-787.

Staudigel, H., G, F. and Giannerini, G., 1986. The history of intrusive activity on the Island of La Palma (Canary Islands). Journal of Volcanology and Geothermal Research, 27: 299-322.

Staudigel, H. and Schmincke, H.U., 1984. The Pliocene seamount series of La Palma / Canary Islands. Journal of Geophysical Research, 89(13): 11195-11215.

Stracke, A., Bizimis, M. and Salters, J.M., 2003. Recycling oceanic crust: quantitative constraints. Geochemistry Geophysics Geosystems, 4(3).

Sun, S.S. and McDonough, W.F., 1989. Chemical and isotopic systematics of oceanic basalts: implications for mantle composition and processes. In: A.D. Saunders and M.J. Norry (Editors), Magmatism in the Ocean Basins. Geological Society Special Publications No. 42, pp. 313-345.

Thirlwall, M., Singer, B.S. and Marriner, G.F., 2000. 39Ar/40Ar ages and geochemistry of the basaltic shield stage of Tenerife, Canary Islands, Spain. Journal of Volcanology and Geothermal Research., 103(1-4): 247-297.

Todt, W., Cliff, R.A., Hanser, A., Hofmann, A .W., 1996. Evaluation of a 202Pb/Pb double spike for high precision lead isotope analyses. In: A. Basu and S. Hart. Earth processes: reading the isotope code. Geophysical Monograph No. 95: 429-437h

Vannucci, R., Bottazzi, P., Wulff-Pedersen, E. and Neumann, E.R., 1998. Partitioning of REE, Y, Sr, Zr and Ti between clinopyroxene and silicate melts in the mantle under La Palma (Canary Islands): implications for the nature of the metasomatic agents. Earth and Planetary Science Letters, 158: 39-51.

Walter, T.R. and Troll, V.R., 2003. Experiments on rift zone evolution in unstable volcanic edifices. Journal of Volcanology and Geothermal Research, 127: 107-120.

Weaver, B.L., 1991. The origin of ocean island basalt end-member compositions: trace element and isotopic constraints. Earth and Planetary Science Letters, 104: 381-397.

Wilson, M. and Downes, H., 1991. Tertiary-Quaternary extension-related alkaline magmatism in Western and Central Europe. Journal of Petrology, 32(4): 811-849.

Wulff-Pedersen, E., Neumann, E.R. and Jensen, B.J., 1996. The upper mantle under La Palma, Canary Islands: formation of Si-K-Na-rich melt and its importance as a metasomatic agent. Contributions to Mineralogy and Petrology, 125: 113-139.

Wulff-Pedersen, E., Neumann, E.R., Vannucci, R., Bottazzi, P. and Ottolini, L., 1999. Silicic melts produced by reaction between peridotite and infiltrating basaltic melts: ion probe data on glasses and minerals in veined xenoliths from La Palma, Canary Islands. Contributions to Mineralogy and Petrology, 137: 59-82.

Yaxley, G.A. and Kamenetsky, V., 1999. In situ origin for glass in mantle xenoliths from southeastern Australia: insights from trace element compositions of glasses and metasomatic phases. Earth and Planetary Science Letters, 172: 97-109.

5. Geochronology

Abstract

New $^{40}Ar/^{39}Ar$ ages for the Cumbre Nueva ridge and the Bejenado volcano from La Palma are reported. These ages were determined with high-resolution incremental heating experiments on separated basaltic matrix and glass fractions. These particular rocks were dated in order to extend the existing age data set of La Palma and to obtain a better time resolution of critical segments in the stratigraphy. The obtained age of 550 ± 20 ka for a glassy Bejenado sample is consistent with previous reported ages (490 ± 60 to 550 ± 10 ka) for this volcano. The $^{40}Ar/^{39}Ar$ ages for the Cumbre Nueva, however, vary from 0.73 ± 0.02 to 3.75 ± 0.39 Ma and are partly significantly older than those of previous studies (0.57 ± 0.01 to 0.83 ± 0.01 Ma). This is most probably related to the analytical techniques used and to minor groundmass alteration.

1. Introduction

Radiometric ages of La Palma volcanic rocks were determined by Abdel-Monem et al. (1972), Staudigel et al. (1986) and Ancochea et al. (1994). These studies were performed using conventional K-Ar dating method on intrusive rocks and on porphyritic samples. The respective whole-rock ages range from 0.19 to 2.0 Ma. However, recent age determinations from La Palma rocks by Guillou et al. (1998, 2001) show that previously published ages are in some cases overestimated (Fig. 1). Two dating techniques, the unspiked K-Ar (Guillou et al., 1998) and $^{40}Ar/^{39}Ar$ (Guillou et al., 2001) methods, were combined in these studies to ensure the overall geological significance of the ages. Altogether 118 radiometric ages from volcanics of La Palma covering the entire subaerial evolution (2.0 Ma to present) have been published (Fig. 1). Despite the comprehensive and accurate age data there are still gaps in the geochronological data set. In particular, no rocks with ages between 410 and 125 ka – immediately after the Cumbre Nueva collapse - have been dated yet. Thus, the current geochronological data do not allow an ultimate discrimination whether this apparent gap from 410 to 125 ka may corresponds to a period of volcanic quiescence, or reflects that older rocks from this period are completely covered by younger Cumbre Vieja lavas, or to incomplete sampling of the initial stages of the Cumbre Vieja. In order to address this question and to obtain a better time resolution of critical segments in the stratigraphy, some more samples from the Bejenado volcano and in particular from outcrops at the structural break between Cumbre Nueva and Cumbre Vieja (Fig. 2) were collected and dated.

Precise age dating of La Palma rocks, however, is difficult. The rocks are relatively young, are partly altered, and they mostly lack separable minerals that contain sufficient K, forcing the use of whole-rocks (groundmass or glass with phenocrysts removed). The whole rocks have comparatively low K contents for alkali-basalts (Table 1) and substantial contents of atmospheric Ar. Some of the problems in dating volcanic rocks by the K-Ar method, such as

Ar loss or excess Ar, or loss of K associated with alteration can be overcome by the $^{40}Ar/^{39}Ar$ technique (e.g. McDougall and Harrison, 1988; Lo et al., 1994). Therefore, we used the incremental $^{40}Ar/^{39}Ar$ method to determine the eruption ages of basaltic rocks from La Palma. However, the small grain size of the groundmass, and contrasting Ca/K ratios of plagioclase, pyroxene and olivine raise the possibility of introducing significant experimental artefacts into the age spectrum as a result of redistribution of ^{39}Ar and ^{37}Ar by recoil during irradiation.

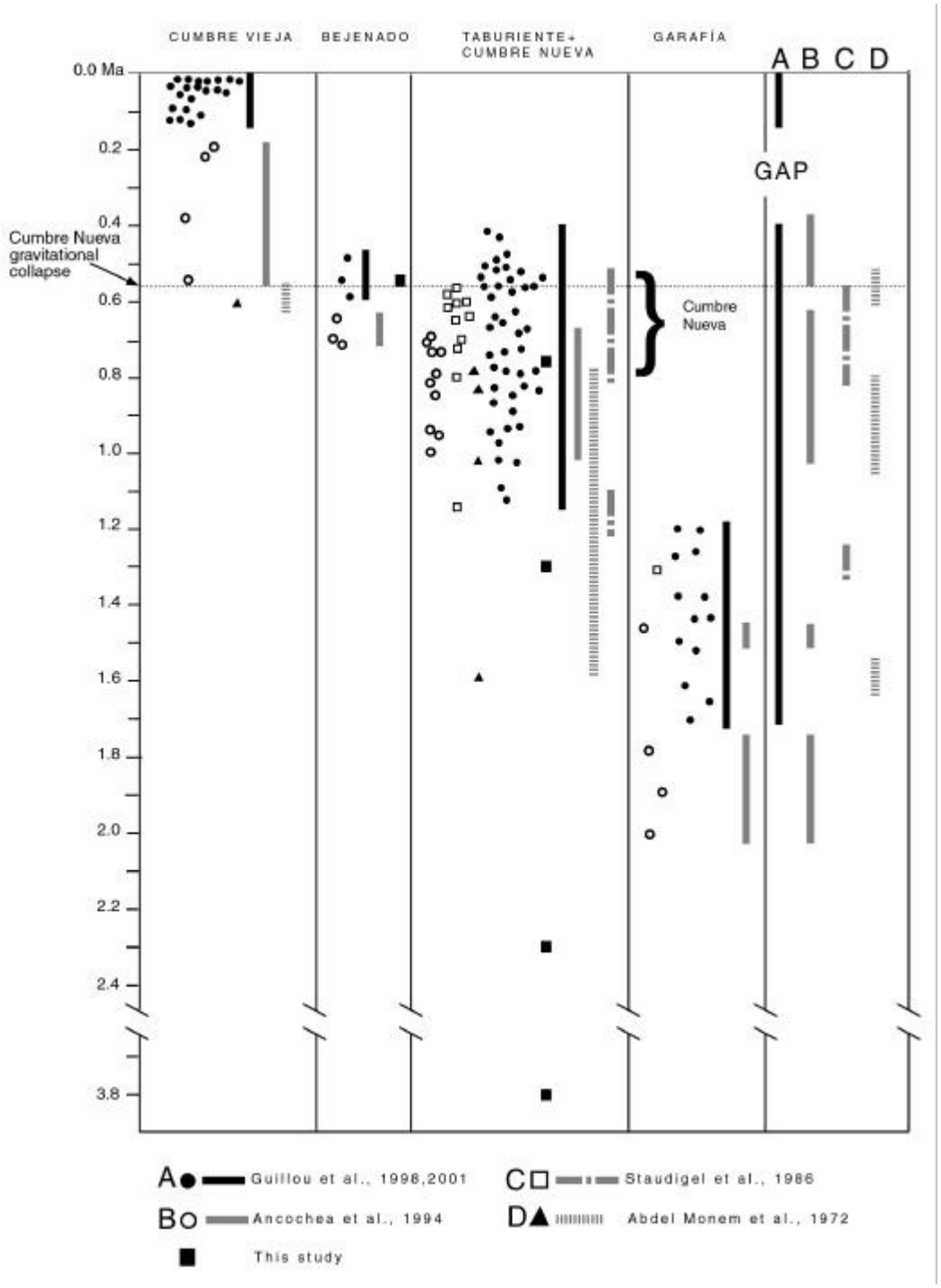

Fig. 1: Published ages of volcanics and intrusives from La Palma (from Carracedo et al., 2001) compared with ages from this study. Ages for Cumbre Vieja rocks after Abdel-Monem et al. (1972) and Ancochea et al. (1994) are overestimated.

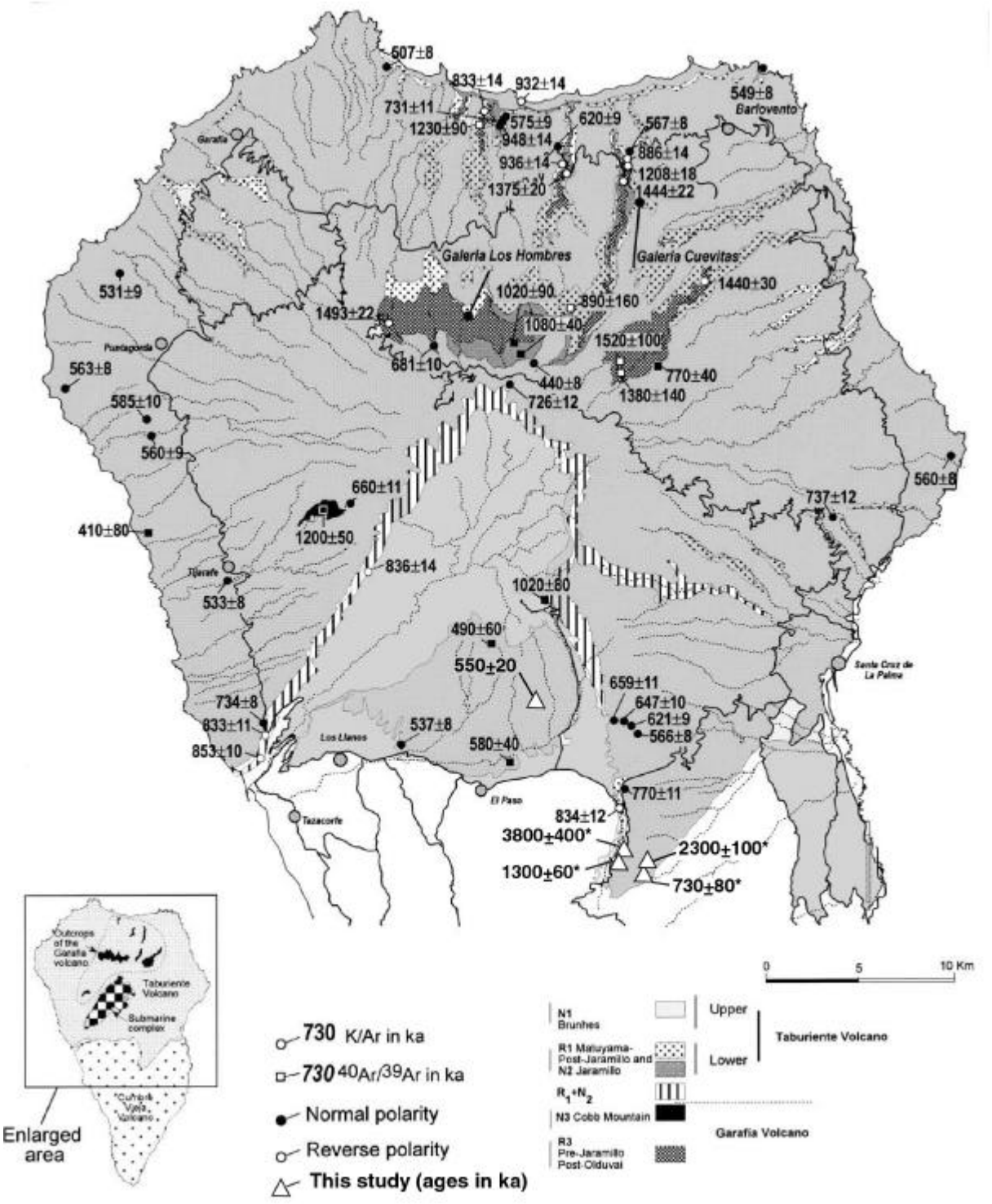

Fig. 2: Distribution of lava flow sequences deduced from K-Ar dating and magnetostratigraphy. Ages and map are taken from Guillou et al. (2001). Numbers with an asterisk identify $^{40}Ar/^{39}Ar$ ages from this study that are obviously too high.

2. Methods

K/Ar and $^{40}Ar/^{39}Ar$ dating method

A detailed description of the theory and methods of the $^{40}Ar/^{39}Ar$ geochronology is given in Faure (1986), York, (1984), McDougall and Harrison (1988) and Kuiper (2004). A brief explanation is given here. $^{40}Ar/^{39}Ar$ geochronology is a variant of K-Ar dating, and is based on the decay of ^{40}K to ^{40}Ar (half-life: 1.25 Ga). There are three naturally occurring isotopes of potassium: ^{39}K (93.2581%); ^{40}K (0.01167%) and ^{41}K (6.7302%). ^{40}K is radioactive and experiences branching decay to ^{40}Ca and ^{40}Ar. Decay to ^{40}Ca is favoured by 88.8% of the ^{40}K atoms, with a decay constant of 0.581×10^{-10} a^{-1}, while decay to ^{40}Ar is favoured by 11.2 % of ^{40}K atoms, with a decay constant of 4.962×10^{-10} a^{-1} (Steiger and Jager, 1977). This chapter is concerned with the ^{40}K to ^{40}Ar branch.

An age can be derived from the $^{40}K/^{40}Ar$ ratio. ^{39}Ar is formed from ^{39}K by irradiation in a nuclear reactor. The amount of ^{39}Ar produced is proportional to the amount of ^{39}K present in the sample. Since the natural abundances of ^{39}K relative to ^{40}K is known, the amount of ^{40}K can be determined and the $^{40}K/^{40}Ar$ ratio and age can be calculated. The main advantage of the $^{40}K/^{39}K$ compared to the $^{40}K/^{39}K$ geochronology, is that only the argon isotopes need to be measured in order to determine the $^{40}K/^{40}Ar$ ratio and age. This measurement is carried out simultaneously on the same specimen. Moreover, Ar loss across grain boundaries can be controlled. In contrast, the conventional K-Ar geochronology requires separate analyses of K and Ar with different instruments and samples. Usually Ar/Ar-dating is carried out by incremental heating technique. This technique consists of measurements of $^{40}Ar/^{39}Ar$ during subsequent steps of incremental heating (e.g. in 200 °C heating steps) up to the melting point or until all argon of the sample has been released. After holding the sample at each particular temperature, the gas is extracted and analysed separately by mass spectrometry to obtain a $^{40}Ar/^{39}Ar$ age. At low temperatures, the weakly bound Ar is released, while at higher temperatures the stronger bound Ar or a later, fast cooling event below the closure temparature (e.g. post-metamorphic) is measured. If the analyzed mineral(s) remained a closed system ever since its formation, the $^{40}Ar^*/^{39}Ar$ ($^{40}Ar^*$ = radiogenic Argon) ratio will be constant across all heating steps. Plateaus are herein defined as the release of 50% or greater of the total ^{39}Ar gas released in five or more successive heating steps concordant with 2s error and showing no resolvable slopes (Fleck et al., 1977). However, if Argon loss has occurred during the sample's history, the ratio will increase with increasing temperature. If the plateau age is reached at relatively low temperatures, disturbance has been weak. Saddle-shaped age spectra point towards excess Argon. The standard age equation can be rewritten:

$$T = 1/? [(^{40}Ar^*/^{39}Ar)(J) + 1] \qquad (1)$$

where J is a measure of the efficiency of conversion of ^{39}K to ^{39}Ar. To determine the rate of conversion in the rector during irradiation, a sample of known K-Ar age (standard) is radiated together with the sample of unknown age. The irradiated standard is also analyzed to obtain its $^{40}*Ar/^{39}Ar$ ratio. The term J in (1) is defined as:

$$J = (e^{?tm} – 1)/(^{40}Ar*/^{39}Ar)_s \qquad (2)$$

where tm is the age of the standard and $(^{40}Ar*/^{39}Ar)_s$ is the ratio of the standard.

Sampling and analytical techniques

20 aphyric and porphyritic rock samples ranging from basanites to alkali basalts and phonolites of La Palma were chosen for age dating. Analyses were carried out on microcrystalline groundmass and glass separates, two ages were determined on plagioclase and hornblende phenocrysts. Two samples additionally contain plagioclase- and/or hornblende phenocrysts which were hand-picked for age determination. Secondary minerals such as zeolithe fillings in vesicles were observed in some samples. The portion of zeolith was minimised by careful hand-picking. Following removal of altered surface, pieces of selected rock samples were crushed to <1 mm, <0.5 mm and <250 mm size and sieved. Matrix chips, fresh glass or plagioclase or hornblende phenocrysts were hand-picked from the 250 – 500 mm fraction under a binocular microscope in order to remove phenocrysts which are potential carriers of inherited Ar (Kaneoka et al., 1983; Lanphere and Dalrymple, 1976; Zeitler and Fitzgerald, 1986). The groundmass separates were then cleaned with distilled H_2O in an ultrasonic disintegrator. Plagioclase- and hornblende crystals and rock matrix chips samples of 5 to 10 mg weigth were placed in drill holes in 99.95 % pure aluminium disks. Sample disks with a three dimensional-array of 27.92 Ma TCR (batch 85G003) sanidine monitor (Duffield and Dalrymple, 1990) were secured together, sealed in an aluminium can, and irradiated with 1 mm Cd shielding at the Geesthacht Research Center. Samples were shielded by a 0.5 mm Cd liner during the 72 hours irradiation at 5 MW (in Position 44) with a neutron fluence of 21 x 1012 N cm $^{-2}$ s^{-1}. TCR standard was measured between 3 and 4 times for each monitor position (4 levels with 8 positions = 32 positions). Samples were analyzed at the IFM-Geomar Geochronology Laboratory using a 25 W Spectra Physics argon ion laser and a MAP 216 series mass spectrometer fitted with a Bauer Singer ion source and a Johnston MM! multiplier. The appropriate *J*- and associated errors were interpolated for each sample position using a three-dimensional least squares cosine plane fit. Between 6.21 mg and 13.46 mg rock/glass fragments of each sample were completely fused. Raw mass spectrometer peaks were corrected for mass discrimination, background values (determined between every 6 samples), and interferencing neutron

reactions on K and Ca using CaF_2 and K_2SO_4 salts that had been irradiated together with the samples. Age uncertainties were calculated by partial differentiation of the standard age equation (Duffield and Dalrymple, 1990) and includes uncertainties in the determination of the flux monitor, J, the blank determination, the regression of the intensities of the individual isotopes and the mass discrimination correction (1.0083 per AMU). Ages and error estimates were calculated for each sample discussed here by calculating the mean apparent age of each population (single fusion ages weighted by the inverse of their variance following the method described by Young (1962), assuming an initial "atmospheric" $^{40}Ar/^{39}Ar$ ratio of 295.5. Isochrons have been calculated as inverse isochrons using York's least square fit accommodates errors in both ratios and correlation of errors (York, 1969). Mean squared weighted deviates (MSWD) were determined for the mean apparent ages and isochron ages in order to test the scatter of the single fusion data (Wendt and Carl, 1991). If the cases where the scatter around the plateaus or isochrons is greater than predicted from the analytical errors, i.e., MSWD > 1, the analytical error has been expanded by multiplying by the $\sqrt{\text{MSWD}}$ (e.g. York, 1969). Errors are quoted at the 2s level. Mean apparent ages, isochron ages and mean square weighted deviates are reported in Table 2. Although only samples with high plagioclase proportions within the groundmass and a low degree of alteration were chosen for age determination, only three samples from the Cumbre Nueva and one Bejenado sample yield reliable plateaus (Fig. 3). Samples which do not meet the criteria for reliable plateaus are not further discussed in this study. Mechanisms which produce discordant age spectra in basalts include Ar loss resulting from devitrification of glass or alteration (Fleck et al., 1977, Renne et al., 1993), redistribution and loss of ^{39}Ar and ^{37}Ar recoil (Huneke and Smith, 1976; Foland et al., 1993), and the presence of excess argon (Lanphere and Dalrymple, 1976; Villa 1991; Kelley, 2003).

3. Petrography

Apart from sample KLP 115, all dated samples that yielded reliable plateaus are basaltic lava flows from the eastern flank (KLP 35, KLP 36) and western flank of the Cumbre Nueva (KLP 87, KLP 89) (Fig. 1, Fig. 2). The basaltic rocks are massive and exhibit porphyric or fine granular aphyric textures. The phenocryst phases are clinopyroxene and olivine in variable amounts. The groundmass is mainly composed of plagioclase laths, clinopyroxene, olivine and Fe-Ti-oxides with average crystal sizes between 5 and 80 µm. Iddingsite occurrs in most samples (except sample KLP 115) as an abundant weathering product and replaces olivine partly to completely. Olivine crystals in sample KLP 89 show sepentinitization along cracks as a result of hydrothermal alteration. Sample KLP 115 is a phonolithic lava flow from the southern flank of Bejenado with glassy groundmass and trachytic texture (<10 % feldspar laths) exhibiting no alteration as e.g. palagonit or devitrification. The phenocrysts consist of

kaersutitic amphibole partly intergrown with clinopyroxene, clinopyroxene and minor apatite, hauyne and titanite.

4. Results and interpretation

Although only samples with high plagioclase proportion within the groundmass and a low degree of alteration were chosen for age determination, only three samples from the Cumbre Nueva and one Bejenado sample yield reliable plateaus (Fig. 3). $^{40}Ar/^{39}Ar$ data and analytical details are given in Table 1 which displays the age results. The $^{40}Ar/^{39}Ar$ age plateaus and isotope correlation diagrams are shown in Fig. 3 and 4.

Laser incremental heating analyses of groundmass separates reveal weighted mean age plateaus between 0.55 to 3.75 Ma (including the error of the neutron fluence monitor). Laser step-heating analysis of groundmass separate of Cumbre Nueva sample KLP 35 yields a disturbed age spectrum (Fig. 3) in the lower temperature range. Its step-heating plateau gives a mean apparent age of 2.33 ± 0.14 Ma (MSWD = 1.0) comprising 67.5% of the ^{39}Ar released. Three Cumbre Nueva samples KLP 36, KLP 87, KLP 89 yield ages of 0.73 ± 0.07, 1.30 ± 0.06 and 3.75 ± 0.39 Ma, respectively, for groundmass separates. These samples have flat age spectrum (Fig. 3) only slightly disturbed in the lowest and highest temperature region. The release spectrum of glass sample KLP 115 from Bejenado define a plateau with an age of 0.55 ± 0.02 Ma comprising 99.9% of ^{39}Ar released (Fig. 2).

Ar loss probably occurred at the lowest temperature steps In all age spectra due to alteration effects. Some scatter is also observed within the plateau intervals, indicating that the different Ar reservoirs are not evenly distributed, and selectively diffused during the heating-temperature intervals.

MSWD values range from 0.45 to 1.40 indicating a general correspondence between expected errors and estimated errors. Uncertainties in the apparent ages of gas released during individual heating steps are relatively large because all groundmass separates samples are highly contaminated with atmospheric argon (i.e. ^{40}Ar, ^{36}Ar), as is indicated by Fig. 4 where melting point data are grouped together close to the $^{36}Ar/^{40}Ar$ axis. For sample KLP 89 a negative inverse isochrone was obtained.

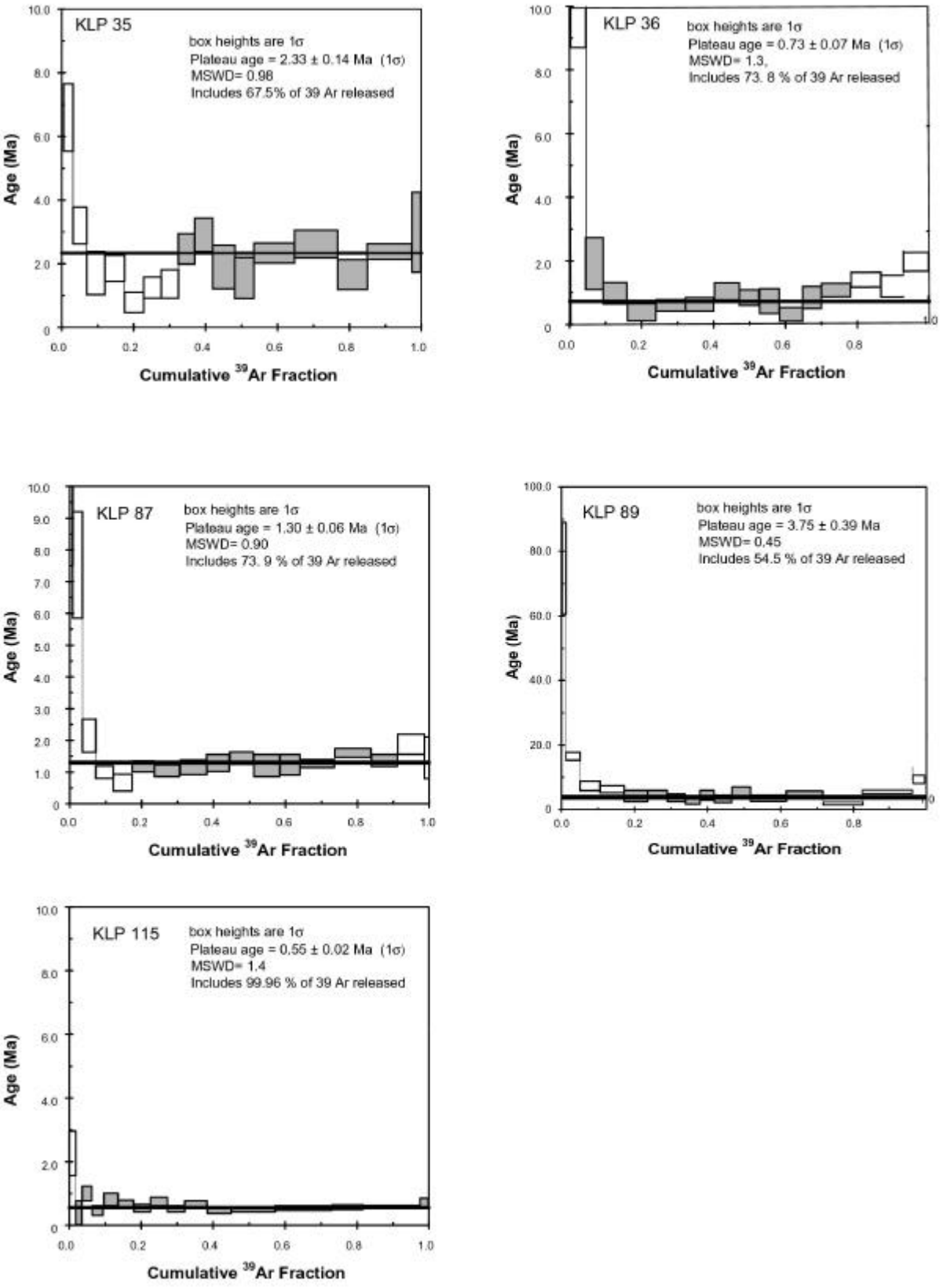

Fig. 3: Results of $^{40}Ar/^{39}Ar$ incremental heating of groundmass and glass separates analyses. Reported $^{40}Ar/^{39}Ar$ dates are weighted age estimates and errors of the plateau fractions at the 1s confidence including ~0.07 % standard deviation in the J value. Plateau ranges and ^{39}Ar fractions as indicated. All samples were analysed using Taylor Creek Rhyolithe (TCR) sanidine (27.92 Ma; Duffield and Dalrymple, 1990) as irradiation monitor standard.

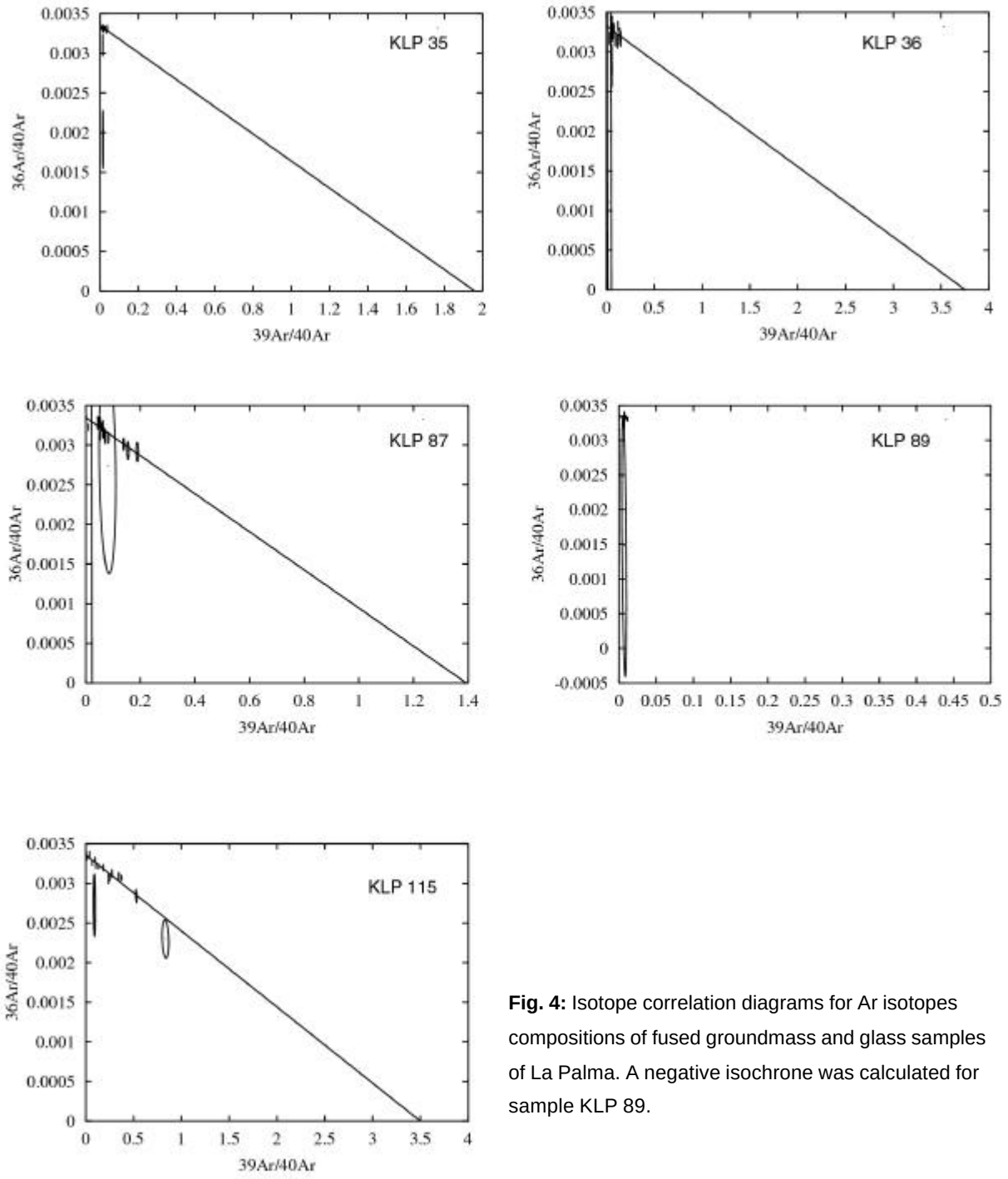

Fig. 4: Isotope correlation diagrams for Ar isotopes compositions of fused groundmass and glass samples of La Palma. A negative isochrone was calculated for sample KLP 89.

5. Discussion

The apparent age information yielded by $^{40}Ar/^{39}Ar$ spectra of groundmass separates from Cumbre Nueva samples (KLP 35, KLP 36, KLP 87, KLP 89) is inhomogeneous over large part of the release pattern indicating a disturbed K-Ar system. Given this fact, the present study deals with the problem of excess argon and Ar recoil of Cumbre Nueva rocks, but also the question how to interpret the $^{40}Ar/^{39}Ar$ age results. Apart from sample KLP 36 (0.73 ± 0.07 Ma), our ages obtained for Cumbre Nueva samples are far outside the age range of Cumbre Nueva rocks by reported by Guillou et al. (1998, 2001) and appear geologically

unreasonable. Their $^{40}Ar/^{39}Ar$ ages and “unspiked” K-Ar ages between 0.57 ± 0.01 and 0.83 ± 0.01 Ma for the Cumbre Nueva are significantly younger than our ages for sample KLP 87, KLP 35 and KLP 89 (1.30 ± 0.06 – 3.80 ± 0.39 Ma). In contrast, our age obtained for Bejenado glass sample KLP 115 (0.55 ± 0.02 Ma) is consistent with rock ages from this volcano (Guillou et al., 1998, 2001) covering a period of 0.49 ± 0.06 to 0.55 ± 0.01 Ma. It is considered that ages obtained by Guillou et al. (1998; 2001) are reliable because they were determined by two different methods ($^{40}Ar/^{39}Ar$ and unspiked K-Ar-technique) from different laboratories, and appear internally and geologically consistent. In addition, the astronomical calibrated time scale (Shackleton, 1990; Hilgen, 1991; Berggren et al., 1995) has been shown to correlate well with $^{40}Ar/^{39}Ar$ ages of transitional polarity lava flows sampled in well-defined stratigraphic sequences (Singer et al., 1999). Guillou et al (1998, 2001) used the Matuyama-Brunhes boundary to check the reliability of the reported $^{40}Ar/^{39}Ar$ and K-Ar ages. Based on stratigraphic relationships, ages for samples KLP 35 (2.30 ± 0.10 Ma), KLP 87 (1.30 ± 0.06 Ma) and KLP 89 (3.80 ± 0.39 Ma) are clearly to high for the following reasons:

(i) Since these samples are taken from the Cumbre Nueva they should be consistent with previously published ages of Cumbre Nueva rocks (0.57 ± 0.01 to 0.83 ± 0.01 Ma; Guillou et al., 2001). However, as indicated in Fig. 1 there are a clear differences between our ages for Taburiente/Cumbre Nueva and those of previous studies. Ages older than ~1.6 Ma for Taburiente/Cumbre Nueva were not reported yet, and it is geologically unlikely that rocks of this age exits at the sample sites.

(ii) Samples KLP 87 (1.30 Ma) and KLP 89 (3.80 Ma) were collected along the same profile section (Fig. 2), at elevations of 1090 m and 1060 m, respectively. Although the ages obtained for these samples are consistent with their field relations and stratigraphic position it is supposed that ages of sample KLP 89 can be discarded. It is simply difficult to reconcile an elevation difference of 30 m with an age difference of 2.5 Ma and a calculated lava accumulation rate of 1.7 mm/a for the Cumbre Nueva (Guillou et al., 1998).

(iii) Sample LP 18 of Guillou et al. (2001) has an age of 0.83 ± 0.01 Ma, which is the oldest reported age of Cumbre Nueva rocks. Therefore, based on stratigraphic evidence, sample KLP 87 has to be younger than 0.83 Ma, because it is clearly situated above the lava flow of LP 18 and a significant discordance between both localities was not observed

There are some possible explanations why the groundmass dating method yield overestimated ages for some Cumbre Nueva samples.

(i) Errors can be related to ^{39}Ar recoil which could produce anomalous old $^{40}Ar/^{39}Ar$ ages (e.g. Walker and McDougall, 1982; Pringle, 1983). During irradiation ^{39}Ar can recoil or be redistributed by as much 0.5 µm, with a mean value of ca. 0.1 µm (McDougall and Harrison, 1988). The effect for coarse-grained material is considered to be negligible. In very fine-

grained volcanic rocks with K-rich and K-poor minerals or with alteration intergrowths, there may be some ^{39}Ar driven by recoil out of the K-rich phase into the K-poor phase. As a consequence, disturbed age spectra can result if these different phases release their gas at different temperatures during step-heating (Foland et al., 1984; Lo and Onstott, 1989; Hanes and York, 1979). Recoil loss of ^{39}Ar in combination with degassing of alteration phases (increasing the atmospheric component) that are located interstitially and on the surfaces of the groundmasses might explain increased apparent ages in the low and highest temperature ranges and lowering of the $^{39}Ar/^{40}Ar$ ratio at constant $^{36}Ar/^{40}Ar$ ratio as observed in Fig.3.

(ii) Secondly, argon concentration can reach levels that cause an $^{40}Ar/^{39}Ar$ age to be significantly older than the event which initialised or reset the isotope system (excess argon; Kelley, 2002). During its cooling history a mineral could trap Ar that was not generated by in situ decay of ^{40}K and has a $^{40}Ar/^{36}Ar$ greater than the present-day atmospheric value of 295.5. In case of excess Ar, the relationship between the parent isotope ^{40}K and its radiogenic daughter isotope ^{40}Ar is disturbed. Therefore calculated ages for minerals affected by excess argon are anomalously high and geological meaningless because some of the excess argon will be misidentified as radiogenic ^{40}Ar (Hanes, 1991). This error is only obvious if the age is too old with regard to the geological relationships or to other geochronological dating methods. A feature of step-heating samples containing excess argon is the saddle or U-shaped $^{40}Ar/^{39}Ar$ plateaus pattern (Lanphere and Dalrymple, 1976; McDougall and Harrison, 1988), in which anomalously high ages are obtained at both low and high temperatures of gas release. The trough of the saddle is minimally contaminated by excess argon and may provide an upper limit for the cooling age of the sample (e.g. Lanphere and Dalrymple, 1976). However, if excess argon is uniformly distributed throughout the sample or if the excess and radiogenic Ar is homogenized during the step-heating experiment, it is possible to obtain a flat plateau pattern corresponding to an anomalous old age (e.g. Foland, 1983; Hanes, 1991; Maboko et al., 1991).

In order to discuss the issue whether ^{39}Ar recoil or excess Ar is responsible for overestimated ages of La Palma samples, I have to point out that uncertainties in the apparent ages during individual incremental heating steps can be related to alteration and improper sample preparation. Alteration of La Palma samples is clearly indicated by the presences of microscopically visible alteration phases (e.g. iddingsite). Koppers et al. (2000) have shown that contamination by atmospheric Ar (i.e. ^{40}Ar, ^{36}Ar) of basalt matrix can be significantly reduced by repeated etching and dissolution of samples in diluted HCL and HNO_3. This procedure preferentially removes alteration products on grain boundaries without affecting

inherited and radiogenic ^{40}Ar, ^{36}Ar, ^{38}Ar components from primary Ar reservoirs. The samples of this study were only washed and cleaned in ultraclean water and in ultrasonic baths.

It is obvious from Fig. (4) that La Palma basaltic samples are highly contaminated by atmospheric argon because melting point data are grouped close to the atmospheric intercept on the $^{36}Ar/^{40}Ar$ axis. Based on the above observations, I conclude that the applied groundmass sample preparation is not suitable for air contaminated La Palma samples even if this sample preparation technique was succesfully applied to other North Atlantic OIB basaltic matrix samples (e.g. Geldmacher et al., 2000; Schwarz et al., 2005).

Conclusion

The age of 550 ± 20 ka for a fresh glass sample from Bejenado volcano and for one Cumbre Nueva sample (730 ± 70 ka) agreed with previously plublished ages for these volcanic edifices. However, obtained $^{40}Ar/^{39}Ar$ step-heating dates for three Cumbre Nueva groundmass samples are overestimated and geologically unreasonable due to contamination of atmospheric argon. In order to obtain better age results in the future, it is recommended to reduce the amount of atmospheric Ar in La Palma samples by acid leaching in diluted HCL and HNO_3.

Table 1: Incremental heating and single-particle total fusion 40Ar/39Ar analyses on groundmass and glass separates from Bejenado and Cumbre Nueva.

					Age spectrum plateau age				Total gas age	Inverse Isochron analysis					
Sample	UTM Coordinates	Elevation m	Rock type	Analysis type	Age ± 1s Ma	^{39}Ar %	MSWD	n (N)	Age ± 1s Ma	Age ± 1s Ma	^{40}Ar/^{36}Ar ± 1s intercept	MSWD	K2O wt%	J	± 1s
Bejenado															
KLP 115	220825 / 3175787	1210	PG	HR-IHA	0.55 ± 0.02	100	1.4	17(20)	0.60 ± 0.03	0.52 ± 0.28	297.67 ± 1.02	1.15	5.60	3.76E-03	± 2.39E-06
Cumbre Nueva															
KLP 35	224111 / 3169290	1220	B	HR-IHA	2.30 ± 0.14	68	1.0	9(20)	2.23 ± 0.13	2.99 ± 2.14	298.57 ± 6.20	2.78	1.40	3.75E-03	± 2.76E-06
KLP 36	224111 / 3169190	1220	B	HR-IHA	0.73 ± 0.07	74	1.3	11(20)	1.70 ± 0.15	1.83 ± 1.50	306.20 ± 2.10	1.81	1.80	3.75E-03	± 2.76E-06
KLP 87	223162 / 3170215	1090	B	HR-IHA	1.30 ± 0.06	74	0.9	10(20)	1.65 ± 0.08	2.73 ± 1.08	305.10 ± 9.13	1.88	1.81	3.75E-03	± 2.76E-06
KLP 89	223390 / 3599950	1060	B	HR-IHA	3.75 ± 0.39	55	0.5	9(20)	5.83 ± 0.34	- ± -	- ± -	-	-	3.76E-03	± 2.39E-06

HR-IHA = High-resolution incremental heating analyses; Reported ^{40}Ar/^{39}Ar dates are weighted age estimates and errors (1s) including uncertainties in the J value. MSWD = Mean Square Weighted Deviates for plateau ages and inverse isochrons calculated for N-1 df. N = total number of heating steps. n = number of heating steps in plateau comprising percent fraction of cumulative 39Ar release. oblique: results rejected because of plateau size deficiency. disturbed spectra or significant differences at 2sigma level (Combined data). K_2O wt% = whole rock or glass content determined by EMS of RFA. Rock types:B = basanite, PG = phonolitic glas.

References

Abdel-Monem, A., Watkins, N.D. and Gast, P.W., 1972. Potassium-argon ages, volcanic stratigraphy, and geomagnetic polarity history of the Canary Islands: Tenerife, La Palma and Hierro. American Journal of Science, 272: 805-825.

Ancochea, A. et al., 1994. Constructive and destructive episodes in the building of a young Oceanic Island, La Palma, Canary Islands, and genesis of the Caldera de Taburiente. Journal of Volcanology and Geothermal Research, 60: 243-262.

Berggren, W.A., Kent, D.V., Swisher III, C.C. and Aubry, M.P., 1995. A revised Cenozoic geochronology and chronostratigraphy. In: W.A. Berggren, D.V. Kent, M.P. Aubry and J. Hardenbol (Editors), Geochronology, Time Scales and Global Stratigraphy Correlation. SEPM Special Publication.

Carracedo, J.C., Badiola, E.R., Guillou, H., de La Nuez, J. and Pérez Torado, F.J., 2001. Geology and Volcanology of La Palma and El Hierro, Western Canaries. Estudios Geologicos, 57(5-6): 157-273.

Duffield, W.A. and Dalrymple, G.B., 1990. The Taylor Creek Rhyolithe of New Mexico: a rapidly emplaced field of domes and lava flows. Bulletin of Volcanology, 52: 475-478.

Fleck, R.J., Sutter, J.F. and Elliott, D.H., 1977. Interpretation of discordant $^{40}Ar/^{39}Ar$ age-spectra of Mesozoic tholeiites from Antarctica. Geochimica et Cosmochimica Acta, 41: 15-32.

Foland, K.A., 1983. $^{40}Ar/^{39}Ar$ incremental heating plateaus for biotites with excess argon. Isotope Geosciences, 1: 3-21.

Foland, K.A., Fleming, T.H., Heimann, A. and Elliot, D.H., 1993. Potassium-argon dating of fine-grained basalts with massive Ar loss: application of $^{40}Ar/^{39}Ar$ technique to plagioclase and glass from Kirkpatrick Basalt, Antartica. Chemical Geology, 107: 173-190.

Foland, K.A., Linder, J.S., Laskowski, T.E. and Grant, N.K., 1984. $^{40}Ar/^{39}Ar$ dating on glauconites: measured 39Ar recoil loss from well-specialized specimen. Isotope Geoscience, 2: 241-264.

Geldmacher, J., Bogaard, P.v.d., Hoernle, K.A. and Schmincke, H.U., 2000. Ar age dating of the Madeira Archipelago and hotspot track (eastern North Atlantic). Geochemistry, Geophysics, Geosystems, 1: Paper number 1999GC000018.

Guillou, H., Carracedo, J.C. and Day, S., 1998. Dating of the upper Pleistocene-Holocene activity of La Palma using the unspiked K-Ar technique. Journal of Volcanology and Geothermal Research, 86: 137-149.

Guillou, H., Carracedo, J.C. and Duncan, R., 2001. K-Ar, $^{40}Ar/^{39}Ar$ ages and magnetostratigraphy of Brunhes and Matuyama lava sequences from La Palma Island. Journal of Volcanology and Geothermal research, 86(1-4): 37-149.

Hanes, J.A., 1991. K-Ar and $^{40}Ar/^{39}Ar$ geochronology: methods and applications. In: L. Heaman and J.N. Ludden (Editors), Short course handbook on applications of radiogenic isotope systems to problems in geology. Mineralogical Association of Canada, Toronto, pp. 498.

Hanes, J.A. and York, D., 1979. A detailed $^{40}Ar/^{39}Ar$ age study of an Abitibi dike from the Canadian Superior Provinz. Canadian Journal of Earth Science, 16: 1060-170.

Hilgen, F.J., 1991. Astronomicla calibration of Gauss to Matuyama sapropels in the Meditarranean and implications for the geomagnetic time scale. Earth and Planetary Science Letters, 104: 226-244.

Huneke, J.C. and Smith, S.P., 1976. The realities of recoil: ^{39}Ar recoil out off small grains and anomalous patterns in $^{39}Ar/^{40}Ar$ dating. Geochimica et Cosmochimica Acta, 7: 1987-2008.

Kaneoka, I., Takaoka, N. and Clague, D.A., 1983. Noble gas systematics for coexisting glass and olivine crystals in basalts and dunite xenoliths from Loihi seamount. Earth and Planetary Science Letters, 66: 427-437.

Kelley, S., 2002. Excess argon in K-Ar and Ar-Ar geochronology. Chemical Geology, 188: 1-22.

Koppers, A.A.P., Satudigel, H. and Wijbrans, J.R., 2000. Dating crystalline groundmass separates of altered Cretaceous seamount basalts by the $^{40}Ar/^{39}$ Ar incremental heating technique. Chemical Geology, 166: 139-158.

Lanphere, M.A. and Dalrymple, G.B., 1976. Identification of excess ^{40}Ar by the $^{40}Ar/^{39}Ar$ age spectrum technique. Earth and Planetary Science Letters, 32: 141-148.

Lo, C.H. and Onstott, T.C., 1989. ^{39}Ar recoil artifacts in cloritized biotite. Geochimica et Cosmochimica Acta, 5: 2697-2711.

Lo, C.-H., Onstott, T.C., Chen, C.-H. and Lee, T., 1994. An assessment of $^{40}Ar/^{39}Ar$ dating for whole-rock volcanic samples from the Luzon Arc near Taiwan. Chemical Geology, 114: 157-178.

Makobo, M.A.H., McDougall, I., Zeitler, P.K. and Fitzgerald, J.D., 1991. Discodant $^{40}Ar/^{39}Ar$ ages from the Miscrave Ranges, central Australia: implications for the significance of hornblende $^{40}Ar/^{39}Ar$ spectra. Chemical Geology, 86: 139-160.

McDougall, I. and Harrison, T., 1988. Geochronology and thermochronology by the $^{40}Ar/^{39}Ar$ method, Oxford.

Pringle, M.S., 1983. Age progressive volcanism in the musician seamounts: a test of the hot spot hypothesis for the late Cretaceous Pacific. In: M.S. Pringle, W. Sager, W.V. Sliter and S. Stein (Editors), The Mesozoic Pacific: Geology, Tectonics and Volcanism. Geophysical Monograph. American Geophysical Union, Washington DC, pp. 187-216.

Renne, P., Walter, R., Verosub, K., Sweitzer, M. and Aronson, J., 1993. New data from Hadar (Ethiopia) support orbitally tuned time scale to 3.3 Ma. Geophysical Research Letters, 20(11): 1067-1070.

Schwarz, S., Klügel, A., van den Bogaard, P. and Geldmacher, J., 2005. Internal structureof a volcanic rift system in the eastern Nort Atlantic: The desertas rift zone Madeira Archepilago. Journal of Volcanology and Geothermal Research, 141: 123-155.

Shackelton, N.J., Berger, A. and Peltier, W.R., 1990. An alternative astronomical calibration of the lower Pleistocene timescale based on ODP site 677. Transaction of the Royal Society Edinburgh, Earth Science 81: 251-261.

Singer, B.S., Hoffman, K.A., Chauvin, A., Coe, R.S. and Pringle, M.S., 1999. Dating transitionally magnetized lavas of the late Matuyama Chron: toward a new $^{40}Ar/^{39}Ar$ timescale of reversals and event. Journal of Geophysical Research, 104: 679-693.

Staudigel, H., G, F. and Giannerini, G., 1986. The history of intrusive activity on the Island of La Palma (Canary Islands). Journal of Volcanology and Geothermal Research, 27: 299-322.

Steiger, R.H. and Jager, E., 1977. Subcommission on geochronology: conventions on the use of decay constants in geo- and cosmochronology. Earth and Planetary Science Letters, 36: 359-362

Villa, I.M., 1991. Excess ar geochemistry in potassic volcanites. Schweizerische Mineralogische Petrographische Mitteilungen, 71: 205-219.

Walker, D.A. and McDougall, I., 1982. $^{40}Ar/^{39}Ar$ and K-Ar dating of altered glassy volcanic rocks: the Dabi volcanics P.N.G. Geochimica et Cosmochimica Acta, 46: 2181-2190

Wendt, I. and Carl, C., 1991. The statistical distribution of the mean squared weighted deviation. Chemical Geology, 86: 275-285.

York, D., 1969. Least squares fitting of a straight line with correlated errors. Earth and Planetary Science Letters, 5: 320-324.

Young, H.D., 1962. Statistical treatment of experimental data. McGraw-Hill, New York, pp. 5101-5112.

Zeitler, P.K. and Fitzgerald, J.D., 1986. Saddle-shaped 40Ar/39Ar age spectra from young, microstructurally complex potassium feldspars. Geochimica et Cosmochimica Acta, 50: 1185-1199.

6. Conclusions

6. Conclusions

The main purpose of this thesis was to improve our understanding of magma evolution and transport mechanisms in rift zones, using La Palma as a case study. Rocks from La Palma have been investigated in detail using $^{40}Ar/^{39}Ar$ geochronology, thermobarometry, fluid inclusion studies, major and trace elements as well as Sr-Nd-Pb isotope analyses. Of special interest was the question whether the currently active Cumbre Vieja rift zone is genetically related to the extinct Taburiente stratovolcano, or whether they represent two distinct volcanoes with their own magma plumbing systems.

The main results of this study are:

1. In all volcanic phases two prominent depth ranges of magma stagnation are constrained by clinopyroxene-melt barometry and fluid inclusion studies: (i) major fractionation levels within the upper mantle, and (ii) temporary stagnation levels in the lower crust close to the Moho. The thermobarometric data indicate a migration of fractionation and stagnation levels to shallower depths from the earlier Taburiente phase to the Recent Cumbre Vieja phase.
2. The thermobarometric data yield significant differences between the extinct Taburiente/Cumbre Nueva and the presently active Cumbre Vieja. Therefore it is proposed that both volcanic systems are not fed by a common magma reservoir, but rather represent two distinct volcanoes.
3. The obtained barometric results show that models for Hawaiian rift zones are not necessarily transferable to North Atlantic rift zones largely, because magma supply rates differ by up to two orders of magnitude and are not high enough for La Palma to develop and maintain a long-lived shallow magma chamber - a characteristic feature of Hawaiian volcanoes. Nevertheless, the migration of magma reservoirs to shallower depths at La Palma over time is analogous to the progressive evolution of crustal magma chambers to shallower depths proposed for Hawaiian volcanoes.
4. Trace element systematics of both older and recent La Palma lavas requires the presence of residual amphibole in their melting region. It is suggested that this amphibole is of lithospheric origin since this phase is not stable in the asthenospheric mantle under most conditions or within a hot mantle plume.
5. Modelling shows that the the trace element systematics of lavas from Taburiente/Cumbre Nueva, Bejenado and Cumbre Vieja cannot be generated by an amphibole-bearing garnet peridotite or any other plausible source. This feature of La Palma lavas is best explained by bulk assimilation of additional apatite (Cumbre Vieja) and amphibole (Taburiente/Cumbre Nueva, Bejenado). The calculations revealed that the high Nb/U ratios of Taburiente/Cumbre Nueva and Bejenado lavas can only be achieved if ~20% amphibole is added to the melt

whereas the high Sm/Yb and La/Yb ratios and high P, Th and U contents of Cumbre Vieja lavas require addition of ~1% apatite to the melt.

6. The isotopic variations of La Palma lavas are best explained by mixing of two components in variable proportions: a more enriched HIMU component closely associated with the inferred mantle plume beneath La Palma, and a more depleted component, DMM-like, from the refractory oceanic lithosphere.

7. The binary mixing trends of La Palma rocks similar to other OIB can be explained from plume-lithosphere interaction. This model implies that plume-derived melts mix with melts at the base of the lithosphere formed by conductive heating of the plume. La Palma magmas represent mixing between deep plume melts and melts formed by partial melting at the boundary of the amphibole-metasomatized lithosphere in variable proportions and have isotopic compositions intermediate between the depleted lithosphere and the plume.

8. The obtained trace element data indicate no progressive geochemical evolution of La Palma magmas but a compositional break between Taburiente/Cumbre Nueva and Bejenado volcanism in the north and Cumbre Vieja volcanism in the south. In addition, the high Nb/U ratios found for many Taburiente/Cumbre Nueva and Bejenado rocks but not for any Cumbre Vieja rocks indicate different metasomatism of the lithosphere beneath northern and southern La Palma. Therefore, the geochemical data are consistent with the interpretation of the thermobarometric data that the old Taburiente/Cumbre Nueva and the young Cumbre Vieja rift represent two distinct volcanoes.

9. $^{40}Ar/^{39}Ar$ step-heating data obtained during this study yield reasonable ages only for one Bejenado sample and one Cumbre Nueva sample, which agree with previously published ages for these volcanoes. The three data for the other samples are far too high and geologically unreasonable, most likely due to contamination by atmospheric argon. In order to obtain better age results in the future, it is concluded that the amount of atmospheric Ar in La Palma samples could be reduced by leaching of the samples in diluted HCL and HNO_3.

Appendix

Appendix A 2.1: Compositions of glasses analyzed for thermobarometry
N denotes number of analyzes averaged, values in parentheses are relative standard deviations (RSD) in percent.

Sample	N	SiO_2	TiO_2	Al_2O_3	FeO*	MnO	MgO	CaO	Na_2O	K_2O	P_2O_5	Total
KLA1620	14	48.6 (0.7)	3.28 (2.1)	17.2 (0.8)	9.51 (2.9)	0.24 (17)	3.47 (2.4)	7.87 (3.8)	5.54 (5.6)	2.97 (4.8)	0.92 (3.3)	99.84
KLA1653	9	47.7 (0.5)	3.28 (2.0)	17.5 (0.8)	9.97 (2.2)	0.23 (16)	3.35 (2.0)	8.03 (1.6)	5.86 (1.1)	3.02 (2.1)	0.94 (2.6)	99.99
KLA1690	15	44.6 (0.5)	4.34 (1.8)	15.3 (1.1)	12.4 (1.4)	0.22 (17)	4.42 (1.2)	10.9 (1.1)	4.53 (2.4)	1.75 (2.6)	0.85 (3.7)	99.50
POS_155-1	10	46.7 (0.6)	3.76 (2.8)	17.4 (0.9)	9.88 (1.4)	0.21 (23)	4.05 (1.5)	9.06 (2.5)	5.29 (1.4)	2.50 (2.7)	0.90 (3.6)	99.65
POS_164-7	15	49.0 (0.5)	2.87 (2.6)	18.7 (0.8)	7.82 (2.6)	0.20 (18)	3.09 (1.7)	7.00 (1.6)	6.45 (0.9)	3.06 (2.0)	0.74 (4.0)	99.13
POS_165-3	10	46.0 (0.6)	3.59 (1.8)	16.8 (0.8)	11.0 (1.5)	0.20 (14)	4.40 (1.6)	10.1 (1.3)	4.51 (1.3)	1.92 (1.6)	0.75 (2.5)	99.29
POS_169-1-9	14	46.4 (0.6)	3.61 (1.8)	16.8 (1.2)	11.1 (2.0)	0.21 (23)	4.19 (3.2)	9.56 (2.3)	4.22 (3.8)	1.94 (4.9)	0.78 (3.6)	98.82
POS_170-2	16	45.5 (0.8)	3.39 (2.9)	16.5 (1.0)	11.5 (2.6)	0.23 (23)	4.30 (3.1)	9.47 (2.4)	5.01 (2.5)	1.77 (3.3)	0.97 (3.4)	98.74
M43_639-1	5	45.5 (0.2)	3.13 (2.1)	15.8 (0.6)	12.5 (1.2)	0.20 (20)	5.64 (1.4)	11.8 (1.1)	4.02 (0.9)	1.35 (2.6)	0.57 (2.7)	100.5
M43_658-2	25	44.5 (1.1)	3.04 (2.4)	15.0 (2.6)	11.5 (2.9)	0.19 (20)	5.75 (1.4)	11.9 (1.1)	3.89 (1.6)	1.32 (2.9)	0.60 (5.2)	97.74
M43_660-2	20	44.5 (0.5)	3.09 (2.3)	15.2 (0.7)	11.5 (1.6)	0.18 (22)	5.39 (1.3)	11.7 (0.8)	3.98 (1.1)	1.38 (2.7)	0.66 (4.9)	97.85
Regular analyses of reference standards (Smithsonian)												
VG-2 Juan de Fuca	22	51.5 (1.0)	1.93 (3.1)	14.1 (1.6)	12.0 (2.4)	0.24 (24)	6.99 (3.1)	11.2 (1.5)	2.66 (1.7)	0.19 (7.6)	0.25 (13)	101.1
VG-A99 Makaopuhi	27	51.6 (1.0)	4.15 (2.6)	12.6 (1.5)	13.4 (2.1)	0.21 (24)	5.05	-2.60	2.67 (2.6)	0.80 (4.4)	0.40 (9.0)	100.3

Appendix A 2.2: Clinopyroxene compositions and calculated temperatures and pressures

	N	rej.	SiO_2	TiO_2	Al_2O_3	FeO	MnO	MgO	CaO	Na_2O	Cr_2O_3	Total	mg#	T [°C]	P [MPa]
KLA1620															
Cpx1	6	0	44.13	3.79	9.50	7.89	0.12	11.85	22.15	0.54	0.013	99.99	72.82	1130	653
Cpx2	6	1	44.72	3.68	8.45	7.84	0.16	12.13	22.23	0.49	0.012	99.72	73.40	1123	578
Cpx6	6	0	44.09	3.86	9.44	7.82	0.14	11.79	22.16	0.52	0.011	99.85	72.88	1128	621
Cpx3	6	1	47.02	2.59	6.64	7.28	0.17	13.31	22.60	0.45	0.023	100.10	76.52	1115	502
Cpx4	6	0	46.50	2.99	7.04	7.43	0.16	13.02	21.99	0.45	0.042	99.64	75.75	1118	514
Cpx5	4	0	48.76	2.15	5.41	6.78	0.13	14.12	22.45	0.41	0.008	100.22	78.78	1109	425
KLA1653															
Cpx1	6	0	44.44	3.79	8.95	7.81	0.47	11.78	22.04	0.52	0.007	99.82	72.89	1116	619
Cpx2	6	0	45.22	3.45	8.35	7.53	0.15	12.29	22.33	0.50	0.020	99.85	74.42	1112	571
Cpx3	6	2	45.71	3.21	7.66	7.60	0.09	12.52	22.27	0.48	0.011	99.57	74.60	1109	550
Cpx4	4	0	47.32	2.74	6.10	7.55	0.18	13.35	22.36	0.40	0.008	100.04	75.91	1098	415
Cpx7	6	0	44.37	3.77	8.93	7.68	0.13	11.77	22.14	0.53	0.010	99.38	73.19	1116	630
Cpx8	6	0	43.68	3.79	9.72	7.88	0.13	11.60	22.21	0.55	0.047	99.61	72.41	1119	650
KLA1690															
Cpx7	6	1	43.15	4.07	10.57	7.98	0.14	11.35	22.11	0.56	0.094	100.03	71.72	1142	767
Cpx8	6	1	44.59	3.62	8.90	8.10	0.15	11.90	22.04	0.47	0.040	99.83	72.37	1131	635
Cpx5	8	0	45.47	2.88	8.24	7.24	0.13	12.53	22.22	0.48	0.160	99.37	75.51	1130	642
Cpx6	7	0	44.49	3.36	9.21	7.58	0.10	11.98	22.01	0.51	0.162	99.40	73.79	1135	684
Cpx3	8	3	45.53	3.25	7.86	7.77	0.13	12.43	21.96	0.44	0.062	99.43	74.04	1126	579
Cpx1	7	1	46.25	2.76	7.57	7.47	0.15	12.51	22.04	0.52	0.062	99.34	74.92	1134	695
Cpx2	7	1	46.44	2.58	7.70	6.96	0.10	12.89	22.26	0.47	0.175	99.59	76.76	1128	621
POS270_155-1															
Cpx1	6	0	41.97	5.04	10.09	8.17	0.11	11.30	22.13	0.54	0.012	99.37	71.13	1141	733
Cpx2	6	0	42.54	4.80	9.63	8.20	0.12	11.48	22.03	0.54	0.015	99.37	71.38	1141	731
Cpx3	6	0	44.37	4.07	8.10	8.00	0.13	12.37	21.91	0.49	0.038	99.51	73.38	1135	660
Cpx4	6	0	42.09	5.14	10.04	8.10	0.13	11.19	22.07	0.55	0.010	99.34	71.11	1143	752
Cpx5	6	0	44.99	3.76	7.69	7.54	0.12	12.72	22.21	0.48	0.018	99.56	75.06	1131	630
POS270_164-7															

Appendix A 2.2 (continued): Clinopyroxene compositions and calculated temperatures and pressures

Cpx1	9	4	45.52	3.01	7.84	7.45	0.16	12.37	22.33	0.55	0.002	99.27	74.76	1122	687
Cpx2	7	0	44.55	3.42	9.02	7.77	0.13	11.87	22.49	0.57	0.002	99.85	73.16	1125	715
Cpx3	6	0	44.96	3.45	8.46	7.69	0.17	12.03	22.08	0.55	0.003	99.42	73.59	1124	696
Cpx4	9	0	43.82	3.78	9.32	7.85	0.16	11.52	22.43	0.60	0.011	99.52	72.34	1128	752
Cpx5	8	0	44.98	3.22	8.42	7.48	0.15	12.12	22.58	0.56	0.014	99.56	74.29	1123	693
Cpx6	7	0	45.70	3.08	7.82	7.57	0.14	12.49	22.44	0.54	0.004	99.79	74.62	1121	666
POS270_165-3															
Cpx1	6	0	45.44	3.25	7.39	8.16	0.13	12.78	21.92	0.40	0.011	99.51	73.62	1128	515
Cpx2	6	0	44.10	3.76	8.65	8.27	0.14	12.06	21.85	0.42	0.012	99.27	72.20	1133	567
Cpx3	7	0	43.63	3.96	8.94	8.31	0.12	11.96	21.91	0.44	0.020	99.32	71.94	1135	588
Cpx4	6	0	44.12	3.76	8.68	8.24	0.14	12.16	21.86	0.43	0.100	99.51	72.45	1134	573
Cpx5	6	0	44.98	3.40	8.02	8.03	0.12	12.53	22.03	0.42	0.007	99.53	73.55	1131	546
POS270_169-1-9															
Cpx1	6	0	44.29	3.66	8.55	8.36	0.13	12.08	21.77	0.46	0.011	99.34	72.03	1137	608
Cpx2	6	0	43.77	3.98	8.90	8.57	0.14	11.89	21.80	0.43	0.006	99.52	71.21	1134	558
Cpx3	6	0	44.64	3.56	8.20	8.22	0.14	12.30	22.06	0.41	0.007	99.56	72.74	1130	518
Cpx4	6	0	45.36	3.37	7.59	8.09	0.15	12.62	21.93	0.40	0.008	99.55	73.55	1127	491
Cpx5	6	0	43.19	4.27	9.37	8.53	0.13	11.56	22.00	0.45	0.015	99.54	70.71	1137	597
POS270_170-2															
Cpx1	6	0	45.66	2.99	7.61	7.88	0.13	12.79	22.12	0.42	0.015	99.63	74.30	1123	533
Cpx2	7	0	44.71	3.38	8.16	8.35	0.17	12.39	21.83	0.44	0.010	99.46	72.57	1127	567
Cpx3	6	0	45.04	3.29	8.16	8.14	0.13	12.52	22.04	0.41	0.018	99.76	73.29	1123	525
Cpx4	6	0	44.36	3.25	8.31	8.33	0.14	12.37	21.72	0.43	0.017	98.92	72.59	1126	555
Cpx5	6	0	44.46	3.50	8.90	8.20	0.11	12.19	21.98	0.43	0.015	99.81	72.60	1127	560
M43_639-1															
Cpx S3	7	2	44.28	3.64	8.59	7.35	0.13	12.03	23.33	0.46	n.a.	99.81	74.47	1157	721
Cpx S4	4	0	45.06	3.23	7.99	8.07	0.15	11.94	22.84	0.39	n.a.	99.66	72.51	1149	601
M43_660-2															
Cpx3	10	0	48.45	1.62	4.81	6.40	0.10	14.40	22.76	0.31	0.243	99.10	80.05	1132	407
Cpx4	15	0	46.17	2.24	7.27	6.94	0.07	13.04	22.72	0.38	0.256	99.09	77.02	1147	578
Cpx5	8	1	47.23	2.12	6.81	6.37	0.11	13.49	22.66	0.36	0.469	99.63	79.07	1144	538
Cpx6	7	1	47.56	2.04	6.70	6.41	0.10	13.54	22.84	0.36	0.376	99.94	79.00	1143	522
Cpx7	6	0	48.47	1.86	5.63	6.69	0.12	14.01	22.66	0.34	0.238	100.01	78.87	1138	473

Appendix A 2.2 (continued): Clinopyroxene compositions and calculated temperatures and pressures

M43_658-2														
Cpx1	15	0	48.55	1.56	4.90	5.85	0.09	14.35	22.85	0.32	0.417	98.89	81.39	1143	473
Cpx2	15	0	47.19	1.96	6.42	6.03	0.06	13.61	22.85	0.35	0.614	99.08	80.10	1149	538
Cpx S8	2	0	47.47	1.69	5.87	5.94	0.11	13.15	23.31	0.39	0.609	98.54	79.78	1153	620
Cpx S1	2	0	47.26	1.75	5.78	5.92	0.13	13.20	23.24	0.40	0.677	98.36	79.91	1155	640
Cpx S5	4	0	45.55	2.49	7.06	6.57	0.13	12.50	23.28	0.45	0.484	98.50	77.24	1162	729
Cpx S6	10	0	47.45	1.90	5.94	5.92	0.11	13.20	23.46	0.39	0.611	98.99	79.90	1153	618
Regular analyses of reference standard Kakanui-Augite (USNM 122142)															
Mean	34	0	50.39	0.78	8.72	6.31	0.14	16.45	15.89	1.25	0.150	100.09	-	-	-
rel. standard dev. (%)			0.4	5.3	4.2	2.0	29.9	1.1	1.5	2.9	15.7				
Regular analyses of reference standard Cr-Augite (USNM 164905)															
Mean	14	0	50.91	0.41	7.51	4.71	0.13	17.68	17.20	0.75	0.877	100.19	-	-	-
rel. standard dev. (%)			0.6	7.1	4.6	2.3	25.5	0.7	1.0	3.7	8.3				

Each analysis represents the average rim composition of a single clinopyroxene.
Temperatures and pressures are calculated using the formulation of Putirka et al. (1996).
N: number of microprobe points; *rej.:* number of outliers rejected for averaging; mg# = molar Mg/(Mg+Fe^{tot})*100.

Appendix A 3.1: Composition of clinopyroxene rims and calculated temperatures and pressures
Each analysis represents the average rim composition of a single clinopyroxene based on 4 to 13 measured points.
Temperatures and pressures are calculated using the formulation of Putirka et al. (1996) and Putirka et al (2003).

Sample		KLP113	KLP113	KLP113	KLP113	KLP113	KLP106	KLP106	KLP106	KLP106	KLP66	KLP6	KLP6	KLP6	KLP6
Cpx#		Cpx2	Cpx3	Cpx1	Cpx4-5	Cpx6	Cpx2	Cpx1	Cpx3	Cpx4	av. Cpx	Cpx5	Cpx1	Cpx6	Cpx2
No. points		6	4	7	8	7	6	6	6	7	4	5	8	6	5
SiO2		46.56	44.61	45.21	45.22	44.69	43.86	45.31	45.06	44.50	45.72	45.52	45.63	46.69	44.15
TiO2		3.31	3.64	3.63	3.58	3.67	4.05	3.44	3.47	3.66	3.65	3.98	4.00	3.53	4.12
Al2O3		7.70	8.72	8.55	8.10	8.87	9.22	7.97	8.26	8.51	7.28	8.63	7.39	6.60	8.97
FeOtot		7.45	7.70	7.74	7.70	7.72	8.11	7.81	7.84	7.88	8.64	7.62	7.70	7.48	7.77
MnO		0.13	0.11	0.13	0.12	0.12	0.11	0.10	0.11	0.12	0.17	0.10	0.16	0.14	0.14
MgO		12.22	11.79	11.75	11.94	11.70	11.51	12.21	12.16	11.84	12.24	11.87	11.96	12.44	11.54
CaO		21.66	21.41	21.38	21.51	21.52	21.76	21.73	21.67	21.76	21.66	22.10	21.95	21.77	21.57
Na2O		0.73	0.70	0.76	0.70	0.73	0.62	0.58	0.59	0.59	0.53	0.60	0.58	0.53	0.57
K2O		0.00	0.01	0.01	0.02	0.00	0.00	0.00	0.01	0.01	0.02	0.01	0.00	0.00	0.00
Cr2O3		0.03	0.06	0.03	0.04	0.05	0.03	0.03	0.14	0.06	0.01	0.01	0.01	0.02	0.01
Total		99.80	98.80	99.21	98.92	99.11	99.29	99.18	99.37	98.94	99.92	100.47	99.4	99.24	99.85
T [°C]:	**PT96**	**1138**	**1138**	**1142**	**1137**	**1141**	**1148**	**1143**	**1145**	**1145**	**1146**	**1108**	**1105**	**1100**	**1108**
P [kbar]:	**PT96**	**8.6**	**8.5**	**9.1**	**8.5**	**8.8**	**8.0**	**7.4**	**7.6**	**7.6**	**7.0**	**6.9**	**6.6**	**6.0**	**6.7**
T [°C]:	**PT03**	**1107**	**1109**	**1112**	**1107**	**1110**	**1130**	**1124**	**1126**	**1126**	**1130**	**1062**	**1058**	**1054**	**1063**
P [kbar]:	**PT03**	**7.4**	**7.4**	**7.8**	**7.3**	**7.6**	**6.9**	**6.4**	**6.5**	**6.6**	**6.0**	**6.1**	**5.9**	**5.5**	**6.0**

PT96 Temperatures and pressures are calculated using the formulation of Putirka et al. (1996)
PT03 Temperatures and pressures are calculated using the formulation of Putirka et al. (1996)

Appendix A 3.1 (continued):

Sample		KLP6	KLP6A	KLP6A	KLP6A	KLP6A	KLP6A	KLP6A	KLP6A	KLP6A	KLP38	KLP38	KLP38	KLP38	KLP115
Cpx#		Cpx3	Cpx2	Cpx8	Cpx3	Cpx5	Cpx6	Cpx7	Cpx4	Cpx1	Cpx1	Cpx 4	Cpx5	Cpx6	Cpx1
No. points		3	8	4	8	3	3	3	6	6	11	8	3	3	5
SiO2		47.56	44.81	43.86	44.53	44.12	45.82	44.95	44.79	45.06	43.31	44.39	43.06	40.74	44.39
TiO2		3.45	4.00	4.69	3.96	4.56	3.92	4.19	3.86	4.12	4.21	3.43	4.03	5.31	3.65
Al2O3		6.67	7.95	8.48	8.47	8.47	7.08	7.99	8.41	7.77	9.47	8.75	9.00	10.49	8.44
FeOtot		7.69	7.64	7.65	7.51	7.67	7.42	7.71	7.65	7.62	8.33	7.60	9.84	9.37	7.19
MnO		0.18	0.13	0.14	0.14	0.13	0.16	0.12	0.13	0.12	0.17	0.15	0.27	0.17	0.14
MgO		12.66	12.01	11.57	11.87	11.57	12.24	11.82	12.03	12.04	11.14	11.89	10.11	10.08	11.92
CaO		21.90	22.13	21.96	22.04	22.00	22.16	22.01	22.06	22.06	22.30	22.73	22.39	22.50	23.03
Na2O		0.56	0.61	0.60	0.62	0.65	0.58	0.62	0.61	0.60	0.62	0.56	0.73	0.63	0.66
K2O		0.01	0.00	0.00	0.00	0.00	0.00	0.00	0.01	0.01	0.02	0.01	0.01	0.02	0.01
Cr2O3		0.02	0.02	0.00	0.01	0.01	0.02	0.02	0.01	0.01	0.02	0.01	0.01	0.03	0.01
Total		100.72	99.32	98.99	99.18	99.2	99.41	99.45	99.57	99.42	99.584	99.512	99.462	99.346	99.441
T [°C]:	**PT96**	**1102**	**1113**	**1113**	**1115**	**1117**	**1109**	**1114**	**1114**	**1112**	**1118**	**1110**	**1125**	**1118**	**1023**
P [kbar]:	**PT96**	**6.3**	**6.5**	**6.5**	**6.7**	**7.0**	**6.1**	**6.6**	**6.5**	**6.4**	**7.2**	**6.3**	**8.3**	**7.1**	**7.3**
T [°C]:	**PT03**	**1056**	**1061**	**1063**	**1064**	**1065**	**1058**	**1063**	**1063**	**1061**	**1041**	**1035**	**1044**	**1042**	**857**
P [kbar]:	**PT03**	**5.7**	**5.6**	**5.6**	**5.7**	**6.0**	**5.3**	**5.7**	**5.6**	**5.5**	**5.3**	**4.7**	**6.0**	**5.3**	**12.2**

PT96 Temperatures and pressures are calculated using the formulation of Putirka et al. (1996)
PT03 Temperatures and pressures are calculated using the formulation of Putirka et al. (1996)

Appendix A 3.1 (continued):

Sample		KLP115	KLP115	KLP115	KLP115	KLP115	KLP115	KLP61	KLP61	KLP61	KLP61	KLP61	KLP35	KLP35	KLP35
Cpx#		Cpx2	Cpx3	Cpx4	Cpx5	Cpx6	Cpx7	Cpx1	Cpx2	Cpx3	Cpx4	Cpx5	Cpx1	Cpx2	Cpx3
No. points		5	8	4	7	6	4	10	11	8	8	7	6	6	6
SiO2		45.35	41.98	45.94	42.93	41.79	43.50	43.63	46.59	46.41	46.60	46.18	47.19	46.07	47.62
TiO2		3.23	4.30	2.80	3.90	4.32	3.60	4.09	2.47	2.53	2.53	2.51	2.38	2.75	2.16
Al2O3		7.61	10.01	6.74	9.48	9.99	8.74	9.32	7.78	7.76	7.74	7.79	7.37	7.95	6.67
FeOtot		7.02	9.17	6.26	9.30	9.04	8.74	8.14	7.07	7.23	7.04	8.45	6.90	7.16	7.04
MnO		0.13	0.24	0.09	0.24	0.24	0.26	0.11	0.10	0.11	0.11	0.18	0.13	0.10	0.13
MgO		12.65	9.90	13.37	10.03	9.89	10.63	11.55	13.15	13.12	13.12	11.89	13.22	12.76	13.44
CaO		23.32	22.54	23.41	22.72	22.65	22.80	22.40	22.01	22.17	22.15	22.36	22.13	22.21	22.18
Na2O		0.57	0.91	0.48	0.92	0.88	0.85	0.44	0.58	0.57	0.54	0.63	0.57	0.56	0.59
K2O		0.01	0.02	0.00	0.01	0.01	0.00	0.00	0.01	0.00	0.00	0.00	0.01	0.01	0.00
Cr2O3		0.02	0.01	0.03	0.01	0.01	0.01	0.01	0.10	0.07	0.05	0.01	0.07	0.03	0.06
Total		99.89	99.086	99.111	99.548	98.824	99.149	99.684	99.858	99.989	99.874	99.983	99.975	99.598	99.901
T [°C]:	**PT96**	**1015**	**1040**	**1007**	**1040**	**1039**	**1110**	**1125**	**1118**	**1023**	**1015**	**1040**	**1007**	**1040**	**1039**
P [kbar]:	**PT96**	**6.2**	**9.5**	**5.1**	**9.5**	**9.3**	**6.3**	**8.3**	**7.1**	**7.3**	**6.2**	**9.5**	**5.1**	**9.5**	**9.3**
T [°C]:	**PT03**	**851**	**867**	**846**	**866**	**866**	**1035**	**1044**	**1042**	**857**	**851**	**867**	**846**	**866**	**866**
P [kbar]:	**PT03**	**11.6**	**13.6**	**10.9**	**13.6**	**13.4**	**4.7**	**6.0**	**5.3**	**12.2**	**11.6**	**13.6**	**10.9**	**13.6**	**13.4**

PT96 Temperatures and pressures are calculated using the formulation of Putirka et al. (1996)
PT03 Temperatures and pressures are calculated using the formulation of Putirka et al. (1996)

Appendix A 3.1 (continued):

Sample		KLP35	KLP35	KLP35	KLP35	KLP103	KLP103	KLP103	KLP103	KLP103	KLP89	KLP89	KLP89	KLP89	KLP89
Cpx#		Cpx4	Cpx4a	Cpx6	Cpx6	Cpx1	Cpx2	Cpx3	Cpx4	Cpx5	Cpx1	Cpx2	Cpx3	Cpx4	Cpx5
No. points		6	6	9	10	14	9	8	5	7	10	7	6	7	6
SiO2		45.01	46.67	46.68	46.57	49.02	47.85	48.07	49.79	50.02	47.20	47.64	47.25	46.77	43.59
TiO2		3.10	2.47	2.43	2.41	1.46	1.96	1.82	1.26	1.24	2.07	2.05	2.22	2.26	3.58
Al2O3		8.18	7.40	7.33	7.49	4.96	5.84	5.60	4.26	4.14	6.32	6.01	5.74	6.93	9.10
FeOtot		7.86	6.85	6.88	7.14	6.03	6.59	6.29	5.55	5.73	7.09	7.08	7.63	7.17	8.32
MnO		0.12	0.12	0.12	0.13	0.08	0.09	0.09	0.09	0.09	0.12	0.14	0.12	0.12	0.13
MgO		12.36	13.20	13.16	13.02	14.71	14.15	14.14	15.24	15.28	13.68	13.77	13.66	13.34	11.87
CaO		22.31	22.26	22.11	22.14	22.45	22.17	21.99	22.41	22.42	22.18	22.35	22.06	22.21	22.04
Na2O		0.50	0.58	0.57	0.58	0.37	0.34	0.34	0.32	0.34	0.39	0.40	0.33	0.41	0.42
K2O		0.00	0.01	0.01	0.00	0.00	0.00	0.01	0.01	0.01	0.00	0.01	0.00	0.00	0.00
Cr2O3		0.05	0.07	0.07	0.06	0.73	0.55	0.74	0.87	0.71	0.20	0.23	0.07	0.17	0.07
Total		99.484	99.64	99.341	99.54	99.812	99.546	99.082	99.794	99.973	99.264	99.669	99.101	99.391	99.119
T [°C]:	**PT96**	**1205**	**1212**	**1211**	**1212**	**1212**	**1210**	**1211**	**1204**	**1206**	**1161**	**1161**	**1151**	**1163**	**1169**
P [kbar]:	**PT96**	**10.5**	**11.6**	**11.5**	**11.5**	**8.7**	**8.2**	**8.3**	**7.6**	**7.9**	**6.5**	**6.6**	**5.2**	**6.8**	**7.2**
T [°C]:	**PT03**	**1213**	**1217**	**1217**	**1218**	**1233**	**1233**	**1234**	**1226**	**1227**	**1155**	**1154**	**1147**	**1158**	**1165**
P [kbar]:	**PT03**	**11.0**	**11.7**	**11.6**	**11.7**	**8.4**	**8.1**	**8.1**	**7.6**	**7.8**	**6.7**	**6.8**	**5.8**	**6.9**	**7.3**

PT96 Temperatures and pressures are calculated using the formulation of Putirka et al. (1996)
PT03 Temperatures and pressures are calculated using the formulation of Putirka et al. (1996)

Appendix A 3.1 (continued):

Sample		KLP80	KLP80	KLP80	KLP80	KLP80	KLP19	KLP19	KLP19	KLP19	KLP19	KLP63	KLP63	KLP63	KLP63
Cpx#		Cpx1	Cpx2	Cpx3	Cpx5	Cpx6	Cpx1	Cpx2	Cpx3	Cpx4	Cpx5	Cpx1	Cpx2	Cpx4	Cpx5
No. points		7	8	9	8	5	9	7	8	8	15	10	8	7	9
SiO2		48.10	47.75	48.14	49.60	48.05	44.50	42.87	45.40	43.76	46.28	43.20	46.85	46.22	45.27
TiO2		1.95	2.08	1.88	1.77	1.74	3.58	4.69	3.71	4.27	3.18	4.07	2.28	2.49	3.14
Al2O3		6.09	5.92	5.82	4.58	4.67	8.36	9.47	7.81	8.78	6.93	9.45	7.51	7.95	7.74
FeOtot		6.59	6.65	6.38	6.32	6.36	7.66	8.29	7.85	8.09	7.63	8.43	7.28	7.34	7.94
MnO		0.12	0.11	0.10	0.11	0.11	0.09	0.11	0.09	0.09	0.10	0.09	0.06	0.07	0.09
MgO		14.24	14.01	14.30	14.97	14.20	11.96	11.11	12.06	11.35	12.47	11.23	13.13	12.95	12.42
CaO		22.03	22.21	22.16	22.18	22.15	22.75	22.40	22.46	22.38	22.37	22.21	22.34	22.18	22.24
Na2O		0.40	0.36	0.39	0.34	0.37	0.43	0.50	0.45	0.49	0.43	0.50	0.52	0.52	0.50
K2O		0.00	0.00	0.01	0.00	0.01	0.00	0.00	0.00	0.00	0.02	0.00	0.00	0.00	0.00
Cr2O3		0.39	0.43	0.40	0.31	0.42	0.01	0.00	0.01	0.01	0.00	0.00	0.05	0.04	0.02
Total		99.901	99.527	99.589	99.802	99.406	99.33	99.438	99.833	99.219	99.404	99.175	100.02	99.757	99.361
T [°C]:	**PT96**	**1171**	**1166**	**1170**	**1160**	**1166**	**1159**	**1169**	**1161**	**1168**	**1158**	**1174**	**1172**	**1174**	**1170**
P [kbar]:	**PT96**	**6.9**	**6.2**	**6.7**	**5.6**	**6.4**	**7.1**	**8.3**	**7.4**	**8.2**	**7.0**	**8.8**	**8.8**	**8.9**	**8.6**
T [°C]:	**PT03**	**1177**	**1172**	**1175**	**1166**	**1169**	**1154**	**1164**	**1156**	**1162**	**1152**	**1173**	**1169**	**1171**	**1168**
P [kbar]:	**PT03**	**6.5**	**6.0**	**6.3**	**5.5**	**6.0**	**7.1**	**8.1**	**7.4**	**8.0**	**7.1**	**9.0**	**9.0**	**9.0**	**8.8**

PT96 Temperatures and pressures are calculated using the formulation of Putirka et al. (1996)
PT03 Temperatures and pressures are calculated using the formulation of Putirka et al. (1996)

Appendix A 3.1 (continued):

Sample		KLP76	KLP76	KLP76	KLP76	KLP76	KLP77	KLP77	KLP41	KLP41	KLP41	KLP41	KLP41	KLP41	KLP112	KLP112	KLP112	KLP112
Cpx#		Cpx1	Cpx2_3	Cpx4	Cpx5	Cpx6	Cpx2	Cpx4	Cpx1	Cpx2	Cpx3	Cpx4	Cpx5	Cpx6	Cpx1	Cpx2	Cpx3	Cpx4
No. points		6	9	8	12	10	9	7	9	12	7	9	7	13	4	6	3	12
SiO2		45.33	42.40	46.62	45.21	41.94	48.34	44.55	45.50	44.74	43.96	42.60	46.94	43.64	44.60	45.35	45.60	44.75
TiO2		3.10	4.18	2.40	3.09	4.52	2.21	3.65	3.12	3.70	3.97	4.71	2.82	4.32	3.57	3.32	3.21	3.46
Al2O3		7.65	9.90	6.75	7.93	10.47	4.87	8.46	7.50	8.25	8.33	9.57	5.56	8.95	9.21	7.98	7.90	8.91
FeOtot		7.55	7.95	6.88	7.24	8.24	7.42	8.02	7.16	7.55	8.04	8.13	7.60	7.83	7.60	7.29	7.42	7.32
MnO		0.09	0.10	0.10	0.11	0.10	0.11	0.09	0.08	0.09	0.10	0.10	0.10	0.09	0.08	0.08	0.09	0.08
MgO		12.30	11.11	13.06	12.29	10.91	14.11	12.10	12.59	12.01	11.65	10.93	13.05	11.44	11.54	12.06	12.08	11.71
CaO		22.40	22.49	22.75	22.49	22.41	21.95	22.35	22.30	22.26	22.19	22.19	22.12	22.13	21.88	22.19	21.99	21.97
Na2O		0.51	0.52	0.46	0.52	0.54	0.28	0.37	0.39	0.41	0.40	0.43	0.32	0.42	0.67	0.58	0.58	0.65
K2O		0.00	0.00	0.00	0.00	0.00	0.01	0.01	0.00	0.00	0.00	0.00	0.00	0.00	0.01	0.01	0.01	0.01
Cr2O3		0.01	0.01	0.10	0.02	0.00	0.08	0.10	0.16	0.09	0.06	0.06	0.05	0.07	0.04	0.05	0.02	0.05
Total		98.936	98.671	99.119	98.911	99.134	99.389	99.705	98.823	99.1	98.684	98.727	98.577	98.891	99.193	98.921	98.898	98.893
T [°C]:	**PT96**	**1151**	**1156**	**1144**	**1153**	**1159**	**1200**	**1220**	**1161**	**1164**	**1163**	**1170**	**1149**	**1168**	**1123**	**1114**	**1114**	**1121**
P [kbar]:	**PT96**	**7.6**	**8.0**	**6.7**	**7.7**	**8.2**	**7.1**	**9.5**	**6.6**	**6.9**	**6.7**	**7.5**	**5.1**	**7.2**	**7.7**	**6.7**	**6.6**	**7.5**
T [°C]:	**PT03**	**1133**	**1140**	**1126**	**1135**	**1143**	**1210**	**1230**	**1150**	**1153**	**1152**	**1159**	**1138**	**1157**	**1090**	**1081**	**1081**	**1087**
P [kbar]:	**PT03**	**7.1**	**7.4**	**6.5**	**7.2**	**7.7**	**8.6**	**10.4**	**6.8**	**7.0**	**6.9**	**7.5**	**5.6**	**7.2**	**6.8**	**6.0**	**6.0**	**6.6**

PT96 Temperatures and pressures are calculated using the formulation of Putirka et al. (1996)
PT03 Temperatures and pressures are calculated using the formulation of Putirka et al. (1996)

Appendix A 3.2: Electron microprobe analyses of basaltic glass or fused groundmass (matrix)

Sample	#	SiO2	TiO2	Al2O3	FeO	MnO	MgO	CaO	Na2O	K2O	P2O5	F	Cl	Total
Taburiente														
KLP 66	31	46.46	3.67	16.47	10.87	0.25	4.19	9.97	4.33	2.21	0.95	0.07	0.10	99.53
KLP 76	22	44.94	3.64	16.52	11.10	0.20	4.96	10.04	4.81	2.10	0.58	0.00	0.03	98.92
KLP 63	26	43.21	4.40	15.33	13.36	0.20	6.19	11.02	4.25	0.90	0.54	0.02	0.02	99.44
KLP 77	23	44.70	3.99	13.62	12.52	0.19	8.32	11.66	2.95	1.31	0.46	0.00	0.02	99.75
KLP 61	23	42.87	4.41	14.98	13.44	0.21	6.41	11.51	3.95	0.73	0.58	0.01	0.15	99.24
Cumbre Nueva														
KLP 103	26	46.24	3.11	13.49	11.59	0.16	8.09	12.59	2.85	0.81	0.44	0.00	0.02	99.39
KLP 89	27	45.30	3.74	15.97	12.49	0.18	5.73	10.64	3.51	1.37	0.56	0.00	0.02	99.51
KLP 80	24	46.25	3.56	15.13	12.06	0.16	5.92	11.32	3.23	1.26	0.54	0.00	0.01	99.45
KLP 41	30	45.31	4.15	16.62	11.68	0.19	5.42	10.60	3.31	1.72	0.62	0.01	0.02	99.63
KLP 19	29	44.26	4.35	15.84	12.45	0.18	5.41	10.84	3.54	1.54	0.60	0.00	0.02	99.04
KLP 38	38	51.23	2.72	18.78	7.83	0.22	2.76	6.66	6.85	3.24	0.55	0.10	0.12	101.05
Bejenado														
KLP 6A	22	49.48	3.32	18.40	8.94	0.20	2.86	7.38	5.69	2.82	0.76	0.10	0.08	100.03
KLP 106	10	46.98	4.09	16.83	11.01	0.19	3.99	9.72	4.12	2.26	0.77	0.08	0.05	100.09
KLP 113	41	46.67	3.72	17.24	10.84	0.19	3.70	8.95	5.19	2.56	0.81	0.08	0.07	100.03
KLP 6	1	48.95	3.30	18.13	9.50	0.21	2.96	7.64	6.52	3.07	0.86	0.07	0.06	101.26
KLP 6	28	48.06	3.40	18.02	9.55	0.19	3.01	7.70	6.53	3.16	0.88	0.10	0.08	100.67
KLP 115	19	53.60	0.74	22.08	4.05	0.16	0.68	2.19	10.46	5.60	0.30	0.10	0.20	100.21
KLP 5	22	54.09	1.40	20.58	4.67	0.13	0.61	1.07	10.47	6.35	0.32	0.19	0.17	100.06
KLP 112	24	46.31	3.79	16.93	10.05	0.13	3.21	8.47	5.44	3.00	1.24	0.30	0.05	98.92

Appendix A 3.3: Fluid inclusion data

Sample	Frag-ment	Fl #	Host mineral	Standard CO2	Standard H2O – KCl	Tm initial	Tm initial corrected	Tm final	Tm final corrected	Th L	Th V	Density	P (MPa) Calculated
Taburiente													
KLA 1804	A	1	Ol	-57.2	-10.7			-57.3	-56.7	19.5		0.774	470.4
KLA 1804	A	2	Ol	-57.2	-10.7			-57.5	-56.9	19.5		0.774	470.4
KLA 1804	A	3	Ol	-57.2	-10.7			-57.4	-56.8	20.4		0.765	458.7
KLA 1804	A	4	Ol	-57.2	-10.7			-57.4	-56.8	17.4		0.796	499.3
KLA 1804	A	5	Ol	-57.2	-10.7			-57.4	-56.8	17.9		0.791	492.2
KLA 1804	B	1	Ol	-57.2	-10.7			-56.9	-56.3	19.5		0.774	470.4
KLA 1804	B	2	Ol	-57.2	-10.7			-57.5	-56.9	18.6		0.783	482.5
KLA 1804	B	3	Ol	-57.2	-10.7			-57.8	-57.2	21.7		0.752	442.7
KLA 1804	B	4	Ol	-57.2	-10.7			-57.4	-56.8	18.0		0.790	490.8
KLA 1804	B	5	Ol	-57.4	-10.7			-57.4	-56.6	18.9		0.780	478.4
KLA 1804	B	6	Ol	-57.4	-10.7			-57.5	-56.7	19.2		0.777	474.4
KLA 1804	B	7	Ol	-57.4	-10.7			-57.4	-56.6	19.5		0.774	470.4
KLA 1804	B	8	Ol	-57.4	-10.7			-57.4	-56.6	19.8		0.771	466.5
KLA 1804	B	9	Ol	-57.4	-10.7			-57.4	-56.6	19.8		0.771	466.5
KLA 1804	C	1	Ol	-57.4	-10.7			-57.4	-56.6	18.7		0.782	481.1
KLA 1804	C	2	Ol	-57.4	-10.7			-57.4	-56.6	16.7		0.803	509.4
KLA 1804	C	3	Ol	-57.4	-10.7			-57.4	-56.6	16.1		0.809	518.1
KLA 1804	C	4	Ol	-57.4	-10.7			-57.4	-56.6	17.3		0.797	500.8
KLA 1804	C	5	Ol	-57.4	-10.7			-57.3	-56.5	20.0		0.769	463.9
KLA 1804	C	6	Ol	-57.4	-10.7			-57.4	-56.6	19.0		0.779	477.1
KLA 1804	C	7	Ol	-57.4	-10.7			-57.8	-57.0	17.9		0.791	492.2
KLA 1804	C	8	Ol	-57.4	-10.7			-57.8	-57.0	18.0		0.790	490.8
KLA 1804	D	1	Ol	-57.3	-10.7			-57.4	-56.7	18.5		0.784	483.9
KLA 1804	D	2	Ol	-57.3	-10.7			-57.4	-56.7	18.5		0.784	483.9
KLA 1804	D	3	Ol	-57.3	-10.7			-57.4	-56.7	18.5		0.784	483.9
KLA 1804	D	4	Ol	-57.3	-10.7			-57.3	-56.6	17.5		0.795	497.9
KLA 1804	D	5	Ol	-57.3	-10.7			-57.3	-56.6	18.6		0.783	482.5
KLA 1804	D	6	Ol	-57.3	-10.7			-57.3	-56.6	18.8		0.781	479.8
KLA 1804	E	1	Ol	-57.3	-10.7			-57.5	-56.8	19.1		0.778	475.7
KLA 1804	E	2	Ol	-57.3	-10.7			-57.5	-56.8	19.0		0.779	477.1
KLA 1804	E	3	Ol	-57.3	-10.7			-57.5	-56.8	18.5		0.784	483.9

Appendix A 3.3: Fluid inclusion data

Sample	Frag-ment	Fl #	Host mineral	Standard CO2	Standard H2O – KCl	Tm initial	Tm initial corrected	Tm final	Tm final corrected	Th L	Th V	Density	P (MPa) Calculated
KLA 1804	E	4	Ol	-57.3	-10.7			-57.5	-56.8	17.7		0.793	495.1
KLA 1804	E	5	Ol	-57.3	-10.7			-57.5	-56.8	17.8		0.792	493.7
KLA 1804	E	6	Ol	-57.3	-10.7			-57.5	-56.8	18.2		0.788	488.0
KLA 1804	F	1	Ol	-57.3	-10.7			-57.5	-56.8	18.7		0.782	481.1
KLA 1804	F	2	Ol	-57.3	-10.7			-57.5	-56.8	18.8		0.781	479.8
KLA 1804	F	3	Ol	-57.3	-10.7			-57.5	-56.8	18.6		0.783	482.5
KLA 1804	F	4	Ol	-57.3	-10.7			-57.5	-56.8	18.9		0.780	478.4
KLA 1804	F	5	Ol	-57.3	-10.7			-57.5	-56.8	17.7		0.793	495.1
KLA 1804	F	6	Ol	-57.3	-10.7			-57.5	-56.8	18.7		0.782	481.1
KLA 1803	A	1	Ol	-57.3	-10.5			-57.4	-56.7	20.9		0.760	452.5
KLA 1803	A	2	Ol	-57.3	-10.5			-57.7	-57.0	21.1		0.758	450.0
KLA 1803	A	3	Ol	-57.3	-10.5			-57.7	-57.0	21.5		0.754	445.1
KLA 1803	A	4	Ol	-57.3	-10.5			-57.4	-56.7	21.2		0.757	448.8
KLA 1803	A	5	Ol	-57.3	-10.5			-57.4	-56.7	19.6		0.773	469.1
KLA 1803	A	6	Ol	-57.3	-10.5			-57.4	-56.7	20.4		0.765	458.7
KLA 1803	A	7	Ol	-57.3	-10.5			-57.4	-56.7	29.0		0.630	317.3
KLA 1803	A	8	Ol	-57.3	-10.5			-57.4	-56.7	29.2		0.622	310.7
KLA 1803	A	9	Ol	-57.3	-10.5			-57.4	-56.7	29.1		0.626	314.0
KLA 1803	C	1	Ol	-57.3	-10.5			-57.4	-56.7	20.5		0.764	457.5
KLA 1803	C	2	Ol	-57.3	-10.5			-57.4	-56.7	20.3		0.766	460.0
KLA 1803	C	3	Ol	-57.3	-10.5			-57.4	-56.7	21.5		0.754	445.1
KLA 1803	C	4	Ol	-57.3	-10.5			-57.3	-56.6	20.4		0.765	458.7
KLA 1803	C	5	Ol	-57.3	-10.5			-57.3	-56.6	20.3		0.766	460.0
KLA 1803	C	6	Ol	-57.2	-10.5			-57.3	-56.7	29.5		0.610	300.3
KLA 1803	C	7	Ol	-57.2	-10.5			-57.3	-56.7	26.1		0.701	385.3
KLA 1803	C	8	Ol	-57.2	-10.5			-57.3	-56.7	26.2		0.699	383.6
KLA 1803	C	9	Ol	-57.2	-10.5			-57.3	-56.7	20.8		0.761	453.7
KLA 1803	C	10	Ol	-57.2	-10.5			-57.2	-56.6	21.4		0.755	446.3
KLA 1803	D	1	Ol	-57.2	-10.5			-57.2	-56.6	25.7		0.707	391.7
KLA 1803	D	2	Ol	-57.6	-10.5			-57.2	-56.2	24.7		0.720	406.0
KLA 1803	D	3	Ol	-57.3	-10.5			-57.2	-56.5	21.1		0.758	450.0
KLA 1803	D	4	Ol	-57.3	-10.5			-57.2	-56.5	20.0		0.769	463.9

Appendix A 3.3: Fluid inclusion data

Sample	Frag-ment	Fl #	Host mineral	Standard CO2	Standard H2O – KCl	Tm initial	Tm initial corrected	Tm final	Tm final corrected	Th L	Th V	Density	P (MPa) Calculated
KLA 1803	D	5	Ol	-57.3	-10.5			-57.2	-56.5	20.2		0.767	461.3
KLA 1803	D	6	Ol	-57.3	-10.5			-57.2	-56.5	20.6		0.763	456.2
KLA 1803	D	7	Ol	-57.3	-10.5			-57.2	-56.5	29.8		0.596	289.2
KLA 1803	D	8	Ol	-57.3	-10.5			-57.2	-56.5	29.5		0.610	300.3
KLA 1803	E	1	Ol	-57.3	-10.5			-57.2	-56.5	21.4		0.755	446.3
KLA 1803	E	2	Ol	-57.3	-10.5			-57.2	-56.5	21.9		0.750	440.3
KLA 1803	E	3	Ol	-57.3	-10.5			-57.2	-56.5	22.1		0.748	437.9
KLA 1803	E	4	Ol	-57.3	-10.5			-57	-56.3	21.1		0.758	450.0
KLA 1803	E	5	Ol	-57.3	-10.5			-57	-56.3	21.5		0.754	445.1
KLA 1803	E	6	Ol	-57.3	-10.5			-57	-56.3	22.8		0.741	429.5
KLA 1803	H	1	Ol	-57.3	-10.5			-57.2	-56.5	22.8		0.741	429.5
KLA 1803	H	2	Ol	-57.3	-10.5			-57.2	-56.5	23.2		0.737	424.7
KLA 1803	H	3	Ol	-57.3	-10.5			-57.2	-56.5	23.9		0.729	416.2
KLA 1803	H	4	Ol	-57.3	-10.5			-57.1	-56.4	24.7		0.720	406.0
KLA 1803	H	5	Ol	-57.3	-10.5			-57.1	-56.4	20.8		0.761	453.7
KLA 1803	H	6	Ol	-57.3	-10.5			-57.1	-56.4	23.3		0.736	423.5
KLA 1803	H	7	Ol	-57.3	-10.5			-57.1	-56.4	22.6		0.743	431.9
Cumbre Nueva													
KLP 22	O	1	Cpx	-56.9	-10.7			-57.0	-56.7	29.1		0.626	314.0
KLP 22	O	2	Cpx	-56.9	-10.7			-57.0	-56.7	28.9		0.634	320.5
KLP 22	O	3	Cpx	-56.9	-10.7			-57.0	-56.7	29.2		0.622	310.7
KLP 22	O	4	Cpx	-56.9	-10.7			-57.0	-56.7	29.9		0.591	285.3
KLP 22	T	1	Cpx	-56.9	-10.7			-57.2	-56.9	30.5		0.558	260.7
KLP 22	N	1	Cpx	-56.9	-10.7			-57.2	-56.9	30.2		0.575	273.3
KLP 22	Z	1	Cpx	-57.0	-10.7			-57.0	-56.6	30.8		0.539	247.5
KLP 22	Z	2	Cpx	-57.0	-10.7			-57.0	-56.6	30.5		0.558	260.7
KLP 22	Z	3	Cpx	-57.0	-10.7			-57.0	-56.6	30.2		0.575	273.3
KLP 22	V	1	Cpx	-57.0	-10.7			-57.1	-56.7	30.3		0.570	269.2
KLP 26	G	1	Cpx	-57.0	-10.7			-56.9	-56.5	29.0		0.630	317.3
KLP 26	G	2	Cpx	-57.0	-10.7			-57.0	-56.6	27.7		0.669	353.5
KLP 26	G	3	Cpx	-57.0	-10.7			-57.0	-56.6	27.9		0.664	348.6

Appendix A 3.3: Fluid inclusion data

Sample	Frag-ment	Fl #	Host mineral	Standard CO2	Standard H2O – KCl	Tm initial	Tm initial corrected	Tm final	Tm final corrected	Th L	Th V	Density	P (MPa) Calculated
KLP 26	G	4	Cpx	-57.0	-10.7			-57.0	-56.6	27.9		0.664	348.6
KLP 26	C	1	Cpx	-57.0	-10.7			-56.9	-56.5	26.7		0.691	374.6
KLP 26	C	2	Cpx	-57.0	-10.7			-56.9	-56.5	26.0		0.703	386.9
KLP 26	C	3	Cpx	-57.0	-10.7			-56.9	-56.5	26.1		0.701	385.3
KLP 26	C	4	Cpx	-57.0	-10.7			-56.9	-56.5	25.4		0.711	396.2
KLP 26	C	5	Cpx	-57.0	-10.7			-56.9	-56.5	25.9		0.704	388.5
KLP 26	C	6	Cpx	-57.0	-10.7			-56.9	-56.5	25.5		0.710	394.7
KLP 26	C	7	Cpx	-57.0	-10.7			-57.0	-56.6	27.0		0.685	368.8
KLP 26	C	8	Cpx	-57.0	-10.7			-57.0	-56.6	27.9		0.664	348.6
KLP 37	E	1	Cpx	-57.1	-10.7			-57.1	-56.6	28.4		0.650	335.4
KLP 37	E	2	Cpx	-57.1	-10.7			-57.1	-56.6	29.0		0.630	317.3
KLP 37	E	3	Cpx	-57.1	-10.7			-57.1	-56.6	29.7		0.601	292.9
KLP 37	E	4	Cpx	-57.1	-10.7			-57.1	-56.6	29.7		0.601	292.9
KLP 37	E	5	Cpx	-57.1	-10.7			-57.1	-56.6	28.4		0.650	335.4
KLP 37	E	6	Cpx	-57.1	-10.7			-57.1	-56.6	28.8		0.637	323.6
KLP 37	E	7	Ol	-57.1	-10.7			-58.0	-57.5	21.8		0.751	441.5
KLP 37	B	1	Ol	-57.1	-10.7			-57.5	-57	26.0		0.703	386.9
KLP 37	B	2	Ol	-57.1	-10.7			-57.5	-57	27.4		0.676	360.3
KLP 37	B	3	Ol	-57.1	-10.7			-57.5	-57	24.6		0.721	407.3
KLP 37	B	4	Ol	-57.1	-10.7			-57.6	-57.1	26.1		0.701	385.3
KLP 37	B	5	Ol	-57.1	-10.7			-57.5	-57	23.6		0.733	419.9
KLP 37	B	6	Ol	-57.1	-10.7			-57.6	-57.1	25.5		0.710	394.7
KLP 37	B	7	Ol	-57.1	-10.7			-57.6	-57.1	26.6		0.693	376.5
KLP 37	B	8	Ol	-57.1	-10.7			-58.0	-57.5	24.2		0.726	412.5
KLP 37	B	9	Ol	-57.1	-10.7			-57.5	-57	23.9		0.729	416.2
KLP 37	B	10	Ol	-57.1	-10.7			-57.4	-56.9	25.5		0.710	394.7
KLP 37	C	1	Cpx	-57.1	-10.7			-57.3	-56.8	27.1		0.683	366.7
KLP 37	C	2	Cpx	-57.1	-10.7			-57.2	-56.7	27.6		0.672	355.8
KLP 37	C	3	Cpx	-57.1	-10.7			-57.2	-56.7	25.7		0.707	391.7
KLP 37	C	4	Cpx	-57.1	-10.7			-57.2	-56.7	27.4		0.676	360.3
KLP 37	C	5	Cpx	-57.1	-10.7			-57.2	-56.7	27.1		0.683	366.7
KLP 37	C	6	Cpx	-57.1	-10.7			-57.2	-56.7	26.5		0.694	378.3

Appendix A 3.3: Fluid inclusion data

Sample	Frag-ment	Fl #	Host mineral	Standard CO2	Standard H2O – KCl	Tm initial	Tm initial corrected	Tm final	Tm final corrected	Th L	Th V	Density	P (MPa) Calculated
KLP 37	C	7	Cpx	-57.1	-10.7			-57.2	-56.7	28.6		0.644	329.6
KLP 37	C	8	Cpx	-57.1	-10.7			-57.2	-56.7	28.6		0.644	329.6
KLP 37	C	9	Cpx	-57.1	-10.7			-57.2	-56.7	28.0		0.662	346.1
KLP 37	C	10	Cpx	-57.1	-10.7			-57.2	-56.7	28.1		0.659	343.5
KLP 37	C	11	Cpx	-57.1	-10.7			-57.2	-56.7	28.2		0.656	340.8
KLP 37	C	12	Cpx	-57.1	-10.7			-57.2	-56.7	28.9		0.634	320.5
KLP 37	G	1	Ol	-57.1	-10.7			-57.5	-57	19.4		0.775	471.7
KLP 37	G	2	Ol	-57.1	-10.7			-58.0	-57.5	17.4		0.796	499.3
KLP 37	G	3	Ol	-57.1	-10.7			-57.5	-57	22.2		0.747	436.7
KLP 37	G	4	Cpx	-57.1	-10.7			-57.1	-56.6	28.1		0.659	343.5
KLP 84	B	1	Ol	-56.9	-10.5			-56.9	-56.6	28.2		0.656	340.8
KLP 84	B	2	Ol	-56.9	-10.5			-56.9	-56.6	28.6		0.644	329.6
KLP 84	B	3	Ol	-56.9	-10.5			-56.9	-56.6	28.6		0.644	329.6
KLP 84	B	4	Ol	-56.9	-10.5			-56.9	-56.6	30.3		0.570	269.2
KLP 84	B	5	Ol	-56.9	-10.5			-56.9	-56.6	27.5		0.674	358.1
KLP 84	B	6	Ol	-56.9	-10.5			-56.9	-56.6	27.8		0.667	351.0
KLP 84	B	7	Ol	-56.9	-10.5			-56.9	-56.6	28.9		0.634	320.5
KLP 84	B	8	Ol	-56.9	-10.5			-56.9	-56.6	29.4		0.614	303.8
KLP 84	A	1	Ol	-56.9	-10.5			-56.9	-56.6	27.3		0.679	362.5
KLP 84	A	2	Ol	-56.9	-10.5			-56.9	-56.6	27.4		0.676	360.3
KLP 84	C	1	Ol	-56.9	-10.5			-57.4	-57.1	29.6		0.605	296.6
KLP 84	C	2	Ol	-56.9	-10.5			-57.4	-57.1	30.0		0.586	281.4
KLP 84	C	3	Ol	-56.9	-10.5			-57.4	-57.1	27.8		0.667	351.0
KLP 84	C	4	Ol	-56.9	-10.5			-57.0	-56.7	28.6		0.644	329.6
KLP 84	C	5	Ol	-56.9	-10.5			-57.2	-56.9	28.2		0.656	340.8
KLP 84	E	1	Cpx	-56.9	-10.5			-57.0	-56.7	30.6		0.552	256.4
KLP 84	E	2	Cpx	-56.9	-10.5			-57.0	-56.7	30.5		0.558	260.7
KLP 84	E	3	Cpx	-56.9	-10.5			-57.0	-56.7	30.5		0.558	260.7
KLP 84	E	4	Cpx	-56.9	-10.5			-57.0	-56.7	30.6		0.552	256.4
KLP 84	E	5	Cpx	-56.9	-10.5			-57.0	-56.7	30.6		0.552	256.4
KLP 84	D	1	Cpx	-56.9	-10.5			-56.9	-56.6	30.2		0.575	273.3
KLP 84	F	1	Cpx	-56.9	-10.5			-56.9	-56.6	30.3		0.570	269.2

Appendix A 3.3: Fluid inclusion data

Sample	Frag-ment	Fl #	Host mineral	Standard CO2	Standard H2O – KCl	Tm initial	Tm initial corrected	Tm final	Tm final corrected	Th L	Th V	Density	P (MPa) Calculated
KLP 84	F	2	Cpx	-56.9	-10.5			-56.9	-56.6	30.7		0.545	252.0
KLP 84	F	3	Cpx	-56.9	-10.5			-56.9	-56.6	30.0		0.586	281.4
KLP 84	F	4	Ol	-56.9	-10.5			-56.9	-56.6	29.0		0.630	317.3
KLP 84	J	1	Ol	-57.0	-10.5			-57.0	-56.6	28.1		0.659	343.5
KLP 84	J	2	Ol	-57.0	-10.5			-57.0	-56.6	27.0		0.685	368.8
KLP 84	J	3	Ol	-57.0	-10.5			-57.0	-56.6	27.1		0.683	366.7
KLP 84	J	4	Ol	-57.0	-10.5			-57.0	-56.6	27.4		0.676	360.3
KLP 84	J	5	Ol	-57.0	-10.5			-57.0	-56.6	28.5		0.647	332.5
KLP 84	J	6	Ol	-57.0	-10.5			-57.0	-56.6	28.0		0.662	346.1
KLP 84	J	7	Ol	-57.0	-10.5			-57.0	-56.6	27.7		0.669	353.5
KLP 84	J	8	Ol	-57.0	-10.5			-57.0	-56.6	28.2		0.656	340.8
KLP 84	K	1	Ol	-57.0	-10.5			-57.0	-56.6	27.5		0.674	358.1
KLP 84	K	2	Ol	-57.0	-10.5			-57.0	-56.6	27.7		0.669	353.5
KLP 84	K	3	Ol	-57.0	-10.5			-57.0	-56.6	27.9		0.664	348.6
KLP 84	K	4	Ol	-57.0	-10.5			-57.0	-56.6	27.1		0.683	366.7
KLP 84	K	5	Ol	-57.0	-10.5			-57.0	-56.6	29.0		0.630	317.3
KLP 84	K	6	Ol	-57.0	-10.5			-57.0	-56.6	27.0		0.685	368.8
KLP 84	K	7	Ol	-57.0	-10.5			-57.0	-56.6	27.1		0.683	366.7
KLP 84	G	1	Ol	-56.9	-10.5			-56.9	-56.5	30.4		0.564	265.0
KLP 84	G	2	Ol	-56.9	-10.5			-56.9	-56.5	30.2		0.575	273.3
KLP 84	G	3	Ol	-56.9	-10.5			-56.9	-56.5	29.4		0.614	303.8
KLP 84	G	4	Ol	-56.9	-10.5			-56.9	-56.5	29.4		0.614	303.8
KLP 84	G	5	Ol	-56.9	-10.5			-56.9	-56.5	30.0		0.586	281.4
KLP 84	I	1	Ol	-57.0	-10.5			-57.0	-56.6	25.3		0.713	397.7
KLP 84	I	2	Ol	-57.0	-10.5			-57.0	-56.6	28.8		0.637	323.6
KLP 88	A I	6	Cpx	-57.0	-10.4	-58.7	-58.3	-57.7	-57.3	23.6		0.733	419.9
KLP 88	A I	7	Cpx	-57.0	-10.4	-58.7	-58.3	-57.7	-57.3	22.0		0.749	439.1
KLP 88	A I	8	Cpx	-57.0	-10.4	-58.7	-58.3	-57.7	-57.3	21.9		0.750	440.3
KLP 88	G	1	Cpx	-57.0	-10.4	-58.9	-58.5	-57.9	-57.5	26.0		0.703	386.9
KLP 88	G	2	Cpx	-57.0	-10.4	-58.9	-58.5	-57.9	-57.5	24.8		0.719	404.6
KLP 88	G	3	Cpx	-57.0	-10.4	-58.9	-58.5	-57.9	-57.5	24.6		0.721	407.3
KLP 88	G	4	Cpx	-57.0	-10.4	-58.9	-58.5	-57.9	-57.5	23.8		0.730	417.5

Appendix A 3.3: Fluid inclusion data

Sample	Frag-ment	Fl #	Host mineral	Standard CO2	Standard H2O – KCl	Tm initial	Tm initial corrected	Tm final	Tm final corrected	Th L	Th V	Density	P (MPa) Calculated
KLP 88	G	5	Cpx	-57.0	-10.4	-58.9	-58.5	-57.9	-57.5	24.6		0.721	407.3
KLP 88	G	6	Cpx	-57.0	-10.4	-58.9	-58.5	-57.9	-57.5	24.8		0.719	404.6
KLP 88	G	7	Cpx	-57.0	-10.4	-58.9	-58.5	-57.9	-57.5	28.3		0.653	338.1
KLP 88	G	8	Cpx	-57.0	-10.4	-59.6	-59.2	-57.9	-57.5	24.6		0.721	407.3
KLP 88	G	9	Cpx	-57.0	-10.4	-59.6	-59.2	-57.9	-57.5	22.9		0.740	428.3
KLP 88	A	1	Cpx	-57.0	-10.4	-58.7	-58.3	-57.7	-57.3	24.0		0.728	415.0
KLP 88	A	2	Cpx	-57.0	-10.4	-58.7	-58.3	-57.7	-57.3	24.1		0.727	413.7
KLP 88	A	3	Cpx	-57.0	-10.4	-58.7	-58.3	-57.7	-57.3	23.5		0.734	421.1
KLP 88	A	4	Cpx	-57.0	-10.4	-58.7	-58.3	-57.7	-57.3	29.5		0.610	300.3
KLP 88	A	5	Cpx	-57.0	-10.4	-58.7	-58.3	-57.7	-57.3	26.8		0.689	372.7
KLP 88	A	6	Cpx	-57.0	-10.4	-58.7	-58.3	-57.7	-57.3	23.1		0.738	425.9
KLP 88	A	7	Cpx	-57.0	-10.4	-58.7	-58.3	-57.7	-57.3	22.5		0.744	433.1
KLP 88	A	8	Cpx	-57.0	-10.4	-58.7	-58.3	-57.7	-57.3	22.1		0.748	437.9
KLP 88	H	1	Cpx	-57.0	-10.4	-59.5	-59.1	-58.5	-58.1	25.0		0.716	401.9
KLP 88	H	2	Cpx	-57.0	-10.4	-59.5	-59.1	-58.5	-58.1	21.6		0.753	443.9
KLP 88	H	3	Cpx	-57.0	-10.4	-59.5	-59.1	-58.5	-58.1	21.7		0.752	442.7
KLP 88	H	4	Cpx	-57.0	-10.4	-59.5	-59.1	-58.5	-58.1	not determined			
KLP 88	H	5	Cpx	-57.0	-10.4	-59.5	-59.1	-58.5	-58.1	25.2		0.714	399.1
KLP 88	H	6	Cpx	-57.0	-10.4	-59.5	-59.1	-58.5	-58.1	25.8		0.706	390.1
KLP 88	H	7	Cpx	-57.0	-10.4	-59.5	-59.1	-58.5	-58.1	21.8		0.751	441.5
KLP 88	H	8	Cpx	-57.0	-10.4	-59.5	-59.1	-58.5	-58.1	22.1		0.748	437.9
KLP 88	H	9	Cpx	-57.0	-10.4	-59.5	-59.1	-58.5	-58.1	27.1		0.683	366.7
KLP 88	H	10	Cpx	-57.0	-10.4	-59.5	-59.1	-58.5	-58.1	21.8		0.751	441.5
KLP 88	H	11	Cpx	-57.0	-10.4	-59.5	-59.1	-58.5	-58.1	25.2		0.714	399.1
KLP 88	I	1	Cpx	-57.1	-10.4	-59.4	-58.9	-58.6	-58.1	24.9		0.718	403.3
KLP 88	I	2	Cpx	-57.1	-10.4	-59.4	-58.9	-58.6	-58.1	24.2		0.726	412.5
KLP 88	I	3	Cpx	-57.1	-10.4	-59.4	-58.9	-58.6	-58.1	24.4		0.724	409.9
Bejenado													
KLP 6B	D	1	Ol	-56.9	-10.5			-57.1	-56.8	25.7		0.707	391.7
KLP 6B	D	2	Ol	-56.9	-10.5			-57.1	-56.8	21.6		0.753	443.9
KLP 6B	D	3	Ol	-56.9	-10.5			-57.5	-57.2	25.8		0.706	390.1

Appendix A 3.3: Fluid inclusion data

Sample	Frag-ment	Fl #	Host mineral	Standard CO2	Standard H2O – KCl	Tm initial	Tm initial corrected	Tm final	Tm final corrected	Th L	Th V	Density	P (MPa) Calculated
KLP 6B	D	4	Ol	-56.9	-10.5			-57.5	-57.2	24.6		0.721	407.3
KLP 112	D	1	Ol	-57.3	-10.4			-57.4	-56.7	11.2		0.856	588.0
KLP 112	D	2	Ol	-57.3	-10.4			-57.4	-56.7	9.9		0.866	604.9
KLP 112	D	3	Ol	-57.3	-10.4			-57.4	-56.7	13.7		0.833	553.2
KLP 112	A	1	Ol	-57.1	-10.4			-57.1	-56.6	27.5		0.674	358.1
KLP 216	F	1	Cpx	-57.1	-10.5			-57.0	-56.5	30.5		0.558	260.7
KLP 216	F	2	Cpx	-57.1	-10.5			-57.0	-56.5	30.5		0.558	260.7
KLP 216	F	3	Cpx	-57.1	-10.5			-56.9	-56.4	30.6		0.552	256.4
KLP 216	F	4	Cpx	-57.1	-10.5			-56.9	-56.4	30.6		0.552	256.4
KLP 216	F	5	Cpx	-57.1	-10.5			-56.9	-56.4	29.6		0.605	296.6
KLP 216	C	1	Cpx	-57.0	-10.5			-57.0	-56.6	29.8		0.596	289.2
KLP 216	C	2	Cpx	-57.0	-10.5			-57.0	-56.6	29.5		0.610	300.3
KLP 216	C	3	Cpx	-57.0	-10.5			-57.0	-56.6	29.6		0.605	296.6
KLP 216	C	4	Cpx	-57.0	-10.5			-57.0	-56.6	29.6		0.605	296.6
KLP 216	C	5	Cpx	-57.0	-10.5			-57.0	-56.6	29.9		0.591	285.3
KLP 216	H	1	Cpx	-57.0	-10.5			-57.2	-56.8	30.3		0.570	269.2
KLP 216	H	2	Cpx	-57.0	-10.5			-57.2	-56.8	30.4		0.564	265.0
KLP 216	H	3	Cpx	-57.0	-10.5			-57.2	-56.8	30.4		0.564	265.0
KLP 216	H	4	Cpx	-57.0	-10.5			-57.3	-56.9	29.5		0.610	300.3
KLP 216	H	5	Cpx	-57.0	-10.5			-57.3	-56.9	29.5		0.610	300.3
KLP 216	H	6	Cpx	-57.0	-10.5			-57.2	-56.8	29.1		0.626	314.0
KLP 216	H	7	Cpx	-57.0	-10.5			-57.2	-56.8	29.8		0.596	289.2
KLP 216	D	1	Cpx	-57.0	-10.5			-57.2	-56.8	30.4		0.564	265.0
KLP 216	D	2	Cpx	-57.0	-10.5			-57.2	-56.8	30.4		0.564	265.0
KLP 216	D	3	Cpx	-57.0	-10.5			-57.2	-56.8	30.4		0.564	265.0
KLP 216	D	4	Cpx	-57.0	-10.5			-57.2	-56.8	30.4		0.564	265.0
KLP 216	A	1	Cpx	-57.0	-10.5			-57.6	-57.2	30.2		0.575	273.3
KLP 216	A	2	Cpx	-57.0	-10.5			-57.6	-57.2	30.2		0.575	273.3
KLP 218	A	1	Cpx	-57.0	-10.5			-57.3	-56.9	29.6		0.605	296.6
KLP 218	A	2	Cpx	-57.0	-10.5			-57.3	-56.9	30.2		0.575	273.3
KLP 218	A	3	Cpx	-57.0	-10.5			-57.3	-56.9	30.1		0.581	277.4
KLP 218	E	1	Cpx	-57.0	-10.5			-57.1	-56.7	30.5		0.558	260.7

Appendix A 3.3: Fluid inclusion data

Sample	Frag-ment	Fl #	Host mineral	Standard CO2	Standard H2O – KCl	Tm initial	Tm initial corrected	Tm final	Tm final corrected	Th L	Th V	Density	P (MPa) Calculated
KLP 218	G	1	Cpx	-57.0	-10.5			-57.3	-56.9	30.1		0.581	277.4
KLP 218	G	2	Cpx	-57.0	-10.5			-57.3	-56.9	30.1		0.581	277.4
KLP 218	G	3	Cpx	-57.0	-10.5			-57.3	-56.9	30.1		0.581	277.4
KLP 218	G	4	Cpx	-57.0	-10.5			-57.3	-56.9	30.1		0.581	277.4
KLP 218	G	5	Cpx	-57.0	-10.5			-57.6	-57.2	30.0		0.586	281.4
KLP 218	G	6	Cpx	-57.0	-10.5			-57.6	-57.2	29.9		0.591	285.3
KLP 218	K	1	Ol	-57.0	-10.5	-57.8	-57.4	-57.6	-57.2	29.0		0.630	317.3
KLP 218	K	2	Ol	-57.0	-10.5	-57.8	-57.4	-57.6	-57.2	28.5		0.647	332.5
KLP 218	K	3	Ol	-57.0	-10.5			-57.6	-57.2	28.8		0.637	323.6
KLP 218	K	4	Ol	-57.0	-10.5			-57.9	-57.5	27.8		0.667	351.0
KLP 218	K	5	Cpx	-57.0	-10.5			-57.9	-57.5	28.3		0.653	338.1
KLP 218	K	6	Cpx	-57.0	-10.5			-57.6	-57.2	29.5		0.610	300.3
KLP 218	K	7	Cpx	-57.0	-10.5			-57.6	-57.2	29.8		0.596	289.2
KLP 218	K	8	Cpx	-57.0	-10.5			-57.5	-57.1	29.4		0.614	303.8
KLP 218	K	9	Cpx	-57.0	-10.5			-57.3	-56.9	28.8		0.637	323.6
KLP 218	M	1	Cpx	-57.0	-10.5			-57.3	-56.9	30.4		0.564	265.0
KLP 218	M	2	Cpx	-57.0	-10.5			-57.3	-56.9	29.9		0.591	285.3
KLP 218	M	3	Cpx	-57.0	-10.5			-57.3	-56.9	30.0		0.586	281.4
KLP 218	M	4	Cpx	-57.0	-10.5			-57.3	-56.9	30.4		0.564	265.0
KLP 218	M	5	Cpx	-57.0	-10.5			-57.3	-56.9	30.2		0.575	273.3
KLP 218	M	6	Cpx	-57.0	-10.5			-57.2	-56.8	30.4		0.564	265.0
KLP 218	M	7	Cpx	-57.0	-10.5			-57.2	-56.8	30.4		0.564	265.0
KLP 218A	A	1	Ol	-57.1	-10.5			-57.1	-56.6	30.3		0.570	269.2
KLP 218A	A	2	Ol	-57.1	-10.5			-57.1	-56.6	30.2		0.575	273.3
KLP 218A	A	3	Ol	-57.1	-10.5			-57.1	-56.6	30.0		0.586	281.4
KLP 218A	A	4	Ol	-57.1	-10.5			-57.1	-56.6	30.3		0.570	269.2
KLP 218A	B	1	Ol	-57.1	-10.5			-57.1	-56.6	29.8		0.596	289.2
KLP 218A	B	2	Ol	-57.1	-10.5			-57.1	-56.6	29.8		0.596	289.2
KLP 218A	B	3	Ol	-57.1	-10.5			-57.1	-56.6	30.1		0.581	277.4
KLP 218A	B	4	Ol	-57.1	-10.5			-57.1	-56.6	30.2		0.575	273.3
KLP 218A	B	5	Cpx	-57.1	-10.5			-57.2	-56.7	30.5		0.558	260.7
KLP 218A	B	6	Cpx	-57.1	-10.5			-57.2	-56.7	30.4		0.564	265.0

Appendix A 3.3: Fluid inclusion data

Sample	Frag-ment	Fl #	Host mineral	Standard CO2	Standard H2O – KCl	Tm initial	Tm initial corrected	Tm final	Tm final corrected	Th L	Th V	Density	P (MPa) Calculated
KLP 218A	B	7	Cpx	-57.1	-10.5			-57.2	-56.7	30.4		0.564	265.0
KLP 218A	B	8	Cpx	-57.1	-10.5			-57.2	-56.7	30.4		0.564	265.0
KLP 218A	C	1	Cpx	-57.1	-10.5			-57.1	-56.6	30.2		0.575	273.3
KLP 218A	C	2	Cpx	-57.1	-10.5			-57.1	-56.6	30.3		0.570	269.2
KLP 218A	C	3	Cpx	-57.1	-10.5			-57.1	-56.6	30.0		0.586	281.4
KLP 218A	C	4	Cpx	-57.1	-10.5			-57.1	-56.6	30.4		0.564	265.0
KLP 218A	C	5	Cpx	-57.1	-10.5			-57.1	-56.6	30.4		0.564	265.0
Cumbre Vieja													
POS 166-3	F	1	Ol	-57.0	-10.5			-58.0	-57.6	22.3		0.746	435.5
POS 166-3	F	2	Ol	-57.0	-10.5			-58.0	-57.6	22.2		0.747	436.7
POS 166-3	A	1	Ol	-57.0	-10.5			-57.0	-56.6	25.7		0.707	391.7
POS 166-3	A	2	Ol	-57.0	-10.5			-56.9	-56.5	23.5		0.734	421.1
POS 166-3	A	3	Ol	-57.0	-10.5			-56.9	-56.5	26.2		0.699	383.6
POS 166-3	A	4	Ol	-57.0	-10.5			-56.9	-56.5	22.4		0.745	434.3
POS 166-3	A	5	Ol	-57.0	-10.5			-56.9	-56.5	22.6		0.743	431.9
POS 166-3	C	1	Ol	-57.0	-10.5			-56.8	-56.4	23.2		0.737	424.7
POS 166-3	C	2	Ol	-57.0	-10.5			-56.8	-56.4	27.8		0.667	351.0
POS 166-3	C	3	Ol	-57.0	-10.5			-56.7	-56.3	26.0		0.703	386.9
POS 166-3	C	4	Ol	-57.0	-10.5			-56.8	-56.4	26.3		0.698	381.9
POS 166-3	C	5	Ol	-57.0	-10.5			-56.8	-56.4	23.5		0.734	421.1
POS 166-3	D	1	Ol	-56.9	-10.5			-57.1	-56.8	19.3		0.776	473.0
POS 166-3	D	2	Ol	-56.9	-10.5			-57.1	-56.8	20.7		0.762	455.0
POS 166-3	D	3	Ol	-56.9	-10.5			-57.1	-56.8	24.8		0.719	404.6
POS 166-3	D	4	Ol	-56.9	-10.5			-57.1	-56.8	20.9		0.760	452.5
POS 166-3	D	5	Ol	-56.9	-10.5			-57.1	-56.8	29.9		0.591	285.3
POS 166-3	D	6	Ol	-56.9	-10.5			-57	-56.7	29.8		0.596	289.2
POS 166-3	L	1	Ol	-56.9	-10.5			-57.2	-56.9	27.1		0.683	366.7
POS 166-3	L	2	Ol	-56.9	-10.5			-57.1	-56.8	25.6		0.708	393.2
POS 166-3	L	3	Ol	-56.9	-10.5			-57.1	-56.8	25.2		0.714	399.1
POS 166-3	L	4	Ol	-56.9	-10.5			-57.2	-56.9	25.1		0.715	400.5
POS 166-3	L	5	Ol	-56.9	-10.5			-57.2	-56.9	23.8		0.730	417.5

Appendix A 3.3: Fluid inclusion data

Sample	Frag-ment	Fl #	Host mineral	Standard CO2	Standard H2O – KCl	Tm initial	Tm initial corrected	Tm final	Tm final corrected	Th L	Th V	Density	P (MPa) Calculated
POS 166-3	L	6	Ol	-56.9	-10.5			-57.1	-56.8	25.4		0.711	396.2
POS 166-3	J	1	Ol	-56.9	-10.5			-56.9	-56.6	28.7		0.641	326.6
POS 166-3	J	2	Ol	-56.9	-10.5			-56.9	-56.6	27.2		0.681	364.7
POS 166-3	K	1	Ol	-56.9	-10.5			-56.9	-56.6	20.6		0.763	456.2
POS 166-3	K	2	Ol	-56.9	-10.5			-56.9	-56.6	20.5		0.764	457.5
POS 166-3	K	3	Ol	-56.9	-10.5			-56.9	-56.6	20.8		0.761	453.7
POS 166-3	G	1	Ol	-56.9	-10.5			-56.8	-56.5	23.4		0.735	422.3
POS 170-1	E	1	Cpx	-57.0	-10.5			-57.6	-57.2	26.1		0.701	385.3
POS 170-1	E	2	Cpx	-57.0	-10.5	-59.4	-59.0	-58.4	-58.0	25.0		0.716	401.9
POS 170-1	E	4	Cpx	-57.0	-10.5			-57.8	-57.4	26.4		0.696	380.1
POS 170-1	E	5	Cpx	-57.0	-10.5			-59.1	-58.7	25.8		0.706	390.1
POS 170-1	E	6	Cpx	-57.0	-10.5			-59.1	-58.7	26.0		0.703	386.9
POS 170-1	E	7	Cpx	-57.0	-10.5			-58.0	-57.6	27.1		0.683	366.7
POS 170-1	E	8	Cpx	-57.0	-10.5			-58.0	-57.6	27.5		0.674	358.1
POS 170-1	E	9	Cpx	-57.0	-10.5	-59.1	-58.7	-58.0	-57.6	27.5		0.674	358.1
POS 170-1	E	10	Cpx	-57.0	-10.5	-59.4	-59.0	-57.3	-56.9	30.9		0.532	242.9
POS 170-1	E	11	Cpx	-57.0	-10.5	-59.4	-59.0	-57.3	-56.9	30.9		0.532	242.9
POS 170-1	E	12	Cpx	-57.0	-10.5	-59.4	-59.0	-57.3	-56.9	30.9		0.532	242.9
POS 170-1	B	1	Cpx	-57.1	-10.5			-57	-56.5	23.9		0.729	416.2
POS 170-1	B	2	Cpx	-57.1	-10.5			-57.3	-56.8	25.2		0.714	399.1
POS 170-1	B	3	Cpx	-57.1	-10.5			-57.3	-56.8	25.2		0.714	399.1
POS 170-1	B	4	Cpx	-57.1	-10.5			-57.3	-56.8	24.0		0.728	415.0
POS 170-1	B	5	Cpx	-57.1	-10.5			-57.2	-56.7	24.4		0.724	409.9
POS 170-1	D	1	Cpx	-57.1	-10.5	-58.3	-57.8	-57.1	-56.6	25.4		0.711	396.2
POS 170-1	D	2	Cpx	-57.1	-10.5	-58.3	-57.8	-57.1	-56.6	25.5		0.710	394.7
POS 170-1	D	3	Cpx	-57.1	-10.5	-58.3	-57.8	-57.1	-56.6	25.5		0.710	394.7
POS 170-1	D	4	Cpx	-57.1	-10.5	-58.5	-58.0	-57.6	-57.1	28.9		0.634	320.5
POS 170-1	D	5	Cpx	-57.1	-10.5	-58.5	-58.0	-57.6	-57.1	28.9		0.634	320.5
POS 170-1	D	6	Cpx	-57.1	-10.5			-57.3	-56.8	26.3		0.698	381.9
POS 170-1	D	7	Cpx	-57.1	-10.5			-57.3	-56.8	26.6		0.693	376.5
POS 170-1	D	8	Cpx	-57.1	-10.5	-58.5	-58.0	-57.8	-57.3	29.1		0.626	314.0
POS 170-1	D	9	Cpx	-57.1	-10.5	-58.5	-58.0	-57.8	-57.3	29.2		0.622	310.7

Appendix A 3.3: Fluid inclusion data

Sample	Frag-ment	Fl #	Host mineral	Standard CO2	Standard H2O – KCl	Tm initial	Tm initial corrected	Tm final	Tm final corrected	Th L	Th V	Density	P (MPa) Calculated
POS 170-1	D	10	Cpx	-57.1	-10.5	-58.2	-57.7	-57.7	-57.2	25.5		0.710	394.7
POS 170-1	D	11	Cpx	-57.1	-10.5	-59.1	-58.6	-57.8	-57.3	26.1		0.701	385.3
POS 170-1	D	12	Cpx	-57.1	-10.5	-58.6	-58.1	-57.6	-57.1	26.2		0.699	383.6
POS 170-1	D	13	Cpx	-57.1	-10.5	-58.2	-57.7	-57.6	-57.1	26.6		0.693	376.5
POS 170-1	C	1	Cpx	-57.1	-10.5			-57	-56.5	23.7		0.731	418.7
POS 170-1	C	2	Cpx	-57.1	-10.5			-57	-56.5	23.7		0.731	418.7
POS 170-1	C	3	Cpx	-57.1	-10.5			-57	-56.5	23.7		0.731	418.7
POS 170-1	C	4	Cpx	-57.1	-10.5			-57.1	-56.6	23.7		0.731	418.7
POS 170-1	C	5	Cpx	-57.1	-10.5			-57.1	-56.6	23.7		0.731	418.7
POS 170-1	I	1	Cpx	-57.0	-10.5	-58.6	-58.2	-57.4	-57.0	27.7		0.669	353.5
POS 170-1	I	2	Cpx	-57.0	-10.5	-58.6	-58.2	-57.4	-57.0	27.9		0.664	348.6
POS 170-1	I	3	Cpx	-57.0	-10.5	-58.6	-58.2	-57.4	-57.0	27.3		0.679	362.5
POS 170-1	I	4	Cpx	-57.0	-10.5	-58.5	-58.1	-57.4	-57.0	27.9		0.664	348.6
POS 170-1	I	5	Cpx	-57.0	-10.5	-58.5	-58.1	-57.4	-57.0	28.6		0.644	329.6
POS 170-1	I	6	Cpx	-57.0	-10.5	-58.2	-57.8	-57.7	-57.3	27.3		0.679	362.5
POS 170-1	I	7	Cpx	-57.0	-10.5	-58.2	-57.8	-57.7	-57.3	27.4		0.676	360.3

Appendix A 3.4: Electron microprobe analyses of standards

	Date	SiO2	TiO2	Al2O3	FeO	MnO	MgO	CaO	Na2O	K2O	P2O5	Cr2O3	NiO	ZnO	F	Cl	Total
EMS IFM-Geomar																	
Sc-Olivine																	
1	4/9/02	40.88	0.01	0.04	9.62	0.15	0.11	0.08	0.00	0.00	0.00	0.02	0.43	-	-	-	99.55
2	4/9/02	40.71	0.01	0.03	9.69	0.11	0.10	0.07	0.00	0.00	0.00	0.02	0.31	-	-	-	98.96
3	4/9/02	40.60	0.02	0.03	9.87	0.14	0.10	0.10	0.00	0.01	0.00	0.03	0.37	-	-	-	100.60
4	4/9/02	39.63	0.01	0.06	9.77	0.13	0.09	0.10	0.00	0.00	0.00	0.00	0.37	-	-	-	99.88
5	4/9/02	41.38	0.04	0.05	9.67	0.17	0.13	0.10	0.00	0.00	0.00	0.03	0.38	-	-	-	100.47
6	4/9/02	41.93	0.04	0.03	9.41	0.12	0.10	0.10	0.00	0.01	0.00	0.03	0.40	-	-	-	100.39
7	4/9/02	41.38	0.04	0.05	9.67	0.17	0.09	0.10	0.00	0.00	0.00	0.03	0.38	-	-	-	100.43
8	18/12/02	41.33	-	-	9.44	0.13	49.64	0.13	-	-	-	0.01	0.33	-	-	-	101.01
9	18/12/02	41.13	-	-	9.28	0.14	49.58	0.10	-	-	-	0.02	0.37	-	-	-	100.59
10	18/12/02	41.02	-	-	9.57	0.15	49.40	0.14	-	-	-	0.02	0.38	-	-	-	100.67
11	18/12/02	40.99	-	-	9.16	0.15	49.55	0.09	-	-	-	0.03	0.33	-	-	-	100.28
12	18/12/02	41.29	-	-	9.36	0.20	49.48	0.09	-	-	-	0.00	0.34	-	-	-	100.75
13	18/12/02	41.18	-	-	9.57	0.11	49.71	0.10	-	-	-	0.00	0.35	-	-	-	100.96
14	20/1/03	40.57	-	-	9.40	0.16	49.43	0.17	-	-	-	0.02	0.31	-	-	-	100.05
15	20/1/03	40.48	-	-	9.55	0.20	49.67	0.09	-	-	-	0.00	0.27	-	-	-	100.25
16	20/1/03	40.40	-	-	9.48	0.17	49.58	0.10	-	-	-	0.03	0.21	-	-	-	99.96
17	20/1/03	40.43	-	-	9.37	0.19	49.67	0.08	-	-	-	0.02	0.28	-	-	-	100.04
18	20/1/03	40.20	-	-	9.33	0.17	49.44	0.10	-	-	-	0.02	0.34	-	-	-	99.58
19	20/1/03	40.42	-	-	9.62	0.15	49.56	0.10	-	-	-	0.03	0.30	-	-	-	100.18
20	11/3/03	41.01	-	-	9.35	0.17	49.63	0.14	-	-	-	0.03	0.20	-	-	-	100.53
21	11/3/03	40.81	-	-	9.62	0.12	49.53	0.19	-	-	-	0.02	0.28	-	-	-	100.57
22	11/3/03	40.63	-	-	9.39	0.16	49.58	0.12	-	-	-	0.02	0.29	-	-	-	100.19
23	11/3/03	40.66	-	-	9.40	0.11	49.61	0.09	-	-	-	0.02	0.28	-	-	-	100.18
25	11/3/03	41.14	-	-	9.52	0.15	49.46	0.10	-	-	-	0.00	0.27	-	-	-	100.63
26	11/3/03	40.72	-	-	9.66	0.13	49.48	0.11	-	-	-	0.00	0.28	-	-	-	100.38
27	11/3/03	40.66	-	-	9.47	0.17	49.13	0.11	-	-	-	0.00	0.25	-	-	-	99.78
28	11/3/03	40.70	-	-	9.74	0.16	49.28	0.11	-	-	-	0.01	0.29	-	-	-	100.27
29	11/3/03	40.24	-	-	9.43	0.15	49.40	0.10	-	-	-	0.00	0.24	-	-	-	99.56
30	11/3/03	40.57	-	-	9.48	0.12	48.94	0.11	-	-	-	0.01	0.23	-	-	-	99.44
mean		**40.80**	**0.03**	**0.04**	**9.51**	**0.15**	**37.57**	**0.11**	**0.00**	**0.00**	**0.00**	**0.02**	**0.31**				**100.21**
std.dev.		**0.45**	**0.02**	**0.01**	**0.16**	**0.03**	**21.51**	**0.02**	**0.00**	**0.00**	**0.00**	**0.01**	**0.06**				**0.48**
Recom.		**40.81**			**9.55**	**0.14**	**49.42**	**0.05**									**100.29**

Appendix A 3.4: Electron microprobe analyses of standards

	Date	SiO2	TiO2	Al2O3	FeO	MnO	MgO	CaO	Na2O	K2O	P2O5	Cr2O3	NiO	ZnO	F	Cl	Total
Kakanuiaugite																	
1	4/9/02	49.65	0.84	8.57	6.27	0.12	16.71	15.63	1.17	0.02	-	0.14	0.09	-	-	-	99.28
2	4/9/02	49.42	0.85	8.50	6.30	0.19	16.76	15.55	1.16	0.00	-	0.19	0.05	-	-	-	99.01
3	4/9/02	50.15	0.78	8.55	6.28	0.14	16.50	15.89	1.17	0.01	-	0.14	0.08	-	-	-	99.70
4	4/9/02	50.18	0.77	8.44	6.14	0.20	16.42	15.71	1.15	0.00	-	0.16	0.03	-	-	-	99.20
5	4/9/02	50.72	0.82	8.43	6.09	0.14	16.55	15.76	1.14	0.01	-	0.16	0.04	-	-	-	99.85
6	4/9/02	50.36	0.79	8.53	6.27	0.09	16.44	15.65	1.13	0.00	-	0.18	0.03	-	-	-	99.48
7	4/9/02	49.58	0.77	8.54	6.37	0.11	16.49	15.77	1.17	0.00	-	0.20	0.07	-	-	-	99.07
8	4/9/02	50.36	0.79	8.50	6.11	0.13	16.49	15.65	1.21	0.00	-	0.17	0.01	-	-	-	99.42
9	4/9/02	51.41	0.83	8.46	6.39	0.15	16.66	15.91	1.18	0.00	-	0.16	0.10	-	-	-	101.25
10	4/9/02	50.27	0.85	8.48	6.52	0.17	16.31	15.75	1.17	0.00	-	0.17	0.05	-	-	-	99.74
11	4/9/02	49.91	0.86	8.46	6.28	0.15	16.30	15.48	1.18	0.00	-	0.17	0.00	-	-	-	98.78
12	4/9/02	49.93	0.77	8.35	6.32	0.15	16.21	15.28	1.19	0.00	-	0.11	0.07	-	-	-	98.39
13	4/9/02	50.23	0.84	8.37	6.29	0.09	16.21	15.79	1.26	0.01	-	0.18	0.00	-	-	-	99.26
14	18/12/02	50.14	0.81	8.68	6.21	0.14	16.47	16.15	1.23	0.01	-	0.16	-	-	-	-	99.99
15	18/12/02	50.08	0.74	8.79	6.38	0.12	16.54	16.17	1.21	0.01	-	0.16	-	-	-	-	100.19
16	18/12/02	50.24	0.80	8.79	6.40	0.17	16.69	16.18	1.22	0.00	-	0.16	-	-	-	-	100.65
17	18/12/02	50.16	0.79	8.77	6.56	0.19	16.66	16.14	1.23	0.02	-	0.18	-	-	-	-	100.69
18	18/12/02	50.65	0.86	8.75	6.39	0.14	16.76	15.78	1.22	0.02	-	0.16	-	-	-	-	100.74
19	18/12/02	50.40	0.78	8.72	6.24	0.18	16.70	15.85	1.20	0.02	-	0.19	-	-	-	-	100.27
20	18/12/02	50.46	0.83	8.70	6.16	0.18	16.63	15.92	1.23	0.01	-	0.19	-	-	-	-	100.30
21	18/12/02	50.36	0.77	8.73	6.48	0.15	16.62	16.21	1.21	0.01	-	0.14	-	-	-	-	100.68
22	18/12/02	50.58	0.75	8.79	6.37	0.16	16.69	15.96	1.22	0.00	-	0.17	-	-	-	-	100.69
23	18/12/02	50.01	0.94	8.68	6.40	0.10	16.64	16.10	1.21	0.02	-	0.17	-	-	-	-	100.29
24	18/12/02	50.47	0.83	8.78	6.37	0.13	16.62	16.06	1.23	0.01	-	0.15	-	-	-	-	100.65
25	18/12/02	50.74	0.80	8.67	6.26	0.17	16.63	16.03	1.20	0.00	-	0.18	-	-	-	-	100.67
26	18/12/02	50.27	0.78	8.68	6.33	0.12	16.79	16.05	1.23	0.00	-	0.17	-	-	-	-	100.41
27	18/12/02	50.58	0.83	8.81	6.44	0.14	16.66	15.98	1.25	0.00	-	0.17	-	-	-	-	100.87
28	18/12/02	50.63	0.79	8.75	6.20	0.13	16.54	15.96	1.22	0.00	-	0.15	-	-	-	-	100.37
29	18/12/02	50.20	0.80	8.73	6.52	0.16	16.58	15.83	1.23	0.00	-	0.19	-	-	-	-	100.24
30	18/12/02	50.51	0.84	8.75	6.36	0.16	16.70	16.02	1.25	0.02	-	0.18	-	-	-	-	100.78
31	18/12/02	50.75	0.77	8.83	6.37	0.11	16.58	16.03	1.20	0.01	-	0.16	-	-	-	-	100.80
32	18/12/02	50.49	0.80	8.72	6.52	0.07	16.59	15.95	1.25	0.01	-	0.16	-	-	-	-	100.55

Appendix A 3.4: Electron microprobe analyses of standards

	Date	SiO2	TiO2	Al2O3	FeO	MnO	MgO	CaO	Na2O	K2O	P2O5	Cr2O3	NiO	ZnO	F	Cl	Total
33	21/2/03	50.28	0.83	8.77	6.43	0.12	16.80	16.05	1.17	0.00	-	0.15	-	-	-	-	100.58
34	21/2/03	50.22	0.77	8.81	6.40	0.08	16.72	16.16	1.19	0.01	-	0.15	-	-	-	-	100.50
35	21/2/03	50.34	0.74	8.53	5.99	0.13	16.45	16.12	1.18	0.00	-	0.16	-	-	-	-	99.63
36	21/2/03	50.74	0.71	8.48	6.32	0.14	16.75	16.02	1.18	0.00	-	0.16	-	-	-	-	100.49
37	21/2/03	50.63	0.82	8.71	6.21	0.15	16.66	16.11	1.17	0.01	-	0.15	-	-	-	-	100.61
38	21/2/03	50.18	0.77	8.73	6.25	0.17	16.67	16.09	1.17	0.02	-	0.16	-	-	-	-	100.20
39	21/2/03	50.41	0.75	8.88	6.24	0.12	16.66	16.27	1.17	0.00	-	0.17	-	-	-	-	100.68
40	21/2/03	50.57	0.76	8.50	6.21	0.13	16.62	16.24	1.19	0.02	-	0.17	-	-	-	-	100.41
41	21/2/03	50.42	0.79	8.58	6.19	0.14	16.62	16.35	1.16	0.00	-	0.15	-	-	-	-	100.41
42	21/2/03	50.69	0.77	8.80	6.57	0.15	16.75	16.32	1.20	0.00	-	0.15	-	-	-	-	101.38
43	21/2/03	50.32	0.72	8.62	6.46	0.12	16.39	16.24	1.16	0.00	-	0.15	-	-	-	-	100.18
44	21/2/03	50.77	0.78	8.52	6.46	0.16	16.68	16.10	1.19	0.00	-	0.18	-	-	-	-	100.83
45	21/2/03	50.18	0.74	8.69	6.27	0.12	16.56	16.14	1.17	0.02	-	0.16	-	-	-	-	100.05
46	21/2/03	50.19	0.76	8.60	6.21	0.09	16.70	16.20	1.19	0.00	-	0.15	-	-	-	-	100.08
47	21/2/03	50.48	0.78	8.67	6.54	0.16	16.71	16.15	1.17	0.00	-	0.16	-	-	-	-	100.80
48	21/2/03	50.18	0.73	8.51	6.30	0.12	16.69	16.30	1.20	0.01	-	0.18	-	-	-	-	100.21
49	11/3/03	50.41	0.77	8.85	6.27	0.13	16.47	15.97	1.22	0.01	-	0.17	-	-	-	-	100.26
50	11/3/03	50.37	0.73	8.68	6.40	0.08	16.54	15.87	1.29	0.00	-	0.10	-	-	-	-	100.06
51	11/3/03	50.50	0.72	8.70	6.34	0.10	16.34	16.03	1.26	0.00	-	0.11	-	-	-	-	100.10
52	11/3/03	50.69	0.69	8.76	6.36	0.09	16.46	15.86	1.28	0.00	-	0.12	-	-	-	-	100.30
53	11/3/03	50.43	0.69	8.75	6.11	0.08	16.48	15.82	1.27	0.00	-	0.10	-	-	-	-	99.72
54	11/3/03	50.70	0.78	8.85	6.07	0.15	16.52	15.96	1.27	0.02	-	0.12	-	-	-	-	100.44
55	11/3/03	50.38	0.77	8.83	6.32	0.07	16.57	15.83	1.25	0.02	-	0.17	-	-	-	-	100.21
56	11/3/03	50.31	0.72	8.69	6.30	0.12	16.51	16.04	1.26	0.00	-	0.11	-	-	-	-	100.07
57	11/3/03	49.69	0.71	8.58	6.35	0.09	16.47	15.95	1.25	0.00	-	0.11	-	-	-	-	99.21
58	11/3/03	50.53	0.74	8.79	6.23	0.15	16.69	16.04	1.27	0.00	-	0.15	-	-	-	-	100.58
59	11/3/03	49.18	0.69	8.49	6.07	0.07	16.46	15.79	1.26	0.00	-	0.10	-	-	-	-	98.11
60	11/3/03	49.78	0.71	8.48	6.22	0.11	16.47	15.86	1.29	0.00	-	0.12	-	-	-	-	99.02
61	11/3/03	49.93	0.70	8.67	6.23	0.13	16.44	15.86	1.25	0.00	-	0.13	-	-	-	-	99.35
62	11/3/03	50.22	0.71	8.66	6.21	0.07	16.42	16.00	1.28	0.00	-	0.12	-	-	-	-	99.68
63	11/3/03	50.01	0.73	8.56	6.31	0.10	16.41	16.10	1.28	0.01	-	0.12	-	-	-	-	99.63
64	11/3/03	49.42	0.68	8.59	6.42	0.04	16.40	15.82	1.27	0.00	-	0.11	-	-	-	-	98.76
65	11/3/03	49.86	0.71	8.58	6.44	0.09	16.51	15.90	1.28	0.00	-	0.10	-	-	-	-	99.45

Appendix A 3.4: Electron microprobe analyses of standards

	Date	SiO2	TiO2	Al2O3	FeO	MnO	MgO	CaO	Na2O	K2O	P2O5	Cr2O3	NiO	ZnO	F	Cl	Total
66	11/3/03	49.95	0.75	8.56	6.21	0.08	16.27	15.80	1.25	0.00	-	0.11	-	-	-	-	98.97
67	11/3/03	50.34	0.70	8.56	6.11	0.11	16.51	16.03	1.26	0.00	-	0.09	-	-	-	-	99.69
68	11/3/03	50.23	0.76	8.82	6.25	0.14	16.51	15.90	1.25	0.00	-	0.14	-	-	-	-	99.97
69	11/3/03	49.88	0.77	8.76	6.49	0.17	16.40	15.99	1.24	0.01	-	0.14	-	-	-	-	99.84
70	11/3/03	49.98	0.75	8.78	6.13	0.09	16.45	15.86	1.26	0.03	-	0.14	-	-	-	-	99.47
71	11/3/03	50.18	0.76	8.68	6.08	0.07	16.57	15.95	1.23	0.00	-	0.15	-	-	-	-	99.67
72	11/3/03	50.16	0.73	8.64	6.13	0.06	16.49	15.97	1.24	0.00	-	0.15	-	-	-	-	99.56
73	11/3/03	49.81	0.72	8.56	6.28	0.08	16.40	16.01	1.22	0.01	-	0.17	-	-	-	-	99.26
74	11/3/03	49.94	0.73	8.73	6.13	0.11	16.42	15.86	1.22	0.01	-	0.15	-	-	-	-	99.29
75	11/3/03	50.13	0.75	8.70	6.26	0.09	16.53	15.83	1.26	0.01	-	0.14	-	-	-	-	99.70
76	11/3/03	50.51	0.82	8.63	6.23	0.12	16.66	16.05	1.23	0.01	-	0.14	-	-	-	-	100.40
77	11/3/03	50.58	0.79	8.77	6.31	0.13	16.66	15.87	1.25	0.01	-	0.14	-	-	-	-	100.50
78	11/3/03	50.40	0.78	8.74	6.33	0.14	16.45	15.95	1.25	0.02	-	0.16	-	-	-	-	100.21
79	11/3/03	50.59	0.73	8.65	6.20	0.11	16.58	15.96	1.18	0.00	-	0.16	-	-	-	-	100.15
80	11/3/03	50.86	0.75	8.73	6.17	0.11	16.60	15.94	1.17	0.00	-	0.17	-	-	-	-	100.50
81	11/3/03	50.36	0.72	8.70	6.30	0.11	16.37	15.92	1.17	0.00	-	0.17	-	-	-	-	99.80
82	11/3/03	50.22	0.75	8.64	6.16	0.10	16.46	16.06	1.15	0.00	-	0.16	-	-	-	-	99.70
83	11/3/03	50.10	0.75	8.67	6.41	0.13	16.52	15.86	1.19	0.00	-	0.18	-	-	-	-	99.82
84	11/3/03	49.97	0.71	8.67	6.08	0.10	16.35	16.18	1.17	0.00	-	0.17	-	-	-	-	99.38
85	11/3/03	50.28	0.74	8.74	6.07	0.13	16.33	15.88	1.20	0.00	-	0.16	-	-	-	-	99.52
86	11/3/03	50.38	0.75	8.59	6.29	0.09	16.47	15.94	1.18	0.00	-	0.12	-	-	-	-	99.80
87	11/3/03	50.38	0.71	8.69	6.05	0.11	16.52	15.81	1.19	0.00	-	0.16	-	-	-	-	99.63
88	9/10/03	50.46	0.76	8.65	6.59	0.15	16.58	15.85	1.29	0.01	-	0.14	0.06	-	-	-	100.54
89	9/10/03	48.15	0.77	8.48	6.51	0.14	16.47	15.86	1.28	0.00	-	0.17	0.02	-	-	-	97.85
90	9/10/03	47.99	0.72	8.45	6.53	0.08	16.38	15.88	1.30	0.01	-	0.15	0.00	-	-	-	97.49
91	9/10/03	47.14	0.70	8.32	6.29	0.05	16.29	15.76	1.29	0.00	-	0.13	0.01	-	-	-	95.98
92	9/10/03	49.98	0.75	8.67	6.34	0.16	16.50	15.98	1.27	0.01	-	0.12	0.01	-	-	-	99.80
93	9/10/03	49.52	0.75	8.56	6.64	0.12	16.55	15.91	1.28	0.00	-	0.16	0.04	-	-	-	99.53
mean		**50.19**	**0.77**	**8.65**	**6.30**	**0.12**	**16.54**	**15.95**	**1.22**	**0.01**		**0.15**	**0.04**				**99.89**
std.dev.		**0.57**	**0.05**	**0.13**	**0.14**	**0.03**	**0.13**	**0.18**	**0.04**	**0.01**		**0.02**	**0.03**				**0.82**
Recom.		**50.73**	**0.74**	**8.73**	**6.77**	**0.13**	**16.65**	**15.82**	**1.27**								**100.44**

Appendix A 3.4: Electron microprobe analyses of standards

	Date	SiO2	TiO2	Al2O3	FeO	MnO	MgO	CaO	Na2O	K2O	P2O5	Cr2O3	NiO	ZnO	F	Cl	Total
Chromaugite																	
1	4/9/02	50.28	0.43	7.17	4.78	0.14	17.78	16.71	0.71	0.01	-	0.97	0.01	-	-	-	99.00
2	4/9/02	50.37	0.41	7.32	4.73	0.09	17.74	16.91	0.74	0.01	-	0.92	0.00	-	-	-	99.24
3	4/9/02	50.68	0.45	7.29	4.67	0.08	17.48	16.96	0.73	0.01	-	0.92	0.10	-	-	-	99.38
4	4/9/02	50.73	0.39	7.36	4.84	0.15	17.56	17.02	0.72	0.00	-	0.92	0.03	-	-	-	99.71
5	4/9/02	50.87	0.42	7.22	4.65	0.09	17.59	16.94	0.71	0.00	-	0.92	0.07	-	-	-	99.47
6	4/9/02	50.79	0.42	7.42	4.74	0.13	17.69	17.04	0.75	0.00	-	0.99	0.09	-	-	-	100.04
7	4/9/02	51.18	0.42	7.21	4.65	0.12	17.61	17.06	0.75	0.02	-	0.94	0.08	-	-	-	100.02
8	4/9/02	50.95	0.42	7.27	4.71	0.16	17.66	16.90	0.72	0.00	-	0.94	0.06	-	-	-	99.80
9	4/9/02	50.58	0.43	7.24	4.67	0.06	17.50	17.14	0.74	0.01	-	0.95	0.02	-	-	-	99.33
10	4/9/02	50.50	0.37	7.36	4.85	0.14	17.55	17.01	0.75	0.00	-	0.94	0.02	-	-	-	99.48
11	4/9/02	49.24	0.43	7.23	4.70	0.13	17.39	16.81	0.74	0.00	-	0.94	0.06	-	-	-	97.67
12	4/9/02	49.10	0.44	7.22	4.80	0.10	17.32	16.72	0.74	0.00	-	0.93	0.07	-	-	-	97.43
13	4/9/02	49.57	0.42	7.26	4.84	0.13	17.23	16.56	0.75	0.01	-	0.96	0.00	-	-	-	97.71
14	4/9/02	51.42	0.43	7.27	4.84	0.14	17.37	16.99	0.75	0.01	-	0.98	0.00	-	-	-	100.19
15	4/9/02	50.35	0.40	7.28	4.84	0.15	17.42	16.94	0.72	0.01	-	0.90	0.03	-	-	-	99.03
16	18/12/02	50.53	0.38	7.51	4.49	0.11	17.73	17.30	0.75	0.02	-	1.00	-	-	-	-	99.52
17	18/12/02	50.06	0.38	7.54	4.60	0.13	17.61	17.50	0.76	0.00	-	0.93	-	-	-	-	99.49
18	18/12/02	50.18	0.41	7.57	4.76	0.14	17.52	17.22	0.76	0.01	-	0.92	-	-	-	-	99.28
19	18/12/02	49.79	0.40	7.51	4.69	0.09	17.71	17.33	0.76	0.01	-	0.99	-	-	-	-	99.82
20	18/12/02	50.46	0.47	7.49	4.53	0.18	17.65	17.36	0.75	0.01	-	0.93	-	-	-	-	100.58
21	18/12/02	50.91	0.43	7.57	4.67	0.11	17.75	17.46	0.75	0.00	-	0.95	-	-	-	-	100.36
22	18/12/02	50.76	0.46	7.54	4.62	0.17	17.72	17.34	0.77	0.02	-	0.96	-	-	-	-	99.89
23	18/12/02	50.48	0.42	7.49	4.68	0.13	17.84	17.15	0.73	0.00	-	0.97	-	-	-	-	100.11
24	18/12/02	50.70	0.42	7.51	4.79	0.14	17.70	17.16	0.74	0.00	-	0.95	-	-	-	-	99.98
25	18/12/02	50.50	0.43	7.52	4.71	0.13	17.71	17.31	0.76	0.00	-	0.92	-	-	-	-	99.98
26	18/12/02	50.49	0.45	7.42	4.82	0.10	17.79	17.25	0.74	0.01	-	0.93	-	-	-	-	100.10
27	18/12/02	50.75	0.39	7.51	4.63	0.13	17.75	17.23	0.75	0.00	-	0.96	-	-	-	-	100.28
28	18/12/02	50.86	0.43	7.51	4.63	0.15	17.73	17.29	0.75	0.00	-	0.93	-	-	-	-	100.38
29	18/12/02	50.83	0.41	7.61	4.68	0.08	17.81	17.30	0.74	0.01	-	0.92	-	-	-	-	100.69
30	18/12/02	50.97	0.40	7.61	4.76	0.13	17.68	17.41	0.76	0.00	-	0.98	-	-	-	-	100.94
31	18/12/02	51.04	0.42	7.53	4.86	0.15	17.76	17.40	0.78	0.02	-	0.99	-	-	-	-	100.26
32	18/12/02	50.86	0.44	7.53	4.65	0.05	17.73	17.32	0.76	0.00	-	0.92	-	-	-	-	100.11

Appendix A 3.4: Electron microprobe analyses of standards

	Date	SiO2	TiO2	Al2O3	FeO	MnO	MgO	CaO	Na2O	K2O	P2O5	Cr2O3	NiO	ZnO	F	Cl	Total
33	18/12/02	50.74	0.42	7.51	4.58	0.12	17.69	17.29	0.76	0.01	-	1.00	-	-	-	-	100.58
34	18/12/02	51.11	0.40	7.52	4.80	0.08	17.75	17.24	0.77	0.00	-	0.93	-	-	-	-	100.35
35	22/1/03	50.64	0.422	7.46	4.81	0.11	17.70	17.53	0.73	0.00	-	0.95	-	-	-	-	100.35
36	22/1/03	50.66	0.39	7.50	4.78	0.08	17.82	17.68	0.75	0.00	-	1.00	-	-	-	-	100.67
37	22/1/03	50.96	0.36	7.18	4.62	0.13	17.83	17.50	0.73	0.02	-	0.92	-	-	-	-	100.23
38	22/1/03	50.65	0.42	7.36	4.56	0.14	17.66	17.50	0.73	0.01	-	0.92	-	-	-	-	99.96
39	22/1/03	50.69	0.40	7.38	4.93	0.13	17.81	17.62	0.72	0.01	-	0.93	-	-	-	-	100.61
40	22/1/03	51.00	0.43	7.44	4.53	0.12	17.71	17.55	0.72	0.01	-	0.91	-	-	-	-	100.44
41	22/1/03	50.71	0.44	7.33	4.78	0.14	17.67	17.67	0.71	0.00	-	0.97	-	-	-	-	100.42
42	22/1/03	50.94	0.42	7.43	4.60	0.13	17.76	17.68	0.72	0.00	-	0.92	-	-	-	-	100.59
43	22/1/03	50.77	0.45	7.41	4.63	0.12	17.79	17.42	0.73	0.00	-	0.89	-	-	-	-	100.21
44	22/1/03	50.64	0.35	7.34	4.80	0.11	17.74	17.60	0.73	0.00	-	0.92	-	-	-	-	100.22
45	22/1/03	50.67	0.42	7.25	4.72	0.11	17.66	17.61	0.71	0.02	-	0.96	-	-	-	-	100.13
46	22/1/03	50.77	0.37	7.50	4.70	0.11	17.83	17.51	0.72	0.02	-	0.96	-	-	-	-	100.48
47	22/1/03	50.69	0.45	7.53	4.59	0.15	17.63	17.54	0.74	0.00	-	0.97	-	-	-	-	100.30
48	22/1/03	50.91	0.42	7.55	4.78	0.12	17.80	17.51	0.72	0.01	-	0.95	-	-	-	-	100.74
49	22/1/03	50.21	0.40	7.36	4.82	0.12	17.59	17.57	0.74	0.01	-	0.95	-	-	-	-	99.77
50	22/1/03	49.98	0.37	7.21	4.83	0.14	17.63	17.59	0.74	0.00	-	0.93	-	-	-	-	99.43
51	11/3/03	50.01	0.43	7.54	4.91	0.10	17.60	17.38	0.74	0.00	-	0.88	-	-	-	-	99.59
52	11/3/03	50.76	0.40	7.52	4.71	0.12	17.65	17.19	0.75	0.00	-	0.84	-	-	-	-	99.93
53	11/3/03	50.68	0.37	7.54	4.92	0.09	17.64	17.31	0.78	0.00	-	0.78	-	-	-	-	100.11
54	11/3/03	50.52	0.35	7.41	4.72	0.11	17.61	17.34	0.80	0.02	-	0.76	-	-	-	-	99.63
55	11/3/03	50.64	0.36	7.40	4.72	0.09	17.69	17.32	0.77	0.00	-	0.78	-	-	-	-	99.78
56	11/3/03	50.66	0.37	7.37	4.59	0.08	17.47	17.13	0.80	0.00	-	0.79	-	-	-	-	99.25
57	11/3/03	50.81	0.40	7.51	4.64	0.12	17.55	17.46	0.76	0.01	-	0.79	-	-	-	-	100.06
58	11/3/03	50.85	0.41	7.45	4.65	0.09	17.53	17.29	0.76	0.01	-	0.86	-	-	-	-	99.89
59	11/3/03	49.89	0.39	7.34	4.53	0.11	17.54	17.48	0.78	0.00	-	0.80	-	-	-	-	98.84
60	11/3/03	50.40	0.35	7.40	4.73	0.08	17.65	17.39	0.77	0.00	-	0.80	-	-	-	-	99.56
61	11/3/03	49.91	0.37	7.34	4.58	0.10	17.47	17.18	0.79	0.00	-	0.78	-	-	-	-	98.53
62	11/3/03	49.40	0.32	7.29	4.63	0.10	17.54	17.32	0.78	0.00	-	0.76	-	-	-	-	98.13
63	11/3/03	49.86	0.33	7.46	4.81	0.14	17.52	17.25	0.80	0.00	-	0.80	-	-	-	-	98.95
64	11/3/03	50.02	0.33	7.33	4.64	0.07	17.59	16.98	0.77	0.00	-	0.75	-	-	-	-	98.48
65	11/3/03	50.35	0.31	7.37	4.86	0.08	17.57	17.32	0.78	0.00	-	0.78	-	-	-	-	99.41

Appendix A 3.4: Electron microprobe analyses of standards

	Date	SiO2	TiO2	Al2O3	FeO	MnO	MgO	CaO	Na2O	K2O	P2O5	Cr2O3	NiO	ZnO	F	Cl	Total
66	11/3/03	50.45	0.34	7.41	4.70	0.10	17.53	17.30	0.79	0.00	-	0.80	-	-	-	-	99.42
67	11/3/03	50.10	0.34	7.44	4.66	0.08	17.69	17.24	0.76	0.00	-	0.78	-	-	-	-	99.08
68	11/3/03	49.83	0.38	7.31	4.75	0.11	17.61	17.00	0.78	0.00	-	0.74	-	-	-	-	98.53
69	11/3/03	50.13	0.33	7.43	4.54	0.10	17.50	17.29	0.81	0.00	-	0.74	-	-	-	-	98.87
70	11/3/03	50.02	0.33	7.42	4.74	0.09	17.57	17.17	0.81	0.00	-	0.77	-	-	-	-	98.93
71	11/3/03	50.37	0.43	7.47	4.65	0.14	17.53	17.28	0.78	0.00	-	0.76	-	-	-	-	99.43
72	11/3/03	50.33	0.42	7.58	4.81	0.06	17.49	17.25	0.77	0.00	-	0.83	-	-	-	-	99.54
73	11/3/03	49.79	0.41	7.49	4.74	0.08	17.57	17.37	0.74	0.01	-	0.82	-	-	-	-	99.02
74	11/3/03	49.82	0.37	7.22	4.78	0.06	17.69	17.31	0.76	0.00	-	0.82	-	-	-	-	98.84
75	11/3/03	49.78	0.38	7.40	4.65	0.08	17.65	17.41	0.76	0.01	-	0.84	-	-	-	-	98.97
76	11/3/03	49.36	0.37	7.29	4.80	0.11	17.62	17.15	0.74	0.01	-	0.82	-	-	-	-	98.27
77	11/3/03	50.07	0.39	7.45	4.69	0.07	17.66	17.15	0.76	0.00	-	0.87	-	-	-	-	99.10
78	11/3/03	50.50	0.40	7.40	4.79	0.07	17.47	17.53	0.74	0.02	-	0.79	-	-	-	-	99.71
79	11/3/03	50.38	0.41	7.41	4.89	0.05	17.57	17.28	0.77	0.01	-	0.82	-	-	-	-	99.58
80	11/3/03	50.54	0.39	7.48	4.75	0.09	17.61	17.26	0.72	0.01	-	0.83	-	-	-	-	99.67
81	11/3/03	50.62	0.42	7.39	4.91	0.11	17.74	17.36	0.76	0.01	-	0.84	-	-	-	-	100.14
82	11/3/03	50.41	0.37	7.44	4.59	1.70	17.71	17.13	0.71	0.00	-	0.82	-	-	-	-	100.89
83	11/3/03	50.38	0.39	7.34	4.63	0.07	17.56	17.20	0.69	0.01	-	0.80	-	-	-	-	99.06
84	11/3/03	50.31	0.39	7.36	4.73	0.10	17.52	17.37	0.69	0.00	-	0.81	-	-	-	-	99.29
85	11/3/03	49.87	0.40	7.35	4.70	0.08	17.51	17.34	0.70	0.00	-	0.82	-	-	-	-	98.77
86	11/3/03	49.68	0.41	7.31	4.61	0.07	17.41	17.30	0.71	0.00	-	0.81	-	-	-	-	98.30
87	11/3/03	50.12	0.36	7.39	4.80	0.09	17.31	17.13	0.69	0.01	-	0.81	-	-	-	-	98.70
88	11/3/03	50.04	0.38	7.49	4.58	0.09	17.39	17.16	0.72	0.00	-	0.82	-	-	-	-	98.65
89	11/3/03	50.48	0.37	7.52	4.69	0.07	17.55	17.21	0.68	0.00	-	0.85	-	-	-	-	99.42
90	11/3/03	50.06	0.35	7.47	4.66	0.08	17.30	17.28	0.71	0.00	-	0.84	-	-	-	-	98.75
91	9/10/03	50.52	0.37	7.44	4.79	0.08	17.59	17.26	0.78	0.02	-	0.83	0.00	-	-	-	99.69
92	9/10/03	49.54	0.35	7.50	4.82	0.09	17.49	17.16	0.77	0.00	-	0.79	0.00	-	-	-	98.49
93	9/10/03	49.01	0.40	7.32	4.88	0.15	17.59	17.38	0.77	0.00	-	0.78	0.01	-	-	-	98.30
94	9/10/03	50.56	0.42	7.39	4.64	0.17	17.63	17.03	0.81	0.00	-	0.85	0.02	-	-	-	99.51
95	9/10/03	50.68	0.41	7.37	4.83	0.12	17.50	17.19	0.80	0.00	-	0.83	0.02	-	-	-	99.75
mean		**50.40**	**0.40**	**7.41**	**4.72**	**0.12**	**17.61**	**17.27**	**0.75**	**0.00**		**0.88**	**0.03**				**99.57**
std.dev.		**0.48**	**0.03**	**0.11**	**0.10**	**0.17**	**0.13**	**0.22**	**0.03**	**0.01**		**0.08**	**0.03**				**0.76**
Recom.		**50.48**	**0.51**	**8.03**	**4.66**	**0.12**	**17.32**	**17.30**	**0.84**			**0.09**					

Appendix A 3.4: Electron microprobe analyses of standards

	Date	SiO2	TiO2	Al2O3	FeO	MnO	MgO	CaO	Na2O	K2O	P2O5	Cr2O3	NiO	ZnO	F	Cl	Total
Ilmenite																	
1	4/9/02	0.00	45.45	0.00	46.61	4.71	0.28	-	-	-	-	0.02	0.00	0.10	-	-	97.17
2	4/9/02	0.05	45.80	0.00	46.35	4.73	0.30	-	-	-	-	0.00	0.07	0.04	-	-	97.32
3	4/9/02	0.00	45.47	0.00	46.52	4.67	0.25	-	-	-	-	0.01	0.00	0.18	-	-	97.11
4	4/9/02	0.02	45.82	0.00	46.09	4.71	0.29	-	-	-	-	0.00	0.03	0.03	-	-	96.99
5	4/9/02	0.03	45.57	0.02	46.84	4.80	0.25	-	-	-	-	0.04	0.00	0.00	-	-	97.55
6	4/9/02	0.02	45.73	0.02	47.02	4.73	0.27	-	-	-	-	0.04	0.04	0.00	-	-	97.86
7	4/9/02	0.00	45.49	0.00	46.26	4.78	0.26	-	-	-	-	0.00	0.01	0.11	-	-	96.91
mean		**0.02**	**45.64**	**0.01**	**46.51**	**4.74**	**0.27**					**0.01**	**0.03**				**97.29**
std.dev.		**0.02**	**0.16**	**0.01**	**0.35**	**0.05**	**0.02**					**0.02**	**0.03**				**0.36**
Recom.			**45.70**		**46.54**	**4.77**	**0.31**										**97.32**
Plagioclase																	
1	4/9/02	50.79	0.07	30.89	0.35	0.00	0.14	13.11	3.42	0.14	0.02	0.00	0.00	-	-	-	98.99
2	4/9/02	50.84	0.04	31.00	0.36	0.01	0.13	13.10	3.36	0.13	0.00	0.02	0.03	-	-	-	99.09
3	4/9/02	51.81	0.01	30.75	0.44	0.01	0.16	13.17	3.37	0.13	0.01	0.00	0.00	-	-	-	99.83
4	4/9/02	52.08	0.05	30.98	0.36	0.00	0.15	13.24	3.45	0.13	0.00	0.01	0.03	-	-	-	100.49
5	4/9/02	50.16	0.02	30.45	0.40	0.00	0.14	12.85	3.40	0.13	0.00	0.01	0.04	-	-	-	97.61
6	4/9/02	52.33	0.04	31.03	0.41	0.01	0.13	13.15	3.41	0.13	0.05	0.00	0.00	-	-	-	100.64
7	4/9/02	51.27	0.06	30.72	0.42	0.00	0.14	13.13	3.46	0.13	0.03	0.00	0.05	-	-	-	99.37
8	11/3/03	51.10	0.02	30.54	0.43	-	0.16	13.92	3.63	0.11	-	-	-	-	-	-	99.91
9	11/3/03	50.84	0.01	30.45	0.38	-	0.16	13.73	3.62	0.13	-	-	-	-	-	-	99.31
10	11/3/03	50.83	0.00	30.43	0.39	-	0.15	13.81	3.66	0.11	-	-	-	-	-	-	99.38
11	11/3/03	51.05	0.00	30.60	0.40	-	0.13	13.90	3.63	0.12	-	-	-	-	-	-	99.83
12	9/10/03	51.49	0.04	30.85	0.38	-	0.16	13.70	3.98	0.12	-	-	-	-	-	-	100.72
13	9/10/03	51.53	0.05	30.69	0.35	-	0.15	13.74	3.93	0.12	-	-	-	-	-	-	100.56
14	9/10/03	50.95	0.07	30.11	0.39	-	0.15	13.39	3.92	0.14	-	-	-	-	-	-	99.11
15	9/10/03	50.89	0.06	30.10	0.41	-	0.14	13.31	3.99	0.13	-	-	-	-	-	-	99.04
16	9/10/03	51.58	0.02	30.33	0.39	-	0.13	13.21	3.96	0.14	-	-	-	-	-	-	99.75
17	9/10/03	51.59	0.05	30.70	0.41	-	0.13	13.62	3.96	0.14	-	-	-	-	-	-	100.60
18	9/10/03	51.79	0.04	30.87	0.38	-	0.16	13.68	3.89	0.14	-	-	-	-	-	-	100.95
19	9/10/03	51.59	0.04	31.00	0.46	-	0.15	13.60	3.94	0.13	-	-	-	-	-	-	100.90

Appendix A 3.4: Electron microprobe analyses of standards

	Date	SiO2	TiO2	Al2O3	FeO	MnO	MgO	CaO	Na2O	K2O	P2O5	Cr2O3	NiO	ZnO	F	Cl	Total
mean		**51.29**	**0.04**	**30.66**	**0.39**	**0.00**	**0.15**	**13.44**	**3.68**	**0.13**	**0.02**	**0.01**	**0.02**				**99.79**
std.dev.		**0.53**	**0.02**	**0.29**	**0.03**	**0.00**	**0.01**	**0.32**	**0.25**	**0.01**	**0.02**	**0.01**	**0.02**				**0.86**
Recom.		**51.25**	**0.05**	**30.91**	**0.46**		**0.14**	**13.64**	**3.45**	**0.18**							**100.17**
Albite																	
1	9/10/03	68.65	0.02	20.25	0.00	-	0.04	0.40	11.71	0.19	-	-	-	-	-	-	101.26
2	9/10/03	68.90	0.00	20.02	0.02	-	0.01	0.25	11.88	0.17	-	-	-	-	-	-	101.26
3	9/10/03	67.16	0.05	19.37	0.03	-	0.00	0.14	11.90	0.16	-	-	-	-	-	-	98.82
4	9/10/03	67.31	0.00	19.64	0.03	-	0.00	0.28	11.87	0.22	-	-	-	-	-	-	99.35
5	9/10/03	68.44	0.02	19.91	0.00	-	0.01	0.31	11.77	0.29	-	-	-	-	-	-	100.76
6	9/10/03	69.44	0.01	20.14	0.02	-	0.00	0.24	11.76	0.19	-	-	-	-	-	-	101.80
7	9/10/03	68.48	0.00	19.89	0.00	-	0.01	0.15	11.77	0.22	-	-	-	-	-	-	100.51
8	9/10/03	68.56	0.00	20.08	0.00	-	0.01	0.29	11.87	0.28	-	-	-	-	-	-	101.09
mean		**68.37**	**0.01**	**19.91**	**0.01**		**0.01**	**0.26**	**11.82**	**0.21**							**100.60**
std.dev.		**0.77**	**0.02**	**0.28**	**0.01**		**0.01**	**0.08**	**0.07**	**0.05**							**1.02**
Recom.		**68.14**	**0.00**	**20.26**	**0.86**		**0.00**	**0.24**	**11.44**	**0.27**							**100.43**
Anorthite																	
1	9/10/03	44.21	0.00	35.68	0.46	-	0.04	19.85	0.54	0.01	-	-	-	-	-	-	100.78
2	9/10/03	44.02	0.02	35.71	0.41	-	0.06	19.93	0.59	0.02	-	-	-	-	-	-	100.76
3	9/10/03	43.34	0.01	34.71	0.50	-	0.07	19.38	0.56	0.01	-	-	-	-	-	-	98.58
4	9/10/03	43.18	0.00	34.91	0.42	-	0.06	19.23	0.57	0.00	-	-	-	-	-	-	98.37
5	9/10/03	43.64	0.01	35.26	0.45	-	0.05	19.49	0.57	0.01	-	-	-	-	-	-	99.48
6	9/10/03	44.33	0.03	35.98	0.44	-	0.04	19.72	0.59	0.00	-	-	-	-	-	-	101.12
7	9/10/03	44.50	0.00	35.94	0.50	-	0.06	19.63	0.55	0.02	-	-	-	-	-	-	101.20
8	9/10/03	44.27	0.01	35.97	0.45	-	0.07	19.80	0.57	0.01	-	-	-	-	-	-	101.14
mean		**43.94**	**0.01**	**35.52**	**0.45**		**0.05**	**19.63**	**0.57**	**0.01**							**100.18**
std.dev.		**0.49**	**0.01**	**0.50**	**0.03**		**0.01**	**0.24**	**0.02**	**0.01**							**1.19**
Recom.		**44.00**	**0.03**	**36.03**	**0.67**		**0.02**	**19.09**	**0.53**	**0.03**							**100.33**

Appendix A 3.4: Electron microprobe analyses of standards

	Date	SiO2	TiO2	Al2O3	FeO	MnO	MgO	CaO	Na2O	K2O	P2O5	Cr2O3	NiO	ZnO	F	Cl	Total
Basaltic glass - Juan de Fuca Ridge VG-2																	
1	4/9/02	50.76	1.90	13.99	11.88	0.19	6.87	11.52	2.68	0.16	0.25	-	-	-	0.00	0.00	100.19
2	4/9/02	49.21	1.98	13.71	11.23	0.24	6.74	11.13	2.62	0.21	0.20	-	-	-	0.00	0.04	97.32
3	4/9/02	50.58	1.91	13.80	12.19	0.15	6.86	11.58	2.67	0.20	0.23	-	-	-	0.00	0.01	100.19
4	4/9/02	49.57	1.86	13.70	11.76	0.19	6.90	11.33	2.63	0.21	0.19	-	-	-	0.00	0.04	98.39
5	4/9/02	50.76	1.90	13.99	11.88	0.19	6.87	11.52	2.68	0.16	0.25	-	-	-	0.00	0.00	100.19
6	4/9/02	49.42	1.91	14.04	11.62	0.18	6.78	11.50	2.63	0.22	0.23	-	-	-	0.00	0.04	98.57
7	4/9/02	50.96	1.84	14.12	11.90	0.31	6.86	11.36	2.67	0.22	0.25	-	-	-	0.00	0.02	100.51
8	4/9/02	49.57	1.86	13.70	11.76	0.19	6.90	11.33	2.64	0.21	0.19	-	-	-	0.00	0.04	98.39
9	4/9/02	50.40	1.96	13.94	11.60	0.21	6.71	11.34	2.64	0.19	0.21	-	-	-	0.00	0.05	99.24
10	4/9/02	50.40	1.86	13.93	12.38	0.24	6.75	11.32	2.66	0.22	0.24	-	-	-	0.00	0.03	100.00
11	4/9/02	49.07	1.96	13.77	12.22	0.18	6.73	11.13	2.66	0.21	0.19	-	-	-	0.00	0.04	98.15
12	4/9/02	51.81	1.91	13.95	12.26	0.10	6.97	11.36	2.71	0.18	0.26	-	-	-	0.00	0.00	101.49
13	4/9/02	51.57	1.89	13.83	12.46	0.18	6.68	11.26	2.77	0.17	0.23	-	-	-	0.00	0.02	101.05
14	4/9/02	48.83	1.91	13.56	12.27	0.20	6.50	10.96	2.73	0.16	0.19	-	-	-	0.00	0.01	97.33
15	4/9/02	50.11	1.99	13.77	12.50	0.19	6.69	11.15	2.71	0.18	0.21	-	-	-	0.00	0.04	99.54
16	4/9/02	51.57	1.89	13.83	12.46	0.18	6.68	11.26	2.77	0.17	0.23	-	-	-	0.00	0.02	101.05
17	4/9/02	49.55	1.84	13.79	12.32	0.27	6.50	11.10	2.67	0.18	0.19	-	-	-	0.00	0.03	98.45
18	4/9/02	50.05	2.00	13.84	12.06	0.20	6.72	11.26	2.69	0.19	0.23	-	-	-	0.00	0.00	99.23
19	4/9/02	50.00	1.93	13.82	12.59	0.17	6.84	11.13	2.69	0.21	0.27	-	-	-	0.00	0.04	99.69
20	4/9/02	51.35	1.85	14.00	12.56	0.25	6.82	11.37	2.74	0.20	0.24	-	-	-	0.00	0.03	101.41
21	4/9/02	50.10	1.94	13.83	12.36	0.21	6.58	10.98	2.72	0.17	0.23	-	-	-	0.00	0.01	99.14
22	4/9/02	50.42	1.93	13.93	12.85	0.20	6.60	11.14	2.66	0.17	0.20	-	-	-	0.00	0.02	100.13
23	18/12/02	50.90	1.91	14.19	11.27	0.25	7.17	11.28	2.64	0.19	0.24	-	-	-	0.01	0.03	100.08
24	18/12/02	50.49	1.90	14.23	12.04	0.22	7.03	11.26	2.65	0.19	0.20	-	-	-	0.00	0.00	100.20
25	18/12/02	50.68	1.98	14.17	12.07	0.27	7.02	11.26	2.70	0.16	0.23	-	-	-	0.00	0.05	100.59
26	18/12/02	50.98	1.94	14.07	11.84	0.22	7.25	11.45	2.69	0.21	0.20	-	-	-	0.00	0.05	100.89
27	18/12/02	50.88	1.88	13.86	12.09	0.26	6.98	11.08	2.70	0.21	0.17	-	-	-	0.00	0.03	100.14
28	18/12/02	51.00	2.07	14.20	12.08	0.20	6.96	11.06	2.69	0.23	0.16	-	-	-	0.00	0.05	100.70
29	18/12/02	51.07	1.95	14.06	12.03	0.24	7.07	11.24	2.68	0.19	0.21	-	-	-	0.00	0.02	100.76
30	18/12/02	50.88	1.97	13.91	11.61	0.19	6.90	10.99	2.72	0.19	0.23	-	-	-	0.01	0.05	99.65
31	18/12/02	50.89	1.99	13.68	11.87	0.20	6.92	11.06	2.72	0.23	0.20	-	-	-	0.00	0.04	99.80
32	18/12/02	51.17	1.97	13.77	12.27	0.13	6.95	10.96	2.72	0.19	0.19	-	-	-	0.00	0.04	100.34

Appendix A 3.4: Electron microprobe analyses of standards

	Date	SiO2	TiO2	Al2O3	FeO	MnO	MgO	CaO	Na2O	K2O	P2O5	Cr2O3	NiO	ZnO	F	Cl	Total
33	18/12/02	50.46	1.97	13.89	12.25	0.31	6.87	11.04	2.69	0.20	0.21	-	-	-	0.00	0.04	99.93
34	18/12/02	50.44	1.96	13.80	12.24	0.30	6.92	10.92	2.79	0.17	0.20	-	-	-	0.00	0.00	99.75
35	18/12/02	50.93	1.88	13.88	11.83	0.20	6.87	10.85	2.70	0.20	0.20	-	-	-	0.00	0.02	99.55
36	18/12/02	50.68	1.94	13.74	12.35	0.31	6.88	11.11	2.70	0.20	0.20	-	-	-	0.00	0.05	100.15
37	22/1/03	50.76	1.92	14.06	12.14	0.20	6.99	10.86	2.72	0.19	0.19	-	-	-	0.00	0.02	100.06
38	22/1/03	50.18	1.92	14.28	11.63	0.21	6.96	11.13	2.65	0.18	0.19	-	-	-	0.00	0.03	99.36
39	22/1/03	49.77	1.83	14.19	12.14	0.16	7.04	10.93	2.74	0.18	0.29	-	-	-	0.00	0.03	99.30
40	22/1/03	50.40	1.84	14.29	12.41	0.10	7.08	11.13	2.65	0.20	0.23	-	-	-	0.00	0.03	100.36
41	22/1/03	50.55	1.97	14.21	11.79	0.25	7.00	11.06	2.70	0.21	0.20	-	-	-	0.00	0.04	99.98
42	22/1/03	49.12	1.80	14.13	11.84	0.23	7.19	10.99	2.64	0.20	0.23	-	-	-	0.00	0.03	98.40
43	22/1/03	50.41	1.89	14.21	12.09	0.21	7.14	11.04	2.59	0.22	0.22	-	-	-	0.00	0.02	100.05
44	22/1/03	50.40	1.85	14.25	11.85	0.14	7.03	11.13	2.61	0.18	0.18	-	-	-	0.00	0.05	99.67
45	22/1/03	50.16	1.82	14.11	12.45	0.23	7.04	10.97	2.65	0.17	0.22	-	-	-	0.00	0.04	99.87
46	22/1/03	50.18	1.88	14.09	12.15	0.20	7.00	10.94	2.66	0.20	0.24	-	-	-	0.00	0.02	99.55
47	22/1/03	50.23	1.81	14.39	11.98	0.22	6.99	11.08	2.61	0.21	0.21	-	-	-	0.00	0.04	99.76
48	22/1/03	50.09	1.94	14.31	12.05	0.26	6.90	11.18	2.55	0.22	0.24	-	-	-	0.00	0.04	99.76
49	22/1/03	50.60	1.95	14.32	11.89	0.21	7.07	11.18	2.67	0.19	0.23	-	-	-	0.00	0.07	100.37
50	22/1/03	51.06	1.84	14.20	11.79	0.16	6.95	10.94	2.63	0.18	0.21	-	-	-	0.00	0.02	99.97
51	22/1/03	50.49	1.92	14.26	11.39	0.27	7.02	11.10	2.65	0.21	0.23	-	-	-	0.00	0.03	99.56
52	22/1/03	51.04	1.82	14.24	12.11	0.24	7.01	11.25	2.62	0.20	0.21	-	-	-	0.02	0.04	100.79
53	22/1/03	50.63	1.90	14.04	11.70	0.19	6.96	10.74	2.60	0.19	0.22	-	-	-	0.00	0.02	99.19
54	22/1/03	50.31	1.91	14.00	11.77	0.17	6.94	10.92	2.67	0.19	0.24	-	-	-	0.00	0.02	99.14
55	22/1/03	50.95	2.02	14.23	12.01	0.20	6.92	10.98	2.62	0.20	0.22	-	-	-	0.00	0.02	100.36
56	22/1/03	50.85	1.90	14.16	12.18	0.23	7.02	10.82	2.70	0.19	0.24	-	-	-	0.00	0.04	100.31
57	22/1/03	50.72	1.92	14.09	12.09	0.18	6.94	11.04	2.66	0.19	0.20	-	-	-	0.00	0.03	100.05
58	22/1/03	51.01	1.79	14.31	11.84	0.25	7.02	11.02	2.59	0.18	0.20	-	-	-	0.00	0.05	100.25
59	22/1/03	49.81	1.90	13.99	12.08	0.21	6.96	10.94	2.71	0.19	0.21	-	-	-	0.00	0.03	99.04
60	22/1/03	50.97	1.87	14.34	12.04	0.14	7.04	10.90	2.59	0.19	0.25	-	-	-	0.00	0.03	100.35
61	22/1/03	51.13	1.85	14.27	11.85	0.27	7.13	11.01	2.68	0.17	0.20	-	-	-	0.00	0.03	100.57
62	22/1/03	50.50	1.91	14.09	11.96	0.23	6.97	10.95	2.70	0.21	0.19	-	-	-	0.00	0.05	99.75
63	22/1/03	49.88	1.93	14.14	11.23	0.21	6.99	10.87	2.64	0.19	0.17	-	-	-	0.00	0.03	98.30
64	22/1/03	50.81	1.91	14.14	12.12	0.25	7.04	10.81	2.67	0.20	0.19	-	-	-	0.00	0.04	100.18
65	22/1/03	50.72	2.03	13.91	12.00	0.26	6.97	10.81	2.74	0.19	0.20	-	-	-	0.00	0.03	99.85

Appendix A 3.4: Electron microprobe analyses of standards

	Date	SiO2	TiO2	Al2O3	FeO	MnO	MgO	CaO	Na2O	K2O	P2O5	Cr2O3	NiO	ZnO	F	Cl	Total
66	22/1/03	49.81	1.85	14.24	12.36	0.18	6.76	10.87	2.73	0.19	0.22	-	-	-	0.00	0.02	99.23
67	22/1/03	50.11	1.87	14.22	12.62	0.19	6.86	10.71	2.70	0.21	0.20	-	-	-	0.00	0.03	99.70
68	22/1/03	50.20	1.89	14.04	12.68	0.22	6.86	10.83	2.73	0.18	0.23	-	-	-	0.00	0.04	99.89
69	22/1/03	50.28	1.94	14.17	12.38	0.18	6.83	11.00	2.66	0.18	0.18	-	-	-	0.00	0.02	99.81
70	22/1/03	50.04	1.88	14.19	12.64	0.23	6.86	10.93	2.66	0.20	0.18	-	-	-	0.00	0.05	99.85
71	22/1/03	50.40	1.85	14.29	12.07	0.19	6.79	10.91	2.67	0.18	0.20	-	-	-	0.00	0.05	99.58
72	22/1/03	50.76	1.94	14.07	12.48	0.14	6.84	10.87	2.72	0.17	0.16	-	-	-	0.00	0.04	100.20
73	22/1/03	50.60	1.90	14.20	12.24	0.16	6.84	10.99	2.74	0.20	0.18	-	-	-	0.00	0.00	100.05
74	22/1/03	50.42	1.95	14.22	12.11	0.19	6.88	10.91	2.70	0.18	0.21	-	-	-	0.00	0.02	99.79
75	22/1/03	50.65	2.03	14.04	12.83	0.16	6.93	10.96	2.70	0.20	0.20	-	-	-	0.00	0.00	100.69
76	22/1/03	50.19	1.90	13.94	12.42	0.23	6.83	11.01	2.69	0.17	0.22	-	-	-	0.00	0.04	99.64
77	22/1/03	50.59	1.93	13.96	12.55	0.24	6.92	10.90	2.68	0.20	0.20	-	-	-	0.00	0.02	100.19
78	22/1/03	51.06	1.95	14.07	12.57	0.22	6.90	10.73	2.77	0.21	0.23	-	-	-	0.00	0.02	100.72
79	22/1/03	51.20	1.96	14.15	12.33	0.21	6.89	10.74	2.70	0.18	0.20	-	-	-	0.00	0.05	100.62
80	22/1/03	51.07	1.93	14.15	12.18	0.16	6.79	10.84	2.61	0.20	0.25	-	-	-	0.00	0.04	100.21
81	22/1/03	50.54	1.84	14.08	11.85	0.29	6.83	10.73	2.67	0.22	0.23	-	-	-	0.00	0.03	99.31
82	22/1/03	50.06	2.06	14.17	11.83	0.19	6.95	10.59	2.62	0.19	0.17	-	-	-	0.00	0.02	98.84
83	22/1/03	50.80	1.95	14.32	12.03	0.19	6.86	10.82	2.67	0.19	0.20	-	-	-	0.00	0.05	100.07
84	22/1/03	50.77	1.87	14.25	11.96	0.22	6.88	10.80	2.70	0.18	0.17	-	-	-	0.00	0.04	99.84
85	22/1/03	51.17	2.00	14.08	12.53	0.21	6.96	10.81	2.74	0.21	0.19	-	-	-	0.00	0.02	100.91
86	22/1/03	50.80	1.99	14.05	12.58	0.18	6.81	10.80	2.71	0.19	0.23	-	-	-	0.00	0.04	100.37
87	22/1/03	50.98	2.01	14.14	12.36	0.20	6.85	10.75	2.74	0.15	0.21	-	-	-	0.00	0.02	100.40
88	22/1/03	50.99	1.94	14.12	12.57	0.24	6.79	10.87	2.70	0.19	0.20	-	-	-	0.00	0.03	100.64
89	22/1/03	50.28	2.03	13.98	12.60	0.16	6.90	10.90	2.70	0.19	0.20	-	-	-	0.01	0.01	99.96
90	22/1/03	50.08	1.86	13.92	12.35	0.25	6.75	10.81	2.75	0.18	0.21	-	-	-	0.00	0.04	99.20
91	22/1/03	50.62	1.85	14.06	12.13	0.21	6.82	11.08	2.71	0.22	0.23	-	-	-	0.00	0.03	99.97
92	22/1/03	50.52	1.92	13.85	11.81	0.22	6.74	11.04	2.71	0.19	0.19	-	-	-	0.00	0.02	99.20
mean		**50.50**	**1.92**	**14.05**	**12.11**	**0.21**	**6.90**	**11.04**	**2.68**	**0.19**	**0.21**				**0.00**	**0.03**	**99.84**
std.dev.		**0.56**	**0.06**	**0.18**	**0.34**	**0.04**	**0.14**	**0.21**	**0.05**	**0.02**	**0.02**				**0.00**	**0.01**	**0.78**
Recom.		**50.81**	**1.85**	**14.06**	**11.84**	**0.22**	**6.71**	**11.12**	**2.62**	**0.19**	**0.20**				**0.20**	**1.20**	**99.62**

Appendix A 3.4: Electron microprobe analyses of standards

	Date	SiO2	TiO2	Al2O3	FeO	MnO	MgO	CaO	Na2O	K2O	P2O5	Cr2O3	NiO	ZnO	F	Cl	Total
CFA trachyte																	
1	18/12/02	60.90	0.22	18.27	2.77	0.13	0.34	1.83	5.38	8.02	0.08	-	-	-	0.16	0.43	98.61
2	18/12/02	61.46	0.04	18.14	2.80	0.28	0.36	1.98	5.52	8.04	0.07	-	-	-	0.13	0.37	99.18
3	18/12/02	61.05	0.12	18.36	2.53	0.25	0.38	1.99	5.36	7.96	0.11	-	-	-	0.15	0.36	98.64
4	18/12/02	61.14	0.25	18.40	2.79	0.20	0.39	1.83	5.51	8.04	0.05	-	-	-	0.17	0.37	99.16
5	22/1/03	61.96	0.27	18.76	2.24	0.20	0.35	1.86	5.47	7.88	0.13	-	-	-	0.15	0.43	99.69
6	22/1/03	61.47	0.13	18.87	2.51	0.16	0.34	1.86	5.44	8.14	0.09	-	-	-	0.14	0.33	99.49
7	22/1/03	60.34	0.34	18.44	3.17	0.22	0.44	2.62	5.24	7.83	0.12	-	-	-	0.15	0.40	99.34
8	22/1/03	61.89	0.17	19.05	2.37	0.11	0.31	1.86	5.21	8.44	0.14	-	-	-	0.10	0.35	100.03
9	22/1/03	61.83	0.26	18.65	2.59	0.20	0.38	1.90	5.47	7.95	0.12	-	-	-	0.20	0.35	99.92
10	22/1/03	61.54	0.34	18.64	2.66	0.22	0.36	1.92	5.50	8.22	0.07	-	-	-	0.11	0.37	99.92
11	22/1/03	61.86	0.32	18.71	2.58	0.28	0.35	1.96	5.49	8.04	0.04	-	-	-	0.13	0.38	100.17
12	22/1/03	61.93	0.25	18.52	2.64	0.16	0.39	1.80	5.41	8.01	0.07	-	-	-	0.12	0.33	99.60
13	22/1/03	61.74	0.23	18.51	2.59	0.20	0.39	1.97	5.43	8.17	0.11	-	-	-	0.12	0.35	99.84
14	11/3/03	61.25	0.55	18.38	2.76	0.13	0.39	1.97	5.58	7.96	0.15	-	-	-	0.12	0.40	99.75
15	11/3/03	60.74	0.50	17.98	3.20	0.11	0.36	1.93	5.56	8.24	0.11	-	-	-	0.18	0.38	99.30
16	11/3/03	61.82	0.29	18.26	3.00	0.11	0.38	1.92	5.64	7.67	0.15	-	-	-	0.19	0.37	99.79
17	11/3/03	60.64	0.47	17.94	2.69	0.08	0.33	1.86	5.59	8.06	0.12	-	-	-	0.20	0.33	98.31
18	11/3/03	60.39	0.37	18.17	3.05	0.18	0.37	1.96	5.65	8.05	0.10	-	-	-	0.17	0.42	98.86
19	11/3/03	60.48	0.44	17.94	2.70	0.13	0.35	1.90	5.61	7.98	0.12	-	-	-	0.21	0.36	98.22
20	11/3/03	60.39	0.37	17.78	2.76	0.12	0.34	1.92	5.62	7.92	0.17	-	-	-	0.20	0.43	98.01
21	11/3/03	60.17	0.32	17.98	2.74	0.11	0.33	1.90	5.68	8.00	0.09	-	-	-	0.17	0.41	97.91
mean		**61.19**	**0.30**	**18.37**	**2.72**	**0.17**	**0.36**	**1.94**	**5.49**	**8.03**	**0.10**				**0.15**	**0.38**	**99.23**
std.dev.		**0.62**	**0.13**	**0.34**	**0.24**	**0.06**	**0.03**	**0.16**	**0.13**	**0.16**	**0.03**				**0.03**	**0.03**	**0.70**
Recom.		**61.63**	**0.42**	**18.53**	**2.65**	**0.18**	**0.42**	**1.84**	**5.37**	**7.98**							**99.71**
Lipari obsidian																	
1	18/12/02	73.92	0.16	12.93	1.61	0.10	0.04	0.80	3.81	5.11	0.04	-	-	-	0.13	0.30	98.93
2	18/12/02	73.42	0.14	12.68	1.43	0.02	0.05	0.75	4.00	5.27	0.04	-	-	-	0.12	0.24	98.20
3	18/12/02	74.12	0.01	13.03	1.44	0.00	0.04	0.79	3.97	5.29	0.01	-	-	-	0.08	0.30	99.08
4	18/12/02	74.09	0.01	13.18	1.17	0.07	0.04	0.77	3.84	5.39	0.06	-	-	-	0.08	0.25	99.01
5	18/12/02	73.66	0.00	12.99	1.78	0.12	0.02	0.75	3.92	5.05	0.01	-	-	-	0.10	0.28	98.73

Appendix A 3.4: Electron microprobe analyses of standards

	Date	SiO2	TiO2	Al2O3	FeO	MnO	MgO	CaO	Na2O	K2O	P2O5	Cr2O3	NiO	ZnO	F	Cl	Total
6	22/1/03	74.09	0.08	13.18	1.23	0.04	0.04	0.75	4.03	4.98	0.04	-	-	-	0.15	0.28	98.96
7	22/1/03	74.01	0.12	13.41	1.41	0.16	0.03	0.75	4.04	5.14	0.04	-	-	-	0.16	0.27	99.57
8	22/1/03	74.34	0.01	13.26	1.57	0.20	0.04	0.73	4.03	5.18	0.02	-	-	-	0.10	0.28	99.77
9	22/1/03	74.21	0.00	13.53	1.53	0.04	0.02	0.74	4.04	5.30	0.02	-	-	-	0.12	0.28	99.88
10	22/1/03	74.32	0.03	13.34	1.28	0.09	0.05	0.76	4.01	5.11	0.04	-	-	-	0.12	0.28	99.43
11	22/1/03	74.58	0.09	13.33	1.58	0.09	0.04	0.72	3.95	5.35	0.03	-	-	-	0.11	0.22	100.11
12	22/1/03	74.20	0.01	13.28	1.17	0.08	0.05	0.72	4.05	5.30	0.07	-	-	-	0.11	0.24	99.27
13	22/1/03	74.76	0.16	13.18	1.25	0.05	0.03	0.79	3.99	5.30	0.01	-	-	-	0.07	0.23	99.86
14	22/1/03	74.55	0.00	13.08	1.42	0.07	0.02	0.74	3.93	5.00	0.01	-	-	-	0.15	0.31	99.26
15	11/3/03	74.12	0.00	13.25	1.42	0.06	0.03	0.81	4.00	5.12	0.03	-	-	-	0.07	0.26	99.23
16	11/3/03	73.68	0.00	12.74	1.47	0.01	0.02	0.71	3.91	5.03	0.03	-	-	-	0.14	0.22	97.94
17	11/3/03	73.91	0.04	12.81	1.60	0.08	0.02	0.75	3.97	5.10	0.04	-	-	-	0.14	0.27	98.71
18	11/3/03	73.45	0.05	13.01	1.66	0.01	0.02	0.73	4.00	4.92	0.04	-	-	-	0.12	0.27	98.28
19	11/3/03	73.47	0.09	12.91	1.58	0.01	0.01	0.72	4.02	5.28	0.04	-	-	-	0.14	0.23	98.49
20	11/3/03	73.50	0.07	12.84	1.57	0.02	0.03	0.75	3.99	5.25	0.03	-	-	-	0.14	0.20	98.37
21	11/3/03	74.03	0.07	12.98	1.63	0.02	0.03	0.67	4.01	5.13	0.02	-	-	-	0.15	0.25	98.98
22	11/3/03	73.04	0.09	12.64	1.74	0.01	0.02	0.74	4.06	5.00	0.03	-	-	-	0.15	0.27	97.78
mean		**73.98**	**0.06**	**13.07**	**1.48**	**0.06**	**0.03**	**0.75**	**3.98**	**5.16**	**0.03**				**0.12**	**0.26**	**98.99**
std.dev.		**0.43**	**0.05**	**0.24**	**0.18**	**0.05**	**0.01**	**0.03**	**0.07**	**0.13**	**0.02**				**0.03**	**0.03**	**0.64**
Recom.		**74.35**	**0.00**	**12.97**	**1.51**	**0.18**	**0.05**	**0.74**	**3.93**	**5.11**							**98.98**
RH 12 rhyolite																	
1	18/12/02	74.38	0.03	13.07	1.42	0.09	0.04	0.73	4.06	4.97	0.05	-	-	-	0.10	0.26	99.21
2	18/12/02	74.25	0.03	13.00	1.39	0.12	0.02	0.76	4.04	4.95	0.03	-	-	-	0.13	0.28	99.03
3	18/12/02	74.03	0.01	13.24	1.30	0.00	0.04	0.82	3.98	4.99	0.00	-	-	-	0.13	0.26	98.80
4	18/12/02	74.26	0.04	13.12	1.32	0.00	0.04	0.82	4.01	5.04	0.10	-	-	-	0.13	0.26	99.16
mean		**74.23**	**0.03**	**13.11**	**1.36**	**0.05**	**0.03**	**0.78**	**4.02**	**4.99**	**0.04**				**0.12**	**0.26**	**99.05**
std.dev.		**0.15**	**0.01**	**0.10**	**0.06**	**0.06**	**0.01**	**0.05**	**0.03**	**0.04**	**0.04**				**0.02**	**0.01**	**0.18**
Recom.		**73.67**	**0.07**	**13.82**	**1.56**	**0.07**	**0.31**	**0.75**	**3.81**	**5.17**	**0.01**						**99.24**

Appendix A 3.4: Electron microprobe analyses of standards

	Date	SiO2	TiO2	Al2O3	FeO	MnO	MgO	CaO	Na2O	K2O	P2O5	Cr2O3	NiO	ZnO	F	Cl	Total
KN 18 Rhyolite																	
1	22/1/03	75.30	0.05	10.87	3.28	0.05	0.03	0.20	5.26	4.49	0.05	-	-	-	0.47	0.23	100.29
2	22/1/03	74.85	0.00	10.94	3.31	0.05	0.02	0.12	5.14	4.52	0.02	-	-	-	0.32	0.21	99.56
3	22/1/03	74.22	0.03	10.84	3.44	0.08	0.00	0.13	5.19	4.58	0.02	-	-	-	0.33	0.29	99.17
4	22/1/03	73.41	0.00	11.03	3.61	0.13	0.00	0.03	5.19	4.42	0.09	-	-	-	0.32	0.23	98.50
5	22/1/03	75.35	0.23	11.01	3.58	0.07	0.02	0.17	5.26	4.57	0.03	-	-	-	0.38	0.26	100.99
6	22/1/03	74.71	0.23	10.76	3.40	0.00	0.02	0.09	5.22	4.61	0.01	-	-	-	0.41	0.27	99.71
7	22/1/03	75.32	0.05	10.84	3.09	0.11	0.01	0.13	5.10	4.40	0.01	-	-	-	0.38	0.27	99.75
8	22/1/03	75.53	0.10	10.76	3.13	0.12	0.01	0.10	5.17	4.53	0.03	-	-	-	0.39	0.22	100.14
9	11/3/03	75.26	0.09	10.57	3.44	0.04	0.01	0.05	5.35	4.57	0.05	-	-	-	0.33	0.24	100.06
10	11/3/03	73.94	0.10	10.63	3.51	0.00	0.01	0.29	5.27	4.46	0.09	-	-	-	0.51	0.23	99.05
11	11/3/03	74.78	0.14	10.87	3.63	0.03	0.00	0.06	5.27	4.60	0.05	-	-	-	0.35	0.23	100.03
12	11/3/03	74.83	0.17	10.62	3.49	0.01	0.00	0.02	5.12	4.54	0.04	-	-	-	0.35	0.22	99.41
13	11/3/03	74.76	0.28	10.57	3.69	0.00	0.00	0.01	5.31	4.38	0.06	-	-	-	0.37	0.26	99.69
14	11/3/03	74.00	0.21	10.41	3.71	0.01	0.00	0.09	5.17	4.42	0.05	-	-	-	0.40	0.20	98.67
15	11/3/03	73.65	0.24	10.52	3.63	0.00	0.00	0.11	5.18	4.50	0.05	-	-	-	0.38	0.19	98.49
16	11/3/03	73.16	0.14	10.42	3.78	0.08	0.01	0.06	5.20	4.51	0.05	-	-	-	0.36	0.28	98.04
mean		**74.57**	**0.13**	**10.73**	**3.48**	**0.05**	**0.01**	**0.10**	**5.21**	**4.50**	**0.04**				**0.38**	**0.24**	**99.47**
std.dev.		**0.75**	**0.09**	**0.20**	**0.20**	**0.05**	**0.01**	**0.07**	**0.07**	**0.07**	**0.02**				**0.05**	**0.03**	**0.78**
Recom.		**74.60**	**0.18**	**10.53**	**3.45**	**0.06**		**0.15**	**5.68**	**4.39**	**0.01**						**100.05**
Basaltic glass - Makapui Lava Lake HI VG-A99																	
1	4/9/02	51.11	3.95	12.65	13.27	0.17	5.09	9.51	2.62	0.79	0.35	-	-	-	0.00	0.04	99.54
2	4/9/02	50.85	4.14	12.58	13.16	0.20	5.00	9.54	2.61	0.78	0.36	-	-	-	0.01	0.03	99.26
3	4/9/02	50.46	4.20	12.53	13.25	0.21	4.95	9.39	2.67	0.75	0.36	-	-	-	0.00	0.04	98.80
4	4/9/02	51.43	3.93	12.69	13.36	0.21	4.98	9.20	2.70	0.82	0.39	-	-	-	0.01	0.00	99.72
5	4/9/02	50.71	4.08	12.35	13.27	0.20	4.97	9.36	2.69	0.81	0.39	-	-	-	0.00	0.02	98.85
6	4/9/02	51.43	3.93	12.69	13.36	0.21	4.98	9.20	2.70	0.82	0.39	-	-	-	0.01	0.00	99.72
7	4/9/02	49.63	3.94	12.58	13.60	0.17	4.87	9.36	2.70	0.81	0.34	-	-	-	0.00	0.01	98.02
8	18/12/02	51.28	4.12	12.85	13.18	0.29	5.23	9.36	2.70	0.79	0.30	-	-	-	0.01	0.04	100.16
9	18/12/02	51.45	4.19	12.62	13.61	0.17	5.24	9.46	2.73	0.78	0.29	-	-	-	0.00	0.04	100.58
10	18/12/02	51.18	4.15	12.54	13.49	0.19	5.32	9.53	2.65	0.83	0.35	-	-	-	0.03	0.00	100.28
11	18/12/02	51.37	4.32	12.47	13.96	0.24	5.28	9.37	2.75	0.85	0.30	-	-	-	0.06	0.03	100.99

Appendix A 3.4: Electron microprobe analyses of standards

	Date	SiO2	TiO2	Al2O3	FeO	MnO	MgO	CaO	Na2O	K2O	P2O5	Cr2O3	NiO	ZnO	F	Cl	Total
12	18/12/02	51.15	4.12	12.65	13.52	0.24	5.08	9.26	2.69	0.81	0.29	-	-	-	0.03	0.02	99.85
13	18/12/02	51.36	4.22	12.60	13.36	0.19	5.18	9.39	2.65	0.80	0.34	-	-	-	0.00	0.01	100.10
14	18/12/02	51.13	4.17	12.61	13.71	0.12	5.11	9.53	2.67	0.81	0.28	-	-	-	0.01	0.01	100.16
15	18/12/02	51.42	4.14	12.53	13.21	0.20	5.17	9.33	2.69	0.79	0.30	-	-	-	0.00	0.00	99.77
16	22/01/02	51.10	3.88	12.83	13.23	0.19	5.05	9.40	2.73	0.83	0.33	-	-	-	0.02	0.03	99.62
17	22/01/02	50.69	4.00	12.71	13.50	0.15	5.06	9.20	2.67	0.77	0.35	-	-	-	0.05	0.00	99.16
18	22/01/02	50.60	4.02	12.78	13.88	0.14	5.06	9.28	2.67	0.81	0.34	-	-	-	0.00	0.03	99.61
19	22/01/02	51.01	4.09	12.75	13.24	0.23	5.04	9.44	2.69	0.81	0.35	-	-	-	0.02	0.02	99.67
20	22/01/02	50.39	4.12	12.84	13.83	0.29	5.24	9.42	2.68	0.78	0.36	-	-	-	0.04	0.02	99.98
21	22/01/02	50.98	4.25	12.73	14.09	0.19	5.09	8.99	2.76	0.73	0.35	-	-	-	0.02	0.03	100.19
22	22/01/02	50.95	4.08	12.92	13.85	0.25	5.13	9.25	2.67	0.78	0.36	-	-	-	0.00	0.01	100.24
23	22/01/02	50.81	4.22	12.98	13.50	0.19	5.18	9.24	2.66	0.81	0.37	-	-	-	0.00	0.03	99.99
24	22/01/02	50.77	4.03	12.98	13.35	0.17	5.14	9.27	2.70	0.74	0.35	-	-	-	0.06	0.00	99.55
25	22/01/02	51.01	4.16	12.61	13.09	0.24	4.96	9.22	2.67	0.77	0.34	-	-	-	0.03	0.02	99.11
26	22/01/02	51.22	4.09	12.71	12.85	0.24	5.10	9.19	2.62	0.77	0.32	-	-	-	0.00	0.01	99.12
27	22/01/02	50.43	4.12	12.91	13.17	0.20	5.03	9.37	2.69	0.85	0.38	-	-	-	0.03	0.02	99.20
28	22/01/02	50.83	4.09	12.74	13.43	0.15	5.10	9.07	2.75	0.79	0.36	-	-	-	0.00	0.02	99.33
29	22/01/02	50.51	4.32	12.50	13.17	0.15	5.12	9.15	2.68	0.82	0.31	-	-	-	0.00	0.04	98.77
30	22/01/02	50.78	4.04	12.61	13.42	0.18	5.09	9.05	2.69	0.77	0.34	-	-	-	0.02	0.03	99.00
31	22/01/02	51.00	3.99	12.80	13.70	0.09	5.24	9.21	2.73	0.77	0.31	-	-	-	0.00	0.05	99.91
32	22/01/02	50.92	4.03	12.83	13.41	0.18	5.13	9.23	2.68	0.83	0.31	-	-	-	0.01	0.04	99.60
33	22/01/02	50.92	4.18	12.83	13.49	0.20	5.19	9.31	2.65	0.83	0.31	-	-	-	0.02	0.03	99.94
34	22/01/02	50.48	4.12	12.68	13.09	0.25	5.06	9.14	2.65	0.75	0.34	-	-	-	0.01	0.02	98.58
35	22/01/02	50.67	4.10	12.88	13.29	0.16	5.18	9.02	2.71	0.79	0.33	-	-	-	0.06	0.02	99.21
36	22/01/02	50.26	4.09	12.73	13.03	0.31	5.00	9.33	2.69	0.79	0.34	-	-	-	0.02	0.00	98.60
37	22/01/02	50.88	4.08	12.85	13.30	0.20	5.10	9.41	2.65	0.75	0.35	-	-	-	0.04	0.03	99.63
38	22/01/02	49.90	4.05	12.75	13.84	0.17	5.09	9.03	2.70	0.83	0.35	-	-	-	0.00	0.01	98.73
39	22/01/02	49.87	4.17	12.74	13.51	0.19	5.23	9.26	2.67	0.78	0.33	-	-	-	0.01	0.00	98.74
40	22/01/02	50.58	4.14	12.75	13.62	0.17	5.13	9.14	2.64	0.79	0.34	-	-	-	0.00	0.01	99.31
41	22/01/02	50.38	4.17	12.74	13.61	0.22	5.18	9.18	2.71	0.77	0.34	-	-	-	0.02	0.02	99.32
mean		**50.83**	**4.10**	**12.71**	**13.43**	**0.20**	**5.11**	**9.28**	**2.68**	**0.79**	**0.34**				**0.02**	**0.02**	**99.51**
std.dev.		**0.44**	**0.10**	**0.14**	**0.27**	**0.04**	**0.10**	**0.14**	**0.03**	**0.03**	**0.03**				**0.02**	**0.01**	**0.61**
Recom.		**50.94**	**4.06**	**12.49**	**13.30**	**0.15**	**5.08**	**9.30**	**2.66**	**0.82**	**0.38**						**99.39**

Appendix A 3.4: Electron microprobe analyses of standards

	Date	SiO2	TiO2	Al2O3	FeO	MnO	MgO	CaO	Na2O	K2O	P2O5	Cr2O3	NiO	ZnO	F	Cl	Total
Kakanui Hornblende																	
1	9/10/03	40.10	5.09	15.60	10.65	0.07	12.53	10.28	2.28	2.04	-	0.03	0.02	-	-	-	98.68
2	9/10/03	40.09	4.95	15.41	10.88	0.07	12.15	10.16	2.33	2.08	-	0.00	0.00	-	-	-	98.11
3	9/10/03	39.00	4.91	14.87	11.19	0.06	12.11	10.19	2.39	2.01	-	0.02	0.01	-	-	-	96.76
4	9/10/03	39.26	4.38	15.17	10.66	0.09	12.10	10.14	2.35	2.07	-	0.00	0.00	-	-	-	96.22
5	9/10/03	39.43	4.68	15.14	10.83	0.08	12.31	10.22	2.35	2.09	-	0.00	0.01	-	-	-	97.12
6	9/10/03	39.40	4.82	14.98	10.42	0.12	12.13	10.25	2.35	2.07	-	0.03	0.07	-	-	-	96.64
7	9/10/03	39.06	5.05	14.95	10.98	0.09	12.16	10.14	2.37	2.11	-	0.00	0.01	-	-	-	96.93
8	9/10/03	39.06	4.94	14.96	10.65	0.11	12.09	10.11	2.30	2.02	-	0.00	0.00	-	-	-	96.23
mean		**39.43**	**4.85**	**15.13**	**10.78**	**0.08**	**12.20**	**10.19**	**2.34**	**2.06**		**0.01**	**0.01**				**97.08**
std.dev.		**0.44**	**0.23**	**0.25**	**0.24**	**0.02**	**0.15**	**0.06**	**0.04**	**0.03**		**0.01**	**0.02**				**0.88**
Recom.		**40.37**	**4.72**	**14.90**	**10.92**	**0.09**	**12.80**	**10.30**	**2.60**	**2.05**							**100.02**
Arenal Hornblende																	
1		41.49	1.15	15.25	11.45	0.12	14.12	11.31	1.88	0.17		0.00	0.00				96.94
2		41.37	1.17	15.21	11.56	0.16	14.27	11.51	1.89	0.21		0.00	0.00				97.35
3		40.90	1.32	15.09	11.42	0.16	14.12	11.48	1.96	0.23		0.04	0.03				96.74
4		40.58	1.37	14.93	11.64	0.16	14.04	11.39	1.88	0.21		0.00	0.06				96.24
5		40.82	1.20	15.07	11.38	0.14	14.09	11.51	1.91	0.18		0.04	0.00				96.34
6		40.24	1.47	14.93	11.77	0.12	14.02	11.36	1.95	0.18		0.01	0.03				96.09
7		40.07	1.31	14.90	11.27	0.13	13.83	11.63	1.94	0.19		0.00	0.01				95.29
8		39.89	1.31	14.75	11.55	0.14	13.92	11.48	1.93	0.18		0.04	0.03				95.22
mean		**40.67**	**1.29**	**15.02**	**11.50**	**0.14**	**14.05**	**11.46**	**1.92**	**0.19**		**0.02**	**0.02**				**96.28**
std.dev.		**0.59**	**0.11**	**0.17**	**0.16**	**0.02**	**0.13**	**0.10**	**0.03**	**0.02**		**0.02**	**0.02**				**0.75**
Recom.		**41.46**	**1.41**	**15.47**	**11.47**	**0.09**	**14.24**	**11.55**	**1.91**	**0.21**							**99.64**

Appendix A 4.1: Sample list and sample localities (see map A5.2)

Sample	Type	Locality	m a.s.l.	UTM Coordinates	Age* (ka)
Taburiente					
KLP 59	Flow	Barranco de Jurado	560	211635 / 3178774	533 ± 8
KLP 61	Flow, ankaramite	Playa de La Veta	230	209200 / 3181641	410 ± 80
KLP 63	Lava flow	Playa de La Veta	230	209200 / 3181641	410 ± 80
KLP 64	Lava flow	Puerto de Puntagorda	190	206600 / 3184585	563 ± 8
KLP 65	Lava flow	Puerto de Puntagorda	190	206600 / 3184585	563 ± 8
KLP 67	Lava flow	Road El Roque - coast	635	208373 / 3184428	585 ± 10
KLP 72	Lava flow, ankaramite	Camino Tagamantera	2170	220657 / 3185249	1080 ± 40
KLP 73	Lava flow	Platform lava of Puntallana, Punta Salinas	90	233314 / 3181378	560 ± 8
KLP 75	Lava flow	Platform lava of Puntallana, Punta Salinas	100	233375 / 3181377	560 ± 8
KLP 77	Lava flow	La Fajana in Barranco de Los Hombres	60	219932 / 3192752	833 ± 14
KLP 207	Lava flow, ankaramite	Barranco Franceses	410	221982 / 3191242	936 ± 14
KLP 208	Lava flow	Barranco Franceses	440	221929 / 3191255	936 ± 14
KLP 209	Lava flow, ankaramite	Barranco Gallego	525	223811 / 3191457	836 ± 14
KLP 221	Lava flow, ankaramite	Track to Marcos y Cordero	1338	224865 / 3185133	770 ± 90
Cumbre Nueva					
KLP 19	Lava flow	Camino de Real	1190	223409 / 3174378	647± 10
KLP 22	Lava flow	Camino de Real	1290	223559 / 3174391	
KLP 23	Lava flow	Camino de Real	1310	223585 / 3174425	
KLP 24	Lava flow	Camino de Real	1350	223703 / 3174442	
KLP 27	Lava flow	Top of Cumbre Nueva	1420	223959 / 3174203	
KLP 35	Lava flow	Track between tunnel and Pared Vieja	1220	224111 / 3169290	
KLP 36	Lava flow	Track between tunnel and Pared Vieja	1220	224111 / 3169290	
KLP 37	Lava flow, ankaramite	Road between tunnel and El Pilar	1177	222869 / 3170011	
KLP 39	Dyke	Road between tunnel and El Pilar	1170	222869 / 3170011	
KLP 41	Lava flow	Road between tunnel and El Pilar	1170	222869 / 3170011	
KLP 80	Lava flow	At the w'side of tunnel	1057	223520 / 3172487	834 ± 12
KLP 85	Lava flow	Road between tunnel and El Pilar	1100	223091 / 3169988	
KLP 87	Lava flow	Road between tunnel and El Pilar	1090	223162 / 3170215	
KLP 88	Dyke	Road between tunnel and El Pilar	1080	223214 / 3170355	
KLP 89	Lava flow	Road between tunnel and El Pilar	1060	223390 / 3170671	
KLP 103	Lava flow	Road between tunnel and El Pilar	1040	223375 / 3171468	

Appendix A 4.1 (continued): Sample list and sample localities

Sample	Type	Locality	m a.s.l.	UTM Coordinates	Age* (ka)
Bejenado					
KLP 105	Lava flow	Road between Bejenado and visitor center	1120	221111 / 3175549	
KLP 106	Lava flow	Road between Bejenado and visitor center	1090	221297 / 3175339	
KLP 205	Lava flow	Road between Bejenado and visitor center	852	221062 / 3174252	
KLP 217	Lava flow	W' flank of Bejenado	523	216627 / 3174620	
Cumbre Vieja					
KLP 47	Lava flow	Playa Nuevo	0	214263 / 3168167	123 ± 3
KLP 48	Lava flow	Road between Puerto Naos and Todoque	108	215410 / 3166139	95 ±
KLP 51	Lava flow	Charco Verde	66	216882 / 3163988	90 ± 3
KLP 52	Lava flow	Charco Verde	120	217243 / 3163539	90 ± 3
KLP 82	Lava flow	Puerto Tazacorte, port entrance	0	212587 / 3171981	120 ± 3
KLP 92	Lava flow	Punta Tigalate, Punta del Poris	85	226360 / 3158586	20 ± 2
KLP 93	Lava flow	Road to Punta del Poris	90	226495 / 3158766	20 ± 2
KLA1210**	Lava flow	Llano del Banco 1949 eruption	1130	220550 / 3167000	1949 A.D.
KLA1507**	Lapilli	Duraznero 1949 eruption	1790	222800 / 3154300	1949 A.D.
KLA1513**	Basanitic bomb	Hoyo Negro	1760	222250 / 3165100	1949 A.D.
TLP 79-1	*Basanite, block of aa lava*	*SW flank of V. de Teneguia, upper part of flow, 1971 eruption*	*327*	*220627 / 3152640*	*1971 A.D.*
TLP 111-1	*Basanite flow, 1 m thick, uppermost unit*	*About halfway between P.I.R.S. and main road, S side of road, 1712 eruption*	*921*	*220118 / 3161870*	*1712 A.D.*
TLP 25-1	*Basanite bomb*	*E flank of V. de San Antonio, 1677 eruption*	*648*	*221447 / 3154102*	*1677 A.D.*
TLP 43-1	*Basanite bomb*	*Southernmost crater of the S. Martin system, 1646 eruption*	*1494*	*222185 / 3159651*	*1646 A.D.*
TLP 76-1	*Basanite flow, pahoehoe*	*Flank eruption near El Puertito, 1646 eruption*	*100*	*224927 / 3156120*	*1646 A.D.*
TLP 50-2	*Basanitic mantle of composite bomb*	*W of spines, by gravel road, 1585 eruption*	*698*	*218829 / 3165200*	*1585 A.D.*
TLP 58-1	*Basanite, pahoehoe*	*Central part of 1480 flow, close to vent, 1480 eruption*	*1151*	*222457 / 3170142*	*1480 A.D.*
TLP 15-1	*Basanite flow*	*Mña La Barquita, by "volcano trail"*	*1618*	*221906 / 3167044*	*1480 A.D.*
TLP 17-1	*Basanite bomb*	*NE of Los Charcos*	*1767*	*222293 / 3165952*	*1480 A.D.*
TLP 19-2	*Tephriphonolite, spatter*	*Near eruptive vent at Nambroque*	*1907*	*222969 / 3164911*	
TLP 23-1	*Basanite bomb*	*Deseada II, 100 m S of peak*	*1925*	*222424 / 3163346*	
TLP 36-1	*Basanite bomb*	*W of Cabrito*	*1761*	*222524 / 3161886*	

Appendix A 4.1: Sample list and sample localities

Sample	Type	Locality	m a.s.l.	UTM Coordinates	Age* (ka)
TLP 38-1	*Basanite bomb*	*Mña Cabrera*	*1630*	*222344 / 3160720*	
TLP 44-1	*Basanite bomb*	*Mña Pelada*	*1390*	*222035 / 3159197*	
TLP 46-1	*Phonotephrite flow*	*Volcan Fuego*	*1227*	*222690 / 3158066*	
TLP 51-2	*Phonolite block, surrounded by tephrite*	*By vent near spines*	*962*	*219502 / 3164907*	*1585 A-D.*
TLP 51-3	*Tephrite, surrounding TLP 51-2*	*By vent near spines*	*962*	*219502 / 3164907*	*1585 A.D.*
TLP 69-1	*Tephrite bomb*	*Vent NW of Mña El Caldero*	*1596*	*223312 / 3167192*	
TLP116-1	*Tephrite bomb*	*Mña del Pino, near TV antenna, by dirt road*	*1000*	*222250 / 3156839*	
TLP 64-1	*Basanite bomb*	*Crater just NE of Birigoyo*	*1647*	*222713 / 3167712*	

*Sample ages are from Guillou et al. (1998, 2001)
**Samples were taken from A. Klügel and prepared and analyzed by T.S. Johansen
Samples in italic were taken, prepared and analyzed by T.S. Johansen

Appendix A 4.2: Composition of fractionation-corrected lavas

Sample	KLP61 Tab.	KLP63 Tab.	KLP65 Tab.	KLP67 Tab.	KLP72 Tab.	KLP73 Tab.	KLP75 Tab.	KLP77 Tab.	KLP207 Tab.	KLP208 Tab.	KLP209 Tab.	KLP221 Tab.	KLP19 C. N.	KLP22 C. N.	KLP23 C. N.	KLP24 C. N.	KLP35 C. N.
SiO2	42.26	42.55	41.82	41.62	42.98	42.26	42.93	43.70	44.48	45.00	46.78	44.48	43.15	42.76	43.75	43.09	42.22
TiO2	3.27	3.34	3.48	3.30	2.97	3.54	3.09	3.39	2.14	3.03	3.03	3.19	3.52	3.18	3.27	3.49	3.45
Al2O3	11.45	11.89	12.15	11.79	10.86	12.54	11.73	12.81	11.01	11.96	12.55	13.99	13.61	11.79	13.10	13.27	12.55
Fe2O3T	13.51	13.35	13.79	13.74	13.01	13.93	12.41	12.94	12.39	13.38	13.31	12.97	13.58	13.27	13.17	13.73	13.76
MnO	0.15	0.15	0.15	0.15	0.14	0.15	0.16	0.15	0.17	0.17	0.16	0.16	0.15	0.16	0.15	0.16	0.16
MgO	13.49	13.33	12.58	12.66	14.37	11.09	13.55	11.46	15.15	10.73	9.21	10.23	10.64	12.17	11.34	9.75	11.65
CaO	11.80	10.96	11.70	11.94	12.98	11.65	10.91	11.38	11.98	11.07	11.12	10.58	10.69	12.64	11.04	10.89	11.95
Na2O	2.65	3.04	2.66	3.07	1.68	3.59	3.51	2.60	1.98	2.53	2.69	2.89	2.82	2.55	2.90	3.14	2.76
K2O	0.52	0.76	1.13	0.84	0.57	0.71	0.88	1.20	0.76	1.11	0.69	1.21	1.30	0.50	1.05	1.23	1.18
P2O5	0.48	0.59	0.64	0.67	0.34	0.59	0.70	0.50	0.29	0.43	0.49	0.59	0.65	0.48	0.56	0.70	0.72
Total	99.58	99.96	100.10	99.76	99.91	100.04	99.87	100.13	100.36	99.41	100.03	100.28	100.12	99.50	100.33	99.44	100.40
Cr	126.8	48.8	45.4	73.8	381.2	189.0	21.5	209.9	939.1	696.2	482.1	302.0	92.0	475.1	149.5	227.7	170.1
Ni	382	390	373	363	414	316	385	300	433	286	245	292	305	352	323	274	331
Rb	10.3	15.8	22.4	10.6	21.3	6.1	9.6	23.5	22.2	27.7	11.9	38.9	32.1	51.6	25.9	36.2	26.7
Sr	574	608	655	658	508	718	693	614	430	584	579	812	856	655	616	901	708
Zr	208	219	203	207	164	300	284	243	155	241	235	333	267	231	264	335	240
Nb	41.7	46.6	49.5	48.1	31.5	66.4	64.1	51.3	40.9	51.1	42.0	58.0	66.7	48.4	54.3	68.6	61.4
Ba	275	346	345	317	207	414	436	359	207	264	211	316	399	313	307	348	440
La	35.2	38.1	42.5	43.0	28.6	47.5	51.0	34.8	31.8	39.5	40.8	62.4	45.3	38.8	40.9	55.0	48.6
Ce	73.6	79.7	90.8	89.8	58.7	101.4	102.5	74.8	61.5	78.4	81.4	127.5	90.0	78.0	88.5	109.7	101.4
Pr	9.08	9.88	10.71	10.37	7.31	12.01	12.47	9.43	7.20	9.40	9.70	14.27	10.39	9.66	10.26	13.13	12.54
Nd	36.8	42.4	44.6	42.4	30.3	44.7	50.3	40.6	27.4	37.2	37.4	52.1	41.8	39.9	43.6	51.0	53.5
Sm	7.47	8.49	8.56	7.66	6.31	9.19	10.00	8.37	5.28	7.63	7.88	8.72	8.50	8.00	8.41	9.88	10.68
Eu	2.41	2.61	2.76	2.48	2.04	2.89	2.99	2.68	1.65	2.28	2.53	2.69	2.49	2.50	2.63	3.04	3.11
Gd	6.82	7.38	7.73	6.79	5.94	7.89	8.09	6.88	4.83	6.55	7.33	6.97	7.24	7.19	7.05	8.24	8.64
Dy	5.06	5.50	5.63	4.78	4.42	5.57	6.07	5.49	3.94	5.09	6.05	5.37	5.12	5.23	5.21	6.14	6.46
Ho	0.88	0.99	0.96	0.84	0.80	0.96	1.08	0.98	0.72	0.90	1.07	0.96	0.91	0.96	0.87	1.01	1.07
Er	2.20	2.49	2.30	2.05	1.98	2.29	2.54	2.44	1.85	2.28	2.59	2.38	2.12	2.26	2.38	2.31	2.79
Yb	1.64	1.76	1.68	1.49	1.44	1.61	1.97	1.78	1.41	1.63	1.89	1.69	1.69	1.71	1.85	1.60	1.97
Pb	2.17	3.15	2.42	2.08	1.55	3.48	3.84	3.24	1.36	1.68	1.22	2.16	1.97	2.51	2.38	2.59	3.59
Th	3.08	3.94	4.05	3.66	2.64	5.65	5.72	3.60	2.45	3.09	2.68	4.23	3.66	3.68	4.07	4.11	4.87
U	0.65	0.86	0.95	0.95	0.63	1.10	1.22	0.89	0.61	0.84	0.69	1.17	0.86	0.82	1.06	1.10	1.08

Tab.: Taburiente, C.N.: Cumbre Nueva, Bej.: Bejenado, C.V.: Cumbre Vieja

Appendix A 4.2 (continued): Composition of fractionation-corrected lavas

Sample	KLP36	KLP37	KLP39	KLP41	KLP80	KLP85	KLP88	KLP89	KLP103	KLP115	KLP114	KLP205	KLP217	KLP48	KLP51	KLP82	KLP92
	C. N.	C. N.	C. N.	C. N.	C. N.	C. N.	C. N.	C. N.	C. N.	Bej.	Bej.	Bej.	Bej.	C.V.	C.V.	C.V.	C.V.
SiO2	42.58	44.35	43.08	43.21	45.05	43.53	42.28	44.09	44.39	42.87	42.39	42.87	45.27	43.01	42.30	45.32	42.94
TiO2	3.47	2.44	3.02	3.30	2.94	3.49	3.48	3.17	2.75	3.34	3.14	3.30	3.08	3.26	3.11	2.71	3.14
Al2O3	13.73	9.13	12.00	13.97	13.05	13.22	11.84	14.11	12.70	14.02	12.80	12.20	14.76	12.82	12.51	15.27	13.66
Fe2O3T	14.05	13.26	13.82	12.37	12.51	13.15	14.61	13.26	13.51	13.58	13.32	13.69	14.17	13.06	12.21	11.49	12.18
MnO	0.16	0.17	0.16	0.15	0.14	0.15	0.16	0.15	0.16	0.17	0.16	0.17	0.16	0.16	0.15	0.16	0.16
MgO	9.64	15.89	13.10	10.53	10.59	10.82	12.23	9.96	11.34	10.40	12.24	11.66	8.26	11.72	12.12	8.70	10.73
CaO	11.18	11.65	11.61	10.48	11.28	10.85	11.89	10.56	11.44	10.42	10.99	11.26	10.09	11.10	10.93	9.17	10.85
Na2O	2.78	1.64	2.08	2.59	2.46	2.65	2.25	2.88	2.39	3.24	2.91	3.10	2.94	3.03	3.42	4.39	3.66
K2O	1.05	0.76	0.90	1.33	1.06	1.21	0.96	1.14	0.72	1.27	0.83	0.88	0.84	1.34	1.52	1.85	1.60
P2O5	0.59	0.37	0.43	0.62	0.55	0.53	0.50	0.58	0.49	0.61	0.56	0.60	0.49	0.69	0.69	0.59	0.70
Total	99.23	99.66	100.18	98.55	99.64	99.61	100.20	99.91	99.88	99.91	99.33	99.73	100.06	100.20	98.96	99.65	99.62
Cr	243	1066	370	239	163	120	453	88	499	321	496	606	206	546	173	235	162
Ni	267	469	384	304	321	313	353	282	322	302	362	332	234	343	358	251	303
Rb	23.5	20.2	19.7	29.1	21.6	25.5	21.7	27.9	14.1	26.7	21.9	34.2	17.1	31.6	36.7	57.9	40.8
Sr	771	525	486	772	692	649	575	694	583	834	720	844	594	863	874	1035	1004
Zr	250	182	176	270	208	335	212	248	186	252	218	266	203	265	279	372	279
Nb	54.5	38.0	35.9	59.8	49.0	55.6	45.7	62.5	47.8	83.4	64.4	73.8	39.4	73.5	74.3	112.2	80.1
Ba	363	214	236	399	349	463	288	338	297	477	416	403	239	475	484	673	580
La	45.5	37.5	31.1	50.8	36.6	39.2	38.1	53.7	37.2	43.0	41.0	44.0	37.4	74.8	70.3	103.2	77.0
Ce	94.7	67.4	66.5	110.5	76.0	83.1	81.9	107.5	77.7	88.9	86.5	87.3	75.7	149.4	141.9	172.1	147.4
Pr	11.4	8.7	8.0	12.6	9.3	10.1	9.7	11.9	9.3	10.3	10.2	10.6	9.1	16.1	15.7	17.0	15.9
Nd	47.0	33.9	33.8	52.0	37.6	42.3	42.1	46.5	39.7	44.4	43.3	42.0	36.1	63.0	62.0	61.2	61.2
Sm	9.20	6.54	6.42	9.48	7.76	8.49	8.26	8.49	7.81	8.54	8.64	8.46	7.57	10.87	10.58	10.07	10.27
Eu	2.92	1.98	2.05	2.87	2.59	2.64	2.68	2.62	2.44	2.67	2.59	2.66	2.43	3.25	3.25	2.99	3.15
Gd	8.12	5.84	5.63	7.40	6.88	7.29	7.17	7.36	7.15	7.28	7.11	7.20	6.98	8.52	8.24	8.23	8.39
Dy	5.63	4.50	4.46	5.78	5.11	5.36	5.35	5.32	5.28	5.04	5.02	5.15	5.68	6.29	5.89	5.70	5.90
Ho	0.93	0.80	0.81	1.05	0.89	0.97	0.92	0.98	0.90	0.86	0.86	0.87	1.02	1.15	1.06	1.02	1.10
Er	2.46	2.00	2.03	2.74	2.16	2.55	2.26	2.45	2.33	2.09	2.05	2.05	2.51	2.77	2.74	2.52	2.62
Yb	1.73	1.49	1.61	2.08	1.55	1.86	1.68	1.94	1.67	1.62	1.47	1.43	1.78	2.06	2.05	2.11	2.05
Pb	2.67	1.45	1.94	3.06	2.62	3.10	2.32	2.57	1.75	2.26	2.19	1.75	1.41	3.50	3.82	6.85	3.95
Th	4.39	2.28	2.76	4.81	3.63	3.63	3.54	5.01	3.79	4.25	4.49	3.36	2.35	8.26	7.33	13.56	8.24
U	1.06	0.60	0.63	1.17	0.84	0.97	0.85	1.23	0.89	1.08	1.03	0.84	0.52	2.17	1.92	5.19	2.20

Tab.: Taburiente, C.N.: Cumbre Nueva, Bej.: Bejenado, C.V.: Cumbre Vieja

Appendix A 4.2 (continued): Composition of fractionation-corrected lavas

Sample	KLP93 C.V.	KLA1210 C.V.	KLA1513 C.V.	TLP231 C.V.	TLP251 C.V.	TLP381 C.V.	TLP431 C.V.	TLP502 C.V.	TLP581 C.V.	TLP641 C.V.	TLP791 C.V.	TLP151 C.V.	TLP171 C.V.	TLP761 C.V.	TLP1111 C.V.	TLP441 C.V.	TLP361 C.V.
SiO2	43.20	43.49	41.87	41.55	43.39	43.73	42.93	43.94	43.73	43.88	43.27	43.57	43.83	42.91	42.91	42.97	42.99
TiO2	3.21	3.16	3.34	3.41	3.33	3.14	3.35	3.32	3.34	3.14	3.30	3.26	3.02	3.38	3.39	3.40	3.16
Al2O3	13.42	13.53	12.84	12.21	13.21	13.65	12.56	13.50	13.67	13.14	13.24	13.44	13.66	12.73	12.61	12.62	13.39
Fe2O3T	12.41	13.12	13.35	13.74	13.28	12.54	13.42	13.03	13.09	12.40	13.72	12.82	12.78	13.25	13.46	13.30	13.34
MnO	0.16	0.17	0.19	0.18	0.17	0.17	0.17	0.16	0.18	0.17	0.16	0.17	0.17	0.16	0.16	0.16	0.18
MgO	10.86	10.48	11.79	11.53	10.83	11.18	11.46	10.67	10.34	11.58	11.19	11.04	10.97	11.42	11.68	11.28	11.35
CaO	11.48	10.53	10.51	11.99	11.30	10.31	12.18	11.03	10.71	10.61	11.15	10.59	11.13	11.93	11.59	12.03	11.29
Na2O	3.80	3.35	2.99	3.89	3.35	3.82	2.99	3.23	3.59	3.55	3.18	3.65	3.33	3.19	3.16	3.21	3.21
K2O	1.12	1.15	1.35	1.63	1.53	1.75	1.34	1.52	1.68	1.72	1.22	1.70	1.45	1.38	1.41	1.40	1.33
P2O5	0.73	0.60	0.67	1.03	0.76	0.81	0.75	0.70	0.79	0.89	0.74	0.87	0.77	0.80	0.79	0.78	0.90
Total	100.39	99.56	98.90	101.16	101.14	101.09	101.15	101.12	101.12	101.09	101.19	101.11	101.10	101.14	101.17	101.15	101.14
Cr	223	285	747	413	263	113	316	239	221	125	197	191	241	254	293	241	269
Ni	308	302	339	330	306	322	338	311	299	338	319	315	321	335	338	328	333
Rb	28.3	24.8	37.0	41.6	36.1	44.7	31.4	35.9	40.8	39.2	25.1	41.4	34.6	31.1	32.5	32.6	27.2
Sr	1011	839	1027	1308	1086	1200	1013	1029	1077	1037	865	1076	859	1018	977	1078	1040
Zr	279	251	300	350	299	348	265	305	341	308	259	317	290	266	262	292	271
Nb	79.0	56.0	76.6	112.7	86.2	91.8	76.0	87.9	95.0	84.2	63.7	88.8	77.9	75.2	76.1	83.3	76.9
Ba	558	352	496	649	545	583	474	494	547	502	385	519	452	485	484	505	478
La	80.2	51.2	66.7	90.0	86.8	88.7	76.0	68.9	79.7	64.9	61.9	73.9	62.2	74.5	73.2	82.7	78.2
Ce	153	101	126	169	162	166	143	133	155	131	128	139	123	149	146	156	151
Pr	16.8	11.9	14.4	19.3	18.0	18.5	15.7	15.2	17.4	14.6	14.6	16.0	14.1	16.4	16.0	17.6	17.2
Nd	64.2	46.3	54.2	74.0	65.0	67.3	60.7	57.0	67.7	58.4	58.5	59.7	55.8	64.5	62.3	67.2	67.3
Sm	11.3	8.8	10.0	13.7	11.6	12.1	10.9	10.4	12.4	11.0	10.6	11.3	10.7	11.4	11.8	11.7	12.3
Eu	3.30	2.71	2.97	4.02	3.57	3.80	3.50	3.36	3.85	3.44	3.38	3.50	3.01	3.48	3.49	3.40	3.55
Gd	8.98	7.94	8.67	10.98	10.14	10.34	9.86	9.52	10.68	9.33	9.23	9.71	8.46	9.37	9.60	10.29	10.36
Dy	6.11	5.36	5.81	7.00	6.87	7.32	6.63	6.60	7.42	6.47	6.33	6.72	6.10	6.59	6.80	6.88	7.20
Ho	1.07	0.95	1.02	1.18	1.24	1.25	1.15	1.15	1.28	1.14	1.10	1.16	1.11	1.14	1.15	1.15	1.21
Er	2.68	2.39	2.62	2.95	3.04	3.23	2.86	2.95	3.21	2.99	2.78	3.01	2.97	2.98	2.95	2.81	3.02
Yb	1.92	1.78	2.02	1.87	2.17	2.45	1.98	2.12	2.33	2.14	1.96	2.11	2.30	2.07	2.14	2.00	2.21
Pb	4.09	2.77	2.93	3.41	3.87	4.00	2.18	3.57	4.30	3.92	2.77	4.40	4.63	3.13	3.60	3.11	3.27
Th	8.64	4.83	7.27	8.53	8.12	8.17	7.15	6.35	7.17	6.09	4.97	6.50	6.68	7.31	6.54	8.34	7.32
U	2.19	1.34	1.87	2.55	2.18	2.30	1.90	1.68	1.95	2.05	1.49	2.06	1.76	1.95	1.84	2.06	1.58

Tab.: Taburiente, C.N.: Cumbre Nueva, Bej.: Bejenado, C.V.: Cumbre Vieja

Appendix A 4.3: XRF analyses of international standards

	JA-2			JB-2			JR-1			JB-3		
Sample	Mean (N=5)	Std.dev.	**Rec. value**	Mean (N=5)	Std.dev.	**Rec. value**	Mean (N=5)	Std.dev.	**Rec. value**	Mean (N=5)	Std.dev.	**Rec. value**
wt.%												
SiO2	56.32	0.24	**56.18**	53.28	0.19	**53.2**	75.06	0.23	**75.41**	50.96	0.15	**51.04**
TiO2	0.67	0.01	**0.67**	1.18	0.01	**1.19**	0.11	0.00	**0.1**	1.41	0.00	**1.45**
Al2O3	15.50	0.07	**15.32**	14.93	0.09	**14.67**	12.71	0.04	**12.89**	17.41	0.05	**16.89**
Fe2O3	6.49	0.02	**6.14**	14.28	0.05	**14.34**	0.90	0.00	**0.96**	12.01	0.04	**11.88**
MnO	0.11	0.00	**0.11**	0.21	0.00	**0.2**	0.10	0.00	**0.1**	0.17	0.00	**0.16**
MgO	7.96	0.03	**7.68**	4.85	0.06	**4.66**	0.25	0.07	**0.09**	5.26	0.03	**5.2**
CaO	6.25	0.02	**6.48**	9.93	0.01	**9.89**	0.70	0.01	**0.63**	9.77	0.01	**9.86**
Na2O	3.03	0.06	**3.08**	2.07	0.08	**2.03**	3.94	0.03	**4.1**	2.76	0.09	**2.82**
K2O	1.75	0.01	**1.8**	0.42	0.01	**0.42**	4.46	0.01	**4.41**	0.77	0.01	**0.78**
P2O5	0.15	0.01	**0.15**	0.10	0.00	**0.1**	0.02	0.00	**0.02**	0.30	0.01	**0.29**
Total	98.43	0.39		101.42	0.32		98.36	0.34		101.01	0.24	
ppm												
Co	24.80	1.10	**30**	49	1.3	**40**	6	0.0	**0.65**	39	1.6	**36.3**
Cr	481.20	3.35	**465**	47	2.5	**27**	<18		**2.3**	79	5.6	**60.4**
Ni	127.60	3.44	**142**	12	1.3	**14.2**	<2		**0.66**	40	1.0	**38.8**
V	123.60	2.70	**130**	586	2.4	**578**	<12		**k.A.**	384	4.5	**383**
Zn	60.80	1.79	**62.7**	106	0.4	**110**	28	1.5	**30**	103	0.8	**106**
Ce	26.60	6.88	**32.7**	15	3.1	**6.77**	59	10.2	**47.1**	17	5.0	**21.5**
La	<14		**16.3**	<4		**2.37**	<14		**19.7**	<14		**8.89**
Nb	10.60	1.34	**9.8**	6	2.3	**0.8**	14	1.1	**15.5**	6	1.3	**2.3**
Ga	15.60	1.52	**16.4**	15	2.5	**17**	17	1.8	**17.6**	19	1.8	**20.7**
Pb	19.80	4.44	**19.3**	11	1.8	**5.4**	20	1.3	**19.1**	9	1.7	**5.5**
Pr	<4		**4.38**	7	1.9	**0.96**	<4		**5.62**	<4		**3.39**
Rb	71.40	1.82	**68**	8	1.2	**6.2**	258	2.2	**257**	16	1.3	**13**
Ba	305.20	14.92	**317**	212	3.4	**208**	39	7.1	**40**	242	18.2	**251**
Sr	245.80	1.30	**252**	177	1.9	**178**	29	0.4	**30**	403	3.5	**395**
Th	5.33	0.58	**4.7**	<4		**0.33**	29	2.0	**26.5**	<4		**1.3**
Y	14.40	0.55	**18.1**	24	0.4	**25**	36	1.1	**45.4**	26	0.8	**27**
Zr	102.80	1.64	**119**	56	1.1	**51.4**	98	1.1	**101**	99	1.1	**98.3**

Appendix A 4.4 (continued): ICP-MS analyses of USGS reference standard BCR-2

					Jan-03			May 03		June 03			Jan-04			July 04
	mass	BCR-2 Rec. ng/g	+/-	41	43	44	57	59	63	76	77	78	79	93
Li	7	*9*	*2.0*	-	-	-	10.0	9.7	-	9.7	9.7	8.0	7.8	8.7
Sc	46	34	3.0	32.6	33.6	30.2	37.9	35.1	16.7	34.8	36.6	35.3	34.8	36.7
V	51	416	14.0	427	425	410	450	434	362	426	449	449	441	460
Cr	52	18	2.0	15.2	14.7	14.5	16.0	14.6	13.5	14.7	16.8	15.6	15.2	19.2
Co	59	37	3.0	36.0	37.3	33.3	42.5	38.5	32.5	36.9	39.6	38.2	37.3	39.3
Ni	60			10.9	8.8	10.5	10.2	9.2	9.6	11.5	12.1	11.8	11.5	11.9
Cu	63	19	2.0	15.2	16.2	15.7	17.5	16.3	13.2	16.3	17.1	16.8	16.4	18.0
Zn	66	127	9.0	134.7	121.1	128.3	122.5	121.3	120.4	131.8	139.7	132.2	130.7	141.4
Ga	69	23	2.0	22.7	21.6	22.5	22.0	22.0	20.2	21.1	21.2	21.9	21.4	23.0
Rb	85	48	2.0	47.2	51.4	45.3	56.4	52.8	35.7	48.7	49.6	47.6	47.1	49.81
Sr	86	346	14.0	344.3	346.9	332.3	361.5	350.3	276.0	348.8	343.0	349.2	347.1	358.23
Y	89	37	2.0	34.0	36.1	32.2	37.0	36.2	20.1	34.3	35.7	37.0	35.8	34.46
Zr	90	188	16.0	193.3	200.0	191.2	207.2	197.3	186.0	193.2	195.2	197.1	196.4	196.59
Nb	93			12.2	12.9	12.1	13.4	12.9	11.7	12.0	11.9	12.3	12.3	12.32
Cs	133	1.1	0.1	1.3	1.2	1.3	1.2	1.2	0.9	1.2	1.3	1.1	1.1	1.1
Ba	138	683	28.0	734.7	772.4	759.5	705.4	739.3	694.6	692.5	671.9	682.9	679.0	663.5
La	139	25	1.0	26.2	29.7	26.6	26.0	28.5	20.0	26.8	27.7	26.4	26.5	25.0
Ce	140	53	2.0	55.2	60.9	55.9	56.4	60.2	54.3	56.5	56.8	54.8	55.6	52.0
Pr	141	6.8	0.3	6.8	7.8	7.2	7.0	7.7	5.3	7.0	7.2	6.8	6.9	6.5
Nd	146	28	2.0	26.9	31.9	30.7	27.7	32.5	23.4	30.4	29.3	29.0	29.2	27.4
Sm	147	*6.7*	*0.3*	6.4	6.8	7.1	5.5	6.4	5.0	6.9	6.8	6.7	6.8	6.7
Eu	151	2	0.1	2.0	2.2	2.1	2.0	2.0	1.3	2.1	2.0	2.0	1.9	1.8
Gd	157	*6.8*	*0.3*	6.9	6.9	7.1	6.3	6.7	4.8	7.2	6.8	6.8	7.0	6.6
Tb	159	*1.07*	0.0	1.0	1.1	1.1	0.9	1.0	0.7	1.1	1.1	1.0	1.0	1.0
Dy	163			6.4	6.7	7.2	5.6	6.3	4.9	6.9	6.7	6.6	6.7	6.2
Ho	165	*1.33*	*0.06*	1.38	1.35	1.39	1.15	1.31	0.95	1.37	1.32	1.30	1.33	1.24
Er	166			3.69	4.02	3.82	3.27	3.91	2.73	3.92	3.86	3.62	3.70	3.35
Tm	169	0.54		0.53	0.58	0.57	0.48	0.54	0.42	0.56	0.54	0.51	0.51	0.45
Yb	172	*3.5*	*0.2*	3.3	3.6	3.6	2.9	3.3	2.5	3.6	3.4	3.4	3.4	3.2
Lu	175	*0.51*	*0.02*	0.49	0.50	0.55	0.42	0.46	0.37	0.54	0.49	0.50	0.51	0.46
Hf	178	4.8	0.2	5.1	5.2	5.7	4.0	4.7	6.7	5.2	4.9	5.1	5.2	4.8
Ta	181			0.91	0.85	0.91	0.79	0.80	0.97	0.86	0.94	0.81	0.83	0.73
Tl	205			0.33	0.36	0.34	0.34	0.31	0.42	0.27	0.33	0.26	0.27	0.21
Pb	208	11	2	12	10	13	9	9	13	10	10	9	9	9
Th	232	*6.2*	*0.7*	7.7	6.8	7.4	5.4	6.0	6.2	6.5	6.8	5.9	6.1	5.3
U	238	1.69	0.2	1.92	1.88	1.97	1.57	1.74	2.43	1.83	1.88	1.57	1.61	1.51

Appendix A 4.4 (continued): ICP-MS analyses of USGS reference standard BIR-1

	mass	BIR-1 rec. ng/g	+/-	Jan-03 44-1	44-2
Sc	**45**	**44**	**1.0**	36.57	37.29
V	**51**	**310**	**11.0**	306	311
Cr	**52**	**370**	**8.0**	346	355
Co	**59**	**52**	**2.0**	44.54	46.00
Ni	**60**	**170**	**6.0**	145	146
Cu	**63**	**125**	**4.0**	102	104
Zn	**66**	**70**	**9.0**	66	67
Ga	**69**	**16**		15.12	15.39
Rb	**85**			0.25	0.23
Sr	**86**	**110**	**2.0**	101	103
Y	**89**	**16**	**1.0**	13.57	13.67
Zr	**90**	**18**	**1.0**	14	14
Nb	**93**			0.58	0.51
Cs	**133**			0.01	0.01
Ba	**138**	**7**		8	7
La	**139**	**0.63**	**0.07**	0.64	0.67
Ce	**140**			1.95	2.02
Pr	**141**			0.39	0.38
Nd	**146**	**2.5**	**0.7**	2.46	2.62
Sm	**147**	***1.1***		1.18	1.22
Eu	**151**	**0.55**	**0.05**	0.54	0.55
Gd	**157**	**1.8**	**0.4**	1.91	1.87
Tb	**159**			0.35	0.37
Dy	**163**	**4**	**1.0**	2.66	2.77
Ho	**165**			0.59	0.61
Er	**166**			1.76	1.83
Tm	**169**			0.27	0.26
Yb	**172**	***1.7***	***0.1***	1.65	1.78
Lu	**175**	***0.26***		0.25	0.27
Hf	**178**	**0.6**	**0.08**	0.65	0.64
Ta	**181**			0.06	0.06
Tl	**205**			0.05	0.05
Pb	**208**	3		4.25	3.40
Th	**232**			0.04	0.04
U	**238**			0.01	0.01

Appendix 4.4 (continued): ICP-MS analyses of USGS reference standard BHVO

	mass	BHVO-2 Rec. ng/g	+/-	Jan-03 44	48	May 03 58
Sc	**45**	**32**	**1.0**	27.73	32.08	33.56
V	**51**	**317**	**11.0**	314.22	317.77	342.42
Cr	**52**	**280**	**19.0**	269.67	289.21	288.44
Co	**59**	**45**	**3.0**	40.13	44.53	48.11
Ni	**60**	**119**	**7.0**	102.99	114.19	122.49
Cu	**63**	**127**	**7.0**	112.33	118.68	126.32
Zn	**66**	**103**	**6.0**	97.57	101.11	95.43
Ga	**69**	**21.7**	**0.9**	22.12	21.59	21.29
Rb	**85**	**9.8**	**1.0**	8.93	9.63	10.40
Sr	**86**	**389**	**23.0**	385.01	368.61	414.86
Y	**89**	**26**	**2.0**	23.87	24.22	26.05
Zr	**90**	**172**	**11.0**	169.90	165.58	180.54
Nb	**93**	***18***	***2.0***	17.61	17.10	19.80
Cs	**133**			0.11	0.13	0.11
Ba	**138**	**130**	**13.0**	146.22	143.68	140.01
La	**139**	**15**	**1.0**	16.55	15.36	16.71
Ce	**140**	**38**	**2.0**	40.10	39.14	40.97
Pr	**141**			5.71	5.49	5.70
Nd	**146**	**25**	**1.8**	26.76	25.97	26.13
Sm	**147**	***6.2***	***0.4***	6.80	6.24	5.51
Eu	**151**			2.28	2.10	2.11
Gd	**157**	***6.3***	***0.2***	6.66	6.41	6.28
Tb	**159**	***0.9***		0.97	0.95	0.90
Dy	**163**			5.94	5.38	4.94
Ho	**165**	***1.04***	***0.04***	1.04	1.05	0.93
Er	**166**			2.80	2.72	2.44
Tm	**169**			0.38	0.35	0.33
Yb	**172**	***2***	***0.2***	2.24	2.08	1.86
Lu	**175**	***0.28***	***0.01***	0.34	0.29	0.25
Hf	**178**	**4.1**	**0.3**	5.21	4.96	3.92
Ta	**181**	***1.4***		1.34	1.43	1.18
Tl	**205**			0.07	0.06	0.09
Pb	**208**			1.81	2.26	1.47
Th	**232**	***1.2***	***0.3***	1.53	1.45	1.19
U	**238**			0.49	0.47	0.42

Appendix A 4.5: Sr-Nd-Pb isotope analyses of standard material

NBS987	87Sr/86Sr		
Feb-April 2003 +July 2004			
N=16	0.710256		
2s (abs)	0.000005		
2s (ppm)	3.7		
Sept-Okt 2003			
N=13	0.710274		
2s (abs)	0.000009		
2s (ppm)	6.2		
Normalizing Factor	-0.000017		
SPEX	143Nd/144Nd		
N=20	0.511712		
2s (abs)	0.000006		
2s (ppm)	5.5		
La Jolla	143Nd/144Nd		
N=12	0.511848		
2s (abs)	0.000005		
2s (ppm)	5.3		
NBS981	206Pb/204Pb	207Pb/204Pb	208Pb/204Pb
N=60	16.900	15.437	36.527
2s (abs)	0.007	0.008	0.027
2s (ppm/amu)	193	181	185
2s (%/amu)	0.019	0.018	0.018

Appendix A 4.6: melting model

C_L concentration of a trace element in the liquid
C_o concentration of a trace element in the source
D_o bulk distribution coefficient for the initial solid
P bulk distribution coefficient of minerals which make up a melt
F fraction of melt produced by partial melting
C_{ass} concentration of a trace element in a liquid which has assimilated minerals
C_{Min} concentration of a trace element in an assimilated mineral
F_L fraction of melt produced by partial melting minus fraction of assimilated minerals
F_{Min} fraction of assimilated mineral in the melt

Assuming the constancy of distribution coefficients during the partial melting process, a batch melting equation can be written as:

$C_L = C_o /[D_o + F(1 – P)]$ (Shaw, 1970) (1)

The concentration of a trace element in a liquid which has completely assimilated mineral phases in different proportions are given by:

$$C_{ass} = C_L * F_L + C_{Min} * F_{Min} \quad (2)$$

Appendix A5.1: Map of samples localities listed in Appendix 1 in chapter 3. Satellite image is available at glc.umiac.umd.edu.

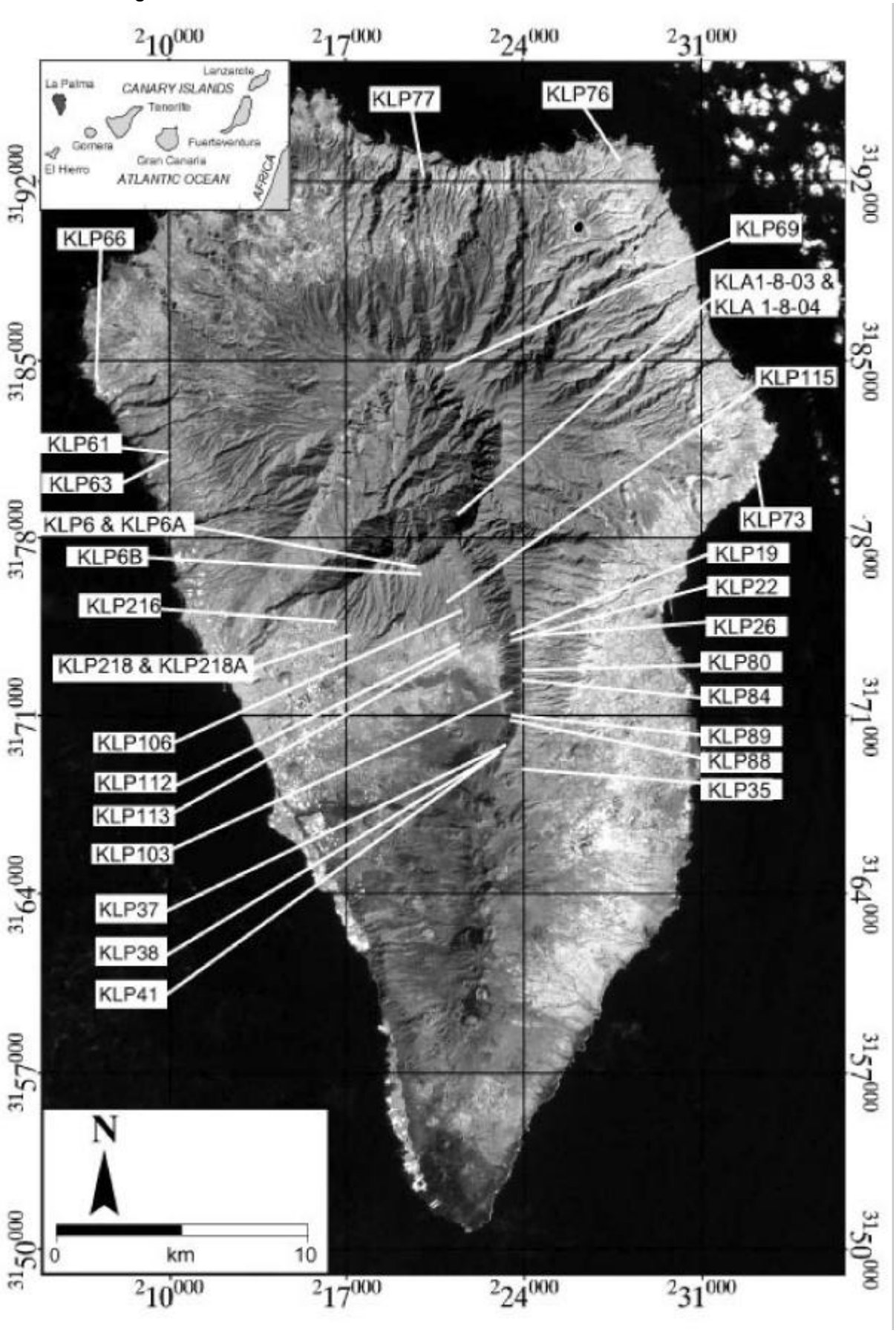

Appendix A5.2: Map of samples localities listed in Table 1 of chapter 4. Satellite image is available at glc.umiac.umd.edu.

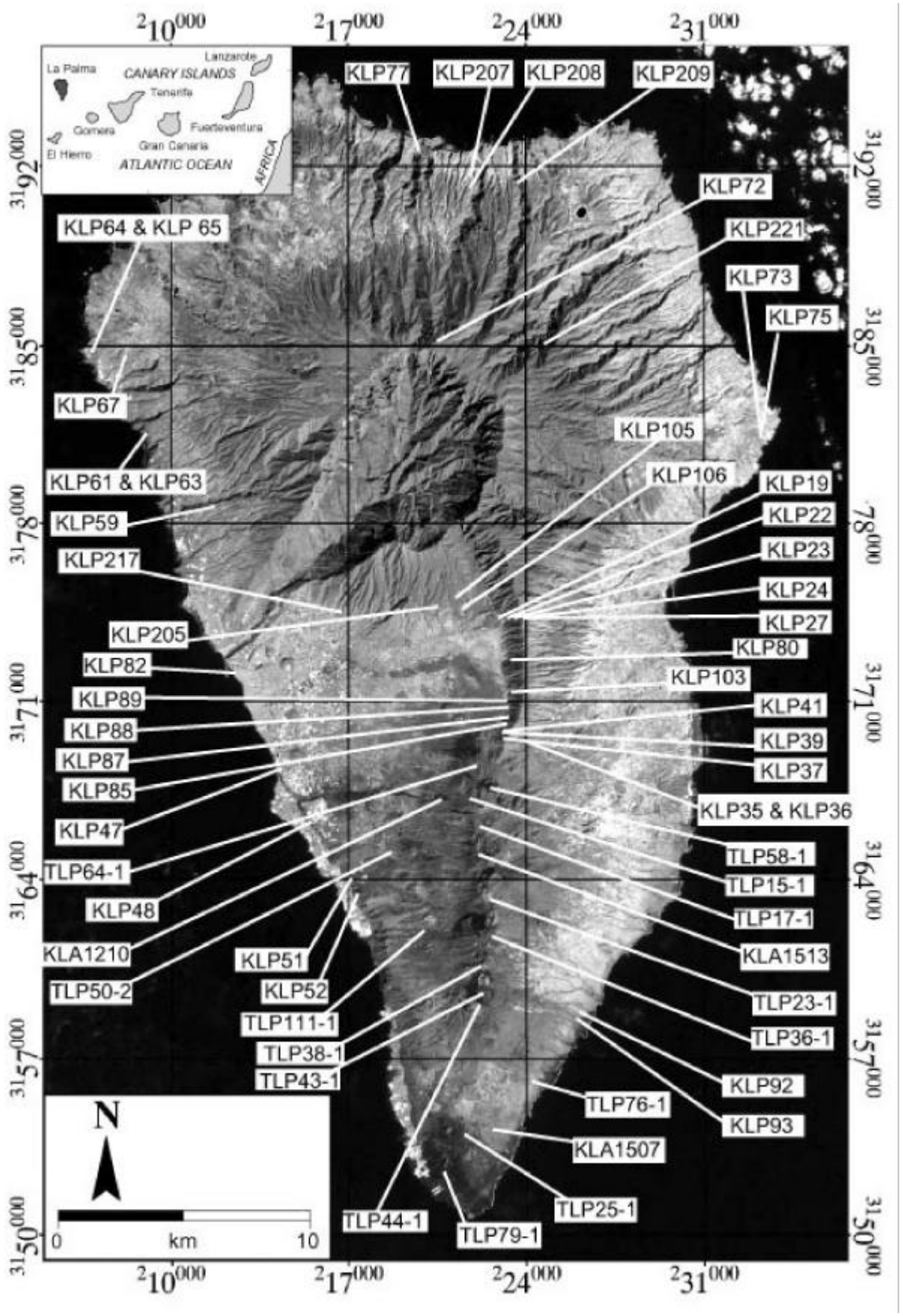

Erklärung

Hiermit versichere ich, dass ich

1. die Arbeit ohne unerlaubte fremde Hilfe angefertigt habe,
2. keine anderen als die von mir angegebenen Quellen und Hilfsmittel benutzt habe und
3. die den benutzten Werken wörtlich oder inhaltlich entnommenen Stellen als solche kenntlich gemacht habe.

Bremen, den

Danksagung

Meinen größten Dank möchte ich Dr. Andreas Klügel aussprechen, der diese Arbeit ermöglicht hat. Als direkter Betreuer stand er immer mit Rat und Tat zur Seite, auch um meine manchmal konfusen Fragen zu beantworten. Als Doktorand kann man sich wirklich keinen besseren Betreuer vorstellen.

Prof. Dr. Olesch sei herzlichst gedankt für die Erstellung des Erstgutachten sowie für die Erlaubnis die Labore der AG “Geologie der Polargebiete” benutzen zu dürfen.

Ein herzliches Dank für moralische und fachliche Unterstützung geht an die ehemaligen Mitglieder der AG “Petrologie der Ozeankruste”: Prof. Dr. C. W. Devey, Dr. K. Lackschewitz, Dr. K. Freitag und Imme Martelock. Außerdem sei meinem Büronkollegen Dr. Burkhard Schramm gedankt für Beantwortung vieler Fragen, die nicht nur fachlich waren. Heike Anders danke ich für die Durchführung der ICP-MS Analysen und den morgendlichen Kaffee. Hervorzuheben ist meine ehemalige Kollegin Dr. Stefanie Schwarz für fachliche Unterstützung und gemeinsames Jammern. Danken möchte ich auch jetzigen und ehemaligen Hiwis, Studenten und Mitgliedern unserer Arbeitsgruppe: Frieder, Anna, Steffi, Almuth, Phillip, Holger, Florence, Bianca und Jutta Ait-Majdari.

Vielen Dank an die Leute vom IFM-Geomar in Kiel, die mir geholfen haben. Besonders ist hierbei Dr. Thor Hansteen hervorzuheben, der nicht nur große Teile der Arbeit Korrektur gelesen hat, sondern sich auch bereit erklärt hat das Zweitgutachten anzufertigen. Dr. Paul van den Bogaard danke ich für die Durchführung der Ar/Ar-Datierungen. Natürlich auch Herzlichen Dank an Prof. Dr. Kaj Hoernle für konstruktive Kritik und den Versuchen mir die Geochemie etwas Näher zu bringen. Nicht zu vergessen den Cumbre Vieja Spezialisten Tor Sigvald, der mir gezeigt hat das es jemanden gibt, der besser als ich Fussballstatistiken runterleiern kann. Dr. Folkmar Hauff bin ich für seine Einführung in die Isotopengeochemie dankbar. Ein herzliches Danke Schön gilt den TechnikernInnen vom IFM-Geomar: Silke Hauff, Dagmar Rau, Jan Sticklus haben u.a. die RFA, Isotopenanalysen und Datierungen durchgeführt, und Mario Thöner unterstützte die Mikrosondenanalysen und versorgte mich immer mit Kaffee.

Für die Durchsicht von Teilen der Arbeit sei folgenden Kollegen an der Uni Bremen gedankt: Dr. B. Emmel, Dr. B. Kleinefeld, Dr. S. Boger, Dr. F. Lisker, Dr. S. Lühning

Bedanken möchte ich mich auch bei den John Zwillingen - Timm für Unterschlupf in Kiel und Uwe für motivierende Gespräche während unserer gemeinsamen Trainingsläufe um den Werdersee.

Herzlichen Dank geht besonders an Sandra, die mich mit ihrem offenem Ohr sowie seelischer und moralischer Unterstützung in allen Lebenslagen begleitet hat..

Abschließend möchte ich mich bei meinen Eltern und der Familie Bolte für ihre Geduld, Vertrauen und Unterstützung bedanken.

Lebenslauf

Name:	Karsten Erwin Erich Galipp
Geburtstag und -ort:	8. März 1971 in Berlin-Spandau
Staatsangehörigkeit:	deutsch
Familienstand:	ledig
Adresse:	Friedrich-Ebert Str. 25, 28199 Bremen
August 1977 - Mai 1991:	Grundschule und Gymnasium in Sudweyhe und Syke
Mai 1991:	Abitur am Gymnasium Syke, Niedersachsen
Oktober 1991 - September 1992:	Geschichtsstudium an der Universität Bremen
Oktober 1992 - März 1996:	Geologiestudium an der TU Clausthal-Zellerfeld
März 1996:	Vordiplom, Gesamturteil: gut
März 1996 - Januar 1997:	Geologiestudium an der Universität Bremen
Februar 1997 - Oktober 1997:	Geologiestudium an der WITS University Johannesburg, Südafrika
November 1997 - Dezember 1999:	Geologiestudium an der Universität Bremen
Dezember 1999:	Abschluß der Diplomprüfung, Gesamturteil: sehr gut
April 2000 - Oktober 2000:	Beschäftigung als Ingenieurgeologe bei der IFB Eigenschenk, Deggendorf
November 2000 - Dezember 2001:	Laborleiter am Institut für Erd- und Grundbau der Fa. DORSCH Consult, München
Seit Januar 2002:	Wissenschaftlicher Mitarbeiter an der Universität Bremen, Fachbereich Geowissenschaften
Seit Oktober 2002:	Hydrologie-Fernstudium an der Universität Hannover